ISSN: 2153-1196 Volume 9, Number 10, September 2018

Scientific Research Publishing

# Journal of Modern Physics

Special Issue on Gravitation, Astrophysics and Cosmology Research

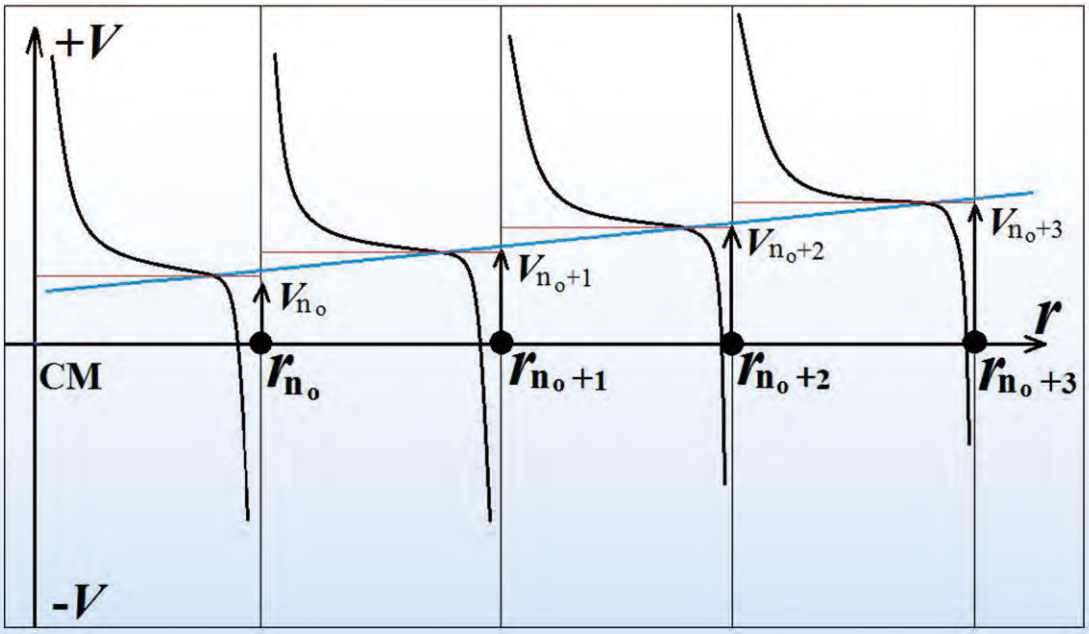


ISSN: 2153-1196

www.scirp.org/journal/jmp

# Journal Editorial Board

**ISSN: 2153-1196 (Print) ISSN: 2153-120X (Online)**
**http://www.scirp.org/journal/jmp**

Scientific Research Publishing

Journal of Modern Physics, 2018, 9, 1867-2020
http://www.scirp.org/journal/jmp
ISSN Online: 2153-120X
ISSN Print: 2153-1196

# Table of Contents

Volume 9 Number 10 September 2018



The figure on the front cover is from the article published in Journal of Modern Physics, 2018, Vol. 9, No. 10, pp. 1883-1905 by Jacob Schaf.

# Journal of Modern Physics (JMP)
# Journal Information

## SUBSCRIPTIONS

The *Journal of Modern Physics* (Online at Scientific Research Publishing, www.SciRP.org) is published monthly by Scientific Research Publishing, Inc., USA.

**Subscription rates:**
Print: $89 per issue.
To subscribe, please contact Journals Subscriptions Department, E-mail: sub@scirp.org

## SERVICES

**Advertisements**
Advertisement Sales Department, E-mail: service@scirp.org

**Reprints (minimum quantity 100 copies)**
Reprints Co-ordinator, Scientific Research Publishing, Inc., USA.
E-mail: sub@scirp.org

## COPYRIGHT



## PRODUCTION INFORMATION

For manuscripts that have been accepted for publication, please contact:
E-mail: jmp@scirp.org

Journal of Modern Physics, 2018, 9, 1867-1882
http://www.scirp.org/journal/jmp
ISSN Online: 2153-120X
ISSN Print: 2153-1196

# Why Flat Space Cosmology Is Superior to Standard Inflationary Cosmology

**Eugene Terry Tatum**

760 Campbell Ln. Ste. 106 #161, Bowling Green, KY, USA
Email: ett@twc.com

**How to cite this paper:** Tatum, E.T. (2018) Why Flat Space Cosmology Is Superior to Standard Inflationary Cosmology. *Journal of Modern Physics*, **9**, 1867-1882.
https://doi.org/10.4236/jmp.2018.910118

**Received:** July 12, 2018
**Accepted:** August 31, 2018
**Published:** September 3, 2018





## Abstract

Following recent Cosmic Microwave Background (CMB) observations of global spatial flatness, only two types of viable cosmological models remain: inflationary models which almost instantaneously attain cosmic flatness following the Big Bang; and non-inflationary models which are spatially flat from inception. Flat Space Cosmology (FSC) is the latter type of cosmological model by virtue of assumptions corresponding to the Hawking-Penrose conjecture that a universe expanding from a singularity could be modeled like a time-reversed black hole. Since current inflationary models have been criticized for their lack of falsifiability, the numerous falsifiable predictions and key features of the FSC model are herein contrasted with standard inflationary cosmology. For the reasons given, the FSC model is shown to be superior to standard cosmology in the following eleven categories: Predictions Pertaining to Primordial Gravity Waves; Cosmic Dawn Early Surprises; Predicting the Magnitude of CMB Temperature Anisotropy; Predicting the Value of Equation of State Term $w$; Predicting the Hubble Parameter Value; Quantifiable Entropy and the Entropic Arrow of Time; Clues to the Nature of Gravity, Dark Energy and Dark Matter; The Cosmological Constant Problem; Quantum Cosmology; Dark Matter and Dark Energy Quantitation; Requirements for New Physics.

## Keywords

Cosmology Theory, Cosmic Inflation, Dark Energy, Cosmic Flatness, CMB Anisotropy, Cosmic Entropy, Emergent Gravity, Black Holes, FSC, Cosmic Dawn, $R_h = ct$ Model

## 1. Introduction and Background

The Boomerang, Wilkinson Microwave Anisotropy Probe (WMAP) and Planck studies of the Cosmic Microwave Background (CMB) have established beyond

all doubt that our universe is spatially flat [1] [2] [3]. All non-flat cosmologies have thus been consigned to the waste basket of history. Andrew Lange, principle investigator for Boomerang, the first study to confirm universal flatness, was decidedly circumspect in his answer to the question on everyone's mind: "Is this final confirmation that cosmic inflation theory is correct?"

One would do well to remember Lange's admonition that one can never *prove* the correctness of cosmic inflation by confirming spatial flatness in the CMB. He emphasized that there might ultimately be other cosmology theories with a non-inflationary mechanism for achieving CMB flatness. While many scientists at the time considered Lange to be unnecessarily conservative with his answer, others have since reiterated this point of view. Physicist Philip Gibbs, for instance, put it this way: "The problem is that no particular model of inflation has been shown to work yet. It is possible that the work has not yet been completed *or that a more recent specific model will be shown to be right*" (emphasis mine) [4].

Given Lange's concerns, physicist Brian Keating and others have set out on a different tack by looking for inflationary B-mode polarization in the CMB. His new book [Keating (2018)] is an excellent glimpse into this new and exciting phase of experimental cosmology. Unfortunately, no primordial gravity waves of inflation have yet been discovered. In 2014, the BICEP2 team jumped the gun and prematurely announced a confirmatory result, only to be proven wrong by a Planck study overlay of B-mode polarizing interstellar dust.

While more sensitive searches for primordial gravity waves of cosmic inflation are being conducted, other cosmologists have taken up the cause of searching for non-inflationary mechanisms to explain cosmic spatial flatness. Some, like myself, have wondered if the universe has always been spatially flat since inception. Certainly, to this point, there is no observational proof otherwise. Even inflationary cosmologists agree that once the universe reaches critical density, it can remain spatially flat for the rest of time. We must remember that inflationary models must achieve spatial flatness to within one part in approximately $10^{60}$ before the first $10^{-32}$ second of cosmic time for inflation to achieve the degree of flatness now observed in the CMB [5]. This is a crucial realization. The only difference between an inflationary universe and a perpetually flat universe from inception is what happens within the first $10^{-32}$ second of cosmic time.

Flat Space Cosmology (FSC) is a remarkably accurate cosmological model which was initially developed as a heuristic mathematical model of the Hawking-Penrose conjecture [6] [7] that a universe smoothly expanding from a singularity can be theoretically treated *within the rules of general relativity* as a time-reversed black hole. Thus, it is perhaps not surprising that FSC makes predictions that closely fit with Planck survey observations. For instance, the Planck Collaboration reported an *observed* global Hubble parameter value of 67.8 +/− 0.9 $km \cdot s^{-1} \cdot Mpc^{-1}$ (68% confidence interval) and FSC *predicts* a current global Hubble parameter value of 66.89 $km \cdot s^{-1} \cdot Mpc^{-1}$, which fits the lower end of the Planck survey range. This FSC calculation is based only upon one free parame-

ter, the Planck study fitting of the CMB temperature peak with a black body at 2.72548 K. This CMB temperature number, plugged into FSC equations first published in 2015 [8] [9] [10] [11] allows for a variety of cosmic parameter calculations fitting very tightly with observations [12].

The five assumptions of FSC, closely adhering to the Hawking-Penrose conjecture, are as follows.

## The Five Assumptions of Flat Space Cosmology

1) The cosmic model is an ever-expanding sphere such that the cosmic horizon always translates at speed of light $c$ with respect to its geometric center at all times *t.* The observer is operationally-defined to be at this geometric center at all times $t$.

2) The cosmic radius $R_t$ and total mass $M_t$ follow the Schwarzschild formula $R_t \cong 2GM_t/c^2$ at all times $t$.

3) The cosmic Hubble parameter is defined by $H_t \cong c/R_t$ at all times $t$.

4) Incorporating our cosmological scaling adaptation of Hawking's black hole temperature formula, at any radius $R_t$, cosmic temperature $T_t$ is inversely proportional to the geometric mean of cosmic total mass $M_t$ and the Planck mass $M_{pl}$. $R_{pl}$ is defined as twice the Planck length (*i.e.,* as the Schwarzschild radius of the Planck mass black hole). With subscript $t$ for any time stage of cosmic evolution and subscript $pl$ for the Planck scale epoch, and, incorporating the Schwarzschild relationship between $M_t$ and $R_t$,

$$\left.\begin{aligned} & k_B T_t \cong \frac{\hbar c^3}{8\pi G\sqrt{M_t M_{pl}}} \cong \frac{\hbar c}{4\pi\sqrt{R_t R_{pl}}} \\ & \begin{cases} M_t \cong \left(\dfrac{\hbar c^3}{8\pi G k_B T_t}\right)^2 \dfrac{1}{M_{pl}} & (\mathrm{A}) \\ R_t \cong \dfrac{1}{R_{pl}}\left(\dfrac{\hbar c}{4\pi k_B}\right)^2\left(\dfrac{1}{T_t}\right)^2 & (\mathrm{B}) \\ R_t T_t^2 \cong \dfrac{1}{R_{pl}}\left(\dfrac{\hbar c}{4\pi k_B}\right)^2 & (\mathrm{C}) \\ t \cong \dfrac{R_t}{c} & (\mathrm{D}) \end{cases} \end{aligned}\right\} \quad (1)$$

5) Total entropy of the cosmic model follows the Bekenstein-Hawking black hole formula [13] [14].

$$S_t \cong \frac{\pi R_t^2}{L_p^2} \quad (2)$$

The first two assumptions are based upon a literal interpretation of the Hawking-Penrose conjecture as it would pertain to a smoothly-expanding Schwarzschild black hole. The third assumption (Hubble parameter) treats maximally redshifted radial photons at the cosmic model horizon as moving with speed of light *c relative* to the geometric center at a distance of horizon radius $R_t$. This is a stipulation of relativity. The fourth assumption is a cosmic

temperature scaling assumption. While it shows similarity to the static Hawking black hole temperature formula, the FSC cosmic model is treated as scaling in Planck mass increments. This allows for dynamic cosmic expansion modeling from the Planck scale epoch. Finally, the fifth assumption utilizes the Bekenstein-Hawking entropy definition, which seems appropriate for a model of the Hawking-Penrose conjecture.

As described in some detail in the seminal FSC papers [Tatum, *et al.* (2015)], the first three assumptions allow for perpetual Friedmann critical density (*i.e.*, perpetual global spatial flatness) of the expanding FSC cosmological model from inception. By dividing the Schwarzschild mass (defined in terms of cosmic radius $R_o$) by the spherical volume, and substituting $c^2/R_o^2$ with $H_o^2$, Friedmann's critical mass density $\rho_0 = \frac{3H_0^2}{8\pi G}$ is achieved for any given moment of observation (hence the subscript "o") in cosmic time. So, *perpetual Friedmann critical density from inception is a fundamental feature of the FSC model.* Furthermore, because a Schwarzschild black hole is clearly allowed within the rules of general relativity, and because Hawking and Penrose have proven the validity of black hole time-reversal for modeling cosmological expansion, *the FSC model, as defined by the rules of black holes, is clearly a general relativity model.* A recent paper [15] has taken the FSC model further by integrating FSC into the Friedmann equations containing a Lambda $\Lambda$ cosmological term. Thus, FSC has been shown to be a scalar dynamic $\Lambda$ dark energy model of the *w*CDM type (wherein equation of state term $w$ is always equal to −1.0). Furthermore, it is well-known that a sufficiently realistic $R_h = ct$ linear model, such as FSC, can fit within the tightest constraints of the Supernova Cosmology Project (SCP) data. The following open source graph from the SCP (**Figure 1**) is offered as proof [16].

One can readily see (by the "Flat" line intersection) that a realistic spatially flat universe model would be an excellent fit with all SCP observations to date.

Currently, there is no certainty about the percentage of the critical density which is attributable to dark matter. Those with knowledge of the observational studies of the ratio of dark matter to visible matter realize the difficulty of determining a precise co-moving value for this ratio at the present time. Galactic and perigalactic distributions of dark matter can be surprisingly variable, as evidenced by the 29 March 2018 report in *Nature* [17] of a galaxy apparently completely lacking in dark matter! Although the 2015 Planck Collaboration consensus is a large-scale approximate ratio of 5.3 parts dark matter to 1 part visible matter, this can only be considered as a rough estimate of the actual *co-moving* ratio, particularly if this ratio varies significantly over cosmic time. A 9.2-to-1 actual ratio in co-moving galaxies remains a possibility, and would change the ratio of total matter mass-energy to dark energy to essentially unity (*i.e.,* 50% matter and 50% dark energy). Thus, the intersection zone of tightest constraints shown in **Figure 1** would then correlate with 0.5 Omega_ matter and 0.5 Omega_Lambda. This is one of several important testable predictions discriminating

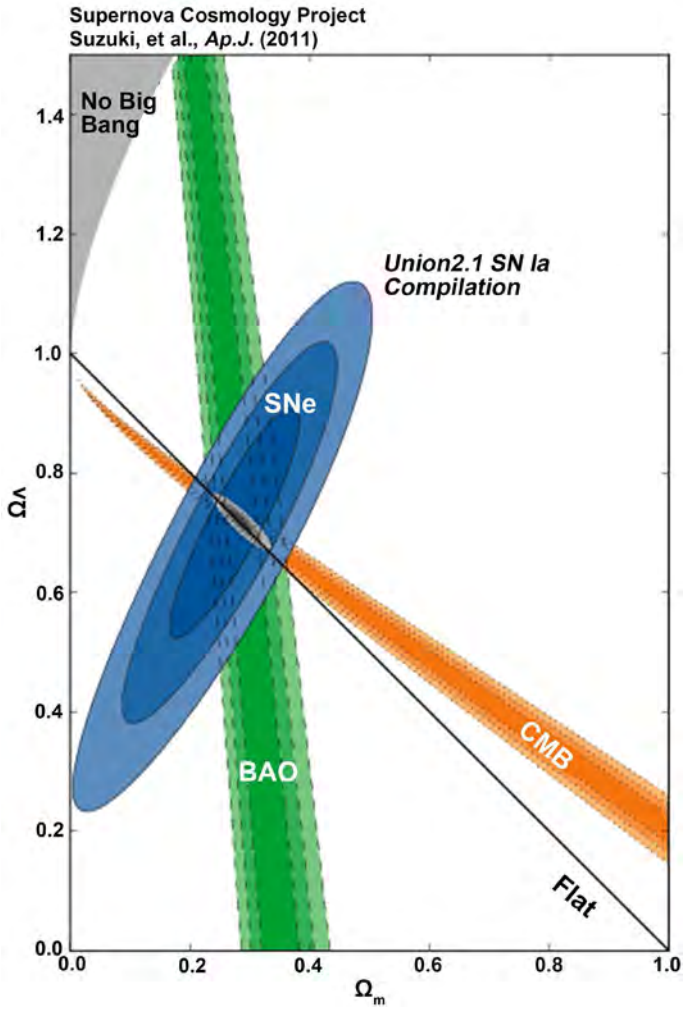


Figure 1. SCP supernovae, BAO and CMB data.

the FSC model from the standard cosmology model. Precise measurements of approximately co-moving galaxies are in order, for comparison with the Planck Collaboration result.

Furthermore, the question of dark energy dominance over total matter energy density remains in doubt. Several recent papers [18] [19] [20] [21] [22] have clearly shown that cosmic acceleration, however small, is not yet *proven*. These are not, of course, arguments against the existence of dark energy. They are only arguments placing some doubt on dark energy *dominance*, and thus cosmic acceleration, as opposed to cosmic coasting (as seen in all competitive $R_h = ct$ models, such as FSC).

The above brief introduction to FSC is for the purpose of showing just one non-inflationary model which fits tightly with astronomical observations to date, including the flatness findings within the CMB. Thus, the words of Lange, Gibbs and Steinhardt [23], who have had serious reservations about the certainty of cosmic inflation, are well worth remembering. Cosmic inflation is definitely not a certainty, particularly in light of the accumulating failures to confirm primor-

dial inflationary gravity waves.

It is the purpose of this paper to present, in Section 2, the predictions and features of FSC which prove its superiority to standard inflationary cosmology. In fact, these predictions and features were embedded in FSC from its inception in 2015.

## 2. Predictions and Features of the FSC Model

### 2.1. Predictions Pertaining to Primordial Gravity Waves

FSC, by the arguments made above with respect to perpetual Friedmann critical density, can readily explain the flatness angular power spectrum of the CMB. Furthermore, this steadily expanding, finite but unbounded, model would not be expected to produce inflationary B-mode primordial gravity waves. Thus, FSC predicts that inflationary B-mode primordial gravity waves will never be confirmed. Such unequivocal confirmation of inflationary waves would falsify FSC. The continued failure to detect such waves (if the sensitivity of detection methods is sufficiently high) should be considered to strongly favor FSC over standard inflationary cosmology.

### 2.2. Cosmic Dawn Early Surprises

As noted in several recent papers [24] [25] [26] standard cosmology cannot easily explain surprisingly early star, galaxy and active galactic nuclei (*i.e.,* quasars and blazars) formation. On the other hand, as detailed in the recent FSC paper entitled, "Temperature Scaling in Flat Space Cosmology in Comparison to Standard Cosmology" [12], temperature differences between the two models are such that cosmic dawn in FSC may have developed as early as 20 million years after the Planck epoch versus approximately 110 million years in standard cosmology. The following graph (**Figure 2**) from the "Temperature Scaling" paper is presented for comparison, with features of the standard model as described in Bowman's recent paper [24].

Hashimoto's paper [25] recently reported the difficulty of explaining their finding of an early galaxy at a redshift $z$ value of 9.11 which suggested galaxy formation no later than about 250 million years after the Big Bang. And yet, a redshift $z$ value of 9.11 is correlated with 174 million years in FSC versus 550 million years in standard cosmology (see how these cosmic times differ in **Figure 2** above). Cosmic dawn in FSC would likely be at 20 - 50 million years after the Planck epoch (the so-called "Big Bang" in standard cosmology) as opposed to the standard cosmology cosmic dawn at 110 - 250 million years, as shown in **Figure 2**.

Thus, FSC is clearly superior to standard cosmology in terms of cosmic dawn early surprises.

### 2.3. Predicting the Magnitude of CMB Temperature Anisotropy

Standard cosmology has difficulty in providing a reasonable explanation for the *magnitude* of the observed CMB temperature anisotropy. Their current

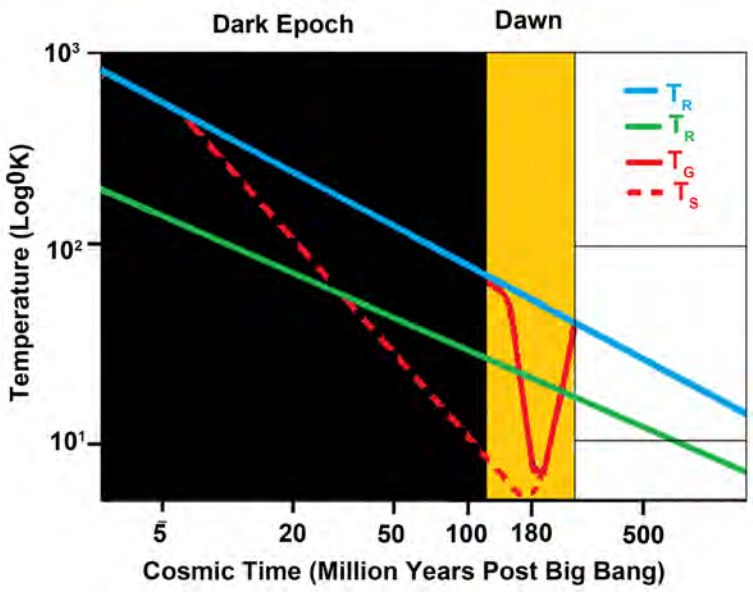


**Figure 2.** Cosmic temperature vs time in standard cosmology (blue) and FSC (green).

explanation appears to be that the CMB pattern represents a magnified Big Bang "quantum fluctuation" event spayed out across the sky. Yet, modeling the physics of such a quantum fluctuation event, including predicting the actual magnitude of the CMB temperature anisotropy, eludes standard cosmology. This would require a deep understanding of quantum gravity, which is lacking at the present time, despite the admirable efforts of string theorists.

The angular power spectrum of the CMB clearly fits with a spatially flat universe. The Boomerang Collaboration reported CMB anisotropy observations closely fitting "the theoretical predictions for a spatially flat cosmological model with an exactly scale invariant primordial power spectrum for the adiabatic growing mode" [27]. Furthermore, the COBE DMR experiment [28] measured a CMB RMS temperature variation of 18 micro Kelvins. This translates to a $dT/T$ anisotropy value of (0.000018)/2.725 equal to $0.66 \times 10^{-5}$. This measurement fits within the range of FSC temperature anisotropy predictions for the beginning and ending of the recombination/decoupling epoch [29]. This result clearly favors FSC.

## 2.4. Predicting the Value of Equation of State Term *w*

For reasons to be described in "Flat Space Cosmology as a Model of Light Speed Expansion—Implications for the Vacuum Energy Density", the FSC model requires that the equation of state $w$ term have a value of exactly −1.0. This fits with the quantum field theory stipulation that the vacuum pressure $p$ corresponding to the zero-state vacuum energy must always be equal in magnitude to the vacuum energy density $\rho$ (*i.e.*, $p = \rho$). For reasons given in the FSC paper, a dark energy dominant universe (as currently believed in standard cosmology) would not meet this quantum field theory stipulation and would have a

*w* value other than exactly −1.0. These are falsifiable predictions for both models. Standard model cosmologists believe our current universe to contain an extremely small *net* negative energy. In other words, they believe in *slight* cosmic acceleration (as opposed to constant velocity light speed expansion), despite current observations of global spatial flatness. However, *if our universe began from a zero energy state, as is often assumed, and the universe now has a non-zero energy density, however small, this would appear to violate conservation of energy*! Thus, there is tension in the standard cosmology model of dark energy dominance, because the Planck Collaboration has reported $w = -1.006$ +/− 0.045. A final consensus value of exactly −1.0, which seems highly likely at the present time, would be in support of FSC and falsify the current belief in dark energy dominance within standard cosmology.

### 2.5. Predicting the Hubble Parameter Value

In standard cosmology, the Hubble parameter value can only be determined by observation. That is to say that there is no theoretical ability within standard cosmology to derive a precise Hubble parameter value. The 2016 Planck Collaboration publication [30] reports the consensus *global* (*i.e.*, CMB) Hubble parameter temperature and lensing value to be 67.8 +/− 0.9 $km \cdot s^{-1} \cdot Mpc^{-1}$ (at the 68% confidence interval). *In FSC, the Hubble parameter is not a free parameter when a precise value of the CMB temperature is known.* The $c/R_o$ FSC value for the Hubble parameter can be determined by simply plugging the measured CMB temperature value $T_o$ of 2.72548 K into relation 1B to get the current FSC radius $R_o$. Dividing speed of light $c$ by $R_o$, according to FSC assumption #3, gives the metric value ($s^{-1}$) of the Hubble parameter $H_o$, which converts to 66.89 $km \cdot s^{-1} \cdot Mpc^{-1}$. Thus, the observed CMB temperature and Hubble parameter values are tightly correlated by FSC theory alone!

Of note, another recently reported measurement of the Hubble parameter [31] is not truly global, but local in nature. Reiss, *et al.*, by measurements based on Type Ia supernovae observations, did not observe the universe on its largest scale, as was the case for the Planck survey CMB observations. Furthermore, observational expectations and formulae for luminosity distance and angular diameter distance (with respect to redshift $z$) differ between the standard cosmology and $R_h = ct$ linear models. This can result in the *illusion* of supernovae acceleration, if not correctly accounted for within the correct cosmological model (see **Figure 3** and **Figure 4** below and the discussion related to these figures). The obvious tension between the Planck CMB observations and Reiss' supernovae observations, with respect to Hubble parameter measurements, may well be the result of such phenomena with respect to distant supernovae observations. In any event, Reiss' outlier Hubble parameter value of approximately 73.24 $km \cdot s^{-1} \cdot Mpc^{-1}$ is not at all relevant to the global FSC model. The fact that FSC tightly correlates its *theoretical* Hubble parameter value (for a CMB temperature of 2.72548 K) with the *observational* Planck survey value is strongly in favor of FSC.

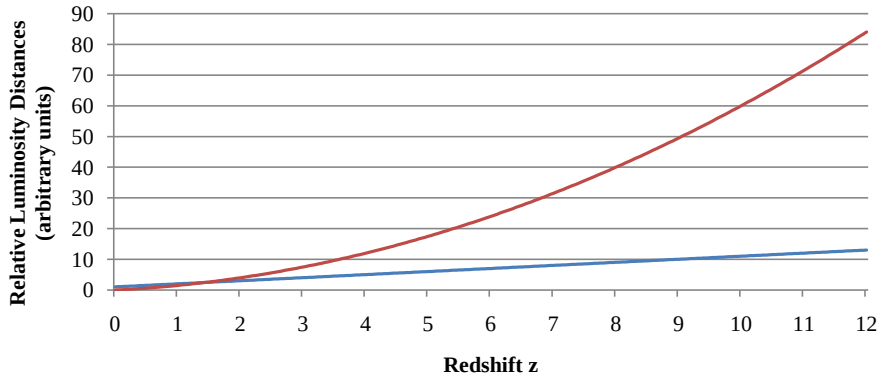


**Figure 3.** Relative luminosity distances vs. redshift *z* for standard (blue) and Milne (red) models.

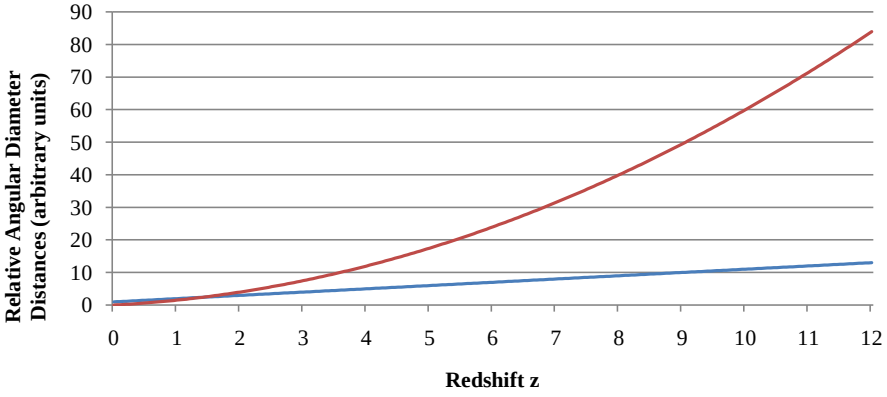


**Figure 4.** Relative angular diameter distances vs. redshift *z* for standard (blue) and Milne (red) models.

## 2.6. Quantifiable Entropy and the Entropic Arrow of Time

One of the problems within the standard inflationary model is in quantifying cosmic entropy. Entropy is typically defined in terms of the total number of possible microstates and the probability of a given set of conditions with respect to that number of microstates. These values are impossible to quantify in an infinite-sized inflationary universe or multiverse. FSC, on the other hand, is a *finite* model with a spherical horizon surface area. Furthermore, since the Bekenstein-Hawking definition of black hole entropy would appear to apply to the FSC model, very precise values for cosmic entropy can be calculated for any time, temperature or radius of the FSC model. Thus, the "entropic arrow of time" is clearly defined and quantified in the FSC model [Tatum, *et al.* (2018)]. The quantifiable entropy of the FSC model allows for model correlations with cosmic entropy theories, such as those of Roger Penrose [32] and Erik Verlinde [33]. Thus, the entropy rules of FSC allow for falsifiability, whereas standard inflationary cosmology is not able to clearly define or quantify entropy or to establish falsifiability in terms of entropy. This feature favors the FSC model, particularly with respect to Verlinde's "emergent gravity" theory described in the next section.

### 2.7. Clues to the Nature of Gravity, Dark Energy and Dark Matter

The reader is referred to the recent FSC paper [15] with this title for an in-depth discussion of how cosmic entropy in the FSC model provides for tantalizing clues with respect to the fundamental nature of gravity. In short, the FSC model is the cosmological model correlate to Verlinde's "emergent gravity" theory [33] [34]. Verlinde's landmark paper from 2011 provides strong theoretical support for gravity being an emergent property of cosmic entropy. The corresponding FSC paper makes a strong case for the correctness of Verlinde's theory. The obvious implications for cosmology are huge. As discussed in the FSC paper, if gravity is an emergent property of cosmic entropy, then dark energy and dark matter are also likely to be emergent properties of cosmic entropy as well. The obvious implication is that galactic and perigalactic features attributed to dark matter (such as gravitational lensing and plate-like galactic rotation) could simply be a large-scale effect of the entropy of the visible galactic matter. Thus, the majority of what is currently being called dark matter may not actually be particulate in nature. If this turns out to be the correct interpretation, then the FSC model predicts that gravity, dark energy and dark matter may be no more definable at the quantum level than consciousness in two connecting neurons.

Following submission and acceptance of the "Clues to the Nature of Gravity, Dark Energy and Dark Matter" paper [15], this author discovered the Brouwer, *et al.* observational reference [35] in support of Verlinde's "emergent gravity" theory as it pertains to dark matter. The discovery of quantum gravity, other than quantum gravity somehow connected to entropy at the quantum level, would falsify Verlinde's "emergent gravity" theory. At present, standard inflationary cosmology, by virtue of its inability to precisely define total cosmic entropy, has no capacity to incorporate Verlinde's theory. This result clearly favors FSC, particularly in light of the above-mentioned observational findings typically ascribed to galactic and perigalactic dark matter.

### 2.8. The Cosmological Constant Problem

The "cosmological constant problem" is a longstanding problem in theoretical physics. It underscores standard cosmology's longstanding problem with uniting general relativity with quantum field theory (QFT). Excellent expositions on this subject have been provided by Weinberg [36] and Carroll [37]. Suffice it to say, QFT predicts a cosmological constant value which differs from observational measurements of the vacuum energy density by a magnitude of approximately $10^{121}$! This discrepancy is so large that it is often referred to as the most embarrassing problem in all of theoretical physics.

In standard cosmology, it has been assumed that the energy density of the cosmic vacuum must be constant over the great span of cosmic time. However, general relativity does indeed allow for the vacuum energy density to be a dynamic scalar over time. Cosmological models incorporating scaling vacuum energy density are called "quintessence" models. FSC is one such model. In FSC,

the vacuum energy density scales downward by 121.26 logs of 10 over the cosmic time interval since the Planck epoch. Perhaps of even greater interest is that the Bekenstein-Hawking cosmic entropy value scales upward in direct proportion to the expanding surface area of the cosmic horizon. If one were to count the current number of Planck radius microstates within the FSC horizon, the model indicates this entropy number to be $10^{121.26}$. Thus, once again, by virtue of the intimate relationship between vacuum energy (*i.e.*, dark energy) and total cosmic entropy, FSC offers a clear-cut explanation for the magnitude difference between the Planck epoch vacuum energy density of the QFT theorists and today's observed vacuum energy density of approximately $10^{-9}$ J·m$^{-3}$. Since the FSC model easily predicts these values, and standard inflationary cosmology has no basis for deriving them, the FSC model is clearly superior with respect to solving the cosmological constant problem.

### 2.9. Quantum Cosmology

The FSC model, by virtue of its appropriately scaling cosmic temperature equation (the first equation listed under FSC assumption #4), can be considered the first successful quantum cosmology model [Tatum, *et al.* (2015)]. By incorporating the values of $T_0$, $\hbar$, $G$, $k_B$, $L_P$, and $\pi$ to as many decimal places as known, the FSC parameters can be shown to closely match astronomical observations, as detailed in the FSC paper entitled, "Temperature Scaling in Flat Space Cosmology in Comparison to Standard Cosmology" [12]. For convenience, the most important FSC quantum cosmology equations are repeated below:

$$R \cong \frac{\hbar^{3/2}c^{7/2}}{32\pi^2 k_B^2 T^2 G^{1/2}} \qquad R_0 \cong \frac{\hbar^{3/2}c^{7/2}}{32\pi^2 k_B^2 T_0^2 G^{1/2}} \tag{3}$$

$$H \cong \frac{32\pi^2 k_B^2 T^2 G^{1/2}}{\hbar^{3/2}c^{5/2}} \qquad H_0 \cong \frac{32\pi^2 k_B^2 T_0^2 G^{1/2}}{\hbar^{3/2}c^{5/2}} \tag{4}$$

$$t \cong \frac{\hbar^{3/2}c^{5/2}}{32\pi^2 k_B^2 T^2 G^{1/2}} \qquad t_0 \cong \frac{\hbar^{3/2}c^{5/2}}{32\pi^2 k_B^2 T_0^2 G^{1/2}} \tag{5}$$

$$M \cong \frac{\hbar^{3/2}c^{11/2}}{64\pi^2 k_B^2 T^2 G^{3/2}} \qquad M_0 \cong \frac{\hbar^{3/2}c^{11/2}}{64\pi^2 k_B^2 T_0^2 G^{3/2}} \tag{6}$$

$$Mc^2 \cong \frac{\hbar^{3/2}c^{15/2}}{64\pi^2 k_B^2 T^2 G^{3/2}} \qquad M_0c^2 \cong \frac{\hbar^{3/2}c^{15/2}}{64\pi^2 k_B^2 T_0^2 G^{3/2}} \tag{7}$$

Current parameters are calculated in the right-hand column. As previously mentioned, the only free parameter in any of these equations is the cosmic temperature. The currently-observed cosmic temperature value: $T_0$ = 2.72548 K. It is truly remarkable that, using only current best measurements of the CMB temperature, the $H_o$ value in Equation (4) can be calculated and fitted to the lower end of the Planck Collaboration observational measurement!

No quantum model exists for standard inflationary cosmology. This obviously favors the FSC model.

### 2.10. Dark Matter and Dark Energy Quantitation

As detailed in the Planck Collaboration report, the ratio of dark matter to visible (baryonic) matter is observed to be approximately 5.3 parts dark matter to 1 part visible matter. However, so little is currently known about precisely detecting and quantifying dark matter that *this ratio is subject to higher revision in the likely event that more dark matter is discovered in the future. For this reason, the Planck Collaboration ratio must be considered as a constraint only on the low end.* Moreover, there are differences between dark matter-to-visible matter ratios observed within galaxies quite near to us (essentially co-movers) and the aforementioned dark matter-to-visible matter ratio determined from Planck survey CMB observations. If the co-moving ratio is ultimately found to be slightly higher by less than a factor of two, to 9.2 parts dark matter to 1 part visible matter (for co-moving galaxies), one can then conclude that total matter energy density *at present* is equal in absolute magnitude to dark energy density. This equality of opposite sign energy densities is what one would expect for a flat universe. Otherwise, if one energy density dominated the other, there should be detectable global spatial curvature corresponding to the dominating energy density. One could, in fact, make a very strong case that the unequivocal spatial flatness of the CMB proves the equality of total matter and dark energy densities at the time of the recombination/decoupling epoch. This should nullify any Planck Collaboration conclusions (such as dark energy dominance) which are obviously contrary to their own observations of flatness.

Despite the fact that FSC and standard cosmology differ *slightly* with respect to the exact percentages of total matter vs. dark energy, there is one thing about this energy density partition on which everyone agrees: it is truly remarkable that total matter energy density and dark energy density are of the same order of magnitude at the present time. As physicist I. I. Rabi once famously remarked, "Who ordered that?!" Standard cosmology simply accepts this "coincidence problem" with no further explanation or rationale. However, FSC stipulates perpetual equality of absolute magnitude of these two energy densities as a *requirement for a spatially flat universe. More importantly, this is a stipulation of the global spatial curvature rules of general relativity*, as discussed in some detail in recent FSC papers [Tatum, *et al.* (2018)]. One can consider this expectation of energy density equality to be a falsifiable FSC prediction with respect to future measurements of total matter energy density vs dark energy density.

With respect to standard cosmology's current belief in cosmic acceleration due to dark energy, the reader is referred to references [18] thru [22] mentioned earlier in this paper. Cosmic acceleration is clearly not proven at the present time, despite the indisputable presence of dark energy. The reader is also referred to this author's recent publication in Journal of Modern Physics entitled, "How a Realistic Linear $R_h = ct$ Model of Cosmology Could Present the Illusion of Late Cosmic Acceleration" [38]. There are relative differences in luminosity distance and angular diameter distance formulae in standard cosmology and $R_h$

= *ct* modified Milne-type models (like FSC). Two comparative graphs from this paper are repeated in Figure 3 and Figure 4.

The significance of the relative luminosity distance and relative angular diameter distance comparisons between these two competing models is paramount. An observer of distant Type Ia supernovae expects particular luminosity distances and angular diameter distances to correspond with particular redshifts. If instead he or she observes greater-than-expected luminosity distances (*i.e.,* unexpected "dimming" of the supernovae) or greater-than-expected angular diameter distances, this can easily be misinterpreted by a standard model proponent as indicative of cosmic acceleration. However, e*ntirely predictable supernova luminosity distances within a realistic Milne-type universe containing matter*, *as opposed to a standard model universe, could be one possible explanation for the Type Ia supernovae observations since* 1998. *Obviously, cosmic acceleration would not then be required to explain these observations.* This possibility, combined with the standard model tension problem presented above (*i.e.*, spatial flatness and dark energy dominance cannot *both* be true at the same time), and the FSC *stipulation* for what the standard model calls the "coincidence problem," strongly favors FSC with respect to its predictions concerning dark matter and dark energy quantitation.

### 2.11. Requirements for New Physics

Inflationary theories require that there be a mysterious *pre-gravity* energy field (called the "inflaton"), which rolls downhill after the moment of the Big Bang and nearly instantaneously inflates the nascent universe to such a size that deviations from global spatial flatness cannot be observed even 14 billion years after the Planck epoch. Standard cosmology maintains that a quantum fluctuation event within a zero energy pre-Big Bang state kicked off the universal expansion. It also maintains that gravity was the first of four fundamental forces to "freeze out" following an exceedingly brief exponential inflationary phase. Standard model cosmologists believe our current universe to contain an extremely small *net* negative energy. In other words, they believe in cosmic acceleration (as opposed to constant velocity light speed expansion), despite observations of extreme flatness. However, *if our universe began from a zero energy state, and now has a net negative energy density, however small, this would appear to violate conservation of energy!* Furthermore, one must ask what exactly is the nature of the force represented by the inflaton field, specifically if gravity did not already exist at the inception of the universe. Cosmic inflation energy appears to be suspiciously like early cosmic dark energy, which we know to be negative gravitational energy in nature. The Big Bang theory is derived from general relativity, which is *entirely* a gravity theory. To require that a gravity theory incorporates a pre-gravity phase within its cosmology, however brief in duration, sounds very much like nonsense. Moreover, cosmic inflation is an ad hoc theory "… contrived with the goal of arranging for the density perturbations to come out right"

[Guth (1997), page 238]. Cosmic inflation, in its many different ad hoc forms, appears to be a deeply flawed theory, as nicely elaborated by one of its founders [Steinhardt (2011)].

Needless to say, a great deal of new physics appears to be required by inflationary cosmology. Not only would a new energy field with ad hoc features be required before gravity "freezes out," but, somewhere along the way, conservation of energy would need to be violated. This must be true if the universe started from zero energy (Guth's "free lunch" idea) and ended with endlessly increasing dark energy dominance. *It must be remembered that inflationary theories preceded the discovery of dark energy*.

According to the FSC model, dark energy density of the early universe was at a remarkably high negative value in balance with the remarkably high positive energy density of matter. Thus, the "repulsive gravity of the inflaton" idea can be seamlessly replaced by FSC's incredibly high dark energy density in the early universe. The reader is reminded that, even in the seminal FSC paper from 2015, the model expands 25 logs of 10 within $10^{-17}$ second. FSC's smoothly progressing light speed expansion does not have the nearly-instantaneous, transient and explosive nature of cosmic inflation. Thus, a future unequivocal discovery of explosive primordial gravity waves is not predicted by the FSC model. Along the lines previously mentioned by Stephen Hawking, cosmic expansion may, in fact, be unbounded in time, with no Big Bang beginning event whatsoever. Whatever may be the case, FSC maintains perpetual spatial flatness, as defined by Friedmann's critical density, and does not require a poorly-understood explosive mechanism to achieve critical density.

Accordingly, FSC does not appear to require any new physics and does not appear to violate conservation of energy. The global energy-density tally is perpetually maintained at a *net* value of zero, as required for a spatially flat expanding universe acting as an isolated system not influenced by external forces. For these reasons, FSC appears to be superior to standard cosmology with respect to requirements for new physics.

## 3. Summary and Conclusions

Following recent precise CMB observations of global spatial flatness, only two types of viable cosmological models remain: inflationary models which almost instantaneously attain cosmic flatness following the Big Bang; and non-inflationary models which are spatially flat from inception. FSC is the latter type of cosmological model by virtue of assumptions corresponding to the Hawking-Penrose conjecture that a universe expanding from a singularity could be modeled like a time-reversed black hole. Since current inflationary models have been criticized for their lack of falsifiability, the numerous falsifiable predictions and key features of the FSC model are herein contrasted with standard inflationary cosmology. For the reasons given, the FSC model is shown to be superior to standard cosmology in the following eleven categories: Predictions Pertaining to

Primordial Gravity Waves; Cosmic Dawn Early Surprises; Predicting the Magnitude of CMB Temperature Anisotropy; Predicting the Value of Equation of State Term $w$; Predicting the Hubble Parameter Value; Quantifiable Entropy and the Entropic Arrow of Time; Clues to the Nature of Gravity, Dark Energy and Dark Matter; The Cosmological Constant Problem; Quantum Cosmology; Dark Matter and Dark Energy Quantitation; Requirements for New Physics.

## Dedications and Acknowledgements

This paper is dedicated to Stephen Hawking and Roger Penrose for their groundbreaking work on black holes and their possible application to cosmology. Dr. Tatum also thanks Rudolph Schild of the Harvard Center for Astrophysics for his support and encouragement.

## Conflicts of Interest

The author declares no conflicts of interest regarding the publication of this paper.

## References

[1] De Bernardis, P., *et al.* (2000) A Flat Universe from High-Resolution Maps of the Cosmic Microwave Background Radiation. arXiv:astro-ph/0004404v1.

[2] Bennett, C.L. (2013) Nine-Year Wilkinson Microwave Anisotropy Probe (WMAP) Observations: Final Maps and Results. arXiv:1212.5225v3 [astro-ph.CO].

[3] Planck Collaboration. (2014) *Astronomy & Astrophysics*, **A23**, 1-48.

[4] Keating, B. (2018) Losing the Nobel Prize. W. W. Norton & Company, New York.

[5] Guth, A.H. (1997) The Inflationary Universe. Basic Books, New York.

[6] Penrose, R. (1965) *Physical Review Letters*, **14**, 57. https://doi.org/10.1103/PhysRevLett.14.57

[7] Hawking, S. and Penrose, R. (1970) *Proceedings of the Royal Society of London A*, **314**, 529-548. https://doi.org/10.1098/rspa.1970.0021

[8] Tatum, E.T., Seshavatharam, U.V.S. and Lakshminarayana, S. (2015) *International Journal of Astronomy and Astrophysics*, **5**, 116-124. https://doi.org/10.4236/ijaa.2015.52015

[9] Tatum, E.T., Seshavatharam, U.V.S. and Lakshminarayana, S. (2015) *Journal of Applied Physical Science International*, **4**, 18-26.

[10] Tatum, E.T., Seshavatharam, U.V.S. and Lakshminarayana, S. (2015) *Frontiers of Astronomy, Astrophysics and Cosmology*, **1**, 98-104.

[11] Tatum, E.T., Seshavatharam, U.V.S. and Lakshminarayana, S. (2015) *International Journal of Astronomy and Astrophysics*, **5**, 133-140. https://doi.org/10.4236/ijaa.2015.53017

[12] Tatum, E.T. and Seshavatharam, U.V.S. (2018) *Journal of Modern Physics*, **9**, 1404-1414. https://doi.org/10.4236/jmp.2018.97085

[13] Bekenstein, J.D. (1974) *Physical Review D*, **9**, 3292-3300. https://doi.org/10.1103/PhysRevD.9.3292

[14] Hawking, S. (1976) *Physical Review D*, **13**, 191-197. https://doi.org/10.1103/PhysRevD.13.191

[15] Tatum, E.T. and Seshavatharam, U.V.S. (2018) *Journal of Modern Physics*, **9**, 1469-1483. https://doi.org/10.4236/jmp.2018.98091

[16] Suzuki, N., *et al.* (2011) The Hubble Space Telescope Cluster Supernovae Survey: V. Improving the Dark Energy Constraints Above Z > 1 and Building an Early-Type-Hosted Supernova Sample. arXiv.org/abs/1105.3470.

[17] van Dokkum, P., *et al.* (2018) *Nature*, **555**, 629-632. https://doi.org/10.1038/nature25767

[18] Tutusaus, I., *et al.* (2017) *Astronomy & Astrophysics*, **602**, A73. arXiv:1706.05036v1

[19] Dam, L.H., *et al.* (2017) *Monthly Notices of the Royal Astronomical Society*, **472**, 835-851. arXiv:1706.07236v2 https://doi.org/10.1093/mnras/stx1858

[20] Nielsen, J.T., *et al.* (2015) *Scientific Reports*, **6**, Article No. 35596. arXiv:1506.01354v1.

[21] Wei, J.-J., *et al.* (2015) *Astronomical Journal*, **149**, 102-112.

[22] Melia, F. (2012) *Astronomical Journal*, **144**, 110. arXiv:1206.6289. https://doi.org/10.1088/0004-6256/144/4/110

[23] Steinhardt, P.J. (2011) *Scientific American*, **304**, 18-25. https://doi.org/10.1038/scientificamerican0411-36

[24] Bowman, J.D. (2018) *Nature*, **555**, 67-70. https://doi.org/10.1038/nature25792

[25] Hashimoto, T. (2018) The Onset of Star Formation 250 Million Years after the Big Bang. arXiv.1805.05966v1 [astro-ph.GA] https://doi.org/10.1038/s41586-018-0117-z

[26] Natarajan, P. (2018) *Scientific American*, **318**, 24-29.

[27] Bucher, M. (2015) Physics of the Cosmic Microwave Background Anisotropy. arXiv:1501.04288v1 [astro-ph.CO]. https://doi.org/10.1142/S0218271815300049

[28] Wright, E.L., *et al.* (1996) *Astrophysical Journal*, **464**, L21-L24. https://doi.org/10.1086/310073

[29] Tatum, E.T. (2018) *Journal of Modern Physics*, **9**, 1484-1490. https://doi.org/10.4236/jmp.2018.98092

[30] Planck Collaboration XIII (2016) *Astronomy & Astrophysics*, **594**, A13. http://arxiv.org/abs/1502.01589

[31] Reiss, A.G., *et al.* (2016) *Astrophysical Journal*, **826**, 56-87. arXiv:1604.01424 [astro-ph.CO].

[32] Penrose, R. (2016) Fashion Faith and Fantasy in the New Physics of the Universe. Princeton University Press, Princeton. https://doi.org/10.1515/9781400880287

[33] Verlinde, E. (2011) *Journal of High Energy Physics*, **4**, 29-55. arXiv:1001.0785v1 [hep-th]. https://doi.org/10.1007/JHEP04(2011)029

[34] Verlinde, E. (2016) Emergent Gravity and the Dark Universe. arXiv:1611.02269v2 [hep-th].

[35] Brouwer, M.M., *et al.* (2016) *Monthly Notices of the Royal Astronomical Society*, 1-14. arXiv:1612.03034v2 [astro-ph.CO].

[36] Weinberg, S. (1989) *Reviews of Modern Physics*, **61**, 1-23. https://doi.org/10.1103/RevModPhys.61.1

[37] Carroll, S. (2001) *Living Reviews in Relativity*, **4**, 5-56. https://doi.org/10.12942/lrr-2001-1

[38] Tatum, E.T. and Seshavatharam, U.V.S. (2018) *Journal of Modern Physics*, **9**, 1397-1403. https://doi.org/10.4236/jmp.2018.97084

Journal of Modern Physics, 2018, 9, 1883-1905
http://www.scirp.org/journal/jmp
ISSN Online: 2153-120X
ISSN Print: 2153-1196

# Dark Matter: An Odd Need Created by Unsuitable Theories of Gravitation. The Higgs Quantum Space Dynamics Gravity Doesn't Need It

**Jacob Schaf**

Instituto de Física, Universidade Federal do Rio Grande do Sul (UFRGS), Porto Alegre, Brazil
Email: schaf@if.ufrgs.br

**How to cite this paper:** Schaf, J. (2018) Dark Matter: An Odd Need Created by Unsuitable Theories of Gravitation. The Higgs Quantum Space Dynamics Gravity Doesn't Need It. *Journal of Modern Physics*, **9**, 1883-1905.
https://doi.org/10.4236/jmp.2018.910119

**Received:** July 11, 2018
**Accepted:** August 31, 2018
**Published:** September 3, 2018





## Abstract

The Higgs theory introduces the idea that space is filled up throughout by a quantum fluid medium, giving mass and mechanical properties to the elementary particles by the Higgs mechanism. This Higgs Quantum Space (HQS) thus governs the inertial motion of matter-energy and is locally their ultimate reference for rest and for motions. On the other hand, motion with respect to the local HQS and not relative motion is the origin of all the effects of velocity on matter, on light and on clocks. In previous works, the author has shown that the HQS, moving round the astronomical bodies according to a Keplerian velocity field $(GM/r)^{1/2}\boldsymbol{e}_{\phi}$, consistent with the local astronomical motions, accurately creates the observed gravitational dynamics and gives rise to all the observed effects of the gravitational fields on light and on clocks. The absence of the solar gravitational slowing on the GPS clocks and the absence of light anisotropy with respect to earth are both the signature of this HQS dynamics. In their orbital motion round the galactic center, the stars carry with them their Keplerian velocity fields. The present work shows that, due to the effects of this orbital velocity on the symmetry of the polarized star Keplerian velocity fields, the collective velocity field, created by them, does not fall with distance as the Keplerian profile ($r^{-1/2}$). Depending on the distribution of the matter density, the velocity of the HQS and the stars can even increase with *r*. The non-Keplerian rotation of the galaxies thus is an intrinsic feature of the HQS dynamics gravitational mechanism, created *without the need of dark matter*.

## Keywords

Dark Matter, Galactic Rotation, Gravitational Fields, Higgs Theory,

General Relativity

## 1. Introduction

The structure of the galaxies is rather different from that of our solar system. While more than 99% of the mass of solar system is concentrated in the central (static) sun, more than 99% of the galactic mass is orbiting, within the thin galactic disk in the form of stars, around the galactic center, under the collective gravitational field created by these orbiting stars. In fact, the solar system too is disk shaped, however, the disk, formed by the planets, satellites and the asteroids all together contains less than 1% of the mass of the solar system. It however is sufficient to give rise to the Pioneer 10 and 11 anomalies as will be explained in Section 4.

Most galaxies are elliptic. Our Milky Way Galaxy is a large, old and barred spiral galaxy, with a central bulge extending out to about $10^4$ light years. The very center of this bulge wobbles a super-massive black hole with millions of solar masses. Beyond the bulge, a swarm of hundreds of billions of stars are all orbiting within a thin disk along direct circular equatorial orbits around the galactic center. The disk extends out to about 5/times $10^4$ light years, beyond which only several dwarf galaxies and globular star clusters are orbiting. The stars in the galactic disk are relatively isolated and well separated from each other by distances of several light years, so that the space within a galaxy is almost empty and the local star fields as well as the motion of the planets are only very weakly perturbed.

## 2. The Non-Keplerian Rotation of the Galaxies Defies the Current Theories of Gravitation

Many published works [1] [2] [3] display star orbital velocity profiles, as a function of the distance from the galactic center, for a number of galaxies. They all show that the orbital velocity of the stars in the galactic disk does not fall with distance from the galactic center as stipulated by the current theories of gravitation. In some galaxies, the orbital velocities even increases with the distance from the galactic center. **Figure 1** displays the observed orbital velocity profile of the stars in the Milky-Way galaxy, together with a typical Keplerian rotation curve. The observed orbital velocity of the stars is much too fast to the gravitational pull and or the spacetime curvature, produced by the content and distribution of visible matter, to hold the Milky-Way together.

It is strange that the systematic discrepancy between the observed galactic rotation profiles and the theoretical predictions, instead of having raised suspicions about the current theories of space and gravitation, have lead to the odd idea that a huge amount of invisible dark matter, 5 times more than the total visible matter in a galaxy, must be responsible for this observed non-Keplerian

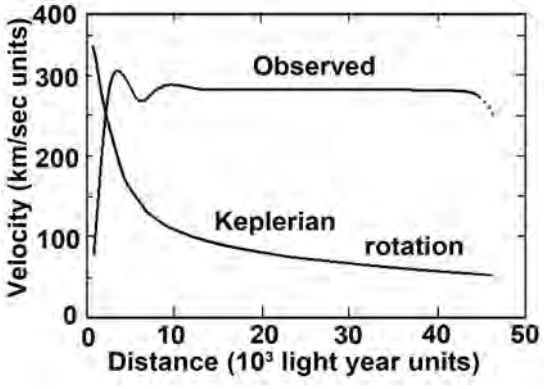


**Figure 1.** The observed orbital velocity profile of the Milky Way galaxy as a function of the distance from the galactic center, together with the typical Keplerian rotation curve, from Ref. [3].

rotation. The idea of the invisible dark matter is much too exotic. To present date nobody has idea what the nature of this dark matter could be. Some people think that it is formed by non-hadronic chargeless particles (WIMPS) that do not scatter, absorb or emit electromagnetic radiation. It is assumed that dark matter is constituted by particles with large masses and to interact with ordinary matter only by gravity. However, if dark matter interacts by gravity, why then is it not concentrated and found within stars and within galaxies? Some people even compute the distribution of dark matter in the form of halos round the galaxies that supposedly can cause the non-Keplerian galactic rotation. In Summary, the observed non-Keplerian rotation of the galaxies is actually among the most serious impasses in the current theories of space and gravitation [4] [5].

Another way to address the problem of the peculiar galactic rotation rate is by the gravitational potential. Several authors [6] have computed the gravitational potential $\left[U\left(r\right)\right]$ as a function of the radial distance from the galactic nucleus for our Milky Way galaxy as well as for other galaxies, with base in the current theories of space and gravitation, taking into account the observed matter distribution in these galaxies. Systematically all these computed gravitational potentials are inconsistent with the observed rotation rate of the galactic disk.

The profile of the gravitational potential can also be obtained by an empirical method, using the circular orbital velocity profile of the stars, like that depicted in **Figure 1**. According to the Virial theorem, the gravitational potential, of a spherically symmetric source, has a very simple relation with the circular orbital velocity $V_{orb}\left(r\right)$. Although this approach is not exact, because galaxies are not spherically symmetric, it is sufficiently precise to provide some clear-cut conclusions. For a central inverse quadratic force field the relation between the gravitational potential and the circular orbital velocity is:

$$U\left(r\right)=-V_{orb}^{2}\left(r\right) \tag{1}$$

**Figure 2** displays the gravitational potential $U\left(r\right)$, calculated, within the galactic border, with the help of Equation (1), using the observed velocity profile

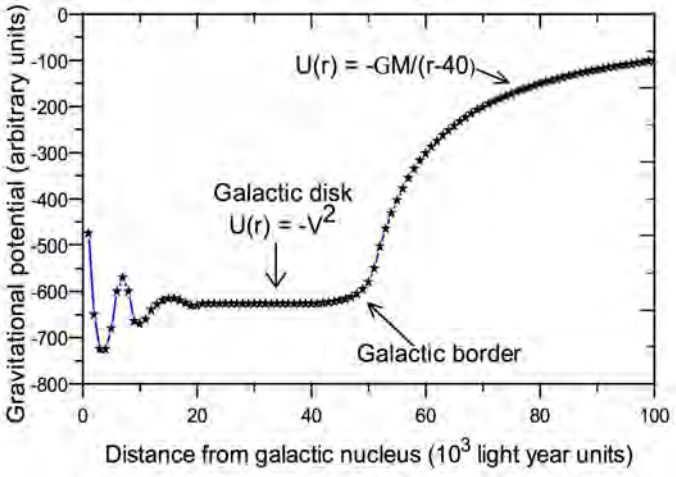


**Figure 2.** The figure depicts the gravitational potential for the Milky-Way galaxy, obtained by making use of Equation (1) and the observed orbital velocity profile in **Figure 1**. Within the galactic disk, this is to be seen as approximately the observed gravitational potential curve. However, beyond the galactic border, on from $(r-40)\times 10^3$ light years in **Figure 2**, the gravitational potential is assumed to follow nearly the usual ($1/r$) dependence, however only on from the galactic border.

of our Milky-Way galaxy in **Figure 1**. The galactic gravitational potential curve, obtained in this way, is to be seen as approximately the observed potential. Especial attention is called to the region within the galactic disk. The result shows that, in this region, the gravitational potential is closely leveled, which, from the Newtonian gravitation viewpoint, means that the force field toward the galactic center is almost zero ( $\boldsymbol{F}(r)=m\boldsymbol{a}(r)=-\boldsymbol{grad}U(r)\sim 0$ ). However, despite this absence, the stars are moving along circular orbits round the galactic center. From the usual mechanics point of view, this breaks fundamental principles of mechanics and seems absurd. Moreover, the spacetime curvature of GR too is well known to be unable to explain these observed orbital motions.

The impasse of the current theories with the observed non-Keplerian galactic gravitational dynamics can be solved in two ways: Or solid evidence must be found that enough dark matter is present at the right place or a fundamentally new gravitational theory must be found that explains this rotation without the need of dark matter. The perspective of success along the first possibility is hopelessly low. Therefore, the present work puts the hope on the second possibility. In the sixties of the past century a series of ground breaking scientific achievements, involving many brilliant scientists, have disclosed the origin of the inertial mass of the elementary particles [7] [8]. Peter Higgs has made the decisive step toward the solution. For this reason the theory is known by his name. The Higgs mechanism, providing inertial mass to the elementary particles, is of vital importance. Without it, the existence of our universe simply would be impossible.

## 3. Briefly the Higgs Quantum Space Dynamics Gravitational Mechanism

The Higgs theory introduces the idea that space is filled up throughout by a quantum fluid medium, a quantum condensate of bosons, analogous to the superconducting condensate (SCC), here to be referred to by Higgs Quantum Space (HQS). Such quantum condensates are not ruled by classical hydrodynamics, however by the principles of quantum mechanics. Likewise the SCC, the HQS forms on spontaneously breaking the $U(1)$ gauge symmetry of the respective boson system and too can be described by a complex macroscopic Ginsburg-Landau like order parameter $\Phi = \phi e^{i\theta}$. In terms of the Real and Imaginary components of $\Phi$ the characteristic form of the potential well, created by the condensate, has the form of a Mexican sombrero $V(\rho) = -n\rho + m\rho^2$, where $n$ is considerably larger than $m$ and $\rho = \Phi^* \Phi$. In this potential well, the minimum of the potential energy occurs not for $\rho = 0$ however for $\rho = n/2m$. This remarkable feature is known as a non-zero vacuum expectation value. However, while the transition temperature of the SCC is very low and is stabilized by an energy gap of only e few meV, the Higgs quantum condensate or Higgs Quantum Space (HQS) is believed to have condensed shortly after the big-bang when the temperature fell through $10^{15}$ K. It moreover is stabilized by a huge energy gap, which, according to the Glashow-Weinberg-Salam electroweak model, achieves more than 200 GeV.

The HQS couples to the vector bosons $W^+$, $W^-$ and $Z_0$, confining and quantizing them, thereby giving them large rest masses by the Higgs mechanism. The HQS also couples indirectly to all the elementary particles porting hypercharges (quarks and leptons) by a Yukawa like mechanism, giving them mass. The Higgs mechanism is the perfect HQS analog of the Meissner effect [9] in superconductivity that couples to the electromagnetic (EM) field, confining and quantizing it and giving inertial mass to the EM field quanta (photons) within superconductors. The first clue that coupling of a field to a quantum condensate gives rise to mass terms was discovered by Anderson in superconductivity [10]. Gauge transformations of the superconducting order parameter $\Psi = \psi e^{i\theta}$, in the presence of a magnetic field, reveal mass terms.

The Higgs theory introduces profound changes in Einstein's view about the nature of the empty space (vacuum). The HQS is much more than simply a local ultimate reference for rest and for motions. It literally governs the inertial motions of matter-energy. This essentially will say that *velocity with respect to the local HQS and not relative velocity is the physical cause of all the effects of motion*. The HQS materializes the local Lorentz frames, turning them into local proper Lorentz frames, *intrinsically stationary with respect to the local HQS*. On the other hand, references not stationary with respect to the local HQS are not proper LFs. The HQS also necessarily is responsible for the gravitational fields because it is mass that creates these fields. It is clear that the HQS plays a fundamental role in the microscopic physics of the quantum world as well as in

the macroscopic world of gravitation. The HQS thus is the link that units quantum physics and gravitation.

Einstein's model of the free-falling inertial references (IRs), proposed in General Relativity to explain the origin of the gravitational dynamics has a serious shortcoming. It cannot give rise to the observed gravitational pull. It cannot because the local free-fall velocity from the infinite $v_{ff} = (2GM/r)^{1/2}$ (local escape velocity) at any point $r_0$ within the gravitational field is constant ($\mathrm{d}v_{ff}/\mathrm{d}t\big|r_0 = 0$). Therefore, a body brought to rest at any given position in the gravitational field and then released, will remain in equilibrium there. Any perturbation however will trigger a runaway departure upward or downward. In fact, within a gravitational field any matter body *that is not thrust by an external force*, must be considered as a free-body. This proves that the nature of the real constant upward force, necessary to prevent the free-fall of such a free body and acting *without producing any upward velocity* along its instantaneous direction, *is clearly of a centripetal nature*. In its turn, the downward reaction force, known as gravitational pull, necessarily is of a centrifugal nature. This will say that the local inertial references are not free falling; however are rotating round an *over-head axis*. The gravitational pull is a spherically symmetric inward centrifuge effect.

In previous publications [11] [12] [13] [14] [15], the author shows that the absence of the gravitational slowing of the GPS clocks by the solar field as well as the absence of light anisotropy with respect to earth demonstrate that the HQS is moving round the sun according to a Keplerian velocity field, consistent with the planetary motions, in which the value of the local velocity is spherically symmetric. This Keplerian velocity field of the HQS is shown to accurately produce all the effects of the gravitational fields on matter, on light and on clocks. In terms of the usual spherical coordinates $[r,\theta,\phi]$ the velocity field of a spherically symmetric source has the very simple form:

$$\mathbf{V}(r) = (GM/r)^{1/2}\,\mathbf{e}_{\phi} \tag{2}$$

This Keplerian velocity field is the quintessence of the gravitational fields.

In this Keplerian velocity field, the velocity of the HQS increases for decreasing radial coordinate $r$ at all positions $[r,\theta,\phi]$ round the gravitational source from the equator to the Poles. Therefore, the local distribution of velocity (velocity gradient) through any infinitesimal region in any $[r,\theta]$ plane, which is parallel to the wave fronts of a particle moving along the $\phi$ coordinate, is consistent with rotation of the local HQS and necessarily of the local inertial reference (IR) *round an overhead axis*. The angular velocity round this overhead axis points along $+\theta$ and can be shown (Refs.(11,12) to be located in the ordinary space at a distance $r$ above the position of the particle. The local rotating references are inertial references because it is the HQS, ruling the inertial motion of matter that is itself so rotating. This will say that a free particle, initially stationary in the ordinary space within this Keplerian velocity field (earth-based laboratory) is implicitly moving with respect to the local (moving)

HQS at a velocity ($\boldsymbol{V}=-\left(GM/r\right)^{1/2}\boldsymbol{e}_{\phi}$). This velocity is implicit because it cannot bve described with respect to the ordinary space. The implicit velocity vector will rotate with the local IR round the same overhead axis at an angular velocity ($\boldsymbol{W}\left(r\right)=\left(GM/r^{3}\right)^{1/2}\boldsymbol{e}_{\theta}$). Consequently, the particle will develop an increasing velocity component along *r*, the acceleration being given by $\boldsymbol{W}\left(r\right)\times\boldsymbol{V}\left(r\right)=-\left(GM/r^{2}\right)\boldsymbol{e}_{r}$. This is exactly the expression for the centrifugal acceleration in a rotating (non-inertial) reference. Here, the non-inertial reference (laboratory) is implicitly rotating (oppositely) with respect to the local IR that is truly rotating in the ordinary space. *Note that this centrifugal acceleration points, from every point, toward the gravitational center*. On the other hand, a particle of mass *m*, stationary with respect to the ordinary space within the Keplerian velocity field Equation (2), will implicitly be moving along a circular path, within the local truly rotating IR, under a real *upward centripetal force* $\boldsymbol{F}_{cp}\left(r\right)=+\left(mGM/r^{2}\right)\boldsymbol{e}_{r}$. The downward reaction force to this real upward centripetal force is a fictitious force, a genuine centrifugal force (gravitational pull) $\boldsymbol{F}_{cf}=-m\boldsymbol{g}\boldsymbol{e}_{r}$. Please see Refs. [11] [12] [13] for the full details. In this HQS dynamics scenario the gravitational pull is identically a usual centrifugal pull toward the gravitational center.

The Keplerian velocity field of the HQS Equation (2), governing the inertial motion of matter-energy, is among all imaginable physical mechanisms the only one that is capable of generate and implement the outside-inside and inside-outside centrifuge scenario, observed within the gravitational fields. No other theory of gravitation can give rise to this intriguing inertial dynamics that is so difficult to grasp. The non-uniform velocity of the HQS in the Keplerian velocity field is the key feature that implements this apparently magic physics. In conclusion, *the gravitational pull is nothing than simply and exactly a centrifugal pull, generated by the Keplerian velocity field of the HQS*. In view of these facts, the present work associates together the central idea of GR, according to which the gravitational pull is an inertial pull and the central idea of the Higgs theory, according to which the HQS governs the inertial motion of matter-energy and replaces Einstein's spacetime curvature by a Keplerian velocity field of the HQS.

In the solar Keplerian velocity field, the orbiting earth, as well as the other planets of the solar system are very closely stationary with respect to the local moving HQS (and the local proper Lorentz frames). This predicts the absence of the gravitational slowing of the GPS clocks by the solar field, as observed. It also predicts the well-known absence of light anisotropy with respect to earth and all the other observed effects of the gravitational fields on light and on clocks. Current theories explain the absence of the solar gravitational slowing on the GPS clocks in terms of the principle of equivalence. However, the GPS clocks too are moving round earth in exactly the same conditions as round the sun, which too should cancel the gravitational slowing by the earth field. This cancelation however is not observed. The GPS clocks move round earth in orbits that make 55 degrees with the earth's equator. This is the relevant difference that is responsible for the non-cancelation of the gravitational slowing of the GPS

clocks by the earth's field. Please see Refs. [11] [12] [13] for the detailed explanation. The absence of the solar gravitational slowing of the GPS clocks and the absence of light anisotropy with respect to the planet earth are both authentic signatures of the true physical mechanism of gravity in action.

The velocity field of the HQS of a galaxy results from the composition of a huge number of the stellar Keplerian velocity fields Equation (2). In order to these stellar velocity fields to build up the galactic velocity field, the individual star velocity fields must be fairly well polarized. They must all be rotating in the same sense as the galactic rotation, round axes that are dominantly parallel to that of the galaxy. In the solar system, the planetary Keplerian velocity fields of the HQS are polarized to a high degree. This is evident from the fact that the planets move all in the same sense along circular orbits round the sun, within the plane of the solar system. Moreover, the planets rotate round nearly parallel axes and the planetary satellites move all in the same sense round these axes along nearly circular orbits closely within the plane of the solar system. The stars in the galaxies too orbit all in the same sense round the galactic center along closely circular orbits within the galactic plane. It seems reasonable to assume that the stellar Keplerian velocity fields rotate all in the same sense as the galactic rotation, round axes dominantly parallel to the galactic rotation axis.

The coming Sections will show that, due to the orbital velocity, the collective galactic velocity field of the HQS, *created by the orbiting stars*, has not the Keplerian form. It does not fall with the radial distance $r$ as in the Keplerian velocity field ($r^{-1/2}$). The reason is that, from the view of an external observer, *the orbital velocity* $v_{orb}$ *of each star subtracts from its local symmetric Keplerian velocity field* Equation (2) *toward the inner side of the orbit, however adds up to it toward the outer side*. Because of this asymmetric effect, the velocity profile in the galactic disk of most galaxies becomes nearly constant with $r$ and, in some galaxies, it even increases with the radial distance. It also naturally depresses the velocity profile within a central region as observed in all galactic velocity profiles. It can even generate a central region with retrograde rotation, as observed in many galaxies. The next Section 3 makes a quantitative analysis for the case of a binary star system that reveals a key feature, which is essential to understand the non-Keplerian rotation of the galaxies. Section 4 constructs a qualitative model that reproduces the observed non-Keplerian rotation of the galaxies *without the need of dark matter*.

## 4. Binary Stars Contain a Key Feature that Unveils the Origin of the Non-Keplerian Rotation of the Galaxies

The crucial question to be answered here is: Why do the orbital velocities of the planets decrease with distance from the gravitational center according to $(1/r)^{1/2}$, while the orbital velocities of the stars in the galactic disk fall less than $(1/r)^{1/2}$ and in many galaxies do not fall at all or even increase with distance r? This is the observational fact that the current theories of gravitation cannot

explain without postulating a huge amount of dark matter. *Here the goal is showing that the gravitational theory, based in the HQS dynamics gravitational mechanism, predicts this non-Keplerian galactic gravitational dynamics without the need of dark matter*. It even reveals incredible details. The origin of this behavior is related with the fact that motion of a gravitational source gives rise to important effects on the velocity field of the HQS, creating the gravitational fields, even for relatively low velocities. In the current theories only very high velocities, comparable to the velocity of light, cause significant changes.

In order to highlight the relevance of the effects of motion of the gravitational sources on their HQS velocity field in a system of bodies gravitating in their self-consistent velocity field, let us begin with the simple case of a binary system of two equal stars. Assume that the velocity fields of both stars are perfectly polarized (velocity fields Equation (2) rotating in the same sense round parallel axes) and that the stars are both moving along the same circular equatorial orbit round the center of mass (CM). Please see a sketch in **Figure 3**. These stars both will be moving along a same circular orbit, together with the local HQS in the collective velocity field of the HQS, created by them. They are each one stationary with respect to the local HQS. The gravitational dynamics of such a binary system has the virtue of disclosing very clearly the effects of the orbital motion of the sources on their velocity fields within the collective gravitational field of the binary system, which is seen by an observer in the non-rotating (XY) reference. These effects unveil the essential clue that is the key to understand the origin of the non-Keplerian galactic gravitational dynamics.

Consider two equal stars with equal masses $M_1 = M_2 = M$, moving in the same circular orbit round their center of mass (CM) and the velocity fields, creating their individual gravitational fields, rotating in the same sense as the orbital motion round parallel axes attached to the center of these gravitational sources, as shown in **Figure 3**. These stars will be com-moving with the local HQS along circular orbits round the CM in the equatorial plane of the collective velocity field of the HQS, creating the gravitational field of the binary. Note that this configuration (axes forming less than 90 degrees) of the velocity fields is the only one leading to a stable bound system. It can be shown that stars with oppositely (anti-parallel) rotating velocity fields of the HQS cannot form a stable bound system, because, on approximating, their opposite velocity fields would add up and gradually cancel, thereby canceling their negative gravitational potentials. Such systems in fact must be anti-gravitating.

The gravitational dynamics of the binary system can be well described by Newtonian mechanics. Balance of the mutual Newtonian gravitational forces $GM^2/(2x_0)^2$ on each star and of the opposite centripetal forces $Mv_{orb}^2/x_0$ leads to the observed orbital velocity $v_{orb}$ of each star round the CM:

$$v_{orb} = \frac{1}{\sqrt{2}}(GM/2x_0)^{1/2} \tag{3}$$

where $2x_0$ is the distance between the two stars and where $x_0$ is a positively defined length (please see **Figure 3**), which is the distance to the CM. Consider

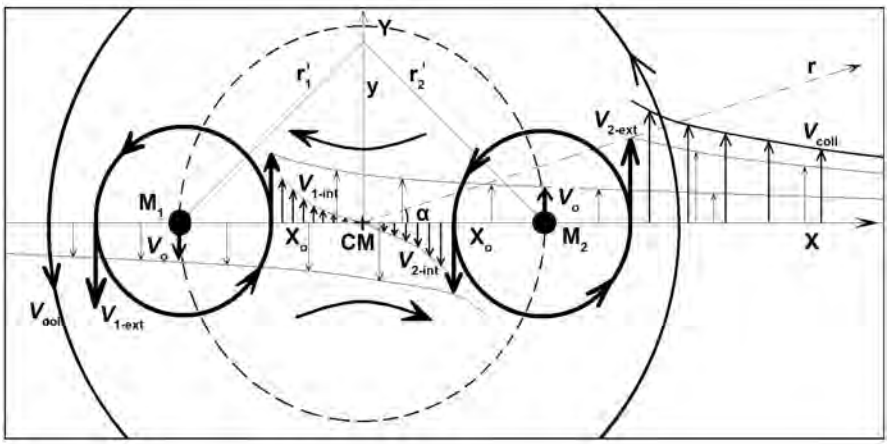


**Figure 3.** View of the velocity fields of the HQS in the equatorial plane of two masses $M_1 = M_2 = M$, moving in the same sense along the same circular orbit round the center of mass (CM) within the equatorial plane of the combined velocity field. The arrows, indicating the velocities are plotted all to scale. Note that, from the perspective of the observer in the non-rotating [X, Y] coordinate axes, the velocity of the HQS, due to the velocity fields of $M_1$ and or of $M_2$, are larger outside than inside the binary orbit.

now a small test particle $m$ moving round an equal, however isolated and static mass $M$ ($M \gg m$) in a circular equatorial orbit having the same radial distance $2x_0$ between $m$ and $M$ as between the masses in the binary. The orbital velocity $v'_{orb}$ of this test particle must be:

$$v'_{orb} = \left(GM/2x_0\right)^{1/2} = \sqrt{2}v_{orb} \tag{4}$$

It immediately is seen that the velocity $v'_{orb}$ in Equation (4) is considerably larger than $v_{orb}$ in Equation (3).

From the viewpoint of the Newtonian gravitational theory there is obviously nothing wrong with Equations (3) and (4). On the other hand, from the viewpoint of the HQS-dynamic gravitational mechanism, the central gravitational source in Equation (4) practically remains stationary at the CM. Therefore this Equation gives the local velocity of the HQS in the Keplerian velocity field round a static mass $M$, exactly as stipulated by Equation (2). However, in the dynamic case of the binary stars, Equation (3) too gives the value of the velocity of the HQS, at the site of $M_1$ and at the site of $M_2$, due to the respective companion star. Otherwise, it would be impossible to their orbits to be circular. Hence, both Equations (3) and (4) describe the velocity of the HQS at the orbits in the respective velocity fields. However, why are these velocities so different?

In the view of the present work, *the difference between* Equations (3) *and* (4) *unveils a key feature that is responsible for the non-Keplerian rotation of the galaxies*. This difference *discloses the effect of the relatively slow orbital velocity of the gravitational sources on the velocity field of the HQS, creating their respective gravitational fields as well as on the collective velocity field* $V_{coll}$, *responsible for the gravitational dynamics of the binary* as viewed by an observer in the static non-rotating (XY) reference (please see **Figure 3**).

However, in the opinion of an observer, moving together with one or the other source of the binary, the respective sources are stationary with respect to the local HQS and the velocity field of the HQS, creating the local gravitational field of each individual source, is closely spherically symmetric, as given by Equation (2), excepting only for small tides. This observer can confirm these facts by light anisotropy experiments and by the rate of his atomic clocks. Nevertheless, from the viewpoint of an observer stationary in the static non-rotating (XY) coordinate axes (please see **Figure 3**), which constitute the reference with respect to which the collective velocity field of the binary must be described, the velocity fields of the individual stars are considerably asymmetric. The value of the velocity of the HQS, at points on the X axis, is much larger outside the orbit of the binary than inside. Moreover, the sense of the velocity of the HQS inside the orbit is opposite to the orbital motion as well as opposite to the considerably higher velocity outside the binary. The circumstance is analogous to the observations of the wheels of a moving car in the view of a resting street observer and of the passenger in the car. In the view of the street observer the lower part of each wheel is stationary on the street, while the upper part is moving at a velocity two times the velocity of the car. However, in the view of the passenger, inside the car, the wheels are rotating symmetrically round their axes.

All these features are fundamental to understand the non-Keplerian gravitational dynamics of galaxies. In the case of the binary, the only possible reason for the reduced velocity of the HQS, at the position of $M_1$ or of $M_2$ is the orbital velocity of the companion star round the center of mass (CM). In fact the orbital velocity of the sources, given by Equation (3), subtracts from the spherically symmetric velocity fields Equation (2) in the reference of each source inside the orbit and adds up to it outside the orbit, as depicted in **Figure 3**.

In order to put in evidence the full effects of motion of the gravitational sources on their velocity fields, consider now, in addition, a small test particle, moving in the collective velocity field of the binary along a direct circular orbit within the orbital plane of the binary. If this orbital motion takes place sufficiently far away from the binary, the asymmetries of the binary field will be minimized. The orbital velocity $v$ of such a test particle is of course given by:

$$v(r)=\sqrt{\frac{G2M}{r}} \tag{5}$$

where $r$ is the distance on from the CM of the binary. For large $r$ Equation (5) too corresponds well to the velocity of the HQS round the binary, however in the collective velocity field round the binary:

$$V_{coll}(r)=\sqrt{\frac{G2M}{r}} \tag{6}$$

In order to reconcile the addition of the velocity fields of $M_1$ and $M_2$ outside the binary with the velocity in the collective velocity field, given by Equation (6), the same orbital velocity that reduces the velocity fields toward the inner side, must increase it outward the binary orbit. It must increase the velocity field $V_1$

toward the left-hand side of $M_1$ and also increase the velocity field $V_2$ toward the right-hand side of $M_2$ as plotted in Figure 3. At distances $r$ much larger than $2x_0$, the addition of the velocity fields of $M_1$ and $M_2$ must reproduce the value, given by Equation (6). Note however that the addition of the velocity fields, due to different sources $M_1$ and $M_2$ along the axis of $X$, must satisfy the *sum rule*:

$$V(r)=\sqrt{\left|V_1^2(r_1)\pm V_2^2(r_2)\right|} \tag{7}$$

The reason of this sum-rule is the fact that the velocity field of the HQS depends on the square-root of the source mass and distances. Taking into account the sum rule Equation (7), the addition of the velocity fields of $M_1$ and $M_2$, *at the* $+X$ *axis* and for large $x$ (large $r$ in Figure 3), takes the form:

$$V_{coll}^2 \sim \frac{G2M}{r}=\frac{1}{2}\frac{GM_1}{x_0+x}+V_{ext,2}^2 \tag{8}$$

Considering that, along the axis of $X$, $r=x$ and the distance from $M_2$ is $x-x_0$ and solving for $V_{ext,2}$ for points on the $+X$ axis, for $x \gg x_0$, the velocity field, produced by $M_2$ is approximately given by:

$$V_{ext,2} \sim \sqrt{\frac{3}{2}}\sqrt{\frac{GM}{x-x_0}} \tag{9}$$

A totally similar result is found toward the left hand side of $M_1$ and hence $\left|V_{ext,1}\right|=\left|V_{ext,2}\right|=V_{ext}$.

Inserting the result of Equation (9) into Equation (8) and adding according to Equation (7), the velocity field of the binary to the right hand side of $M_2$ (along points on $+X$), for large $x$, which means large $r$, is:

$$V_{coll}=\sqrt{\frac{3}{2}\frac{GM}{x-x_0}+\frac{1}{2}\frac{GM}{x_0+x}} \sim \left(G2M/r\right)^{1/2} \tag{10}$$

This reproduces the result of Equation (6) for large $r$. The procedure to obtain $V_{coll}$ to the left hand side of $M_1$ is analogous and the result is identical.

This result shows that effectively the same orbital velocity that, in the view of the static observer in the (XY) reference, reduces the velocity fields of $M_1$ and or $M_2$ (Equation (2)) by a factor $(1/2)^{1/2}$ toward the inner side in Figure 3, enhances the velocity fields of $M_1$ and $M_2$ by a factor $(3/2)^{1/2}$ toward the outer side. This is of course not for nothing. Clearly, *the reason is the orbital velocity of the sources*. This result shows that, while the *contribution of* $M_1$ to the collective velocity field, at points on the axis of $X$ toward the right hand side of $M_2$ is only $(1/4)V_{coll}$, the contribution of $M_2$ is $3/4V_{coll}$. An analogous conclusion is valid at the left hand side of $M_1$, however with the roles of $M_1$ and $M_2$ interchanged. Hence, while, from the viewpoint of the static (XY) reference, the effects of the orbital velocity on the velocity fields of the individual stars change considerably the symmetry of the velocity fields of the individual stars, they do not affect significantly the value of the collective (total) velocity field far outside from the binary. The effective collective velocity field, outside de binary, is closely the same as in the case, in which the two sources are static.

In conclusion, toward the inner side of the binary, on the axis of $X$, the orbital velocity $v_{orb}$ subtracts from the spherically symmetric velocity fields (Equation (2)) of each source, in consonance with Equation (7):

$$V_{int} = \sqrt{\frac{GM}{x'} - v_{orb}^2} = \frac{1}{\sqrt{2}}\sqrt{\frac{GM}{x'}} \tag{11}$$

where $x'$ is the distance on from either $M_1$ or $M_2$ toward the inner side and beyond respectively toward $+\infty$ or $-\infty$ along the $X$ axis. However, outward the binary, either toward the left on from $M_1$ in Figure 3 or toward the right on from $M_2$, the orbital velocity adds up to the respective spherically symmetric velocity field Equation (2), in consonance with Equation (7):

$$V_{ext} = \sqrt{\frac{GM}{x'} + v_{orb}^2} = \sqrt{\frac{3}{2}}\sqrt{\frac{GM}{x'}} \tag{12}$$

where $x'$ is the distance toward the left on from either $M_1$ or toward the right on from $M_2$ in Figure 3, along the axis of $X$ and to respectively $-\infty$ or $+\infty$.

In the view of an observer, stationary on the $X$ axis of the non-rotating (XY) reference, far away at the right hand side of $M_2$, $M_2$ contributes $(3/2)GM/x'$ to the total gravitational potential of the rotating binary, the total value of which is $U(x') = G2M/r$, while $M_1$ contributes only $(1/2)GM/(2x_0 + x')$ to it. An analogous conclusion is valid at the left hand side of $M_1$, where however the roles of $M_1$ and $M_2$ are interchanged. The origin of the difference between the contributions of $M_1$ and $M_2$ to the effective gravitational potential is, besides their different positions, principally their orbital velocities. This view of the static (XY) observer is of fundamental importance, because it is exactly the view of the gravitational dynamics we usually make about the stars within galaxies. Note that in the view of the current gravitational theories, the effect of the low orbital velocities on the gravitational potential of the individual sources is totally irrelevant. In these theories the gravitational potential depends only on the position and not on the velocity of the sources. However, the total gravitational potential far away outside the binary, predicted by both approaches, are the same $U \sim G2M/r$.

The results expressed by Equations (11) and (12) and plotted in Figure 3 are a unique feature of the present HQS-dynamic gravitational mechanism. It arises from the fact that the gravitational dynamics is created by the Keplerian velocity fields of the moving sources. None of the current theories of gravitation can give rise to the features expressed by Equations (11) and (12). These equations show that, while the velocity field, created by $M_2$ at its left hand side, is downward and has the value $-(1/2)^{1/2}(GM/x')^{1/2}$, at the right hand side it is upward and has the value $+(3/2)^{1/2}(GM/x')^{1/2}$. In these expressions $x'$ is the distance on from the position of $M_2$ to either sides. Hence, going in Figure 3 along the positive $X$ axis, on from the CM, there is an upward velocity step $\Delta V$, from $-(1/2)^{1/2}(GM/x')^{1/2}$ to $+(3/2)^{1/2}(GM/x')^{1/2}$, created by $M_2$:

$$\Delta V = \left[\sqrt{\frac{3}{2}} + \sqrt{\frac{1}{2}}\right]\sqrt{\frac{GM}{x'}} \sim 1.93\sqrt{\frac{GM}{x'}} \tag{13}$$

Note that this addition is not ruled by Equation (7) because the velocities are of the same mass. Going along the $X$ axis toward the left hand side in **Figure 3**, on from the CM, there is an analogous velocity step at the position of $M_1$, however increasing the (opposite) downward velocity (please see **Figure 3**). Note also that the magnitude of the velocity step depends on the square-root of the mass $M$ as well as of $x'$, the distance from this mass. For instance, the velocity of the HQS in the solar Keplerian velocity field achieves 436 km/sec at the solar surface. However, at distances of the first neighbor star (Alfa Centaurus) the velocity is only about 60 meters/sec. The sun thus creates on its surface a velocity step of 872 km/sec from side to side and only of about 120 meters/sec at the distances of Alfa Centaurus.

The velocity steps created by the stars in the binary are a key feature that is fundamental in the building up of the velocity field of the HQS, ruling the non-Keplerian galactic gravitational dynamics. In this building up, it is important to perceive that the upward orbital velocity step of $M_2$ in **Figure 3** and given by Equation (13), does not only increase the upward velocity at the right hand side of $M_2$, according to Equation (12), however also decreases the downward velocity at its left hand side, as given by Equations (11). This shows that the total magnitude of the velocity step, created by $M_2$, is the same as in the static situation, however shifted by the orbital velocity.

The obvious conclusion from the above analysis is that the Keplerian velocity fields of the individual stars in the galactic disk act all in the sense of opposing the Keplerian reduction $(1/r)^{1/2}$ of the galactic velocity field. In this modified Keplerian dependence, the velocity outside the orbit that is increased by the orbital velocity, as well as the velocity inside the orbit, decreased by the orbital velocity, both act together in the sense of locally opposing the Keplerian decrease of the velocity as a function of the distance from the galactic center. In some galaxies this effect is strong enough to invert the velocity gradient so much that the velocity, instead of decreasing, effectively increases with $r$. However, beyond the border of the galactic disk, where the mass density falls strongly toward zero, the galactic velocity field of course tends to recover the Keplerian $(1/r)^{1/2}$ dependence.

In-between the orbiting stars of the binary system the velocity fields of the HQS, due to $M_1$ or $M_2$ at the axis of $X$, are opposite to each other (please see **Figure 3**). Moreover, they are reduced by their orbital velocity given by Equation (3), as given by Equation (11). Along the $X$ axis, the addition of these internal velocity fields, according to Equation (7), shows that, close to $M_1$, the upward velocity field of $M_1$ dominates and close to $M_2$ the downward velocity field of $M_2$ is dominant. The internal velocity field rotates in the opposite sense to that of the external velocity field. In-between the two masses, the resultant collective velocity field, as a function of the position $x$ and along the axis of $X$, is

given by:

$$V_{int}(x)=\sqrt{\left|V_1^2-V_2^2\right|}=\sqrt{\left|\frac{1}{2}\frac{GM_1}{x_0+x}-\frac{1}{2}\frac{GM_2}{x_0-x}\right|} \tag{14}$$

where $x_0$ is positively defined, but $x$, in the term of $M_1$, is initially negative, but becomes positive beyond the origin (CM), while, in the term of $M_2$, $x$ is initially positive, but becomes negative below the origin of the (XY) system. If $M_1=M_2$, the resultant velocity at the origin is zero ($V_{int}(x=0)=0$). If $x=-x_0$, $V_{int}(x)$ points upwards and is large near $M_1$ (see **Figure 3**) and for $x=+x_0$, $V_{int}(x)$ points downwards and is large near $M_2$. The opposite velocity field within the binary orbit is not at all strange. In many galaxies, a central region rotates oppositely to the external disk. NGC 7331 is a well-known example in which the central bulge is rotating oppositely to the galactic disk. [16]

In the other regions of the XY plane, the velocity field is strongly affected by continuity and conservation of volume. However, for large $r$ the velocity field tends to the form given by Equation (6). Along the axis of Y, the velocity of the HQS increases continuously for decreasing $y$, however the velocity gradient gradually falls and vanishes at $y=0$. The difficulty to describe the velocity field in such regions however is specific to the binary system. For more symmetric systems, like galaxies, this problem becomes irrelevant.

Finally, the collective velocity field of the HQS, generated by a binary system, necessarily is locally non-symmetric about the center of mass. On rotating in the ordinary space, binaries naturally induce oscillations (4π per orbit) in the magnitude of the collective velocity field of the HQS in the (XY) plane. These oscillations of the velocity field and of the gravitational field intensity expand at the velocity of light and are known as gravitational waves. Hence, while the rotation of circularly symmetric systems does not create oscillations of the velocity field and no gravitational waves, binary systems naturally create oscillations and emit gravitational waves. They are the most efficient mechanism in nature generating gravitational waves.

## 5. A Model for the Observed Non-Keplerian Rotation of the Galaxies, without the Need of Dark Matter

In the solar system, the sun and the planets rotate all in the same sense round axes closely parallel to the axis of the solar system. Moreover, the orbital motions of the planets round the sun and the orbital motions of their satellites all move along direct and closely circular equatorial orbits within the plane of the solar system. These orbital motions demonstrate that the Keplerian velocity fields, creating the gravitational fields of the sun, of the planets as well as of their satellites are highly polarized. The only significant deviation from this highly ordered dynamics is the rotation of Uranus and the orbital motions of its satellites. This however visibly is an exception, visibly due to a strong perturbation, like a catastrophic collision. In order to build up the galactic velocity field of the HQS, the velocity fields Equation (2) of the individual stars, too must be fairly

well polarized. It is well-known that the stars in the galactic disk too are moving all along nearly direct circular orbits in the same sense round the galactic center. Presently the orbits of their planets are largely unknown. It however seems quite reasonable to assume that the rotation axes of the stellar velocity fields of the HQS, creating the stellar gravitational fields, are fairly well polarized. Their velocity fields of the HQS must be rotating dominantly in the same sense as the rotation of the galaxy, round axes that make an angle lower than 90 degrees with the rotation axis of the galaxy. The rotation axis of our solar system is well-known to make about 63 degrees with respect to the rotation axis of the Milky-Way galaxy. This angular deviation may be related with the spiraled structure of our galaxy. Adequate addition of the star velocity fields must generate the galactic velocity field of the HQS that rules the galactic gravitational dynamics.

The previous Section 3 makes a quantitative analysis of the gravitational dynamics of a binary star system from the viewpoint of the HQS-dynamics gravitational mechanism. Now, consider an increasing number of stars, moving in the same sense along the same circular orbit round the CM and their velocity fields of the HQS rotating all in the same sense as their orbital motions, round axes that are all parallel to each other. **Figure 4** displays a sketch of the collective velocity field, created by a system of eight equal stars. The figure shows that, with an increasing number of stars, the velocity in the collective velocity field increases and becomes smoother.

Note that the velocity in the internal collective velocity field is opposite to the velocity in the external collective velocity field. A stagnation point exists at the center as well as between each pair of stars. Each one of the eight stars is stationary with respect to the local moving HQS in the collective velocity field. These eight stars simply are carried round the CM by the HQS in the local collective velocity field.

In order to extend the model of the star-loop in **Figure 4** closer to the realistic situation of the galactic disk, consider now multiple concentric and coplanar circular orbit loops with larger and larger radii and each loop containing a very large number of stars, rotating all in the same sense and moving in the same sense round the CM. **Figure 5** is a representation of the velocity profile of the velocity field of the HQS as well as of the estimated effective velocity of the stars (blue line) through four successive loops in an intermediate region of $r$ for a case in which the density of stars is constant with the distance $r$ from the galactic center. This means equal linear density of matter along each star loop and equal velocity steps at each loop.

Precise computation of the velocity field of a galaxy, containing hundreds of billions of stars, obviously requires formidable computational means. Here only a qualitative estimate is possible, which however convincingly shows that the HQS-dynamics gravitational mechanism consistently and naturally leads to the observed non-Keplerian rotation of the galaxies and moreover reveals some

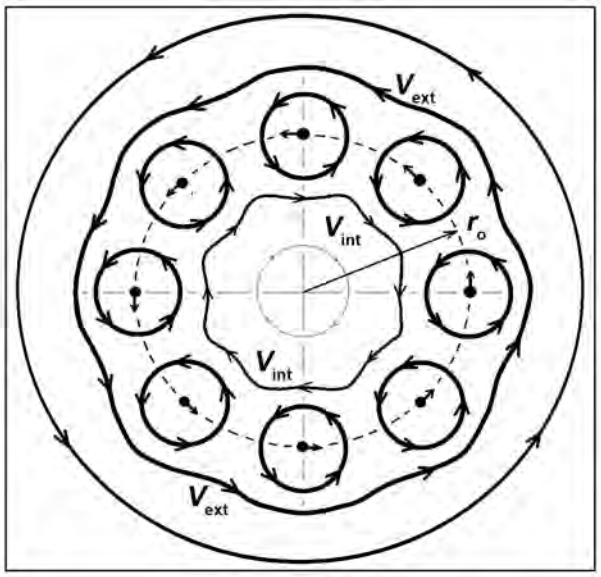


**Figure 4.** Sketch of the collective velocity field, generated by the polarized velocity fields of eight equal stars, moving together with the local HQS along the same circular orbit round the CM. The strength of the velocity field is qualitatively indicated by the wideness of the velocity tracks.

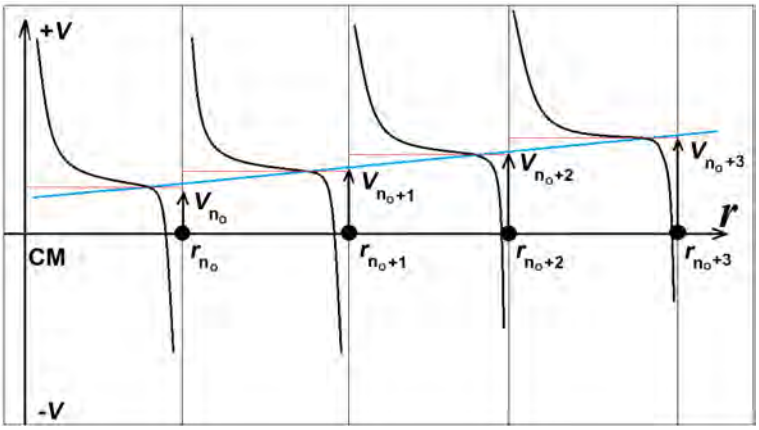


**Figure 5.** Sketch of the velocity profile of the collective velocity field of the HQS of a system of a large number of concentric star loops as a function of the distance from the galactic center. The sketch shows the velocity profile along one given $r$ coordinate within the loop disk, through four intermediate star loops, for a case, in which the star density is constant with $r$. The distance from the CM to the numbered and equally spaced loops is indicated by $r_n$ ($n = 1, 2, 3, \cdots$). The outward distance on from any given star loop $r_n$ is $r - r_n$, and the separation between successive concentric loops $r_{n+1} - r_n$ may be constant.

important and incredible details. For instance, continuing the blue line in Figure 5 to the left for nearly two loop intervals, the rotation velocity may fall to zero. Continuing to the left, the rotation velocity of the star loops may invert and become retrograde, which strongly enhances the retrograde rotation within the

central region. In many galaxies such retrograde rotation is observed.

In the star loop model, each star loop creates a velocity step $\Delta V$ in the form of Equation (13), where however $M$, the effective mass depends on the local mass density in the loop. Each star loop contributes to the collective velocity field of the HQS. This contribution however depends on the orbital velocity of the star loop. Within the galactic disk, each star loop acts in the sense of opposing the Keplerian decrease $(1/r)^{1/2}$ of the velocity field. It enhances the prograde velocity field outside each star loop, however depresses the opposite velocity field toward the inside. However, if the orbital velocity inverts, the enhancement inverts too, which stabilizes an internal region with retrograde rotation.

In terms of the gravitational potential, the successive star loops act each one in the sense of lowering the gradient of the collective (negative) gravitational potential. Depending on the mass density, the gravitational potential can become leveled or even fall with $r$, as is generally observed in an internal region and can also take place in some region of $r$ within the galactic disk. From the viewpoint of the current gravitational theories, the stars in the galactic disk too attenuate the slope of the gravitational potential within the galactic disk. However, in these theories the attenuation is much too small to match the observations. The reason is that, in these theories, the effect on the profile of the gravitational potential within the galaxy depends only on the position of the gravitational sources (stars) and not on their orbital velocity.

In the region of $r$, where the star density is constant as a function of $r$, the velocity of the HQS in the collective galactic velocity field as well as the orbital velocity of the stars within the galactic disk necessarily increases with $r$. However, in the real galaxies the mass density variations with $r$ are specific for each galaxy. Depending on the mass density as a function of $r$, an internal region about the galactic center may form that wholly rotates in the retrograde sense. NGC 7331 [16] is a well-known example in which the bulge rotates in a sense opposite to that of the external galactic disk, indicating that the mass density in the disk is especially high. Many other examples exist, in which retrograde rotation in an internal region is observed. The authors of Ref. [16] tried to understand the possible origin of this retrograde rotation in terms of catastrophic collisions, successive aggressions etc. However, none of these attempts was successful and the mystery remains unsolved to present date. In the present HQS gravitational mechanism the steep decrease of the orbital velocity profile near to the galactic center as well as the observed retrograde rotation in the internal region of many galaxies are perfectly natural features of the galactic velocity field that has a straightforward explanation. Beyond the galactic border, where only some (planetary) dwarf-galaxies and globular star clusters orbit round the galaxy, the star density in the galactic disk falls steeply and the galactic velocity field tends to recover the Keplerian $(1/r)^{1/2}$ dependence.

The star loop model, developed here, is only a qualitative description. It however can convincingly explain the observed features of the observed galactic

gravitational dynamics and even predict incredible details, without the need of dark matter. In particular it predicts the profound depression in the star orbital velocity profile. Such depression is present in the velocity profiles of practically all galaxies. It also predicts the possibility of a central region with retrograde rotation, if the mass density is high enough around this central region.

Although the star loop model is only qualitative, it lets clear that the HQS-dynamic gravitational mechanism is the appropriate physics background that naturally accounts for the non-Keplerian rotation of the galaxies without the need of dark matter. It shows that the stars in the galactic disk strongly attenuate the characteristic slope of the Keplerian velocity field Equation (2), leading to the observed non-Keplerian rotation of the galaxies. It even naturally predicts the retrograde rotation, observed at the center of many galaxies.

The planets in the solar system too constitute a disk round the sun, however a very tenuous one with irregular mass distribution and containing less than 1% of the matter of the solar system. The disk of the planets however is sufficient to attenuate a little bit the slope of the solar Keplerian velocity field and the gradient of its gravitational potential until the border of the solar system, where it regains the Keplerian dependence. This has the consequence that the gravitational acceleration of the solar field increases a little bit on going out beyond the border of the solar system. This may explain the Pioneer anomaly. The Pioneer anomaly is a very small but well-defined (anomalous) increase in the solar gravitational acceleration on the Pioneer 10 and Pioneer 11 spacecrafts, observed as they moved out in two opposite directions beyond the border of the solar system [17] [18]. To now this anomalous acceleration has no explanation.

The null results of the Michelson light experiments searching for light anisotropy due to the orbital and cosmic motion of earth demonstrate that the solar system, despite its orbital velocity of about 230 km/sec round the galactic center, is very closely stationary with respect to the local HQS ruling the inertial motion of matter and the propagation of light. However, our solar system obviously cannot be a privileged exception. All the other stars within the galactic disk must equally be closely com-moving with the local HQS in the galactic non-Keplerian velocity field. This shows that the equator of the galactic velocity field, creating the galactic gravitational field, coincides with the galactic disk. The stars are of course not constrained to move along these circular orbits by gravitational forces. These circular motions also cannot be explained in terms of spacetime curvature of GR. In the view of the HQS dynamics gravitational mechanism, analogously as the planets are carried round the sun by the HQS in the solar Keplerian velocity field, the solar system and the other stars are carried along circular equatorial orbits round the galactic center by the HQS in the galactic velocity field. These stars are locally stationary with respect to the local moving HQS, analogously as earth and the other planets of the solar system are stationary with respect to the local HQS in the solar Keplerian velocity field. This explains the null results of the light anisotropy experiments, searching for light anisotropy with respect to the planet earth in spite of its orbital motion round

the sun and in spite of the orbital motion of the solar system round the center of the Milky Way galaxy.

Likewise the planets are stationary with respect to the local HQS and carried round the sun by the solar Keplerian velocity field, the stars are stationary and carried round the galactic center by the galactic non-Keplerian velocity field. This explains why the orbital velocity of the planets falls according to $(GM/r)^{1/2}$, while the stars in the galactic disk does not fall so. However, both the planets as well as the stars in the galactic disk move along circular orbits *without the need of a central force field* because it is the HQS itself that so moves. This state of affairs is corroborated by the absence of the gravitational slowing of the GPS clocks by the solar field as well as by the absence of the light anisotropy with respect to the planet earth. However, on the other hand, the observed null results of the light anisotropy experiments on earth show that the solar system, as well as the other stars of the Milky-Way galaxy, is stationary with respect to the local moving HQS in the galactic velocity field. These observations are corroborated too by a large number of other observations, described in Refs. [11] [12] [13] [14] [15] All these observations *confirm the signature of the true physical mechanism of gravity in action*.

In conclusion, clocks moving with earth and with the solar system or with any other star in the galactic disk are very closely stationary with respect to the local HQS and run all naturally synchronous. They all show very closely the same universal proper time. However, the relative velocities between the planets, stationary with respect to the local HQS in their respective orbits, introduce well known frequency shifts. These frequency shifts however are not due to relative velocity. They are due to wavelength stretching or contraction, due to the deformation of the HQS in the solar Keplerian velocity field along their optical path. It can be shown that these frequency shifts are totally equivalent to the usual Doppler effects for the respective observed relative velocities in the ordinary space.

From a more general viewpoint, the observed isotropy of light, with respect to our planet earth, moving with the solar system in the Milky-Way galaxy and with the Milky-Way galaxy in the local region of space, also demonstrates that the recession between the galaxies and the expansion of the universe necessarily is concomitant with the expansion of the HQS itself. All the astronomical bodies throughout the universe are very nearly stationary with respect to the local moving HQS in the respective gravitational fields as well as with respect to the concomitantly expansion of the universe. This leads to the universality of the laws of physics independently from Einstein's Principle of Relativity. This problem will be the subject of another article on dark energy.

## 6. The Desperate Hunt for Dark Matter

Actually many groups around the world are searching for observational evidence of dark matter in the motion and collision of galaxies and in the motion within

galactic clusters. Dark matter by definition is not observable via the electromagnetic spectrum. It however is believed to interact with matter via gravity and the weak nuclear force. It thus may indirectly be observable via gravitational perturbations on matter and on light. The gravitational effects of dark matter are believed to be responsible for the non-Keplerian rotation of the galaxies. People also are associating observed anomalous star streams and motions of galaxies with effects by dark matter. Dark matter also is believed to gravitationally affect the propagation of light, causing anomalous gravitational light lensing effects by galaxies and galactic clusters.

All these observations however are much too tenuous to give significant evidence for the existence of the enormous amount of dark matter that is estimated to be five times larger than the whole visible matter-energy in the universe. Some cosmologists [19] [20] suggest that dark matter simply may not exist and that it is a strange need, created by the current flawed theories of gravitation. It also is suggested that gravity is not a fundamental force; however an emergent phenomenon, due to some ignored physical mechanism, like entropic effects.

In the present work, gravity too is not seen as a fundamental force. It is seen as the result of inertial motions (wave propagation) within a moving spatial medium (HQS) that materializes the local Lorentz frames and governs the inertial motion of matter-energy. Likewise the Meissner effect in superconductors, the Higgs mechanism too may develop macroscopic screening velocity fields (currents) of the HQS round the astronomical bodies in the form of Keplerian velocity fields Equation (2) or the non-Keplerian galactic velocity fields, thereby macroscopically confining (expelling out) the matter fields and thereby reducing its energy. The preceding sections show that the velocity field of the HQS, created by the orbiting stars in the galaxies, has a non-Keplerian form. This non-Keplerian velocity field of the HQS straightforwardly explains the non-Keplerian rotation of the galaxies, without the need of dark matter. From this viewpoint, the anomalous star streams, observed near to galaxies and within galactic clusters as well as the apparently anomalous motions of galaxies, are caused simply by the extended velocity fields of the HQS beyond the galactic borders, where this velocity field tends to recover the Keplerian dependence. The dark matter hunters may simply be seeing effects of the HQS tempests, caused by neighboring interacting galaxies and galactic clusters.

## 7. Concluding Comments

The HQS dynamics gravitational mechanism is naturally appropriate to account for the gravitational dynamics in the solar system, without the need of postulating arcane spacetime geometry or postulating exotic dark matter. The non-Keplerian rotation of the galaxies is by far the clearest and most critical observation that the current theories cannot explain. The HQS dynamics gravitational mechanism naturally predicts this non-Keplerian rotation without

the need of dark matter. No other theory of gravitation can do so, without requiring an enormous amount of exotic dark matter. The present work shows that the velocity of the HQS, within the galactic disk of most galaxies, is nearly constant as a function of the distance $r$ from the galactic center. The velocity gradient of the HQS (central force field) is very low. However, despite the absence of a central force field, the stars move along circular orbits. Within the galactic velocity field of the HQS, the effective velocity $c'$ of light is given by $\boldsymbol{c}' = \boldsymbol{c} + \boldsymbol{V}$, where $\boldsymbol{c}$ is the fixed velocity of light with respect to the local moving HQS and $\boldsymbol{V}$ is the local velocity of the HQS itself. The effective velocity of light traversing a galactic disk perpendicularly to the disk is expected to be lower. If the direction is not normal to the galactic disk, it also must be additionally delayed in the retrograde side and advanced at the prograde side. It however will undergo no significant change of direction. Hence, the light lensing effect on light traversing the galactic disk, if it exists at all, is very low. However, beyond the border of the galactic disk, the velocity field tends to recover the Keplerian $(1/r)^{1/2}$ dependence. The refraction rate of light, coming through this region from the back of galaxies, may be strong enough to be observed. This effect is analogous to that giving rise to the light lensing effect by the solar field, please see Section 5.5 of Ref. [11]. In fact, the *refraction rate* outside the galactic border is much smaller than that near to the sun. However, while the light lensing effect by the solar field is produced in about 13.5 milliseconds, in galaxies the excess time delay of light through the retrograde side or time gain in the prograde side may be of days or even of years. It hence can result in considerably large angular deflections. The solar Keplerian velocity field of the HQS along $\phi$ has a large velocity gradient (toward the sun) in the whole region. However, the galactic velocity field has a considerable velocity gradient only beyond the border of the galaxies and of colliding galaxies. Therefore, while the refraction of light by the solar field is relevant through the whole retrograde and also the whole prograde hemispheres, refraction by a galaxy or galactic clusters occurs only in limited regions around the border of the galactic disk. Refraction by the galactic field is typically a non-local effect, because it takes place well outside the gravitational source. This precisely is what is seen in the obtained measurements of the light lensing in galaxies, in colliding galaxies and galactic clusters [21]. The refracted light is diffuse because the galaxies, emitting the light, are extended objects and their lensing cannot produce a well resolved image. An idea that is often seen in the literature, asserts that a galaxy can move through another galaxy with very little interaction, likewise a swarm of birds flying through another swarm of birds. From the view of the present work, this is well far from reality. In the present view, besides possible collisions between stars, there is the collision between the two HQS velocity fields Equation (2). These velocity fields do not obey the principle of superposition, like electromagnetic pulses, however, they add up according to $(\boldsymbol{V}_1 + \boldsymbol{V}_2)^{1/2}$. Therefore, colliding galaxies is a much more complex affair.

## Conflicts of Interest

The author declares no conflicts of interest regarding the publication of this paper.

## References


[1] Rubin, V. and Ford Jr, W.K. (1970) *Astrophysical Journal*, **159**, 379. https://doi.org/10.1086/150317

[2] Rubin, V., Thonnard, N. and Ford Jr, W.K. (1980) *Astrophysical Journal*, **238**, 471-487. https://doi.org/10.1086/158003

[3] Remmen, G. (2010) *Journal of Undergraduate Research in Physics*, **19**, 1.

[4] Schaf, J. (2017) *World Journal of Research and Review* (*WJRR*), **4**, 68.

[5] Schaf, J. (2015) *Universal Journal of Physics and Application*, **9**, 189.

[6] Barbanis, B. and Prendergast, K.H. (1966) *The Astronomical Journal*, **72**, 215. https://doi.org/10.1086/110220

[7] Higgs, P.W. (1964) *Physical Review Letters*, **13**, 508. https://doi.org/10.1103/PhysRevLett.13.508

[8] Englert, F. and Brout, R. (1964) *Physical Review Letters*, **13**, 321. https://doi.org/10.1103/PhysRevLett.13.321

[9] Meissner, W. and Ochsenfeld, R. (1933) *Naturwissenschaften*, **21**, 787-788. https://doi.org/10.1007/BF01504252

[10] Anderson, P.W. (1963) *Physical Review*, **130**, 439. https://doi.org/10.1103/PhysRev.130.439

[11] Schaf, J. (2018) *Journal of Modern Physics*, **9**, 1111-1143. https://doi.org/10.4236/jmp.2018.95068

[12] Schaf, J. (2018) *Journal of Modern Physics*, **9**, 395-418. https://doi.org/10.4236/jmp.2018.93028

[13] Schaf, J. (2017) The True Origin of the Gravitational Dynamics. Sc. Res. Publishing, Inc., USA.

[14] Schaf, J. (2015) *Universal Journal of Physics and Application*, **9**, 141.

[15] Schaf, J. (2014) *Recent Progress in Space Technology*, **4**, 44.

[16] Prada, F., Gutierrez, C., Peletier, R.F. and McKeith, C.D. (1996) Astrophysics. arXiv:astro-ph/9602142.

[17] Turyshev, S.G. and Toth, V.T. (2010) General Relativity and Quantum Cosmology. arXiv:1001.3686v1.

[18] Anderson, J.D., Laing, P.A., Lau, E.L., Liu, A.S., Nieto, M.M. and Turyshev, S.G. (2002) *Physical Review D*, **65**, Article ID: 082004. https://doi.org/10.1103/PhysRevD.65.082004

[19] Verlinde, E. (2016) High Energy Physics—Theory; General Relativity and Quantum Cosmology. arXiv:1611.02269v28.

[20] Verlinde, E. (2010) High Energy Physic—Theory. arXiv:1001.0785v1.

[21] Siegel, E. (2017) The Bullet Cluster Proves Dark Matter Exists, But Not for the Reason Most Physicists Think.

Journal of Modern Physics, 2018, 9, 1906-1934
http://www.scirp.org/journal/jmp
ISSN Online: 2153-120X
ISSN Print: 2153-1196

# Star Physics and Measurement Data

**Boris V. Vasiliev**

Independent Researcher, Dubna, Russia
Email: bv.vasiliev@yandex.com

**How to cite this paper:** Vasiliev, B.V. (2018) Star Physics and Measurement Data. *Journal of Modern Physics*, **9**, 1906-1934.
https://doi.org/10.4236/jmp.2018.910120

**Received:** May 28, 2018
**Accepted:** August 31, 2018
**Published:** September 3, 2018



## Abstract

Astrophysics = the star physics was beginning its development without a supporting of measurement data, which could not be obtained then. Still astrophysics exists without this support, although now astronomers collected a lot of valuable information. This is the main difference of astrophysics from all other branches of physics, for which foundations are measurement data. The creation of the theory of stars, which is based on the astronomical measurements data, is one of the main goals of modern astrophysics. Below, the principal elements of star physics based on data of astronomical measurements are described. The theoretical description of a hot star interior is obtained. It explains the distribution of stars over their masses, mass-radius-temperature and mass-luminosity dependencies. All theoretical predictions are in a good agreement with the known measurement data, which confirms the validity of this consideration.

## Keywords

Electric Polarization, Plasma, Stellar Mass, Stellar Temperature, Stellar Radius

## 1. Introduction

### 1.1. Astrophysics and Astronomical Measurements

It is obvious that the primary goal of modern astrophysics is to create a star theory that can explain the dependencies of parameters of stars and of the Sun, which are measured by astronomers.

The technical progress of astronomical measurements in the last decade has revealed the existence of different relationships that associate together the physical parameters of the stars.

To date, such data have accumulated about a dozen: they are dependencies of temperature-radius-luminosity-mass of stars, the spectra of seismic oscillations of the sun, distribution of stars on mass, the dependence of the magnetic fields

of stars from their moments and speeds of rotation, etc.

All these relationships are defined by phenomena occurring inside stars. So the theory of the internal structure of stars should be based on these quantitative data as on boundary conditions.

Existing theories of stellar interiors can not explain the new data. The modern astrophysics[1] prefers a speculative approach. It elaborates qualitative theories of stars that are not pursued to such quantitative estimates, which could be compared with the data of astronomers. Everything is done in such a way as if the new astronomical data are absent. Of course, the astrophysical community knows about the existence of dependencies of stellar parameters which were measured by astronomers. However, in modern astrophysics, it is accepted to think, that if an explanation of a dependency is not found, that it can be referred to the category of empirical one and it needs no explanation. The so-called empirical relations of stellar luminosities and temperatures—the Hertzsprung-Russell diagram—are known about the hundred years, but its quantitative explanation is not found.

The reason that prevents to explain these relationships is due to the wrong choice of the basic postulates of modern astrophysics. Despite of the fact that all modern astrophysics believes that the stars consist from a plasma, it historically turned out that the theory of stellar interiors does not take into account the electric polarization of the plasma, which must occur within stars under the influence of their gravitational field. Modern astrophysics believes that the gravity-induced electric polarization (GIEP) of stellar plasma is small and it should not be taken into account in the calculations, as this polarization was not taken into account in the calculations at an early stage of development of astrophysics, when a plasma structure of stars was not known. However, plasma is an electrically polarized substance, and an exclusion of the GIEP effect from the calculation is unwarranted. Moreover, without taking into account of the GIEP-effect, the equilibrium stellar matter can not be correctly founded and a theory would not be able to explain the astronomical measurements. Accounting GIEP gives the theoretical explanation for the all observed dependence.

As shown below, the account of the gravity-induced electric polarization of the intra-stellar plasma gives possibility to develop a model of the star, in which all main parameters—the mass of the star, its temperature, radius and luminosity—are expressed by certain combinations of world constants and the individuality of stars is determined by only two parameters—the mass and charge number of nuclei, from which the plasma of these stars is composed. It gives the quantitatively and fairly accurate explanation of all dependencies, which were measured by astronomers.

The important feature of this stellar theory, which is built with the GIEP

[1]The modern astrophysics has a whole series of different branches. It is important to stress that all of them except the physics of hot stars beyond the scope of this consideration; we shall use the term "astrophysics" here and below in its initial meaning—as the physics of stars.

acconting, is the lack of a collapse in the final stage of the star development, as well as "black holes" that could be results from a such collapse.

The main features of this concept were previously published in [1]-[6].

### 1.2. The Basic Postulate of Astrophysics

We can assume that modern astrophysics emerged in the early twentieth century and milestone of this period was the work R. Emden 《Die Gaskugeln》. It has laid the basis for the description of stars as gas spheres. Gases can be characterized by different dependencies of their density from pressure, ie they can be described by different polytropes. According to Emden the equations of state of the gases producing the stars determine their characteristics—it can be either a dwarf, or a giant, or main sequence star, etc. The such approach to the description of stars determined the choice of postulates needed for the theory.

Any theory based on its system of postulates.

The first basic postulate of astrophysics—the Euler equation—was formulated in a mathematical form by L.Euler in a middle of 18th century for the "terrestrial" effects description. This equation determines the equilibrium condition of liquids or gases in a gravitational field:

$$\gamma \boldsymbol{g} = -\nabla P. \tag{1}$$

According to it the action of a gravity forth $\gamma \boldsymbol{g}$ ($\gamma$ is density of substance, $\boldsymbol{g}$ is the gravity acceleration) in equilibrium is balanced by a forth which is induced by the pressure gradient in the substance.

All modern models of stellar interior are obtained on the base of the Euler equation. These models assume that pressure inside a star monotone increases depthward from the star surface. As a star interior substance can be considered as an ideal gas which pressure is proportional to its temperature and density, all astrophysical models predict more or less monotonous increasing of temperature and density of the star substance in the direction of the center of a star.

While we are talking about materials with atomic structure, there are no doubt about the validity of this equation and its applicability. This postulate is surely established and experimentally checked be "terrestrial" physics. It is the base of an operating of series of technical devices—balloons, bathyscaphes and other.

Another prominent astrophysicist first half of the twentieth century was A. Eddington. At this time I. Langmuir discovered the new state of matter—plasma. A. Eddington was first who realized the significance of this discovery for astrophysics. He showed that the stellar matter at the typical pressures and temperatures, should be in the plasma state.

The polarizability of atomic matter is negligible.[2] There was not necessary to take into account a polarization while there was a speech about the model, in

[2]If you do not take account of ferroelectrics, piezoelectrics and other similar substances. Their consideration is not acceptable here.

which the stars are composed of atomic gases.

But plasma is an electrically polarized substance.

**It Is Necessary to Take into Account GIEP of Intra-Stellar Plasma**

Therefore, at consideration of a plasma equilibrium, the term describing its possible electrical polarization $\mathfrak{P}$ should be saved in the Euler equation:

$$\gamma \boldsymbol{g} + \mathfrak{P}\nabla\mathfrak{P} + \nabla P = 0, \tag{2}$$

This leads to the possibility of the existence of a fundamentally new equilibrium state of stellar matter, at which it has a constant density and temperature:

$$\nabla P = 0$$

$$\gamma \boldsymbol{g} + \mathfrak{P}\nabla\mathfrak{P} = 0, \tag{3}$$

that radically distinguishes this equilibrium state from equilibrium, which is described by Equation (1).

The technical progress of astronomical measurements in the last decade discovered that the physical parameters of the stars are related together.

However, these new data do not fit to models of modern astrophysics.

## 2. The Energy-Favorable State of Hot Dense Plasma

### 2.1. The Properties of a Hot Dense Plasma

#### 2.1.1. A Hot Plasma and Boltzman's Distribution

Free electrons being fermions obey the Fermi-Dirac statistic at low temperatures. At high temperatures, quantum distinctions in behavior of electron gas disappear and it is possible to consider electron gas as the ideal gas which obeys the Boltzmann's statistics. At high temperatures and high densities, all substances transform into electron-nuclear plasma. There are two tendencies in this case. At temperature much higher than the Fermi temperature $T_F = \frac{\mathcal{E}_F}{k}$ (where $\mathcal{E}_F$ is Fermi energy), the role of quantum effects is small. But their role grows with increasing of the pressure and density of an electron gas. When quantum distinctions are small, it is possible to describe the plasma electron gas as a the ideal one. The criterium of Boltzman's statistics applicability

$$T \gg \frac{\mathcal{E}_F}{k}. \tag{4}$$

hold true for a non-relativistic electron gas with density $10^{25}$ particles in $cm^3$ at $T \gg 10^6 \mathrm{K}$.

At this temperatures, a plasma has energy

$$\mathcal{E} = \frac{3}{2} kTN \tag{5}$$

and its EOS is the ideal gas EOS:

$$P = \frac{NkT}{V} \tag{6}$$

But even at so high temperatures, an electron-nuclear plasma can be considered as ideal gas in the first approximation only. For more accurate description its properties, the specificity of the plasma particle interaction must be taken into account and two main corrections to ideal gas law must be introduced.

The first correction takes into account the quantum character of electrons, which obey the Pauli principle, and cannot occupy levels of energetic distribution which are already occupied by other electrons. This correction must be positive because it leads to an increased gas incompressibility.

Other correction takes into account the correlation of the screening action of charged particles inside dense plasma. It is the so-called correlational correction. Inside a dense plasma, the charged particles screen the fields of other charged particles. It leads to a decreasing of the pressure of charged particles. Accordingly, the correction for the correlation of charged particles must be negative, because it increases the compressibility of electron gas.

### 2.1.2. The Hot Plasma Energy with Taking into Account the Correction for the Fermi-Statistic

The energy of the electron gas in the Boltzmann's case ( $kT \gg \mathcal{E}_F$ ) can be calculated using the expression of the full energy of a non-relativistic Fermi-particle system [7]:

$$\mathcal{E} = \frac{2^{1/2} V m_e^{3/2}}{\pi^2 \hbar^3} \int_0^\infty \frac{\varepsilon^{3/2} \mathrm{d}\varepsilon}{e^{(\varepsilon-\mu_e)/kT}+1}, \tag{7}$$

expanding it in a series. ( $m_e$ is electron mass, $\varepsilon$ is the energy of electron and $\mu_e$ is its chemical potential).

In the Boltzmann's case, $\mu_e < 0$ and $|\mu_e/kT| \gg 1$ and the integrand at $e^{\mu_e/kT} \ll 1$ can be expanded into a series according to powers $e^{\mu_e/kT-\varepsilon/kT}$. If we introduce the notation $z = \frac{\varepsilon}{kT}$ and conserve the two first terms of the series, we obtain

$$I \equiv (kT)^{5/2} \int_0^\infty \frac{z^{3/2}\mathrm{d}z}{e^{z-\mu_e/kT}+1} \approx (kT)^{5/2} \int_0^\infty z^{3/2} \left( e^{\frac{\mu_e}{kT}-z} - e^{2\left(\frac{\mu_e}{kT}-z\right)} + \cdots \right) \mathrm{d}z \tag{8}$$

or

$$\frac{I}{(kT)^{5/2}} \approx e^{\frac{\mu_e}{kT}} \Gamma\left(\frac{3}{2}+1\right) - \frac{1}{2^{5/2}} e^{\frac{2\mu_e}{kT}} \Gamma\left(\frac{3}{2}+1\right) \approx \frac{3\sqrt{\pi}}{4} e^{\mu_e/kT} \left(1 - \frac{1}{2^{5/2}} e^{\mu_e/kT}\right). \tag{9}$$

Thus, the full energy of the hot electron gas is

$$\mathcal{E} \approx \frac{3V}{2} \frac{(kT)^{5/2}}{\sqrt{2}} \left(\frac{m_e}{\pi\hbar^2}\right)^{3/2} \left( e^{\mu_e/kT} - \frac{1}{2^{5/2}} e^{2\mu_e/kT} \right). \tag{10}$$

Using the definition of a chemical potential of ideal gas (of particles with spin = 1/2) [7]

$$\mu_e = kT \log\left[\frac{N_e}{2V}\left(\frac{2\pi\hbar^2}{m_e kT}\right)^{3/2}\right] \tag{11}$$

we obtain the full energy of the hot electron gas

$$\mathcal{E}_e \approx \frac{3}{2}kTN_e\left[1+\frac{\pi^{3/2}}{4}\left(\frac{a_B e^2}{kT}\right)^{3/2} n_e\right], \tag{12}$$

where $a_B = \frac{\hbar^2}{m_e e^2}$ is the Bohr radius.

### 2.1.3. The Correction for Correlation of Charged Particles in a Hot Plasma

At high temperatures, the plasma particles are uniformly distributed in space. At this limit, the energy of ion-electron interaction tends to zero. Some correlation in space distribution of particles arises as the positively charged particle groups around itself preferably particles with negative charges and vice versa. It is accepted to estimate the energy of this correlation by the method developed by Debye-Hükkel for strong electrolytes [7]. The energy of a charged particle inside plasma is equal to $e\varphi$, where $e$ is the charge of a particle, and $\varphi$ is the electric potential induced by other particles on the considered particle.

This potential inside plasma is determined by the Debye law [7]:

$$\varphi(r) = \frac{e}{r}e^{-\frac{r}{r_D}} \tag{13}$$

where the Debye radius is

$$r_D = \left(\frac{4\pi e^2}{kT}\sum_a n_a Z_a^2\right)^{-1/2} \tag{14}$$

For small values of ratio $\frac{r}{r_D}$, the potential can be expanded into a series

$$\varphi(r) = \frac{e}{r} - \frac{e}{r_D} + \cdots \tag{15}$$

The following terms are converted into zero at $r \to 0$. The first term of this series is the potential of the considered particle. The second term

$$\mathcal{E} = -e^3\sqrt{\frac{\pi}{kTV}}\left(\sum_a N_a Z_a^2\right)^{3/2} \tag{16}$$

is a potential induced by other particles of plasma on the charge under consideration. And so the correlation energy of plasma consisting of $N_e$ electrons and ( $N_e/Z$ ) nuclei with charge $Z$ in volume $V$ is [7]

$$\mathcal{E}_{corr} = -e^3\sqrt{\frac{\pi n_e}{kT}}Z^{3/2}N_e \tag{17}$$

## 2.2. The Energy-Preferable State of a Hot Plasma

### 2.2.1. The Energy-Preferable Density of a Hot Plasma

Finally, under consideration of both main corrections taking into account the inter-particle interaction, the full energy of plasma is given by

$$\mathcal{E} \approx \frac{3}{2} kTN_e \left[ 1 + \frac{\pi^{3/2}}{4} \left( \frac{a_B e^2}{kT} \right)^{3/2} n_e - \frac{2\pi^{1/2}}{3} \left( \frac{Z}{kT} \right)^{3/2} e^3 n_e^{1/2} \right] \tag{18}$$

The plasma into a star has a feature. A star generates the energy into its inner region and radiates it from the surface. At the steady state of a star, its substance must be in the equilibrium state with a minimum of its energy. The radiation is not in equilibrium of course and can be considered as a star environment. The equilibrium state of a body in an environment is related to the minimum of the function ([7] §20):

$$\mathcal{E} - T_o S + P_o V, \tag{19}$$

where $T_o$ and $P_o$ are the temperature and the pressure of an environment. At taking in to account that the star radiation is going away into vacuum, the two last items can be neglected and one can obtain the equilibrium equation of a star substance as the minimum of its full energy:

$$\frac{\mathrm{d}\mathcal{E}_{\text{plasma}}}{\mathrm{d}n_e} = 0. \tag{20}$$

Now taking into account Equation (18), one obtains that an equilibrium condition corresponds to the equilibrium density of the electron gas of a hot plasma

$$n_e^{\text{equilibrium}} \equiv n_\star = \frac{16}{9\pi} \frac{Z^3}{a_B^3} \approx 1.2 \times 10^{24} Z^3 \text{ cm}^{-3}, \tag{21}$$

It gives the electron density $\approx 3 \times 10^{25} \text{cm}^{-3}$ for the equilibrium state of the hot plasma of helium.

### 2.2.2. The Estimation of Temperature of Energy-Preferable State of a Hot Stellar Plasma

As the steady-state value of the density of a hot non-relativistic plasma is known, we can obtain an energy-preferable temperature of a hot non-relativistic plasma.

The virial theorem [7] [8] claims that the full energy of particles $E$, if they form a stable system with the Coulomb law interaction, must be equal to their kinetic energy $T$ with a negative sign. Neglecting small corrections at a high temperature, one can write the full energy of a hot dense plasma as

$$\mathcal{E}_{\text{plasma}} = U + \frac{3}{2} kTN_e = -\frac{3}{2} kTN_e. \tag{22}$$

where $U \approx -\frac{G\mathbb{M}^2}{\mathbb{R}_0}$ is the potential energy of the system, $G$ is the gravitational constant, $\mathbb{M}$ and $\mathbb{R}_0$ are the mass and the radius of the star.

As the plasma temperature is high enough, the energy of the black radiation

cannot be neglected. The full energy of the stellar plasma depending on the particle energy and the black radiation energy

$$\mathcal{E}_{\text{total}} = -\frac{3}{2}kTN_e + \frac{\pi^2}{15}\left(\frac{kT}{\hbar c}\right)^3 VkT \tag{23}$$

at equilibrium state must be minimal, *i.e.*

$$\left(\frac{\partial \mathcal{E}_{\text{total}}}{\partial T}\right)_{N,V} = 0. \tag{24}$$

This condition at $\frac{N_e}{V} = n_\star$ gives a possibility to estimate the temperature of the hot stellar plasma at the steady state:

$$\mathbb{T}_\star \approx Z\frac{\hbar c}{ka_B} \approx 10^7 Z \text{ K}. \tag{25}$$

The last obtained estimation can raise doubts. At "terrestrial" conditions, the energy of any substance reduces to a minimum at $T \to 0$. It is caused by a positivity of a heat capacity of all of substances. But the steady-state energy of star is negative and its absolute value increases with increasing of temperature (Equation (22)). It is the main property of a star as a thermodynamical object. This effect is a reflection of an influence of the gravitation on a stellar substance and is characterized by a negative effective heat capacity. The own heat capacity of a stellar substance (without gravitation) stays positive. With the increasing of the temperature, the role of the black radiation increases ($\mathcal{E}_{br} \sim T^4$). When its role dominates, the star obtains a positive heat capacity. The energy minimum corresponds to a point between these two branches.

## 3. The Gravity Induced Electric Polarization in a Dense Hot Plasma

### 3.1. Plasma Cells

The existence of plasma at energetically favorable state with the constant density $n_\star$ and the constant temperature $\mathbb{T}_\star$ puts a question about equilibrium of this plasma in a gravity field. The Euler equation in commonly accepted form Equation (1) disclaims a possibility to reach the equilibrium in a gravity field at a constant pressure in the substance: the gravity inevitably must induce a pressure gradient into gravitating matter. To solve this problem, it is necessary to consider the equilibrium of a dense plasma in an gravity field in detail. At zero approximation, at a very high temperature, plasma can be considered as a "jelly", where electrons and nuclei are "smeared" over a volume. At a lower temperature and a high density, when an interpartical interaction cannot be neglected, it is accepted to consider a plasma dividing in cells [9]. Nuclei are placed at centers of these cells, the rest of their volume is filled by electron gas. Its density decreases from the center of a cell to its periphery. Of course, this dividing is not freezed. Under action of heat processes, nuclei move. But having a small mass, electrons have time to trace this moving and to form a permanent electron cloud around

nucleus, *i.e.* to form a cell. So plasma under action of a gravity must be characterized by two equilibrium conditions:

- the condition of an equilibrium of the heavy nucleus inside a plasma cell;
- the condition of an equilibrium of the electron gas, or equilibrium of cells.

### 3.2. The Equilibrium of a Nucleus Inside Plasma Cell Filled by an Electron Gas

At the absence of gravity, the negative charge of an electron cloud inside a cell exactly balances the positive charge of the nucleus at its center. Each cell is fully electroneutral. There is no direct interaction between nuclei.

The gravity acts on electrons and nuclei at the same time. Since the mass of nuclei is large, the gravity force applied to them is much larger than the force applied to electrons. On the another hand, as nuclei have no direct interaction, the elastic properties of plasma are depending on the electron gas reaction. Thus er have a situation, when the force applied to nuclei must be balanced by the force of the electron subsystem. The cell obtains an electric dipole moment $d_s$, and the plasma obtains polarization $\mathfrak{P} = n_s d_s$, where $n_s$ is the density of the cell.

It is known [10], that the polarization of neighboring cells induces in the considered cell the electric field intensity

$$E_s = \frac{4\pi}{3}\mathfrak{P}, \tag{26}$$

and the cell obtains the energy

$$\mathcal{E}_s = \frac{d_s E_s}{2}. \tag{27}$$

The gravity force applied to the nucleus is proportional to its mass $Am_p$ (where $A$ is a mass number of the nucleus, $m_p$ is the proton mass). The cell consists of $Z$ electrons, the gravity force applied to the cell electron gas is proportional to $Zm_e$ (where $m_e$ is the electron mass). The difference of these forces tends to pull apart centers of positive and negative charges and to increase the dipole moment. The electric field $E_s$ resists it. The process obtains equilibrium at the balance of the arising electric force $\nabla\mathcal{E}_s$ and the difference of gravity forces applied to the electron gas and the nucleus:

$$\nabla\left(\frac{2\pi}{3}\frac{\mathfrak{P}^2}{n_s}\right) + \left(Am_p - Zm_e\right)\boldsymbol{g} = 0 \tag{28}$$

Taking into account, that $\boldsymbol{g} = -\nabla\psi$, we obtain

$$\frac{2\pi}{3}\frac{\mathfrak{P}^2}{n_s} = \left(Am_p - Zm_e\right)\psi. \tag{29}$$

Hence,

$$\mathfrak{P}^2 = \frac{3GM_r}{2\pi r} n_e \left(\frac{A}{Z}m_p - m_e\right), \tag{30}$$

where $\psi$ is the potential of the gravitational field, $n_s = \frac{n_e}{Z}$ is the density of cell (nuclei), $n_e$ is the density of the electron gas, $M_r$ is the mass of a star containing inside a sphere with radius *r*.

### 3.3. The Equilibrium in Plasma Electron Gas Subsystem

Nonuniformly polarized matter can be represented by an electric charge distribution with density [10]

$$\tilde{\varrho} = \frac{divE_s}{4\pi} = \frac{div\mathfrak{P}}{3}. \tag{31}$$

The full electric charge of cells placed inside the sphere with radius *r*

$$Q_r = 4\pi\int_0^r \tilde{\varrho} r^2 \mathrm{d}r \tag{32}$$

determinants the electric field intensity applied to a cell placed on a distance *r* from center of a star

$$\tilde{\boldsymbol{E}} = \frac{Q_r}{r^2} \tag{33}$$

As a result, the action of a nonuniformly polarized environment can be described by the force $\tilde{\varrho}\tilde{E}$. This force must be taken into account in the formulating of equilibrium equation. It leads to the following form of the Euler equation:

$$\gamma \boldsymbol{g} + \tilde{\varrho}\tilde{\boldsymbol{E}} + \nabla P = 0 \tag{34}$$

## 4. The Internal Structure of a Star

It was shown above that the state with the constant density is energetically favorable for a plasma at a very high temperature. The plasma in the central region of a star can possess by this property. The calculation made below shows that the mass of central region of a star with the constant density—the star core—is equal to 1/2 of the full star mass. Its radius is approximately equal to 1/10 of radius of a star, *i.e.* the core with high density take approximately 1/1000 part of the full volume of a star. The other half of a stellar matter is distributed over the region placed above the core. It has a relatively small density and it could be called as a star atmosphere.

### 4.1. The Plasma Equilibrium in the Star Core

In this case, the equilibrium condition (Equation (28)) for the energetically favorable state of plasma with the steady density $n_s = const$ is achieved at

$$\mathfrak{P} = \sqrt{G}\gamma_\star r, \tag{35}$$

Here the mass density is $\gamma_\star \approx \frac{A}{Z} m_p n_\star$. The polarized state of the plasma can be described by a state with an electric charge at the density

$$\tilde{\rho} = \frac{1}{3} div \mathfrak{P} = \sqrt{G}\gamma_\star, \tag{36}$$

and the electric field applied to a cell is

$$\tilde{\boldsymbol{E}} = \frac{\boldsymbol{g}}{\sqrt{G}}. \tag{37}$$

As a result, the electric force applied to the cell will fully balance the gravity action

$$\gamma \boldsymbol{g} + \tilde{\varrho}\tilde{\boldsymbol{E}} = 0 \tag{38}$$

at the zero pressure gradient

$$\nabla P = 0. \tag{39}$$

### 4.2. The Main Parameters of a Star Core (in Order of Values)

At known density $n_\star$ of plasma into a core and its equilibrium temperature $\mathbb{T}_\star$, it is possible to estimate the mass $\mathbb{M}_\star$ of a star core and its radius $\mathbb{R}_\star$. In accordance with the virial theorem[3], the kinetic energy of particles composing the steady system must be approximately equal to its potential energy with opposite sign:

$$\frac{G\mathbb{M}_\star^2}{\mathbb{R}_\star} \approx k\mathbb{T}_\star \mathbb{N}_\star. \tag{40}$$

where $\mathbb{N}_\star = \frac{4\pi}{3}\mathbb{R}_\star^3 n_\star$ is full number of particle into the star core.

With using determinations derived above (21) and (25) derived before, we obtain

$$\mathbb{M}_\star \approx \frac{\mathbb{M}_{Ch}}{(A/Z)^2} \tag{41}$$

where $\mathbb{M}_{Ch} = \left(\frac{\hbar c}{Gm_p^2}\right)^{3/2} m_p$ is the Chandrasekhar mass.

The radius of the core is approximately equal

$$\mathbb{R}_\star \approx \left(\frac{\hbar c}{Gm_p^2}\right)^{1/2} \frac{a_B}{Z(A/Z)}. \tag{42}$$

where $A$ and $Z$ are the mass and the charge number of atomic nuclei the plasma consisting of.

### 4.3. The Equilibrium State of the Plasma Inside the Star Atmosphere

The star core is characterized by the constant mass density, the charge density, the temperature and the pressure. At a temperature typical for a star core, the plasma can be considered as ideal gas, as interactions between its particles are small in comparison with $k\mathbb{T}_\star$. In atmosphere, near surface of a star, the

[3]Below we shell use this theorem in its more exact formulation.

temperature is approximately by $3 \div 4$ orders smaller. But the plasma density is lower. Accordingly, interparticle interaction is lower too and we can continue to consider this plasma as ideal gas.

In the absence of the gravitation, the equilibrium state of ideal gas in some volume comes with the pressure equalization, *i.e.* with the equalization of its temperature $T$ and its density $n$. This equilibrium state is characterized by the equalization of the chemical potential of the gas $\mu$ (Equation (11)).

### 4.4. The Radial Dependence of Density and Temperature of Substance Inside a Star Atmosphere

For the equilibrium system, where different parts have different temperatures, the following relation of the chemical potential of particles to its temperature holds ([7], §25):

$$\frac{\mu}{kT} = const \tag{43}$$

As thermodynamic (statistical) part of chemical potential of monoatomic ideal gas is ([7], §45):

$$\mu_T = kT \ln\left[\frac{n}{2}\left(\frac{2\pi\hbar^2}{mkT}\right)^{3/2}\right], \tag{44}$$

we can conclude that at the equilibrium

$$n \sim T^{3/2}. \tag{45}$$

In external fields the chemical potential of a gas ([7] §25) is equal to

$$\mu = \mu_T + \mathcal{E}^{\text{potential}} \tag{46}$$

where $\mathcal{E}^{\text{potential}}$ is the potential energy of particles in the external field. Therefore in addition to fulfillment of condition Equation (45), in a field with Coulomb potential, the equilibrium needs a fulfillment of the condition

$$-\frac{GM_r\gamma}{rkT_r} + \frac{\mathfrak{P}_r^2}{2kT_r} = const \tag{47}$$

(where $m$ is the particle mass, $M_r$ is the mass of a star inside a sphere with radius $r$, $\mathfrak{P}_r$ and $T_r$ are the polarization and the temperature on its surface. As on the core surface, the left part of Equation (47) vanishes, in the atmosphere

$$M_r \sim rkT_r. \tag{48}$$

Supposing that a decreasing of temperature inside the atmosphere is a power fuction with the exponent $x$, its value on a radius $r$ can be written as

$$T_r = \mathbb{T}_\star\left(\frac{\mathbb{R}_\star}{r}\right)^x \tag{49}$$

and in accordance with Equation (45), the density

$$n_r = n_\star\left(\frac{\mathbb{R}_\star}{r}\right)^{3x/2}. \tag{50}$$

At assumption that the powers of $r$ in the right and the left parts of condition Equation (48) are equal, we obtain $x = 4$.

Thus, at using power dependencies for the description of radial dependencies of density and temperature, we obtain

$$n_r = n_\star \left( \frac{\mathbb{R}_\star}{r} \right)^6 \tag{51}$$

and

$$T_r = \mathbb{T}_\star \left( \frac{\mathbb{R}_\star}{r} \right)^4. \tag{52}$$

### 4.5. The Mass of the Star Atmosphere and the Full Mass of a Star

After integration of Equation (51), we can obtain the mass of the star atmosphere

$$\mathbb{M}_A = 4\pi \int_{\mathbb{R}_\star}^{\mathbb{R}_0} (A/Z) m_p n_\star \left( \frac{\mathbb{R}_\star}{r} \right)^6 r^2 \mathrm{d}r = \frac{4\pi}{3} (A/Z) m_p n_\star \mathbb{R}_\star^3 \left[ 1 - \left( \frac{\mathbb{R}_\star}{\mathbb{R}_0} \right)^3 \right] \tag{53}$$

It is equal to its core mass

(to $\frac{\mathbb{R}_\star^3}{\mathbb{R}_0^3} \approx 10^{-3}$), where $\mathbb{R}_0$ is radius of a star.

Thus, the full mass of a star

$$\mathbb{M} = \mathbb{M}_A + \mathbb{M}_\star \approx 2\mathbb{M}_\star \tag{54}$$

### 4.6. The Energy of a Star

The virial theorem ([7] [8]) is applicable to a system of particles if they have a finite moving into a volume $V$. If their interaction obeys to the Coulomb's law, their potential energy $\mathcal{E}^{\text{potential}}$, their kinetic energy $\mathcal{E}^{\text{kinetic}}$ and pressure $P$ are in the ratio:

$$2\mathcal{E}^{\text{kinetic}} + \mathcal{E}^{\text{potential}} = 3PV. \tag{55}$$

On the star surface, the pressure is absent and for the particle system as a whole:

$$2\mathcal{E}^{\text{kinetic}} = -\mathcal{E}^{\text{potential}} \tag{56}$$

and the full energy of plasma particles into a star

$$\mathcal{E}(\text{plasma}) = \mathcal{E}^{\text{kinetic}} + \mathcal{E}^{\text{potential}} = -\mathcal{E}^{\text{kinetic}}. \tag{57}$$

Let us calculate the separate items composing the full energy of a star.

### 4.7. The Kinetic Energy of Plasma

The kinetic energy of plasma into a core:

$$\mathcal{E}_\star^{\text{kinitic}} = \frac{3}{2} k \mathbb{T}_\star \mathbb{N}_\star. \tag{58}$$

The kinetic energy of atmosphere:

$$\mathcal{E}_a^{\text{kinetic}} = 4\pi\int_{\mathbb{R}_\star}^{\mathbb{R}_0}\frac{3}{2}k\mathbb{T}_\star n_\star\left(\frac{\mathbb{R}_\star}{r}\right)^{10} r^2\mathrm{d}r \approx \frac{3}{7}\left(\frac{3}{2}k\mathbb{T}_\star\mathbb{N}_\star\right) \tag{59}$$

The total kinetic energy of plasma particles

$$\mathcal{E}^{\text{kinetic}} = \mathcal{E}_\star^{\text{kinetic}} + \mathcal{E}_a^{\text{kinetic}} = \frac{15}{7}k\mathbb{T}_\star\mathbb{N}_\star \tag{60}$$

## 4.8. The Potential Energy of Star Plasma

Inside a star core, the gravity force is balanced by the force of electric nature. Correspondingly, the energy of electric polarization can be considered as balanced by the gravitational energy of plasma. As a result, the potential energy of a core can be considered as equal to zero.

In a star atmosphere, this balance is absent.

The gravitational energy of an atmosphere

$$\mathcal{E}_a^G = -4\pi G\mathbb{M}_\star\frac{A}{Z}m_p n_\star\int_{\mathbb{R}_\star}^{\mathbb{R}_0}\frac{1}{2}\left[2-\left(\frac{\mathbb{R}_\star}{r}\right)^3\right]\left(\frac{\mathbb{R}_\star}{r}\right)^6 r\mathrm{d}r \tag{61}$$

or

$$\mathcal{E}_a^G = \frac{3}{2}\left(\frac{1}{7}-\frac{1}{2}\right)\frac{G\mathbb{M}_\star^2}{\mathbb{R}_\star} = -\frac{15}{28}\frac{G\mathbb{M}_\star^2}{\mathbb{R}_\star} \tag{62}$$

The electric energy of atmosphere is

$$\mathcal{E}_a^E = -4\pi\int_{\mathbb{R}_\star}^{R_0}\frac{1}{2}\rho\varphi r^2\mathrm{d}r, \tag{63}$$

where

$$\tilde{\varrho} = \frac{1}{3r^2}\frac{\mathrm{d}\mathfrak{P}r^2}{\mathrm{d}r} \tag{64}$$

and

$$\tilde{\varphi} = \frac{4\pi}{3}\mathfrak{P}r. \tag{65}$$

The electric energy:

$$\mathcal{E}_a^E = -\frac{3}{28}\frac{G\mathbb{M}_\star^2}{\mathbb{R}_\star}, \tag{66}$$

and total potential energy of atmosphere:

$$\mathcal{E}_a^{\text{potential}} = \mathcal{E}_a^G + \mathcal{E}_a^E = -\frac{9}{14}\frac{G\mathbb{M}_\star^2}{\mathbb{R}_\star}. \tag{67}$$

The equilibrium in a star depends both on plasma energy and energy of radiation.

## 4.9. The Temperature of a Star Core

### 4.9.1. The Energy of the Black Radiation

The energy of black radiation inside a star core is

$$\mathcal{E}_\star(br)=\frac{\pi^2}{15}k\mathbb{T}_\star\left(\frac{\mathbb{R}_\star}{\hbar c}\right)^3\mathbb{V}_\star. \tag{68}$$

The energy of black radiation inside a star atmosphere is

$$\mathcal{E}_a(br)=4\pi\int_{R_\star}^{R_0}\frac{\pi^2}{15}k\mathbb{T}_\star\left(\frac{k\mathbb{T}_\star}{\hbar c}\right)^3\left(\frac{\mathbb{R}_\star}{r}\right)^{16}r^2\mathrm{d}r=\frac{3}{13}\frac{\pi^2}{15}k\mathbb{T}_\star\left(\frac{k\mathbb{T}_\star}{\hbar c}\right)^3\mathbb{V}_\star. \tag{69}$$

The total energy of black radiation inside a star is

$$\mathcal{E}(br)=\mathcal{E}_\star(br)+\mathcal{E}_a(br)=\frac{16}{13}\frac{\pi^2}{15}kT_\star\left(\frac{kT_\star}{\hbar c}\right)^3V_\star=1.23\frac{\pi^2}{15}kT_\star\left(\frac{kT_\star}{\hbar c}\right)^3V_\star \tag{70}$$

#### 4.9.2. The Full Energy of a Star

In accordance with Equation (57), the full energy of a star

$$\mathcal{E}^{\text{star}}=-\mathcal{E}^{\text{kinetic}}+\mathcal{E}(br) \tag{71}$$

*i.e.*

$$\mathcal{E}^{\text{star}}=-\frac{15}{7}k\mathbb{T}_\star\mathbb{N}_\star+\frac{16}{13}\frac{\pi^2}{15}k\mathbb{T}_\star\left(\frac{k\mathbb{T}_\star}{\hbar c}\right)^3\mathbb{V}_\star. \tag{72}$$

The steady state of a star is determined by a minimum of its full energy:

$$\left(\frac{\mathrm{d}\mathcal{E}^{\text{star}}}{\mathrm{d}\mathbb{T}_\star}\right)_{\mathbb{N}=const,\mathbb{V}=const}=0, \tag{73}$$

it corresponds to the condition:

$$-\frac{15}{7}\mathbb{N}_\star+\frac{64\pi^2}{13\times15}\left(\frac{k\mathbb{T}_\star}{\hbar c}\right)^3\mathbb{V}_\star=0. \tag{74}$$

Together with Equation (21) it defines the equilibrium temperature of a star core:

$$\mathbb{T}_\star=\left(\frac{25\times13}{28\pi^4}\right)^{1/3}\left(\frac{\hbar c}{ka_B}\right)Z\approx Z\times2.13\times10^7\ \mathrm{K} \tag{75}$$

### 4.10. Main Parameters

#### 4.10.1. The Star Mass

The virial theorem connect kinetic energy of a system with its potential energy. In accordance with Equations (67) and (60)

$$\frac{9}{14}\frac{G\mathbb{M}_\star^2}{\mathbb{R}_\star}=\frac{30}{7}k\mathbb{T}_\star\mathbb{N}_\star. \tag{76}$$

Introducing the non-dimensional parameter

$$\eta=\frac{G\mathbb{M}_\star\dfrac{A}{Z}m_p}{\mathbb{R}_\star k\mathbb{T}_\star}, \tag{77}$$

we obtain

$$\eta=\frac{20}{3}=6.67, \tag{78}$$

and at taking into account Equations.(21) and (75), the core mass is

$$\mathbb{M}_{\star}=\left[\frac{20}{3}\left(\frac{25\times 13}{28}\right)^{1/3}\frac{3}{4\times 3.14}\right]^{3/2}\frac{\mathbb{M}_{Ch}}{\left(\frac{A}{Z}\right)^{2}}=6.84\frac{\mathbb{M}_{Ch}}{\left(\frac{A}{Z}\right)^{2}} \tag{79}$$

The obtained equation plays a very important role, because together with Equation (54), it gives a possibility to predict the total mass of a star:

$$\mathbb{M}=2\mathbb{M}_{\star}=\frac{13.68\mathbb{M}_{Ch}}{\left(\frac{A}{Z}\right)^{2}}\approx\frac{25.34\mathbb{M}_{\odot}}{\left(\frac{A}{Z}\right)^{2}}. \tag{80}$$

The comparison of obtained prediction Equation (80) with measuring data gives a method to check our theory. Although there is no way to determine chemical composition of cores of far stars, some predictions can be made in this way. At first, there must be no stars which masses exceed the mass of the Sun by more than one and a half orders, because it accords to limiting mass of stars consisting from hydrogen with $A/Z=1$. Secondly, the action of a specific mechanism [6] can make neutron-excess nuclei stable, but it don't give a base to suppose that stars with $A/Z>10$ (and with mass in hundred times less than hydrogen stars) can exist. Thus, the theory predicts that the whole mass spectrum must be placed in the interval from 0.25 up to approximately 25 solar masses. These predications are verified by measurements quite exactly. The mass distribution of binary stars[4] is shown in **Figure 1** [11].

It is important, that the mass spectrum of binary stars (**Figure 1**) consists of series of well-isolated lines which are representing the stars with integer values of ratios $A/Z=3,4,5,\cdots$, corresponding hydrogen-3,4,5 ... or helium-6,8,10 ... (also line with the half-integer ratio $A/Z=3/2$, corresponding, probably, to helium-3, Be-6, C-9...). The existence of stable stars with ratios $A/Z\geq 3$ raises questions. It is generally assumed that stars are composed of hydrogen-1, deuterium, helium-4 and other heavier elements with $A/Z\approx 2$. Nuclei with $A/Z\geq 3$ are the neutron-excess and so short-lived, that they can not build a long-lived stars. Neutron-excess nuclei can become stable under the action of mechanism of neutronization, which is acting inside the dwarfs. It is accepted to think that this mechanism must not work into the stars. The consideration of the effecting of the electron gas of a dense plasma on the nucleus is described in [6]. These calculations show that the electron gas of dense plasma should also lead to the neutronization mechanism and to the stabilization of the neutron-excess nuclei. This explains the existence of a stable of stars, where the plasma consists of nuclei with $A/Z\geq 3$.

At considering of (**Figure 1**), the question is arising: why there are so few stars, which are composed by very stable nuclei of helium-4? At the same time, there are many stars with $A/Z=4$, *i.e.* consisting apparently of a hydrogen-4, as well

[4]The use of these data is caused by the fact that only the measurement of parameters of binary star rotation gives a possibility to determine their masses with satisfactory accuracy.

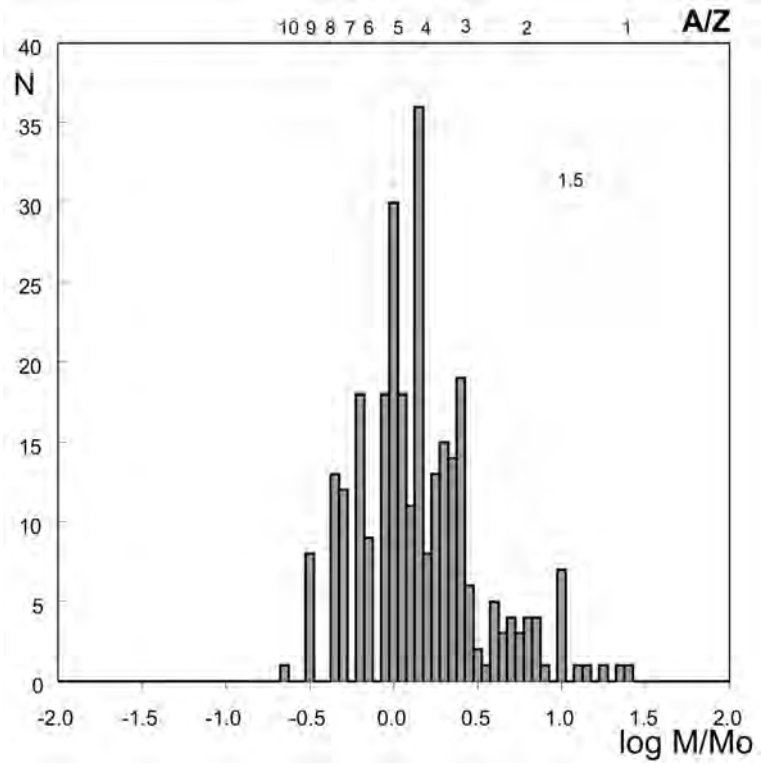


**Figure 1.** The mass distribution of binary stars [11]. On abscissa, the logarithm of the star mass over the Sun mass is shown. Solid lines mark masses, which agree with selected values of A/Z from Equation (80).

as stars with $A/Z = 3/2$, which hypothetically could be composed by another isotope of helium - helium-3. This equation is discussed in [6].

It is important to note, that according to Equation (80) the Sun must consist from a substance with $A/Z = 5$. This conclusion is in a good agreement with results of consideration of solar oscillations [5].

### 4.10.2. Radii of Stars

Using Equation (21) and Equation (79), we can determine the star core radius:

$$\mathbb{R}_{\star} = 1.42 \frac{a_B}{Z(A/Z)} \left( \frac{\hbar c}{G m_p^2} \right)^{1/2} \approx \frac{9.79 \times 10^{10}}{Z(A/Z)} \text{cm}. \tag{81}$$

The temperature near the star surface is relatively small. It is approximately by 3 orders smaller than it is inside the core. Because of it at calculation of surface parameters, we must take into consideration effects of this order, *i.e.* it is necessary to take into account the gravity action on the electron gas. At that it is convenient to consider the plasma cell as some neutral quasi-atom (like the Thomas-Fermi atom). Its electron shell is formed by a cloud of free electrons.

Each such quasi-atom is retained on the star surface by its negative potential energy

$$\left( \mathcal{E}_{\text{gravitational}} + \mathcal{E}_{\text{electric}} \right) < 0. \tag{82}$$

The electron cloud of the cell is placed in the volume $\delta V = \frac{4\pi}{3} r_s^3$, (where $r_s \approx \left(\frac{Z}{n_e}\right)^{1/3}$) under pressure $P_e$. The evaporation of plasma cell releases energy $\mathcal{E}_{PV} = P_e V_s$, and the balance equation takes the form:

$$\mathcal{E}_{\text{gravitational}} + \mathcal{E}_{\text{electric}} + \mathcal{E}_{PV} = 0. \tag{83}$$

In cold plasma, the electron cloud of the cell has energy $\mathcal{E}_{PV} \approx e^2 n_e^{1/3}$. In very hot plasma at $kT \gg \frac{Z^2 e^2}{r_s}$, this energy is equal to $\mathcal{E}_{PV} = \frac{3}{2} ZkT$. On the star surface these energies are approximately equal:

$$\frac{k\mathbb{T}_0}{e^2 n_e^{1/3}} \approx \frac{1}{\alpha}\left(\frac{\mathbb{R}_0}{\mathbb{R}_\star}\right)^2 \approx 1. \tag{84}$$

One can show it easily, that in this case

$$\mathcal{E}_{PV} \approx 2Z\sqrt{\frac{3}{2} kT \cdot e^2 n_e^{1/3}}. \tag{85}$$

And if to take into account Equations (51)-(52), we obtain

$$\mathcal{E}_{PV} \approx 1.5 Zk\mathbb{T}_\star \left(\frac{\mathbb{R}_\star}{\mathbb{R}_0}\right)^3 \sqrt{\alpha\pi} \tag{86}$$

The energy of interaction of a nucleus with its electron cloud does not change at evaporation of the cell and it can be neglected. Thus, for the surface

$$\mathcal{E}_{\text{electric}} = \frac{2\pi\mathfrak{P}^2}{3n_s} = \frac{2G\mathbb{M}_\star}{\mathbb{R}_0}\left(Am_p - Zm_e\right). \tag{87}$$

The gravitational energy of the cell on the surface

$$\mathcal{E}_{\text{gravitational}} = -\frac{2G\mathbb{M}_\star}{\mathbb{R}_0}\left(Am_p + Zm_e\right). \tag{88}$$

Thus, the balance condition Equation (83) on the star surface obtains the form

$$-\frac{4G\mathbb{M}_\star Zm_e}{\mathbb{R}_0} + 1.5 Zk\mathbb{T}_\star \left(\frac{\mathbb{R}_\star}{\mathbb{R}_0}\right)^3 \sqrt{\alpha\pi} = 0. \tag{89}$$

### 4.10.3. The $\mathbb{R}_\star/\mathbb{R}_0$ Ratio and $\mathbb{R}_0$

With account of Equation (52) and Equations (78)-(77), we can write

$$\frac{\mathbb{R}_0}{\mathbb{R}_\star} = \left(\frac{\sqrt{\alpha\pi}}{2\eta}\frac{A}{Z}\frac{m_p}{m_e}\right)^{1/2} \approx 4.56\sqrt{\frac{A}{Z}} \tag{90}$$

As the star core radius is known Equation (81), we can obtain the star surface radius:

$$\mathbb{R}_0 \approx \frac{4.46\times 10^{11}}{Z\left(A/Z\right)^{1/2}} \text{cm}. \tag{91}$$

#### 4.10.4. The Temperature of a Star Surface

At known Equation (52) and Equation (75), we can calculate the temperature of external surface of a star

$$\mathbb{T}_0 = \mathbb{T}_\star \left( \frac{\mathbb{R}_\star}{\mathbb{R}_0} \right)^4 \approx 4.92 \times 10^5 \frac{Z}{\left( A/Z \right)^2} \tag{92}$$

#### 4.10.5. The Comparison with Measuring Data

The mass spectrum (**Figure 1**) shows that the Sun consists basically from plasma with $A/Z = 5$. The radius of the Sun and its surface temperature are functions of $Z$ too. This values calculated at $A/Z = 5$ and differen $Z$ are shown in **Table 1**.

One can see that these calculated data have a satisfactory agreement the measured radius of the Sun

$$\mathbb{R}_\odot = 6.96 \times 10^{10} \text{ cm} \tag{93}$$

and the measured surface temperature

$$\mathbb{T}_\odot = 5850 \text{ K} \tag{94}$$

at $Z = 3$.

The calculation shows that the mass of core of the Sun

$$\mathbb{M}_\star \left( Z = 3, A/Z = 5 \right) \approx 9.68 \times 10^{32} \text{ g} \tag{95}$$

i.t. almost exactly equals to one half of full mass of the Sun

$$\frac{\mathbb{M}_\star \left( Z = 3, A/Z = 5 \right)}{\mathbb{M}_\odot} \approx 0.486 \tag{96}$$

in full agreement with Equation (54).

In addition to obtained determinations of the mass of a star Equation (80), its temperature Equation (92) and its radius Equation (91) give possibility to check the calculation, if we compare these results with measuring data. Really, dependencies measured by astronomers can be described by functions:

$$\mathbb{M} = \frac{Const_1}{\left( A/Z \right)^2}, \tag{97}$$

$$\mathbb{R}_0 = \frac{Const_2}{Z \left( A/Z \right)^{1/2}}, \tag{98}$$

**Table 1.** The calculated stellar parameters.

| $Z$ | $\mathbb{R}_\odot$, cm (calculated (91)) | $\mathbb{T}_\odot$, K (calculated (92)) |
|---|---|---|
| 1 | $2.0 \times 10^{11}$ | 1961 |
| 2 | $1.0 \times 10^{11}$ | 3923 |
| 3 | $6.65 \times 10^{10}$ | 5885 |
| 4 | $5.0 \times 10^{10}$ | 7845 |

$$\mathbb{T}_0 = \frac{Const_3 Z}{\left(A/Z\right)^2}. \tag{99}$$

If to combine they in the way, to exclude unknown parameter $Z$, one can obtain relation:

$$\mathbb{T}_0 \mathbb{R}_0 = Const \mathbb{M}^{5/4} \tag{100}$$

Its accuracy can by checked. For this checking, let us use the measuring data of parameters of masses, temperatures and radii of close binary stars [12] (see [6]). The results of these measurements are shown in **Figure 2**, where the dependence according to Equation (100). It is not difficult to see that these data are well described by the calculated dependence. It speaks about successfulness of our consideration.

## 5. The Thermodynamic Relations of Intra-Stellar Plasma

### 5.1. The Thermodynamic Relation of Star Atmosphere Parameters

Hot stars steadily generate energy and radiate it from their surfaces. This is non-equilibrium radiation in relation to a star. But it may be a stationary radiation for a star in steady state. Under this condition, the star substance can be considered as an equilibrium. This condition can be considered as quasi-adiabatic, because the interchange of energy between both subsystems—radiation and substance—is stationary and it does not result in a change of entropy of substance. Therefore, at consideration of state of a star atmosphere, one can base it on equilibrium conditions of hot plasma and the ideal gas law for adiabatic condition can be used for it in the first approximation.

It is known, that thermodynamics can help to establish correlation between steady-state parameters of a system. Usually, the thermodynamics considers systems at an equilibrium state with constant temperature, constant particle density and constant pressure over all system. The characteristic feature of the considered system is the existence of equilibrium at the absence of a constant temperature and particle density over atmosphere of a star. To solve this problem, one can introduce averaged pressure

$$\hat{P} \approx \frac{G\mathbb{M}^2}{\mathbb{R}_0^4}, \tag{101}$$

averaged temperature

$$\hat{T} = \frac{\int_{\mathbb{V}} T \mathrm{d}V}{V} \sim \mathbb{T}_0 \left( \frac{\mathbb{R}_0}{\mathbb{R}_\star} \right) \tag{102}$$

and averaged particle density

$$\hat{n} \approx \frac{\mathbb{N}_A}{\mathbb{R}_0^3} \tag{103}$$

After it by means of thermodynamical methods, one can find relation between parameters of a star.

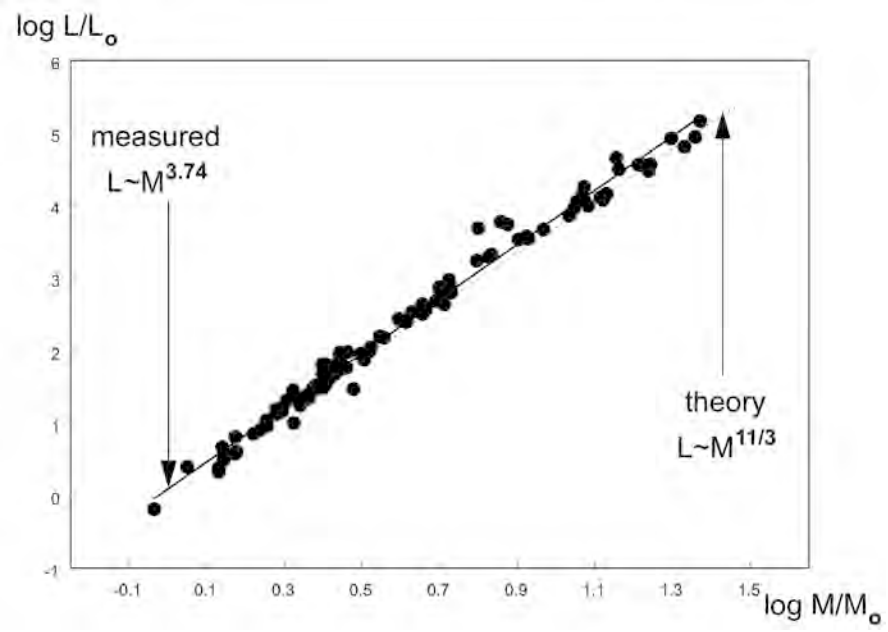


**Figure 2.** The relation between main parameters of stars (Equation (100)) and corresponding data of astronomical measurements for close binary stars are shown. These astronomical data were collected for the first time by K.F. Khaliullinin in his dissertation [12] (in Russian) and with his permission is republished in [6].

### 5.1.1. The $c_P/c_V$ Ratio

At a movement of particles according to the theorem of the equidistribution, the energy $kT/2$ falls at each degree of freedom. It gives the heat capacity $c_v = 3/2k$.

According to the virial theorem [7] [8], the full energy of a star should be equal to its kinetic energy (with opposite sign), so as full energy related to one particle

$$\mathcal{E} = -\frac{3}{2}kT \tag{104}$$

In this case the heat capacity at constant volume (per particle over Boltzman's constant $k$) by definition is

$$c_V = \left(\frac{\mathrm{d}E}{\mathrm{d}T}\right)_V = -\frac{3}{2} \tag{105}$$

The negative heat capacity of stellar substance is not surprising. It is a known fact and it is discussed in Landau-Lifshitz course [7]. The own heat capacity of each particle of star substance is positive. One obtains the negative heat capacity at taking into account the gravitational interaction between particles.

By definition the heat capacity of an ideal gas particle at permanent pressure [7] is

$$c_P = \left(\frac{\mathrm{d}W}{\mathrm{d}T}\right)_P, \tag{106}$$

where $W$ is enthalpy of a gas.

As for the ideal gas [7]

$$W - \mathcal{E} = NkT, \tag{107}$$

and the difference between $c_P$ and $c_V$

$$c_P - c_V = 1. \tag{108}$$

Thus in the case considered, we have

$$c_P = -\frac{1}{2}. \tag{109}$$

Supposing that conditions are close to adiabatic ones, we can use the equation of the Poisson's adiabat.

### 5.1.2. The Poisson's Adiabat

The thermodynamical potential of a system consisting of $N$ molecules of ideal gas at temperature $T$ and pressure $P$ can be written as [7]:

$$\Phi = const \cdot N + NT \ln P - Nc_P T \ln T. \tag{110}$$

The entropy of this system

$$S = const \cdot N - N \ln P + Nc_P \ln T. \tag{111}$$

As at adiabatic process, the entropy remains constant

$$-NT \ln P + Nc_P T \ln T = const, \tag{112}$$

we can write the equation for relation of averaged pressure in a system with its volume (The Poisson's adiabat) [7]:

$$\hat{P} V^{\tilde{\gamma}} = const, \tag{113}$$

where $\tilde{\gamma} = \frac{c_P}{c_V}$ is the exponent of adiabatic constant. In considered case taking into account of Equations.(106) and (105), we obtain

$$\tilde{\gamma} = \frac{c_P}{c_V} = \frac{1}{3}. \tag{114}$$

As $V^{1/3} \sim \mathbb{R}_0$, we have for equilibrium condition

$$\hat{P} \mathbb{R}_0 = const. \tag{115}$$

## 5.2. The Mass-Radius Ratio

Using Equation (101) from Equation (115), we use the equation for dependence of masses of stars on their radii:

$$\frac{\mathbb{M}^2}{\mathbb{R}_0^3} = const \tag{116}$$

This equation shows the existence of internal constraint of chemical parameters of equilibrium state of a star. Indeed, the substitution of obtained determinations Equation (91) and (92)) into Equation (116) gives:

$$Z \sim \left(A/Z\right)^{5/6} \tag{117}$$

Simultaneously, the observational data of masses, of radii and their temperatures

was obtained by astronomers for close binary stars [12]. The dependence of radii of these stars over these masses is shown in **Figure 3** on double logarithmic scale. The solid line shows the result of fitting of measurement data $\mathbb{R}_0 \sim \mathbb{M}^{0.68}$. It is close to theoretical dependence $\mathbb{R}_0 \sim \mathbb{M}^{2/3}$ (Equation (116)) which is shown by dotted line.

If parameters of the star are expressed through corresponding solar values $\rho \equiv \frac{\mathbb{R}_0}{\mathbb{R}_\odot}$ and $\mu \equiv \frac{\mathbb{M}}{\mathbb{M}_\odot}$, that Equation (116) can be rewritten as

$$\frac{\rho}{\mu^{2/3}} = 1. \tag{118}$$

Numerical values of relations $\frac{\rho}{\mu^{2/3}}$ for close binary stars are obtained from Table [12] (see [6]).

### 5.3. The Mass-Temperature and Mass-Luminosity Relations

Taking into account Equations (52), (25) and (42) one can obtain the relation between surface temperature and the radius of a star

$$\mathbb{T}_0 \sim \mathbb{R}_0^{7/8}, \tag{119}$$

or accounting for Equation (116)

$$\mathbb{T}_0 \sim \mathbb{M}^{7/12} \tag{120}$$

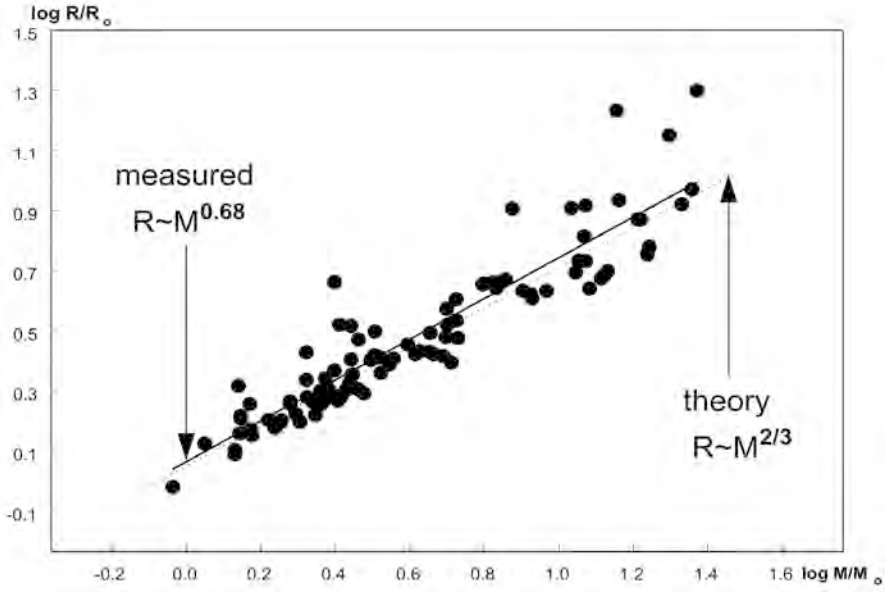


**Figure 3.** The dependence of radii of stars over the star mass. Here the radius of stars is normalized to the sunny radius, the stars masses are normalized to the mass of the Sum. The data are shown on double logarithmic scale. The solid line shows the result of fitting of measurement data $\mathbb{R}_0 \sim \mathbb{M}^{0.68}$. The theoretical dependence $\mathbb{R}_0 \sim \mathbb{M}^{2/3}$ (Equation (116)) is shown by the dotted line. These astronomical data were collected for the first time by K.F. Khaliullinin in his dissertation [12] (in Russian) and with his permission is republished in [6].

The dependence of the temperature on the star surface over the star mass of close binary stars [6] [12] is shown in **Figure 4**. Here the temperatures of stars are normalized to the sunny surface temperature (5875 C), the stars masses are normalized to the mass of the Sum. The data are shown on double logarithmic scale. The solid line shows the result of fitting of measurement data ( $\mathbb{T}_0 \sim \mathbb{M}^{0.59}$ ). The theoretical dependence $\mathbb{T}_0 \sim \mathbb{M}^{7/12}$ (Equation (120)) is shown by dotted line.

If parameters of the star are expressed through corresponding solar values $\tau \equiv \frac{\mathbb{T}_0}{\mathbb{T}_\odot}$ and $\mu \equiv \frac{\mathbb{M}}{\mathbb{M}_\odot}$, that Equation (120) can be rewritten as

$$\frac{\tau}{\mu^{7/12}} = 1. \tag{121}$$

Numerical values of relations $\frac{\tau}{\mu^{7/12}}$ for close binary stars are shown in the last table of [6].

The analysis of these data leads to few conclusions. The averaging over all tabulated stars gives

$$\left\langle \frac{\tau}{\mu^{7/12}} \right\rangle = 1.007 \pm 0.07. \tag{122}$$

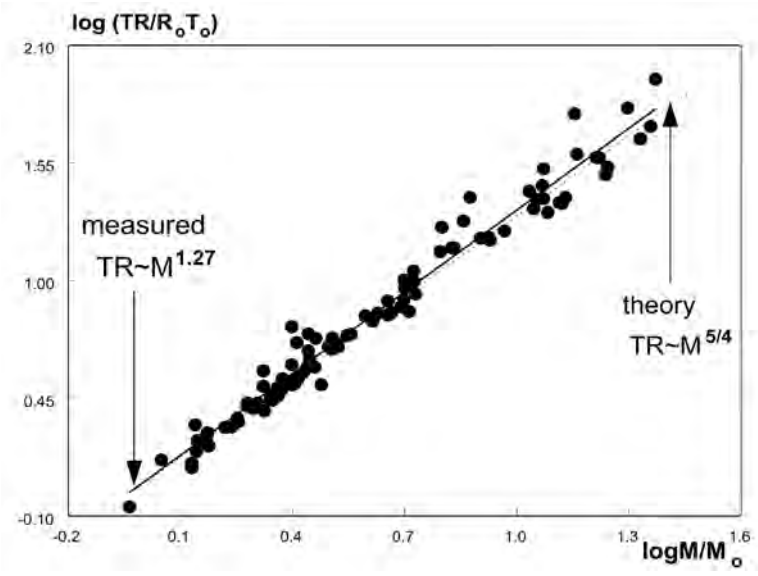


**Figure 4.** The dependence of the temperature on the star surface over the star mass of close binary stars. Here the temperatures of stars are normalized to surface temperature of the Sun (5875 C), the stars masses are normalized to the mass of Sum. The data are shown on double logarithmic scale. The solid line shows the result of fitting of measurement data ( $\mathbb{T}_0 \sim \mathbb{M}^{0.59}$ ). The theoretical dependence $\mathbb{T}_0 \sim \mathbb{M}^{7/12}$ (Equation (120)) is shown by dotted line. These astronomical data were collected for the first time by K.F. Khaliullinin in his dissertation [12] (in Russian) and with his permission is republished in [6].

and we can conclude that the variability of measured data of surface temperatures and stellar masses has statistical character. Secondly, Equation (121) is valid for all hot stars (exactly for all close binary stars).

The problem with the averaging of $\frac{\rho}{\mu^{2/3}}$ looks different. There are a few of giants and super-giants in this Table. The values of ratio $\frac{\rho}{\mu^{2/3}}$ are more than 2 for them. It seems that, if to exclude these stars from consideration, the averaging over stars of the main sequence gives value close to 1. Evidently, it needs in more detail consideration.

The luminosity of a star

$$\mathbb{L}_0 \sim \mathbb{R}_0^2 \mathbb{T}_0^4. \tag{123}$$

at taking into account (Equation (116)) and (Equation (120)) can be expressed as

$$\mathbb{L}_0 \sim \mathbb{M}^{11/3} \sim \mathbb{M}^{3.67} \tag{124}$$

This dependence is shown in **Figure 5**.

It can be seen that all calculated interdependencies $\mathbb{R}(\mathbb{M})$, $\mathbb{T}(\mathbb{M})$ and $\mathrm{L}(\mathbb{M})$ show a good qualitative agreement with the measuring data. At that it is important, that the quantitative explanation of mass-luminosity dependence discovered at the beginning of 20th century is obtained.

## The Compilation of the Results of Calculations

Let us put together the results of calculations. It is energetically favorable for the star to be divided into two volumes: the core is located in the central area of the star and the atmosphere is surrounding it from the outside (**Figure 6**).

The core has the radius:

$$\mathbb{R}_\star = 2.08 \frac{a_B}{Z(A/Z)} \left( \frac{\hbar c}{G m_p^2} \right)^{1/2} \approx \frac{1.41 \times 10^{11}}{Z(A/Z)} \text{cm}. \tag{125}$$

It is roughly equal to 1/10 of the stellar radius.

At that the mass of the core is equal to

$$\mathbb{M}_\star = 6.84 \frac{\mathbb{M}_{Ch}}{\left( \frac{A}{Z} \right)^2}. \tag{126}$$

It is almost exactly equal to one half of the full mass of the star.

The plasma inside the core has the constant density

$$n_\star = \frac{16}{9\pi} \frac{Z^3}{a_B^3} \approx 1.2 \times 10^{24} Z^3 \text{ cm}^{-3} \tag{127}$$

and constant temperature

$$\mathbb{T}_\star = \left( \frac{25 \times 13}{28\pi^4} \right)^{1/3} \left( \frac{\hbar c}{k a_B} \right) Z \approx Z \times 2.13 \times 10^7 \text{ K}. \tag{128}$$

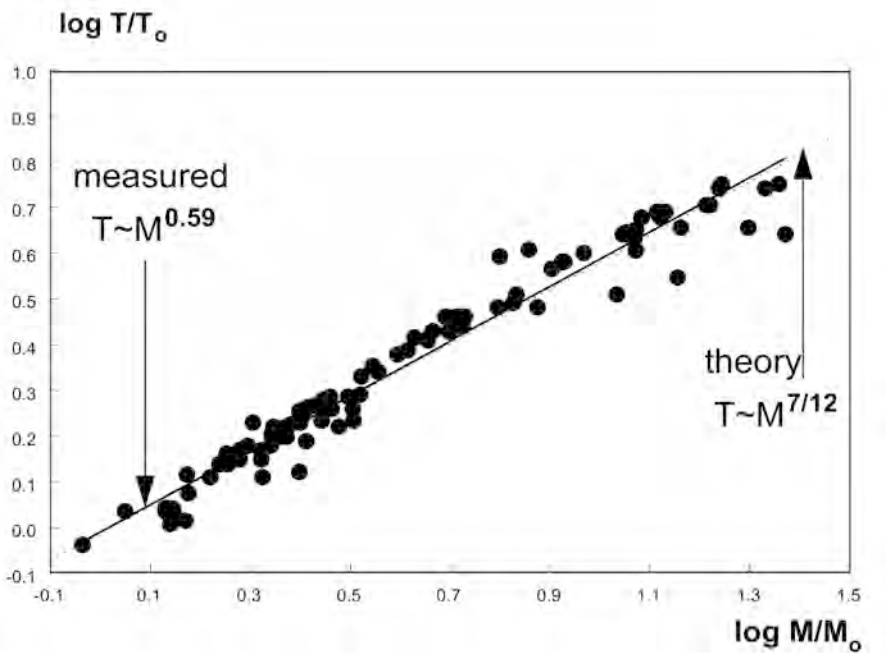


**Figure 5.** The dependence of star luminosity on the star mass of close binary stars. The luminosities are normalized to the luminosity of the Sun, the stars masses are normalized to the mass of the Sum. The data are shown on double logarithmic scale. The solid line shows the result of fitting of measurement data $\mathbb{L} \sim \mathbb{M}^{3.74}$. The theoretical dependence $\mathbb{L} \sim \mathbb{M}^{11/3}$ (Equation (124)) is shown by dotted line. These astronomical data were collected for the first time by K.F. Khaliullinin in his dissertation [12] (in Russian) and with his permission is republished in [6].

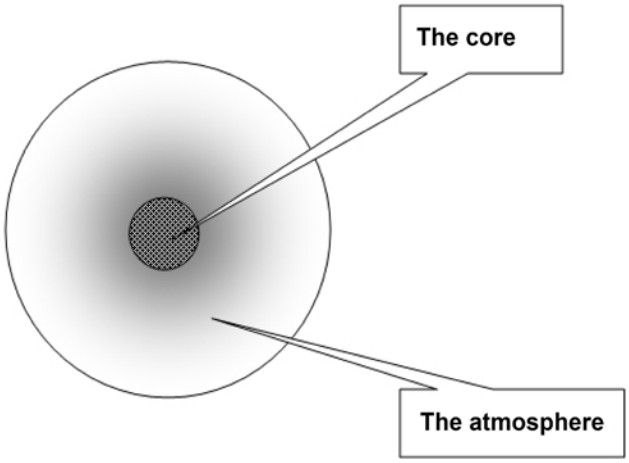


**Figure 6.** The schematic of the star interior.

The plasma density and its temperature are decreasing at an approaching to the stellar surface:

$$n_e(r) = n_\star \left( \frac{\mathbb{R}_\star}{r} \right)^6 \tag{129}$$

and

$$T_r = \mathbb{T}_\star \left( \frac{\mathbb{R}_\star}{r} \right)^4 . \tag{130}$$

The external radius of the star is determined as

$$\mathbb{R}_0 = \left( \frac{\sqrt{\alpha\pi}}{2\eta} \frac{A}{Z} \frac{m_p}{m_e} \right)^{1/2} \mathbb{R}_\star \approx \frac{6.44 \times 10^{11}}{Z\left(A/Z\right)^{1/2}} \text{cm} \tag{131}$$

and the temperature on the stellar surface is equal to

$$\mathbb{T}_0 = \mathbb{T}_\star \left( \frac{\mathbb{R}_\star}{\mathbb{R}_0} \right)^4 \approx 4.92 \times 10^5 \frac{Z}{\left(A/Z\right)^2} \tag{132}$$

### 5.4. About 《Black Holes》

It seems that the idea about the 《black holes》 existence is organic related to the suggestion about an inevitable collapse of large cosmic bodies on the last stage of their evolutions. However, the models of collapsing masses were appearing as a consequence of the rejection from attention of the gravity induced electric polarization of the intra-stellar plasma. At a thermal energy lowering, the gravitational contraction of cooling star is balanced by a counteraction of electrically polarized plasma. If to take into account this mechanism, the possibility of collapse must be excludes.

It allows newly to take a look on the 《black hole》 problem.

In accordance with the standard approach, the Schwarzshield radius of 《black hole》 with mass $M_{bh}$ is

$$r_{bh} = \frac{2GM_{bh}}{c^2} \tag{133}$$

and accordingly the average density of 《black holes》:

$$\gamma_{bh} = \frac{3c^6}{32\pi M_{bh}^2 G^3}. \tag{134}$$

The estimations are showing that all large inwardly-galactic objects of all classes—stars, dwarves, pulsars, giants—possess the mass of the order $M_{Ch}$ (or $10M_{Ch}$). As the density of these objects are small relatively to the limit Equation (134). As result, a searching of 《black hole》 inside stellar objects of our Galaxy seems as hopeless.

On the other hand, stellar objects, consisting of hot relativistic plasma—a quasars, in accordance with their mass and density, may stay 《black holes》. The process of collapse is not needed for their creation. As the quasar mass $M_{qu} \gg M_{Ch}$, all other stellar objects must organize their moving around it and one can suppose that a 《black hole》 can exist at the center of our Galaxy.

## 6. Conclusions

Evidently, the main conclusion from the above consideration consists in statement of the fact that now there are quite enough measuring data to place

the theoretical astrophysics on a reliable foundation. All above measuring data are known for a relatively long time. The traditional system of view based on the Euler equation in the form Equation (1) could not give a possibility to explain and even to consider with due proper attention to these data. Taking into account the gravity induced electric polarization of plasma and a change starting postulate gives a possibility to obtain results for explanation of measuring data considered above.

Basically these results are the following.

Using the standard method of plasma description leads to the conclusion that at conditions characteristic for the central stellar region, the plasma has the minimum energy at constant density $n_\star$ and at the constant temperature $\mathbb{T}_\star$.

This plasma forms the core of a star, where the pressure is constant and gravity action is balanced by the force of the gravity induced by the electric polarization. The virial theorem gives a possibility to calculate the stellar core mass $\mathbb{M}_\star$ and its radius $\mathbb{R}_\star$. At that the stellar core volume is approximately equal to 1/1000 part of full volume of a star.

The remaining mass of a star located over the core has a density approximately thousand times smaller and it is convenient to name it a star atmosphere. At using thermodynamical arguments, it is possible to obtain the radial dependence of plasma density inside the atmosphere $n_a \approx r^{-6}$ and the radial dependence of its temperature $\mathbb{T}_a \approx r^{-4}$.

It gives a possibility to conclude that the mass of the stellar atmosphere $\mathbb{M}_a$ is almost exactly equal to the stellar core mass.Thus, the full stellar mass can be calculated. It depends on the ratio of the mass and the charge of nuclei composing the plasma. This claim is in a good agreement with the measuring data of the mass distribution of binary stars (and close binary stars too).[5] At that it is important that the upper limit of masses of both binary stars and close binary stars is in accordance with the calculated value of the mass of the hydrogen star. The obtained formula explains the origin of sharp peaks of stellar mass distribution. They evidence that the substance of these stars has a certain value of the ratio $A/Z$. In particular, the solar plasma consists of nuclei with $A/Z = 5$.

Knowing temperature and substance density on the core and knowing their radial dependencies, it is possible to estimate the surface temperature $\mathbb{T}_0$ and the radius of a star $\mathbb{R}_0$. It turns out that these measured parameters must be related to the star mass with the ratio $\mathbb{T}_0\mathbb{R}_0 \sim \mathbb{M}^{5/4}$. It is in a good agreement with measuring data.

Using another thermodynamical relation—the Poisson's adiabat—gives a way to determine the relation between radii of stars and their masses $\mathbb{R}_0^3 \sim \mathbb{M}^2$, and between their surface temperatures and masses $\mathbb{T}_0 \sim \mathbb{M}^{5/7}$. It gives the quantitative explanation of the mass-luminosity dependence.

The model described above gives a quite satisfactory quantitative explanation

[5]The measurement of parameters of these stars has a satisfactory accuracy only.

to other astronomical data, such as seismic oscillations of the solar surface, magnetic fields of stars, etc. [5].

The concept of star evolution, including their collapse and "black hole" formation, is flawed.

## Conflicts of Interest

The author declares no conflicts of interest regarding the publication of this paper.

## References

[1] Vasiliev, B.V. (2001) *Nuovo Cimento B*, **116**, 617-634.

[2] Vasiliev, B.V. (1997) *Nuovo Cimento B*, **112**, 1361-1372.

[3] Vasiliev, B.V. (1996) *Nuovo Cimento B*, **110**, 381-389.

[4] Vasiliev, B. (2014) *Universal Journal of Physics and Application*, **2**, 257-262.

[5] Vasiliev, B. (2014) *Universal Journal of Physics and Application*, **2**, 284-301.

[6] Vasiliev, B. (2014) *Universal Journal of Physics and Application*, **2**, 228-243.

[7] Landau, L.D. and Lifshits, E.M. (1980) Statistical Physics. 3rd Edition, Vol. 1, Pergamon, Oxford.

[8] Vasiliev, B.V. and Luboshits, V.L. (1994) *Physics-Uspekhi*, **37**, 345. https://doi.org/10.1070/PU1994v037n04ABEH000018

[9] Leung, Y.C. (1984) Physics of Dense Matter. Science Press/World Scientific, Beijing and Singapore.

[10] Landau, L.D. and Lifshits, E.M. (1980) Electrodynamics of Condensed Matter. 3rd Edition, Vol. 1, Pergamon, Oxford.

[11] Heintz, W.D. (1978) Double Stars. In: *Geophysics and Astrophysics Monographs*, Vol. 15, Springer, Dordrecht. https://doi.org/10.1007/978-94-009-9836-0

[12] Khaliullin, K.F. (2004) Dissertation. Sternberg Astronomical Institute, Moscow.

Journal of Modern Physics, 2018, 9, 1935-1940
http://www.scirp.org/journal/jmp
ISSN Online: 2153-120X
ISSN Print: 2153-1196

# Flat Space Cosmology as a Model of Penrose's Weyl Curvature Hypothesis and Gravitational Entropy

**Eugene Terry Tatum**

760 Campbell Ln. Ste. 106 #161, Bowling Green, KY, USA
Email: ett@twc.com

**How to cite this paper:** Tatum, E.T. (2018) Flat Space Cosmology as a Model of Penrose's Weyl Curvature Hypothesis and Gravitational Entropy. *Journal of Modern Physics*, **9**, 1935-1940.
https://doi.org/10.4236/jmp.2018.910121

**Received:** July 2, 2018
**Accepted:** September 1, 2018
**Published:** September 4, 2018



## Abstract

FSC is shown to be an excellent model of Penrose's Weyl curvature hypothesis and his concept of gravitational entropy. The assumptions of FSC allow for the minimum entropy at the inception of the cosmic expansion and rigorously define a cosmological arrow of time. This is in sharp contrast to inflationary models, which appear to violate the second law of thermodynamics within the early universe. Furthermore, by virtue of the same physical assumptions applying at any cosmic time *t*, the perpetually-flat FSC model predicts the degree of scale invariance observed in the CMB anisotropy pattern, without requiring an explosive and exceedingly brief inflationary epoch. Penrose's concepts, as described in this paper, provide support for the idea that FSC models gravitational entropy and Verlinde's emergent gravity theory.

## Keywords

Flat Space Cosmology, Cosmology Theory, Gravitational Entropy, Weyl's Curvature Hypothesis, Black Holes, Cosmic Inflation, Cosmic Flatness, Cosmic Microwave Background

## 1. Introduction and Background

If the expanding universe follows the second law of thermodynamics, then the total cosmic entropy of each earlier epoch in time *must* have had a lower value. The various theories of cosmic inflation appear to ignore this stipulation, as detailed by Roger Penrose in his 2016 book entitled, *Fashion, Faith and Fantasy in the New Physics of the Universe* [1]. Penrose makes a convincing argument that the *gravitational* entropy state of the earliest universe (*i.e.*, *before* the supposed inflationary epoch at $10^{-37}$ to $10^{-32}$ second of cosmic time) must have been ex-

ceedingly low, even in comparison to the post-inflationary universe. This is in stark contrast to the belief on the part of inflationists that inflation "solves" the problem posed by an extremely chaotic (*i.e.*, high entropy) Big Bang quantum fluctuation event as a beginning of the universe. Yet, as Penrose points out, any such inflationary solution would be either a violation of the second law or an unnecessary solution to a non-existent problem (*i.e.*, that inflation began in a smooth flat patch of primordial space-time). So, in Penrose's view, a theory of cosmic inflation is either a violation of physics or, at best, completely unnecessary. Others have expressed similar concerns with inflationary theory, including one of its founders [2].

In 1979, before any theories of inflation were proposed, Penrose first addressed the tension between the remarkable apparent homogeneity and isotropy of the universe (also inherent in the FLRW model) and the second law requirement of extremely low beginning entropy. He introduced the concept of "gravitational entropy", wherein the ongoing clustering of stars and galaxies, and the formation of black holes, is in the direction of ever-greater total cosmic entropy. Thus, in stark contrast to the thermal entropy of a gas, the total entropy of a gravitating system can be considered to be lowest at its smallest scale and its most homogeneous gravitational state. In his "Weyl curvature hypothesis" [3], Penrose associates the lowest entropy state of the earliest universe with a vanishing Weyl curvature tensor. Thus, if one wishes to consider the theoretical possibility of a "Big Bang" from a singularity condition, under this hypothesis, the universe begins "free of independent gravitational degrees of freedom" [Penrose (2016), pages 371-374]. Operationally, one can consider this to be a "zero" gravitational entropy state with respect to any future positive gravitational entropy values of the expanding universe. This gravitational entropy concept is a key feature of the Flat Space Cosmology (FSC) model [4] and Erik Verlinde's "emergent gravity" (entropic gravity) theory [5] [6]. The concept of gravitational entropy also allows for a very tight FSC correlation with the observed anisotropy magnitude ($0.66 \times 10^{-5}$ dT/T) in the cosmic microwave background (CMB) [7].

The Weyl curvature hypothesis and the FSC model both provide for a cosmological arrow of time [8]. This is in contrast to the standard inflationary model, which has no effective means by which the law of entropy can be obeyed if the model starts with a highly chaotic and high entropy quantum fluctuation event.

One of the current sources of tension between the most recent CMB observations [9] and standard inflationary cosmology is the assertion of global cosmological spatial flatness and dark energy dominance. The assertion of flatness stipulates a Friedmann curvature $k$ term value of zero, while the assertion of dark energy dominance stipulates a small negative value to the $k$ term. *Both stipulations cannot be true at the same time!* Furthermore, while the near scale-invariance of the CMB power spectrum is commonly touted to be a validation of inflationary cosmology, scale invariance is even easier to explain in FSC. Scale invariance in a cosmological model essentially means that the same laws of physics apply to any

scale of the cosmological model. Thus, one would *expect* a large degree of self-similarity between adjacent cosmological epochs in a spatially-flat model in which the same set of basic assumptions is prescribed to occur at any cosmological time *t*. The following section presents the current five basic assumptions of FSC.

## 2. The Five Assumptions of FSC

FSC models the Hawking-Penrose conjecture that a smoothly-expanding cosmic system beginning from a singularity can be modeled *within the rules of general relativity* as a time-reversed black hole. Hence, the assumptions of FSC are as follows:

1) The cosmic model is an ever-expanding sphere such that the cosmic horizon always translates at speed of light $c$ with respect to its geometric center at all times *t*. The observer is operationally-defined to be at this geometric center at all times $t$.

2) The cosmic radius $R_t$ and total mass $M_t$ follow the Schwarzschild formula $R_t \cong 2GM_t/c^2$ at all times $t$.

3) The cosmic Hubble parameter is defined by $H_t \cong c/R_t$ at all times $t$.

4) Incorporating our cosmological scaling adaptation of Hawking's black hole temperature formula, at any radius $R_t$, cosmic temperature $T_t$ is inversely proportional to the geometric mean of cosmic total mass $M_t$ and the Planck mass $M_{pl}$. $R_{pl}$ is defined as twice the Planck length (*i.e.*, as the Schwarzschild radius of the Planck mass black hole). With subscript $t$ for any time stage of cosmic evolution and subscript $pl$ for the Planck scale epoch, and, incorporating the Schwarzschild relationship between $M_t$ and $R_t$,

$$\left.\begin{aligned} & k_B T_t \cong \frac{\hbar c^3}{8\pi G\sqrt{M_t M_{pl}}} \cong \frac{\hbar c}{4\pi\sqrt{R_t R_{pl}}} \\ & \begin{cases} M_t \cong \left(\dfrac{\hbar c^3}{8\pi G k_B T_t}\right)^2 \dfrac{1}{M_{pl}} & (\mathrm{A}) \\ R_t \cong \dfrac{1}{R_{pl}}\left(\dfrac{\hbar c}{4\pi k_B}\right)^2 \left(\dfrac{1}{T_t}\right)^2 & (\mathrm{B}) \\ R_t T_t^2 \cong \dfrac{1}{R_{pl}}\left(\dfrac{\hbar c}{4\pi k_B}\right)^2 & (\mathrm{C}) \\ t \cong \dfrac{R_t}{c} & (\mathrm{D}) \end{cases} \end{aligned}\right\} \quad (1)$$

5) Total entropy $S_t$ of the cosmic model follows the Bekenstein-Hawking black hole formula [10] [11], wherein $R_t$ is the cosmic radius at time $t$ and $L_p$ is the Planck length.

$$S_t \cong \frac{\pi R_t^2}{L_p^2} \quad (2)$$

These model assumptions correlate very closely with current observations, as

detailed in "Clues to the Fundamental Nature of Gravity, Dark Energy and Dark Matter" and "Temperature Scaling in Flat Space Cosmology in Comparison to Standard Cosmology" [Tatum, *et al.* (2018)]. It should be remembered that all five of these assumptions apply to every second of the FSC cosmological model. Hence, *scale invariance to the degree seen in the CMB anisotropy pattern is a prediction of FSC and must not be considered the exclusive domain of inflationary models*.

## 3. Perpetual Friedmann's Critical Density in FSC

As described in some detail in the seminal FSC papers [12] [13] [14] [15], the first three assumptions allow for perpetual Friedmann's critical density (*i.e.*, perpetual global spatial flatness) of the expanding FSC cosmological model from inception. By dividing the Schwarzschild mass (defined in terms of cosmic radius $R_o$) by the spherical volume, and substituting $c^2/R_o^2$ with $H_o^2$, Friedmann's critical mass density $\rho_0 = \frac{3H_0^2}{8\pi G}$ is achieved for any given moment of observation (hence the subscript "*o*") in cosmic time. So, *perpetual Friedmann's critical density* (*i.e., perpetual spatial flatness*) *from inception is a fundamental feature of the FSC model.* For example, the current observational *global* Hubble parameter $H_o$ value is calculated by the FSC model to be 66.89325791854758 km·s$^{-1}$·Mpc$^{-1}$, which fits the lower end range of the 2015 Planck Collaboration consensus observational value of 67.8 +/− 0.9 km·s$^{-1}$·Mpc$^{-1}$ (68% confidence interval), as shown in the FSC "Clues" paper in the July 2018 issue of *Journal of Modern Physics.*

## 4. Gravitational Entropy in FSC

FSC models the Hawking-Penrose conjecture that a smoothly-expanding cosmic system beginning from a singularity can be modeled *within the rules of general relativity* as a time-reversed black hole. Thus, assumption #5 defining FSC entropy by $S_t \cong \frac{\pi R_t^2}{L_p^2}$ at all times $t$ seems appropriate. As of yet, there appear to be no known scale limitations of a cosmological model which follows the above assumptions. And yet, each successively earlier stage of the FSC model *must* have a lower (gravitational) entropy value by virtue of the assumption that the entropy of a black hole scales according to $R^2$. Thus, it is shown by the above theoretical considerations and model assumptions that FSC is a model of Penrose's Weyl curvature hypothesis, his concept of gravitational entropy, and Verlinde's theory of emergent gravity.

## 5. Summary and Conclusions

FSC has been shown to be an excellent model of Penrose's Weyl curvature hypothesis and his concept of gravitational entropy. The assumptions of FSC allow for the minimum entropy at the inception of the cosmic expansion and rigo-

rously define a cosmological arrow of time. This is in sharp contrast to inflationary models, which appear to violate the second law of thermodynamics within the early universe. Furthermore, by virtue of the same physical assumptions applying at any cosmic time *t*, the perpetually-flat FSC model predicts the degree of scale invariance observed in the CMB anisotropy pattern, without requiring an explosive and exceedingly brief inflationary epoch. Penrose's concepts, as described in this paper, provide support for the idea that FSC models gravitational entropy and Verlinde's emergent gravity theory.

## Dedications and Acknowledgements

This paper is dedicated to Dr. Stephen Hawking and Dr. Roger Penrose for their groundbreaking work on black holes and their possible application to cosmology. Dr. Tatum also thanks Dr. Rudolph Schild of the Harvard Center for Astrophysics for his past support and encouragement.

## Conflicts of Interest

The authors declare no conflicts of interest regarding the publication of this paper.

## References

[1] Penrose, R. (2016) Fashion Faith and Fantasy in the New Physics of the Universe. Princeton University Press, Princeton, US. https://doi.org/10.1515/9781400880287

[2] Steinhardt, P.J. (2011) *Scientific American*, **304**, 18-25. https://doi.org/10.1038/scientificamerican0411-36

[3] Penrose, R. (1979) Singularities and Time-Asymmetry. In: Hawking, S.W. and Israel, W., Eds., *General Relativity*: *An Einstein Centenary Survey*, Cambridge University Press, Cambridge, 581-638.

[4] Tatum, E.T. and Seshavatharam, U.V.S. (2018) *Journal of Modern Physics*, **9**, 1469-1483. https://doi.org/10.4236/jmp.2018.98091

[5] Verlinde, E. (2010) On the Origin of Gravity and the Laws of Newton. arXiv:1001.0785v1 [hep-th].

[6] Verlinde, E. (2016) Emergent Gravity and the Dark Universe. aeXiv:1611.02269v2 [hep-th].

[7] Tatum, E.T. (2018) *Journal of Modern Physics*, **9**, 1484-1490. https://doi.org/10.4236/jmp.2018.98092

[8] Tatum, E.T. and Seshavatharam, U.V.S. (2018) *Journal of Modern Physics*, **9**, 1404-1414. https://doi.org/10.4236/jmp.2018.97085

[9] Planck Collaboration XIII. (2016) *Astronomy & Astrophysics*, **594**, A13.

[10] Bekenstein, J.D. (1974) *Physical Review D*, **9**, 3292-3300. https://doi.org/10.1103/PhysRevD.9.3292

[11] Hawking, S. (1976) *Physical Review D*, **13**, 191-197. https://doi.org/10.1103/PhysRevD.13.191

[12] Tatum, E.T., Seshavatharam, U.V.S. and Lakshminarayana, S. (2015) *International Journal of Astronomy and Astrophysics*, **5**, 116-124. https://doi.org/10.4236/ijaa.2015.52015

[13] Tatum, E.T., Seshavatharam, U.V.S. and Lakshminarayana, S. (2015) *Journal of Applied Physical Science International*, **4**, 18-26.

[14] Tatum, E.T., Seshavatharam, U.V.S. and Lakshminarayana, S. (2015) *Frontiers of Astronomy, Astrophysics and Cosmology*, **1**, 98-104.

[15] Tatum, E.T., Seshavatharam, U.V.S. and Lakshminarayana, S. (2015) *International Journal of Astronomy and Astrophysics*, **5**, 133-140. https://doi.org/10.4236/ijaa.2015.53017

Journal of Modern Physics, 2018, 9, 1941-1945
http://www.scirp.org/journal/jmp
ISSN Online: 2153-120X
ISSN Print: 2153-1196

# Cosmic Time as an Emergent Property of Cosmic Thermodynamics

**Eugene Terry Tatum[1], U. V. S. Seshavatharam[2]**

[1]760 Campbell Ln. Ste. 106 #161, Bowling Green, KY, USA
[2]Honorary Faculty, I-SERVE, S. No-42, Hitex Road, Hitech City, Hyderabad, India
Email: ett@twc.com, seshavatharam.uvs@gmail.com

**How to cite this paper:** Tatum, E.T. and Seshavatharam, U.V.S. (2018) Cosmic Time as an Emergent Property of Cosmic Thermodynamics. *Journal of Modern Physics*, **9**, 1941-1945.
https://doi.org/10.4236/jmp.2018.910122

**Received:** July 19, 2018
**Accepted:** September 1, 2018
**Published:** September 4, 2018



## Abstract

This paper, in conjunction with recent Flat Space Cosmology (FSC) publications, provides theoretical support for cosmic time being an emergent property of cosmic entropy and temperature. Therefore, if Verlinde's "emergent gravity" theory is correct, both time and gravity are most fundamentally emergent properties of cosmic thermodynamics. Since emergent properties within complex systems with a huge number of degrees of freedom are often not definable at the smallest scales, these results suggest that quantum time and quantum gravity may be no more definable than consciousness within two connecting neurons. String theorists now struggling to define quantum space-time and quantum gravity should bear this in mind.

## Keywords

Flat Space Cosmology, Cosmology Theory, Emergent Gravity, Dark Matter, Cosmic Entropy, Entropic Arrow of Time, Universal Temperature, Black Holes

## 1. Introduction and Background

A common dictionary definition of time is that it is "the measure of duration". However, this definition is somewhat unsatisfying, because "duration" is simply a synonym for "time". Einstein's definition of time as "what a clock measures" is correct, of course, but gets us no closer to a fundamental understanding of time. The difficulty with the philosophical question "What is time?" is that one cannot define time in a fundamental way using only words, because any word definition of time invariably must use another word which can only be defined in terms of time [1].

The only alternative to defining time in words is to use a more rigorous form

of symbolic logic, namely mathematics. Mathematics is essentially rigorous logic without the use of words, with the only exception to rigor being that some beginning set of assumptions ultimately derived from word logic is necessary as a starting point of any mathematical derivation. As proven in Godel's theorem, all mathematical systems must start with at least one unprovable assumption.

Aside from issues concerning starting assumptions, even with the use of mathematical equations, it is not necessarily easy to define time in a fundamental way. Every student of elementary physics learns the equation $vt = s$, where $v$ stands for velocity, $t$ stands for time, and $s$ stands for distance travelled. Algebraic rearrangement defines time by $t = s/v$ (*i.e.*, time as distance divided by velocity). However, this equation gets us no closer to a fundamental meaning of time than a word definition, because the physics definition of velocity can only be given in terms of time. When we search all other Gallilean and Newtonian physics equations incorporating a time symbol $t$, we invariably find at least one other variable within each equation which can only be defined in terms of time.

It was not until the 19$^{th}$ and early 20$^{th}$ centuries that time could be redefined in a non-Newtonian way. The first important breakthrough appears to have been Maxwell's discovery of a fundamental velocity (*i.e.*, speed of light $c$) which was entirely derivable from Faraday's laws of electromagnetism, *which did not incorporate a time variable!* Then, in 1905, Einstein conclusively proved that $c$ is a fundamental constant of nature which is completely unshackled from the Newtonian concept of absolute time, and the tautological time definitions that come with it.

Of even greater importance, for the purposes of this introduction, was Ludwig Boltzmann's concept of entropy, which also did not incorporate a time variable. Entropy allowed for a probabilistic, but inevitable, sequence progression (*i.e.*, *progressive change*) within highly complex systems with many degrees of freedom, including the cosmos itself. Unfortunately, Boltzmann didn't live long enough to see the potential cosmic consequences of his second law definition, because the universe in his day was widely believed to be infinite, eternal and unchanging.

It was not until Edwin Hubble's discovery of an expanding universe that Einstein and the rest of the scientific world recognized the importance of understanding universal parameters in terms of their fundamental relationship to cosmic time. This opened the way for thinking of cosmic time as being somehow deeply connected to cosmic entropy. The idea of a cosmic "entropic arrow of time" was seriously entertained, although, until recent developments, no one had any idea how to mathematically define cosmic entropy in terms of cosmic time, particularly for infinite universe theories or cosmic models with no definable finite horizon.

The recent developments began with the Bekenstein-Hawking definition of black hole entropy [2] [3] and its possible application to cosmological models according to

$$S_t \cong \frac{\pi R_t^2}{L_p^2} \tag{1}$$

wherein $S_t$ represents cosmic entropy at time $t$, $R_t$ represents the cosmic radius at time $t$, and $L_p$ represents the Planck length. Furthermore, the Hawking-Penrose conjecture that a universe smoothly expanding from a singularity could be modeled as a time-reversed black hole was another development. Such a model implies an ever-expanding, but definable and finite, cosmic horizon with a surface area which is directly proportional to the total entropy of the cosmic system at each point in cosmic time. Finally, the Flat Space Cosmology (FSC) model incorporated into spatially-flat universe Friedmann equations [4] completed this development using the inspiration of the Hawking-Penrose conjecture. The purpose of the current paper is to show how algebraic rearrangements from this July 2018 *Journal of Modern Physics* FSC paper may provide for a more fundamental understanding of cosmic time.

## 2. Results

An entropic arrow of cosmic time is rigorously defined in FSC according to the following equation

$$t \cong \left(\frac{L_p}{c\sqrt{\pi}}\right)\sqrt{S_t} \tag{2}$$

wherein $t$ represents cosmic time, $L_p$ represents the Planck length, $c$ is speed of light and $\sqrt{S}$ is the square root of Bekenstein-Hawking's entropy $S$ at time $t$ [see Equation (1)]. As detailed in the FSC references [4] and [5], Bekenstein-Hawking's entropy is a unitless ratio, and the correct-scaling entropy term in FSC is $\sqrt{S}$. The reason for this is simply that cosmic entropy in terms of $\sqrt{S}$ scales in exactly the same way as cosmic time $t$ (60.63 logs of 10 from the Planck scale). Furthermore, the FSC "Universal Temperature" $T_U$ scale [5], which is defined in a one-to-one correspondence to the Kelvin scale $T$ by $T_U = T^2$, scales *downward* from the Planck scale temperature by 60.63 logs of 10 as time scales *upward* from the Planck scale time by 60.63 logs of 10. This allows for a *thermodynamic arrow of time in the form of*

$$t \cong \left(\frac{\hbar L_p c^4}{32\pi^2 k_B^2 G}\right) T_U^{-1} \cong \left(\frac{\hbar L_p c^4}{32\pi^2 k_B^2 G}\right) T^{-2} \tag{3}$$

wherein $T_U$ and $T$ are defined as above and the other terms are well-known constants.

## 3. Discussion

The above FSC definitions of cosmic time are in terms of cosmic entropy $\sqrt{S}$, cosmic Universal Temperature $T_U$, and temperature $T$ in the Kelvin scale. Thus, in this cosmological model, *cosmic time appears to be fundamentally an emergent property of cosmic thermodynamics*. Furthermore, Erik Verlinde has re-

cently suggested very persuasively that gravity and its manifestations (including dark matter and dark energy) are also emergent properties of cosmic entropy [6] [7]. The paper entitled "Clues to the Fundamental Nature of Gravity, Dark Energy and Dark Matter" [Tatum, *et al.* (2018)] shows how FSC appears to be the cosmological model correlate to Verlinde's "emergent gravity" theory. Furthermore, as detailed in the July 2018 *Journal of Modern Physics* paper entitled "A Potentially Useful Dark Matter Index" [8], there now appear to be at least four recent observational studies [9] [10] [11] [12] in support of Verlinde's "emergent gravity" theory, particularly with respect to observations currently attributed to "dark matter." In addition, our own July 2018 *Journal of Modern Physics* paper entitled "Equivalence between a Gravity Field and an Unruh Acceleration Temperature Field as a Possible Clue to 'Dark Matter'" [13] provides further theoretical support for "dark matter" not actually being particulate in nature. Thus, it appears likely that additional persuasive evidence in support of Verlinde's "emergent gravity" theory will be forthcoming. For the time being, one must keep an open mind. However, if Verlinde's theory is correct, *both time and gravity are most fundamentally emergent properties of cosmic thermodynamics*.

## 4. Summary and Conclusions

The current paper, in conjunction with recent FSC publications, provides theoretical support for cosmic time being an emergent property of cosmic entropy and temperature. Therefore, if Verlinde's "emergent gravity" theory is correct, both time and gravity are most fundamentally emergent properties of cosmic thermodynamics. Since emergent properties within complex systems with a huge number of degrees of freedom are often not definable at the smallest scales, quantum time and quantum gravity may be no more definable than consciousness within two connecting neurons. String theorists now struggling to define quantum space-time and quantum gravity should bear this in mind.

## Dedications and Acknowledgements

Both authors dedicate this paper to the late Dr. Stephen Hawking and to Dr. Roger Penrose for their groundbreaking work on black holes and their possible application to cosmology. Dr. Tatum thanks Dr. Rudolph Schild of the Harvard Center for Astrophysics for his past support and encouragement. Author Seshavatharam UVS is indebted to professors Brahmashri M. Nagaphani Sarma, Chairman, Shri K. V. Krishna Murthy, founding Chairman, Institute of Scientific Research in Vedas (I-SERVE), Hyderabad, India, and to Shri K. V. R. S. Murthy, former scientist IICT (CSIR), Govt. of India, Director, Research and Development, I-SERVE, for their valuable guidance and great support in developing this subject.

## Conflicts of Interest

The authors declare no conflicts of interest regarding the publication of this paper.

## References


[1] Muller, R.A. (2016) Now—The Physics of Time. W.W. Norton & Company, New York.

[2] Bekenstein, J.D. (1974) *Physical Review D*, **9**, 3292-3300. https://doi.org/10.1103/PhysRevD.9.3292

[3] Hawking, S. (1976) *Physical Review D*, **13**, 191-197. https://doi.org/10.1103/PhysRevD.13.191

[4] Tatum, E.T. and Seshavatharam, U.V.S. (2018) *Journal of Modern Physics*, **9**, 1469-1483. https://doi.org/10.4236/jmp.2018.98091

[5] Tatum, E.T. and Seshavatharam, U.V.S. (2018) *Journal of Modern Physics*, **9**, 1404-1414. https://doi.org/10.4236/jmp.2018.97085

[6] Verlinde, E. (2010) On the Origin of Gravity and the Laws of Newton. arXiv:1001.0785v1 [hep-th].

[7] Verlinde, E. (2016) Emergent Gravity and the Dark Universe. aeXiv:1611.02269v2 [hep-th].

[8] Tatum, E.T. (2018) *Journal of Modern Physics*, **9**, 1564-1567. https://doi.org/10.4236/jmp.2018.98097

[9] Van Dokkum, P., *et al.* (2018) *Nature*, **555**, 629-632. https://doi.org/10.1038/nature25767

[10] Posti, L. and Helmi, A. (2018) Mass and Shape of the Milky Way's Dark Matter Halo with Globular Clusters from Gaia and Hubble. arXiv:1805.01408v1 [astro-ph.GA].

[11] Brouwer, M.M., *et al.* (2016) *Monthly Notices of the Royal Astronomical Society*, **000**, 1-14. arXiv:1612.03034v2 [astro-ph.CO].

[12] Genzel, R., *et al.* (2017) *Nature*, **543**, 397-401. https://doi.org/10.1038/nature21685

[13] Tatum, E.T. and Seshavatharam, U.V.S. (2018) *Journal of Modern Physics*, **9**, 1568-1572. https://doi.org/10.4236/jmp.2018.98098

Journal of Modern Physics, 2018, 9, 1946-1953
http://www.scirp.org/journal/jmp
ISSN Online: 2153-120X
ISSN Print: 2153-1196

# Calculating Radiation Temperature Anisotropy in Flat Space Cosmology

**Eugene Terry Tatum**

760 Campbell Ln. Ste. 106 #161, Bowling Green, KY, USA
Email: ett@twc.com

**How to cite this paper:** Tatum, E.T. (2018) Calculating Radiation Temperature Anisotropy in Flat Space Cosmology. *Journal of Modern Physics*, **9**, 1946-1953.
https://doi.org/10.4236/jmp.2018.910123

**Received:** July 12, 2018
**Accepted:** September 1, 2018
**Published:** September 4, 2018



## Abstract

The purpose of this paper is to show how one can use the FSC model of gravitational entropy to calculate cosmic radiation temperature anisotropy for any past cosmic time $t$ since the Planck scale. Cosmic entropy follows the Bekenstein-Hawking definition, although in the correct-scaling form of $\sqrt{S}$, which scales 60.63 logs of 10 from the Planck scale. In the FSC model, cosmic radiation temperature anisotropy $A_t = (t/t_o)$. The derived past anisotropy value can be compared to current co-moving anisotropy defined as unity $(t_o/t_o)$. Calculated in this way, current gravitational entropy and temperature anisotropy have maximum values, and the earliest universe has the lowest entropy and temperature anisotropy values. This approach comports with the second law of thermodynamics and the theoretical basis of the Sachs-Wolfe effect, gravitational entropy as defined by Roger Penrose, and Erik Verlinde's "emergent gravity" theory.

## Keywords

Flat Space Cosmology, Cosmic Microwave Background, CMB Anisotropy, Cosmology Theory, Cosmic Entropy, Gravitational Entropy, Black Holes, Standard Cosmology

## 1. Introduction and Background

In the July 2018 issue of *Journal of Modern Physics*, the paper entitled, "How the CMB Anisotropy Pattern Could Be a Map of Gravitational Entropy" [1] presents the rationale for Flat Space Cosmology (FSC) calculations of gravitational entropy in the form of $\sqrt{S}$. The theoretical basis for doing so is the Sachs-Wolfe effect [2]. The Sachs-Wolfe effect is widely considered to be the source of large angular scale temperature fluctuations in the cosmic microwave background (CMB). However, in a spatially flat universe, the Sachs-Wolfe effect can also be

considered to be the source of the smaller angular scale fluctuations of the CMB temperature anisotropy [3]. The Boomerang Collaboration [4] reported CMB anisotropy observations closely fitting "the theoretical predictions for a spatially flat cosmological model with an exactly scale invariant primordial power spectrum for the adiabatic growing mode" [Bucher (2015), page 6]. Thus, this theoretical basis for the Sachs-Wolfe effect as a measure of "gravitational potential" appears to explain the tight correlation between the FSC CMB anisotropy calculations and the observed CMB anisotropy [5] [6] [7].

Furthermore, the FSC CMB anisotropy paper and its companion paper [8] in the July 2018 *Journal of Modern Physics* show how the FSC model dovetails nicely with Erik Verlinde's concept of "emergent gravity" as an emergent property of cosmic entropy [9] [10] and Roger Penrose's concept of gravitational entropy [11] based upon his "Weyl's curvature hypothesis" [12] [13].

The purpose of this paper is to show how the FSC CMB anisotropy paper opens the way for a definition of cosmic radiation temperature anisotropy *at any cosmic temperature T*, whether it is in the form of "Universal Temperature" $T_U$, as defined in FSC reference [14], or in the Kelvin temperature scale. Although the FSC CMB anisotropy paper shows how to calculate the gravitational entropy ratios relating entropies at given *years* of cosmic time since the Planck epoch, these values can also be calculated in given *seconds* of cosmic time since the Planck epoch. This allows for the first year cosmic times and gravitational entropies to be correlated second-by-second as shown below (see Equation (3)). Therefore, cosmic radiation temperature anisotropy is not only predicted by FSC for the CMB recombination/decoupling "last scattering surface" but also for *any other cosmic time t.*

The rationale for generalizing the radiation temperature anisotropy calculations to be presented herein can be summarized as follows: Sachs and Wolfe used a gravitational redshift theoretical argument that radiation temperature anisotropy could be a result of inhomogeneous gravitational particle clustering. So, while they applied their argument in anticipation of refined CMB anisotropy observations, *there was nothing particularly special about the CMB emission event with respect to their gravitational redshift argument*. The recombination/decoupling event concerned photon emission, making the event observable. However, the coupling of electrons with protons to form the first hydrogen atoms should have no impact whatsoever on gravitational particle clustering. As explained in reference [1], the Sachs-Wolfe effect is now widely considered to be the theoretical basis for large angular scale radiation temperature fluctuations. Furthermore, *in a spatially flat universe*, *the Sachs-Wolfe effect can also be considered to be the source of the smaller angular scale fluctuations of the CMB temperature anisotropy* [3]. Therefore, based upon this scale-invariant flat universe Sachs-Wolfe effect, the calculation method presented in reference [1] and herein is believed to be generalizable to any other gravitational particle clustering stage (*i.e.*, gravitational entropy stage) of universal expansion.

The reader will maximally benefit in reading the present paper after first reading FSC references [1] [8] and [14]. FSC is a mathematical model of the Hawking-Penrose conjecture that a universe smoothly expanding from a singularity can be treated, under general relativity, much like a time-reversal of giant black hole collapse to a singularity. A brief introductory review of the FSC assumptions, and their justification, is provided below. The five assumptions of FSC are:

## The Five Assumptions of Flat Space Cosmology

1) The cosmic model is an ever-expanding sphere such that the cosmic horizon always translates at speed of light $c$ with respect to its geometric center at all times *t.* The observer is operationally-defined to be at this geometric center at all times $t$.

2) The cosmic radius $R_t$ and total mass $M_t$ follow the Schwarzschild formula $R_t \cong 2GM_t/c^2$ at all times $t$.

3) The cosmic Hubble parameter is defined by $H_t \cong c/R_t$ at all times $t$.

4) Incorporating our cosmological scaling adaptation of Hawking's black hole temperature formula, at any radius $R_t$, cosmic temperature $T_t$ is inversely proportional to the geometric mean of cosmic total mass $M_t$ and the Planck mass $M_{pl}$. $R_{pl}$ is defined as twice the Planck length (*i.e.,* as the Schwarzschild radius of the Planck mass black hole). With subscript $t$ for any time stage of cosmic evolution and subscript $pl$ for the Planck scale epoch, and, incorporating the Schwarzschild relationship between $M_t$ and $R_t$,

$$\left.\begin{aligned} & k_B T_t \cong \frac{\hbar c^3}{8\pi G\sqrt{M_t M_{pl}}} \cong \frac{\hbar c}{4\pi\sqrt{R_t R_{pl}}} \\ & \begin{cases} M_t \cong \left(\dfrac{\hbar c^3}{8\pi G k_B T_t}\right)^2 \dfrac{1}{M_{pl}} & (\mathrm{A}) \\ R_t \cong \dfrac{1}{R_{pl}}\left(\dfrac{\hbar c}{4\pi k_B}\right)^2 \left(\dfrac{1}{T_t}\right)^2 & (\mathrm{B}) \\ R_t T_t^2 \cong \dfrac{1}{R_{pl}}\left(\dfrac{\hbar c}{4\pi k_B}\right)^2 & (\mathrm{C}) \\ t \cong \dfrac{R_t}{c} & (\mathrm{D}) \end{cases} \end{aligned}\right\} \quad (1)$$

5) Total entropy of the cosmic model follows the Bekenstein-Hawking black hole formula [13] [14].

$$S_t \cong \frac{\pi R_t^2}{L_p^2} \quad (2)$$

The first two assumptions are based upon a literal interpretation of the Hawking-Penrose conjecture as it would pertain to a smoothly-expanding Schwarzschild black hole. The third assumption (Hubble parameter) treats maximally redshifted radial photons at the cosmic model horizon as moving

with speed of light *c relative* to the geometric center at a distance of horizon radius $R_t$. This is a stipulation of relativity. The fourth assumption is a cosmic temperature scaling assumption. While it shows similarity to the static Hawking black hole temperature formula, the FSC cosmic model is treated as scaling in Planck mass increments. This allows for dynamic cosmic expansion modeling from the Planck scale epoch. Finally, the fifth assumption utilizes the Bekenstein-Hawking entropy definition, which seems appropriate for a model of the Hawking-Penrose conjecture. The numerous observational correlations of FSC are given in references [8] and [14].

## 2. Calculating Radiation Temperature Anisotropy in FSC

Equation (11) from reference [14] gives an FSC cosmic time value of $10^{11.58}$ seconds at the beginning of the recombination/decoupling epoch (3000 K). This equation is repeated here as Equation (3):

$$T^2 t_s = 3.426525959553982 \times 10^{18}\ \mathrm{K}^2 \cdot \mathrm{s} \tag{3}$$

wherein cosmic temperature $T$ is in degrees $K$ and cosmic time $t_s$ is in seconds since the Planck epoch. For reasons given in the reference [1] Discussion section, the "end of decoupling" event happened in the FSC model at $10^{12.6}$ seconds (at a temperature of 924.63 K) after the Planck epoch. The Planck epoch is the cosmic time of the Planck-scale universe and is often considered to be the approximate moment of the "Big Bang" in standard cosmology. FSC reference [8] derives

$$\sqrt{S} = \frac{c\sqrt{\pi}}{L_p} t \tag{4}$$

showing the direct proportionality relationship between gravitational entropy $\sqrt{S}$ and cosmic time $t$. Speed of light $c$ and Planck length $L_p$ are assumed to be constants over cosmic time. Thus, if we normalize the proportionality constant to unity and operationally define $\sqrt{S}$ in terms of seconds,

$\sqrt{S}$ = $10^{-42.965}$ at $10^{-42.965}$ second of cosmic time at Planck temperature 5.6 × $10^{30}$ K;

$\sqrt{S}$ = $10^{11.58}$ at $10^{11.58}$ seconds of cosmic time at CMB beginning temperature 3000 K;

$\sqrt{S}$ = $10^{12.6}$ at $10^{12.6}$ seconds of cosmic time at end-of-decoupling temperature 924.63 K;

$\sqrt{S}$ = $10^{17.66}$ at $10^{17.66}$ seconds of cosmic time at current temperature 2.72548 K.

The above CMB emission epoch gravitational entropies ($10^{11.58}$ and $10^{12.6}$) can then be related to current cosmic entropy ($10^{17.66}$), in ratio form, as follows:

[$\sqrt{S}$ at the beginning of CMB emission]/[$\sqrt{S}$ at current time] = 8.25 × $10^{-7}$ (0.825 × $10^{-6}$);

[$\sqrt{S}$ at the ending of CMB emission]/[$\sqrt{S}$ at current time] = 8.69 × $10^{-6}$ (0.869 × $10^{-5}$).

These derived values of the beginning and ending CMB radiation temperature anisotropy are the same as those calculated in reference [1]. This value range fits the COBE DMR CMB $dT/T$ anisotropy measurement of $0.66 \times 10^{-5}$, as well as with the WMAP and Planck report anisotropy estimates of "approximately" $10^{-5}$.

Thus, if this process for calculating the CMB radiation temperature anisotropy as gravitational entropy ratios can be generalized and extended all the way back to the Planck epoch (and conceivably beyond), the formula for doing such calculations is:

$$A_t = \sqrt{S}_t / \sqrt{S}_o = t/t_o \tag{5}$$

wherein $A_t$ is the radiation temperature anisotropy at cosmic time $t$, $\sqrt{S}_t$ is the gravitational entropy (cosmic entropy) at cosmic time $t$, $\sqrt{S}_o$ is the gravitational entropy (cosmic entropy) at current time $t_o$, and $t/t_o$ is the ratio of these time values. This radiation temperature anisotropy formula can also be substituted by other FSC parameters correlated to $\sqrt{S}_t$, as seen in reference [8]. Thus,

$$A_t = R_t / R_o \tag{6}$$

wherein $R_t$ is the cosmic radius at cosmic time $t$ and $R_o$ is the current observed cosmic radius.

$$A_t = T_o^2 / T_t^2 \tag{7}$$

wherein $T_o$ is the current cosmic radiation temperature in degrees Kelvin (2.72548 K) and $T_t$ is the cosmic radiation temperature in degrees Kelvin at cosmic time $t$.

$$A_t = T_{Uo} / T_{Ut} \tag{8}$$

wherein $T_{Uo}$ is the current cosmic radiation temperature in Universal Temperature units and $T_{Ut}$ is the cosmic radiation temperature in Universal Temperature units at cosmic time $t$. As indicated in reference [14], $T_{Ut}$ is defined by $T_{Ut} = T_t^2$.

Based upon this calculation method, the following **Figure 1** and **Figure 2** can be presented. For comparison, the reader is referred to Figure 1 and Figure 5 in reference [14]. The lines are linear because the vertical and horizontal axes scale in a logarithmic fashion.

**Figure 1** shows how radiation temperature anisotropy and total cosmic entropy in the form of $\sqrt{S}$ scales with respect to cosmic time $t$ and Kelvin temperature $T$. CMB starting and ending values are denoted by the white circles.

**Figure 2** shows how radiation temperature anisotropy and total cosmic entropy in the form of $\sqrt{S}$ scales with respect to cosmic time $t$ and Universal Temperature $T_U$. CMB starting and ending values are denoted by the white circles.

## 3. Discussion

Extensive comparisons between FSC and standard inflationary cosmology are given in reference [15]. Standard inflationary cosmology has no theoretical basis

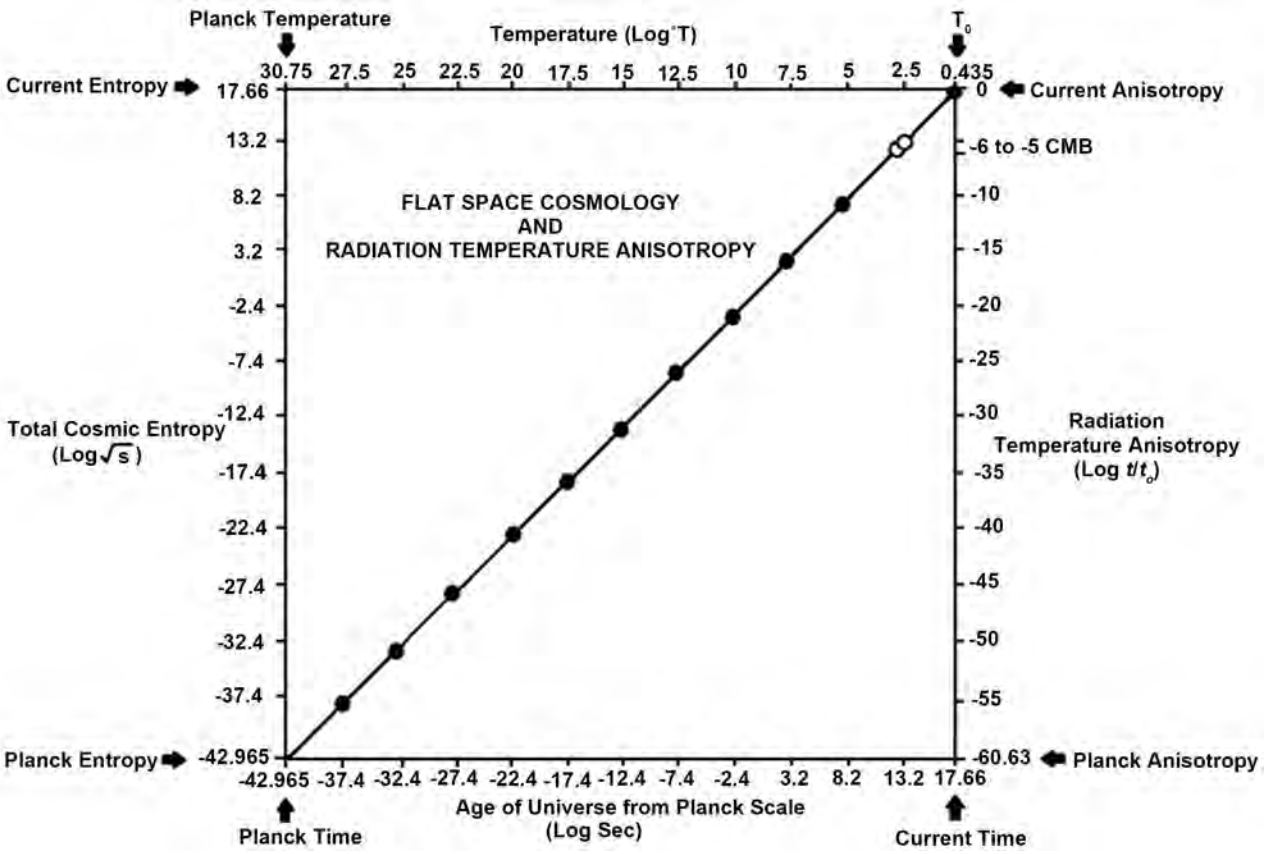


**Figure 1.** Total entropy, Kelvin temperature T, and temp anisotropy.

for predicting and calculating radiation temperature anisotropy at any given cosmic time. Thus, standard model practitioners can only guess as to the possible reasons why the CMB anisotropy pattern has a $dT/T$ RMS anisotropy value of 18 micro-Kelvins/2.725 K = $0.66 \times 10^{-5}$, as measured in the COBE DMR experiment [Wright (1996)]. Current speculation seems to favor a CMB pattern produced by a "quantum fluctuation" Big Bang event smoothed out by cosmic inflation and splayed out across the sky. It is even proposed that a "quantum fluctuation" CMB pattern somehow must provide important clues to the nature of gravity at the quantum scale (*i.e.*, "quantum gravity").

In contrast, the FSC model, as detailed in references [1] and [8], indicates that the CMB pattern could simply be a map of gravitational entropy. The theoretical basis for this interpretation owes much to the prior work of Sachs and Wolfe, Hawking, Penrose and Verlinde, as discussed in both FSC papers. Verlinde's papers [9] [10], in particular, address the deep correlation between cosmic entropy and gravity. Thus, given the FSC success in correlating gravitational entropy in the form of $\sqrt{S}$ with the observed anisotropy of the CMB pattern, the current paper proposes a reasonable extension of the same rationale to calculating radiation temperature anisotropy at any past cosmic time $t$ relative to current cosmic anisotropy. For comparison purposes, current co-moving anisotropy can be defined as unity [*i.e.*, $\log(t_o/t_o) = 0$].

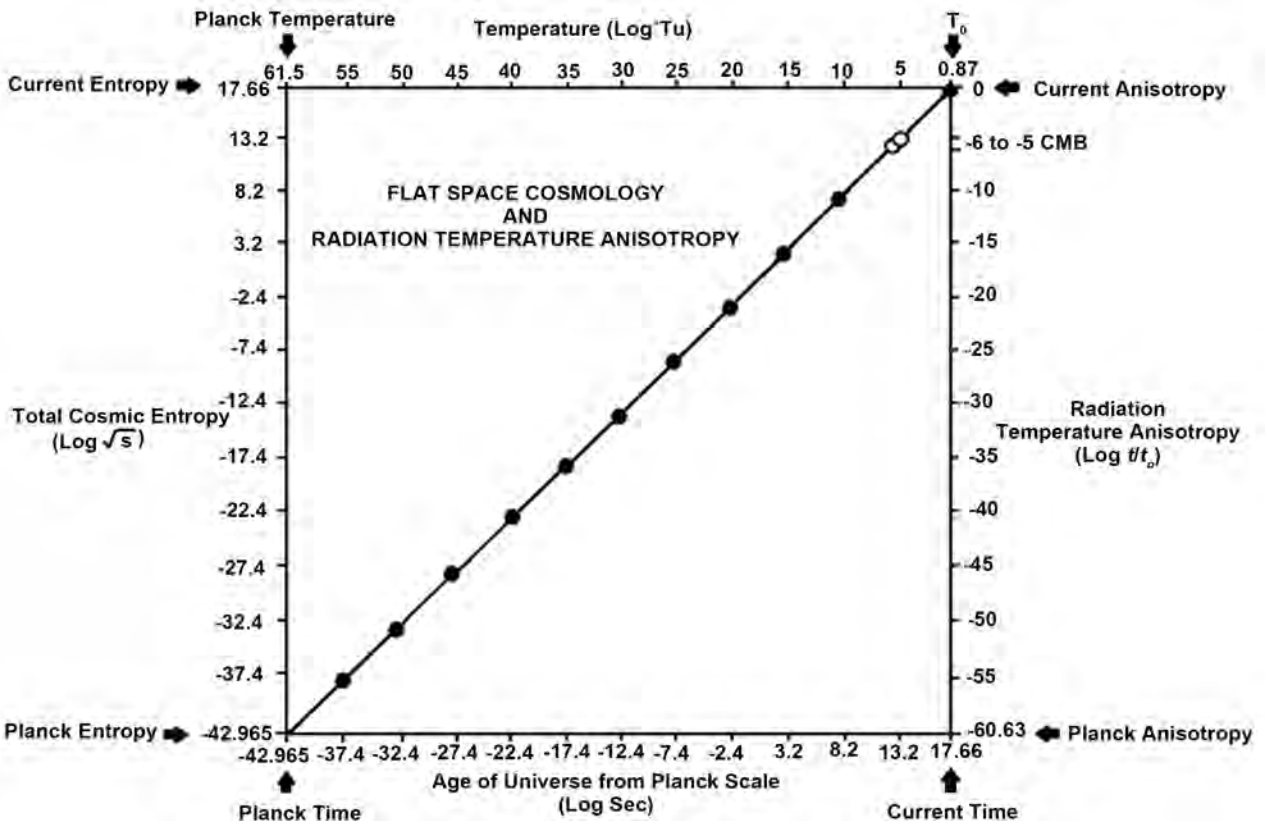


**Figure 2.** Total entropy, universal temperature $T_U$, and temp anisotropy.

Note that, by this definition of current co-moving anisotropy, current gravitational entropy and temperature anisotropy have maximum values, and the earliest universe has the lowest entropy and temperature anisotropy values. This approach comports with the second law of thermodynamics and the theoretical basis of the Sachs-Wolfe effect, gravitational entropy as defined by Roger Penrose, and Erik Verlinde's "emergent gravity" theory.

## 4. Summary and Conclusions

The purpose of this paper has been to show how one can use the FSC model of gravitational entropy to calculate cosmic radiation temperature anisotropy for any past cosmic time $t$ since the Planck scale. In the FSC model, cosmic radiation temperature anisotropy $A_t = (t/t_o)$. The derived past anisotropy value can be compared to current co-moving anisotropy defined as unity $(t_o/t_o)$. Calculated in this way, current gravitational entropy and temperature anisotropy have maximum values, and the earliest universe has the lowest entropy and temperature anisotropy values. This approach comports with the second law of thermodynamics and the theoretical basis of the Sachs-Wolfe effect, gravitational entropy as defined by Roger Penrose, and Erik Verlinde's "emergent gravity" theory.

## Dedications and Acknowledgements

This paper is dedicated to the late Dr. Stephen Hawking and Dr. Roger Penrose

for their groundbreaking work on black holes and their possible application to cosmology. Dr. Tatum also thanks Dr. Rudolph Schild of the Harvard Center for Astrophysics for his past support and encouragement.

## Conflicts of Interest

The author declares no conflicts of interest regarding the publication of this paper.

## References

[1] Tatum, E.T. (2018) *Journal of Modern Physics*, **9**, 1484-1490. https://doi.org/10.4236/jmp.2018.98092

[2] Sachs, R.K. and Wolfe, A.M. (1967) *Astrophysical Journal*, **147**, 73. https://doi.org/10.1086/148982

[3] Bucher, M. (2015) Physics of the Cosmic Microwave Background Anisotropy. arXiv:1501.04288v1 [astro-ph.CO].

[4] De Bernardis, P., *et al.* (2000) A Flat Universe from High-Resolution Maps of the Cosmic Microwave Background Radiation. arXiv:astro-ph/0004404v1.

[5] Wright, E.L., *et al.* (1996) *Astrophysical Journal*, **464**, L21-L24. https://doi.org/10.1086/310073

[6] Bennett, C.L. (2013) Nine-Year Wilkinson Microwave Anisotropy Probe (WMAP) Observations: Final Maps and Results. arXiv:1212.5225v3 [astro-ph.CO].

[7] Planck Collaboration. (2014) *Astronomy & Astrophysics*, **A23**, 1-48.

[8] Tatum, E.T. and Seshavatharam, U.V.S. (2018) *Journal of Modern Physics*, **9**, 1469-1483. https://doi.org/10.4236/jmp.2018.98091

[9] Verlinde, E. (2010) On the Origin of Gravity and the Laws of Newton. arXiv:1001.0785v1 [hep-th].

[10] Verlinde, E. (2016) Emergent Gravity and the Dark Universe. aeXiv:1611.02269v2 [hep-th].

[11] Penrose, R. (2016) Fashion Faith and Fantasy in the New Physics of the Universe. Princeton University Press, Princeton, US. https://doi.org/10.1515/9781400880287

[12] Penrose, R. (1979) Singularities and Time-Asymmetry. In: Hawking, S.W. and Israel, W., Eds., *General Relativity: An Einstein Centenary Survey*, Cambridge University Press, Cambridge, 581-638.

[13] Tatum, E.T. (2018) *Journal of Modern Physics*, **9**, 1935-1940. https://doi.org/10.4236/jmp.2018.910121

[14] Tatum, E.T. and Seshavatharam, U.V.S. (2018) *Journal of Modern Physics*, **9**, 1404-1414. https://doi.org/10.4236/jmp.2018.97085

[15] Tatum, E.T. (2018) *Journal of Modern Physics*, **9**, 1867-1882. https://doi.org/10.4236/jmp.2018.910118

Journal of Modern Physics, 2018, 9, 1954-1969
http://www.scirp.org/journal/jmp
ISSN Online: 2153-120X
ISSN Print: 2153-1196

# Gravity in View of the Theory of Orbiting Binary Stars

**Stefan L. Hahn**

Retired Professor, Institute of Radioelectronics and Multimedia Technology, Warsaw University of Technology, Warsaw, Poland
Email: st.hahn@wp.pl

**How to cite this paper:** Hahn, S.L. (2018) Gravity in View of the Theory of Orbiting Binary Stars. *Journal of Modern Physics*, **9**, 1954-1969.
https://doi.org/10.4236/jmp.2018.910124

**Received:** June 7, 2018
**Accepted:** September 10, 2018
**Published:** September 13, 2018





## Abstract

In this paper, we investigate orbiting of two stars having equal masses. We consider two models: with a circular orbit and with two elliptical orbits having a common center of a mass located in a common focal point. In the case of the circular orbit, we applied the notion of the instantaneous complex frequency. The paper is illustrated with numerous formulas, derivations and discussion of results.

## Keywords

Gravity, Inertia, Complex Frequency, Curvature Radius

## 1. Introduction

Three years ago, the author presented a paper describing the gravitational forces as a result of anisotropic energy exchange between baryonic matter and quantum vacuum [1]. Here, we try to show that the theory of circulation of double stars around a common center of mass yields arguments in favor of the above theory. Our goal can be achieved by investigating orbiting of two stars having equal masses. We present two such models: the first one with a circular orbit and the second one with two elliptical orbits with a common center of a mass located in a common focal point. The presented mathematical descriptions of the above models are derived by the author and certainly only the methods of derivations are new. Most of the results belong to the existing knowledge. As regards the circular orbit, we applied the notion of the instantaneous complex frequency. We introduce the following notations:

- MKS system of units is applied.
- Ellipse: $a$—semi-major axis, $b$ = semi-minor axis, $\varepsilon$—eccentricity;
- $s(t)=\alpha(t)+j\omega(t)$—instantaneous complex frequency;

- $G = 6.67384 \times 10^{-11}\left[\mathrm{m}^3/\left(\mathrm{kg}\cdot\mathrm{s}^2\right)\right]$—gravitational constant;
- $(\rho, \varphi)$—polar coordinates of the ellipse centered at the focus;
- $\rho_c$—curvature radius;
- $P$—power;
- $E$—energy;
- $F$—force;
- $T$ = orbital period.

## 2. A Model of a Double Star of Equal Mass Orbiting on a Circular Orbit

Figure 1 shows a circular orbit of a constant radius $\rho_0$. Both stars are separated by the distance $l_0 = 2\rho_0$. The angular position of the first star is defined by the phasor $\psi_1(t) = \rho_0 \exp(j\omega_0 t); \varphi_1(t) = \omega_0 t$, and the second by $\psi_2(t) = \rho_0 \exp(j\omega_0 t + \pi); \varphi_2(t) = \omega_0 t + \pi$. This system is described by the equality of two forces: the gravitational force of attraction and the centrifugal inertial force.

For the circular orbit of Figure 1 (no inspiral), the two forces are collinear and have opposite directions. They should have the same magnitude. This equality of forces is described by

$$\boldsymbol{F}_g = \frac{Gm^2}{4\rho_0^2} = \boldsymbol{F}_c = m\omega_0^2\rho_0. \tag{1}$$

We get the following time-independent relations between the angular velocity $\omega_0$ and the radius $\rho_0$:

$$\rho_0 = \sqrt[3]{\frac{Gm}{4\omega_0^2}} \quad \text{or} \quad \omega_0 = \sqrt{\frac{Gm}{4\rho_0^3}}. \tag{2}$$

The orbital tangential velocity is $v_0 = \omega_0\rho_0$. Therefore, the kinetic energy of the system is $E_k = mv_0^2$ and the potential energy $E_p = -2\rho_0\left|\boldsymbol{F}_g\right|$. The potential energy is negative. Its value equals twice the kinetic energy. Therefore, the total energy of the system is negative and time independent. Several authors derived formulae for calculation of the power of gravitational waves emitted by the system of Figure 1. The derivations apply linearized version of Einstein's theory of relativity. Let us present two examples:

Valeria Ferrari [2] derived the following formulae; $P = \frac{32}{5}\frac{G^4}{c^5}\frac{\mu^2 M^3}{l_0^5}[\mathrm{W}]$, where $\mu = \frac{m_1 m_2}{M}$, $M = m_1 + m_2$ and $l_0 = 2\rho_0$ is the orbital separation. If $m_1 = m_2$, we get

$$P = \frac{2}{5}\frac{G^4}{c^5}\frac{m^5}{\rho_0^5}[\mathrm{W}]. \tag{3}$$

In the book of Gasperini [3], we find $P = \frac{32}{5}\frac{G}{c^2}a^4\omega_0^6[\mathrm{W}]$, where $a$ is wrongly defined as one half of the orbital separation. Deleting this error and insertion

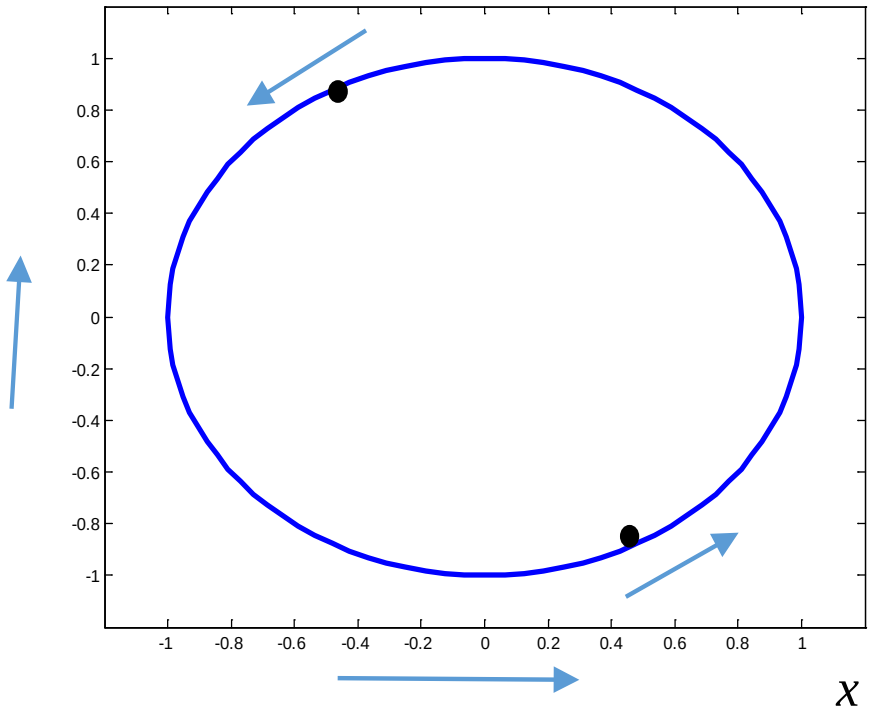


**Figure 1.** The circular orbit of binary stars. Cartesian coordinates ($x$, $y$).

the formula (2), we get again (3). The above presented well known theory does not explain the phenomenon of inspiral. The famous observations by Taylor and Hulse [4] [5] [6], of the binary pulsar PSR1913+16 have shown that the stars inspiral. The instantaneous radius $\rho(t)$ decrease and the instantaneous angular velocity $\omega(t)$ increase. In order to explain this phenomenon we introduced a description of the circular system using the notion of instantaneous complex frequency [7] [8].

## 3. Instantaneous Complex Frequency Description of the Circular Binary System

We have to show that due to the emission of gravitational waves, the trajectory of the stars is not circular since the instantaneous radius decrease in time and the angular velocity and tangential velocity increase in time. The stars are orbiting along spirals (**Figure 2**). A convenient method of description of this phenomenon is the notion of instantaneous complex frequency. The phasor representing the first star has the form

$$\psi_1(t) = \rho_0 \exp\left[\int_0^t s(t)\mathrm{d}t + j\varphi(0)\right];\ s(t) = \alpha(t) + j\omega(t) \tag{4}$$

and the second one

$$\psi_2(t) = \rho_0 \exp\left[\int_0^t s(t)\mathrm{d}t + j\left[\varphi(0) + \pi\right]\right], \tag{5}$$

$\alpha(t)$ is called instantaneous radial frequency and $\omega(t)$—instantaneous angular frequency. The instantaneous radius is $\rho(t) = \rho_0 \exp\left[\int_0^t \alpha(t)\mathrm{d}t\right]$. In the

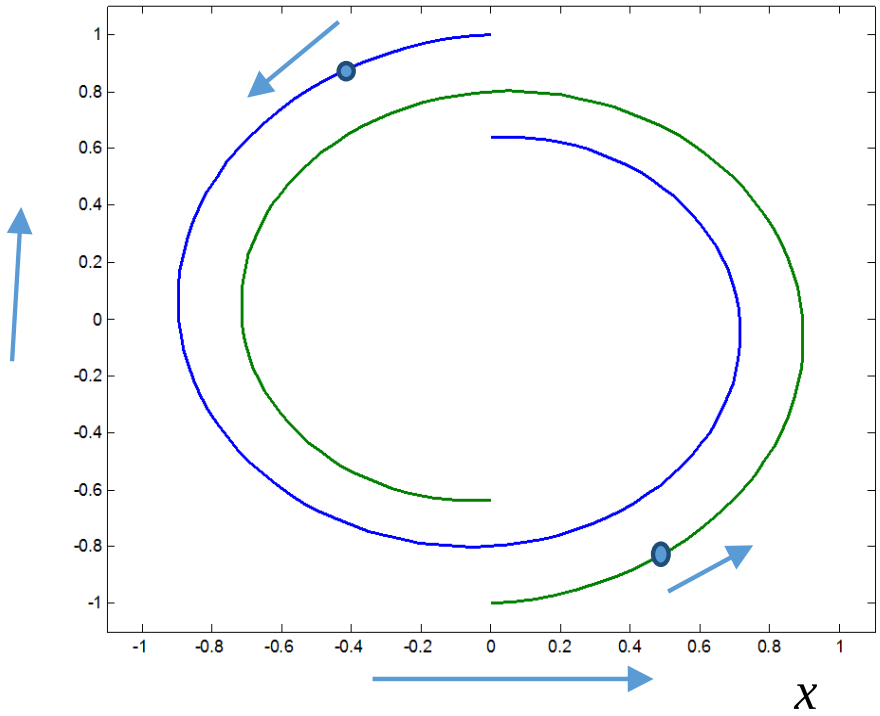


**Figure 2.** Inspiral orbits with enlarged rate of inspiral of binary stars. Cartesian coordinates (*x, y*).

simplest description of the properties of inspiral, the instantaneous complex frequency is time independent: $s(t)=-\alpha_0+j\omega_0$. In this case, the Cartesian coordinates of the orbit are:

- For the first star $x(t)=\rho_0\exp(-\alpha_0 t)\cos(\omega_0 t)$;
  $y(t)=\rho_0\exp(-\alpha_0 t)\sin(\omega_0 t)$;
- For the second $x(t)=-\rho_0\exp(-\alpha_0 t)\cos(\omega_0 t)$;
  $y(t)=-\rho_0\exp(-\alpha_0 t)\sin(\omega_0 t)$.

We have to explain why the stars accelerate by orbiting along the inspiral orbit. Let us show that the gravitational force $F_g=\dfrac{Gm^2}{4\rho^2(t)}$ and the centrifugal force $F_c=m\omega_0^2\rho_c$ differ by magnitude and direction. The orbital distance $2\rho(t)=2\rho_0\exp\left[-\int_0^t\alpha(t)\mathrm{d}t\right]$ is a line connecting the mass centers through the origin (0, 0) and defines the direction of gravitation force. Differently, the direction of the centrifugal force $F_c$ is defined by the curvature radius $\rho_c$. The geometry of the addition of the two forces is presented in **Figure 3** (with large rate of inspiral). In the case $\alpha(t)=-\alpha_0$, the angle $\gamma$ is given by the formulae (see **Appendix 1**)

$$\tan\left(\gamma(t=0)\right)=-\frac{\alpha_0}{\omega_0},\ \sin\left(\gamma(t=0)\right)=\frac{-\alpha_0/\omega_0}{\sqrt{1+\left(\alpha_0/\omega_0\right)^2}},$$
$$\cos\left(\gamma(t=0)\right)=\frac{1}{\sqrt{1+\left(\alpha_0/\omega_0\right)^2}}. \tag{6}$$

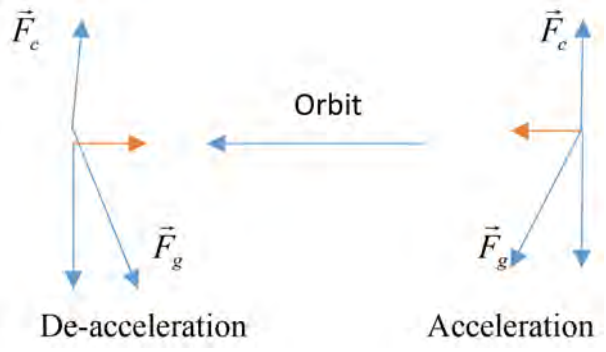


**Figure 3.** The gravitation force $\boldsymbol{F}_g$ is not collinear with the centripetal force $\boldsymbol{F}_c$ the forces $\boldsymbol{F}_c$ and $\boldsymbol{F}_g\cos(\gamma)$ cancel and $\boldsymbol{F}_g\sin(\gamma)$ has the direction of the tangent of the orbit causing de-acceleration (right) or deceleration (left).

The inspiral orbit is defined by the equation

$$\text{Gravitational force}\times\cos\left[\gamma(t)\right]=\text{Centrifugal force}. \tag{7}$$

However, there is a tangential force (see **Figure 3**)

$$\text{Tangential force}=F_{\tan}=\text{Gravitational force}\times\sin\left[\gamma(t)\right]. \tag{8}$$

However, for the quasi-circular orbit, the tangential force is extremely small. This force induces acceleration of the mass $m$ given by

$$a(t)=m\boldsymbol{F}_{\tan}. \tag{9}$$

In consequence, the instantaneous angular frequency is increasing in time

$$\omega(t)=\omega_0+\int_0^t a(t)\mathrm{d}t=\frac{2\pi}{T(t)} \tag{10}$$

where $T(t)$ is a decreasing instantaneous period. The energies of the system also increase in time. The instantaneous tangential velocity of the stars is

$$v(t)=\omega(t)\rho_c(t). \tag{11}$$

The curvature radius is (see **Appendix 2**)

$$\rho_c(t)=\rho_0\mathrm{e}^{-\alpha_0 t}\frac{\left(1+\left(\alpha_0/\omega_0\right)^2\right)^{3/2}}{1-\left(\alpha_0/\omega_0\right)^2}. \tag{12}$$

The instantaneous kinetic energy of both stars is $E_k(t)=mv^2(t)$ and the instantaneous negative potential energy is $E_p(t)=F_g\rho(t)=-\dfrac{Gm^2}{4\rho(t)}$. We start the investigations with Equation (2). We can define the value of the radius $\rho_0$ or of $\omega_0$ but not of both. Our choice is the value $\omega_0=2\pi/T_0=2.259554\times10^{-4}\left[\mathrm{rad/s}\right]$; $T_0=2.788720\times10^4\left[\mathrm{s}\right]$ measured by Taylor and Hulse [8]. Using (2), we get the following values: the radius $\rho_0=9.706500\times10^8\left[\mathrm{m}\right]$. The tangential velocity equals $v=\omega_0\rho_0=2.193236\times10^6\left[\mathrm{m/s}\right]$ (about 219 km/s). The kinetic energy of both stars is $E_k=mv^2=1.346134\times10^{41}\left[\mathrm{J}\right]$ and the negative potential energy

(magnitude twice of $E_k$) is $E_p = -Gm^2/(2\rho_0) = -2.692268\times10^{41}[\mathrm{J}] = -2E_k$. The total energy of the system is negative. The power of the gravitational waves emitted by the system given by Equation (3) is $P = 6.523698\times10^{23}[\mathrm{W}]$.

**1) Estimation of the value of the radial frequency $\alpha_0$**

The decrease of the radius of the circular model in one period $T_0$ is

$$\rho_1 = \rho_0 \mathrm{e}^{-\alpha_0 T_0} = \rho_0 \mathrm{e}^{-2\pi(\alpha_0/\omega_0)}. \tag{13}$$

We have an increase of the negative value of the potential energy

$$E_{p1} = -\frac{Gm^2}{4\rho_1} \approx -\frac{Gm}{4\rho_0}(1+2\pi\alpha_0/\omega_0). \tag{14}$$

Therefore, we get the increase

$$\nabla E_{p1} \approx \frac{-Gm}{4\rho_0}(2\pi\alpha_0/\omega_0). \tag{15}$$

Assuming arbitrary that this increase should be equal to the energy emitted by gravitational waves during one period we get

$$\nabla E_{p1} \approx \frac{-Gm}{4\rho_0}(2\pi\alpha_0/\omega_0) = PT_0 = P2\pi/\omega_0. \tag{16}$$

Therefore,

$$\alpha_0 \approx -\frac{P}{E_p}[\mathrm{s}^{-1}] = -6.526980\times10^{23}/2.692268\times10^{41} = -2.424343\times10^{-18}. \tag{17}$$

**2) The increase of the angular frequency (or decrease of the period $T_0$) during the inspiral**

Taylor and Hulse have measured that the period of the PSR system decreases by 76.5 μs per year [6]. Let us derive a formula for this decrease for the circular system. We insert in Equation (2) $\rho(t) = \rho_0 \mathrm{e}^{-\alpha_0 t}$ in place of $\rho_0$ getting

$$\omega(t) = \sqrt{\frac{Gm}{4\rho_0^4 \mathrm{e}^{-3\alpha_0 t}}} = \omega_0 \mathrm{e}^{\frac{3}{2}\alpha_0 t} \quad \rightarrow T(t) = T_0 \mathrm{e}^{-\frac{3}{2}\alpha_0 t}. \tag{18}$$

The decrease of the period per year is

$$\nabla T_{\mathrm{year}} = T_0 - T(t_{\mathrm{year}}) = T_0\left[1-\mathrm{e}^{-\frac{3}{2}\alpha_0 t_{\mathrm{year}}}\right] \approx -\frac{3}{2}T_0\alpha_0 t_{\mathrm{year}} = 3.18022\times10^{-6}[\mathrm{s}]. \tag{19}$$

It is more than one order of magnitude smaller in comparison to 76, 5 μs per year of the PSR system. Therefore, the circular model cannot be applied to describe the properties of the PSR elliptical system.

**3) The increase of the negative value of the potential energy**

The potential energy at the moment $t = 0$ is

$$E_p(0) = -\frac{Gm^2}{2\rho_0} = -2.692268\times10^{41}[\mathrm{J}]. \tag{20}$$

The value after one year is

$$E_p(t_{\mathrm{year}}) = -\frac{Gm^2}{2\rho_0 \mathrm{e}^{-\alpha_0 t_{\mathrm{year}}}}[\mathrm{J}]. \tag{21}$$

The increase is

$$\nabla E_p = E_p(0)\left(\mathrm{e}^{\alpha_0 t_{\text{year}}} - 1\right) = -2.052708\times 10^{31}\left[\mathrm{J}\right]. \tag{22}$$

The division by $t_{\text{year}}$ yields the power

$$P = \frac{\nabla E_p}{t_{\text{year}}} = -6.526917\times 10^{23}\left[\mathrm{W}\right], \tag{21}$$

*i.e.*, exactly the value defined by Equation (3) which represents the power of the emitted gravitational waves. This result validates the correctness of Equation (17) defining $\alpha_0$ and Equation (19) defining the delay per year. The negative sign of this power is applied in the book of Gasperini [3] with no comment. We found that the authors of reference [9] derived a formula with a negative sign of the gravitational "Poynting vector" also with no comment.

**4) The inspiral time**

The main goal of this paper is to validate the explanation of the nature of gravity presented in [1]. Having this in mind, let us describe only briefly the process of inspiral. During each period the radius $\rho(t) = \rho_0 \exp\left(-\int_0^t \alpha(t)\mathrm{d}t\right)$ is a bit shorter, each next period is shorter corresponding to an increase of the angular frequency which is a function of time. As well, the instantaneous radial frequency increases with time. The angular frequency is

$$\omega(t) = \sqrt{\frac{Gm^2}{4\rho^3(t)}} = \omega_0 \mathrm{e}^{\frac{3}{2}\alpha_0 t}; \quad \alpha(t) = \alpha_0. \tag{22}$$

We get

$$T(t) = T_0 \mathrm{e}^{-\frac{3}{2}\alpha_0 t} \quad \text{and} \quad \nabla T(t) = T_0 - T(t) = T_0\left[1 - \mathrm{e}^{-\frac{3}{2}\alpha_0 t}\right] \approx \frac{-3}{2} T_0 \alpha_0 t. \tag{23}$$

The instantaneous radius is

$$\rho(t) = \rho_0 \exp\left[-\int_0^t \alpha(t)\mathrm{d}t\right] \approx \rho_0 \mathrm{e}^{-\alpha_0 t}; \ \alpha(t) \approx \alpha_0. \tag{24}$$

The decrease of the radius during a year is

$$\nabla\rho_{\text{year}} = \rho_0\left(1 - \mathrm{e}^{-\alpha_0 t_{\text{year}}}\right). \tag{25}$$

The overestimated number of years of the total inspiral (overestimated since calculated using the constant value $\alpha_0$) is

$$\text{Number of years} = \frac{\rho_0}{\nabla\rho_{\text{year}}} = \frac{1}{1 - \mathrm{e}^{-\alpha_0 t_{\text{year}}}} \approx \frac{\sim 1}{\alpha_0 t_{\text{year}}} = 1.098\times 10^{10}\left[\text{years}\right]. \tag{27}$$

**5) Concluding remarks about the circular system**

During a single revolution, the emitted power may be classified as time independent since the increase is negligible. The directional pattern $\sigma(\Omega)\left[\mathrm{W/steradian}\right]$ is circular symmetric with maximum radiation in the plane of the circle. The total energy of the system during a single revolution has a negligible time dependence. The radiation is emitted in twice the orbital fre-

quency with a circular polarization [2]. In long times, there is an increase of the power and the negative energy of the system. Therefore, assuming that the gravitational waves carry positive energy, the emission is at the cost of increasing negative energy of the system. The presented theory of inspiral is valid only in the frame of a linear gravitation. The phenomena in the last stage of inspiral are certainly governed by nonlinear effects. Recently, the LIGO system registered a chirp like signal of duration about 0.17 [s] emitted by two black holes shortly before the collapse [10] [11]. Certainly, a linear theory is unable to describe this signal.

## 4. The Theoretical Model of the Binary Pulsar PSRB1913+16

The PSR system differs considerably from the above described circular system. The two stars are orbiting along elliptical orbits (see **Figure 4**) around a common center of mass located in the focus. We consider again equal masses $m_1 = m_2 = m$. The data of this system measured by Taylor and Hulse are presented in **Appendix 1**. In the circular model, the distance between the stars, the angular velocity $\omega$, the tangential velocity and the potential and kinetic energies could be classified as constant during a single orbital time. This is not the case in the PSR system. For example, the velocity changes from $v_{\max} = 450$ [km/s] to 120 [km/s]. These changes overshadow by several orders the inspiral change due to the emission of gravitational waves.

**1) The description of the elliptical orbits in polar coordinates centered at the focus**

The elliptical orbit of the first star can be defined in polar coordinates ($\rho$, $\varphi$) centered at the right focus of the left ellipse (**Figure 4**). The radius $\rho$ in terms of the angle $\varphi$ is given by the formula

$$\rho(\varphi) = a\frac{1-\varepsilon^2}{1+\varepsilon\cos(\varphi)} \tag{28}$$

and for the second one centered in the left focus of the right ellipse is

$$\rho(\varphi) = a\frac{1-\varepsilon^2}{1-\varepsilon\cos(\varphi+\pi)} \tag{29}$$

Note that the angle $\varphi$ is a function of time. However, our derivations have the form of functions of $\varphi$. The inverse function $t(\varphi)$ has no closed form. Our goals do not require the presentation of these relations.

For $\varphi = 0$, we get periastrone separation $= 2a[1-\varepsilon]$ and for $\varphi = \pi$, the apastrone separation $= 2a[1+\varepsilon]$. The insertion of the semi-major axis $a = 9.7506\times10^8[\mathrm{m}]$ and eccentricity $\varepsilon = 0.617733$ yields (see [6]):

Periastron separation $= 7.45466\times10^8[\mathrm{m}]$ and

Apastron separation $= 3.154477\times10^8[\mathrm{m}]$.

**2)** ***Why the stars accelerate and decelerate?***

In the previous section, we explained why the stars on a circular orbit accelerate. For a circular orbit, this acceleration is extremely small. Differently, in the

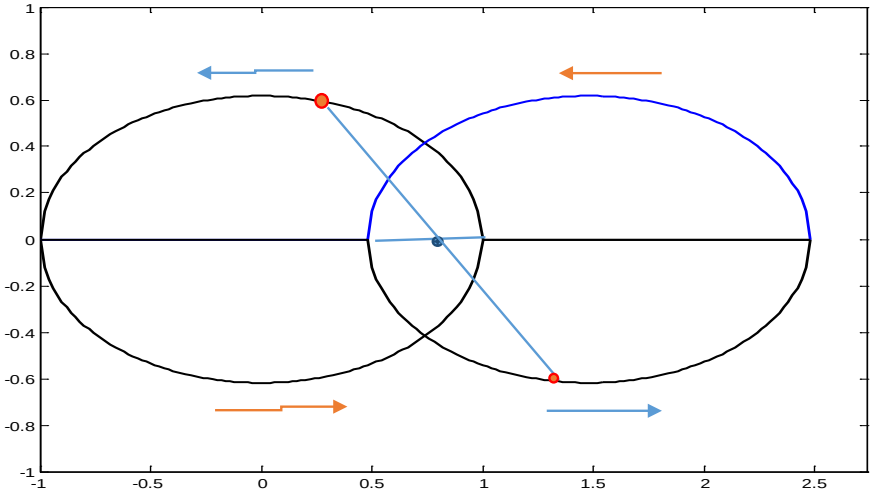


**Figure 4.** The elliptical orbits of the PSR system. The stars (red points) rotate anti clock. Blue arrows: deceleration. Red arrows: acceleration.

case of the two elliptical orbits we have large accelerations and decelerations during each period. Again, the gravitational attraction force is given by

$$\boldsymbol{F}_g(\varphi)=\frac{Gm^2}{4\rho^2(\varphi)}[\mathrm{N}] \tag{30}$$

and the centrifugal force is given by

$$\boldsymbol{F}_c(t)=m\omega^2(\varphi)\rho_c(\varphi)[\mathrm{N}] \tag{31}$$

where $\rho_c$ is the curvature radius of the ellipse and the angular velocity is defined by the rotation of the curvature radius. Again, the force vectors have different direction defined by the angle $\gamma$. The gravitational force can be represented by a vector sum of two perpendicular terms (**Figure 3**). The term

$$\boldsymbol{F}_g(\varphi)\cos(\gamma)=\frac{Gm^2}{4\rho^2(\varphi)}\cos(\gamma)[\mathrm{N}] \tag{32}$$

has the direction of (30) perpendicular to the tangent of the ellipse and the term

$$\boldsymbol{F}_g(\varphi)\sin(\gamma)=\frac{Gm^2}{4\rho^2(\varphi)}\sin(\gamma)[\mathrm{N}] \tag{33}$$

represents a tangential force. Equating the terms (31) and (32) yields the following formula for the local angular velocity (local means the function of $\varphi$).

$$\omega(\varphi)=\sqrt{\frac{Gm\cos(\gamma)}{4\rho(\varphi)\rho_c(\varphi)}}[\mathrm{rad/s}]. \tag{34}$$

The local tangential acceleration is

$$a(\varphi)=\boldsymbol{F}_g(\varphi)\sin(\gamma)/m=\frac{Gm}{4\rho^2(\varphi)}\sin(\gamma)\left[\mathrm{m/s^2}\right]. \tag{35}$$

The local velocity of the stars by orbiting from periastrone to apastron is (deceleration)

$$v(\varphi) = v_{\max} - \int_0^{\pi} a(\varphi)\mathrm{d}\varphi \tag{36}$$

and in opposite direction (acceleration)

$$v(\varphi) = v_{\min} + \int_{\pi}^{2\pi} a(\varphi)\mathrm{d}\varphi . \tag{37}$$

The mean velocity (in terms of $\varphi$) is the same for both directions

$$v_{\text{mean}} = \frac{1}{\pi}\int_0^{\pi} v(\varphi)\mathrm{d}\varphi . \tag{38}$$

The local tangential velocity is alternatively defined as

$$v(\varphi) = \omega(\varphi)\rho_c(\varphi) \tag{39}$$

Where $\rho_c$ is the local curvature radius (see Figure 5). The local velocity is shown in Figure 6. The maximum value equals 448.172 [km/s] and the minimum 106.287 (compare with **Appendix 1**).

Note that in this model, the maxima and minima of the velocity are located near the periastrone and apastrone (not exactly at these locations). The mean value in terms of $\varphi$ (as in Equation (38)) is 269.782 [km/s]. The time average is

$$\overline{v}(t) = \frac{\text{circumference of ellipse}}{\text{time of a single revolution}} = 181.757\left[\text{km/s}\right]. \tag{40}$$

The local average differs from the time average by the factor 1.319. The local angular velocity is shown in Figure 7.

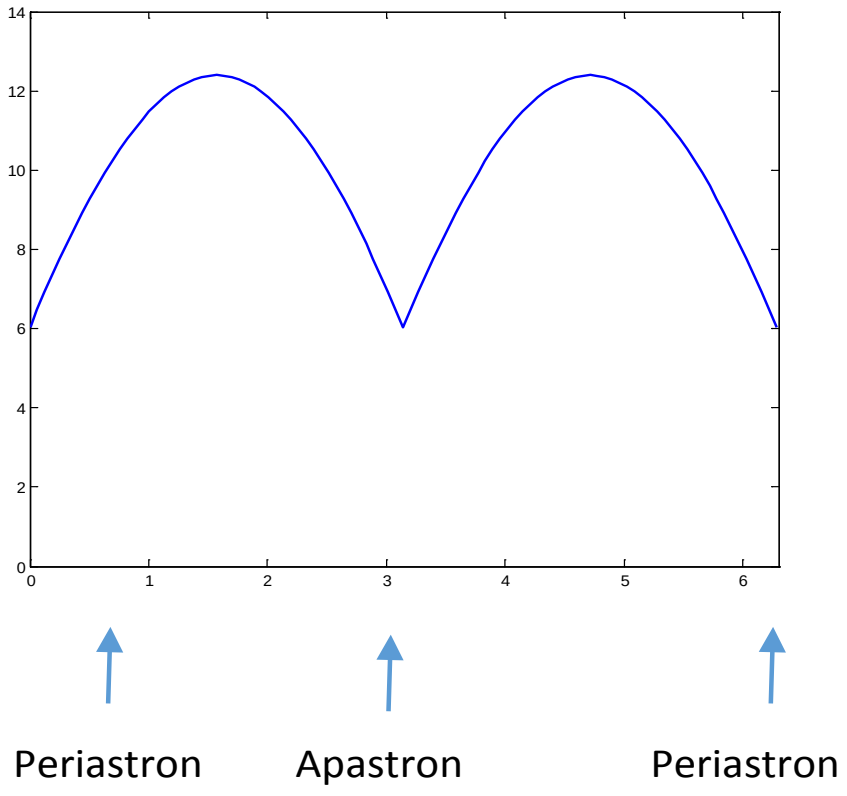


Figure 5. Curvature radius in terms of $\varphi$. Vertical scale $\times 10^8$.

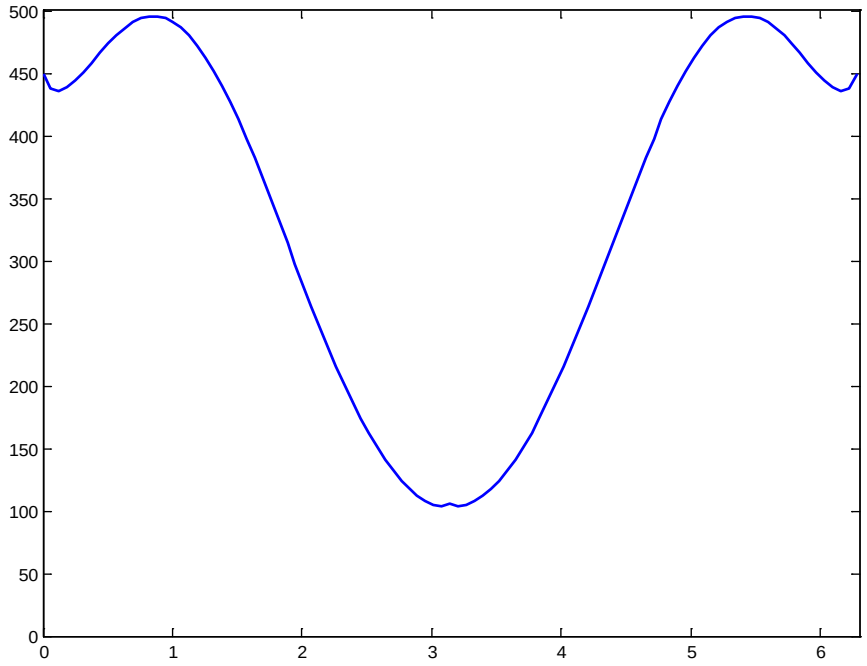


Figure 6. Orbital velocity [km/s] in terms of $\varphi$. Note the localization of $v_{\max}$ not at periastron.

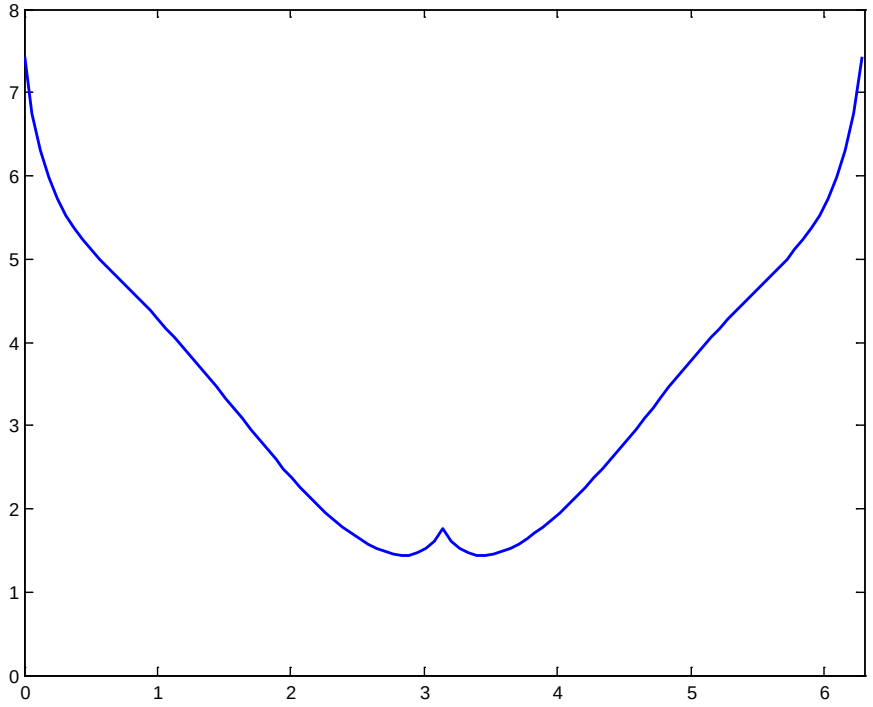


Figure 7. Angular velocity $\omega$ (rad/s) in terms $\varphi$. Vertical scale $10^{-8}$.

### 3) Kinetic and potential energies in the PSR system

The local kinetic energy is (Figure 8)

$$E_k(\varphi) = mv^2(\varphi)[\mathrm{J}] \tag{41}$$

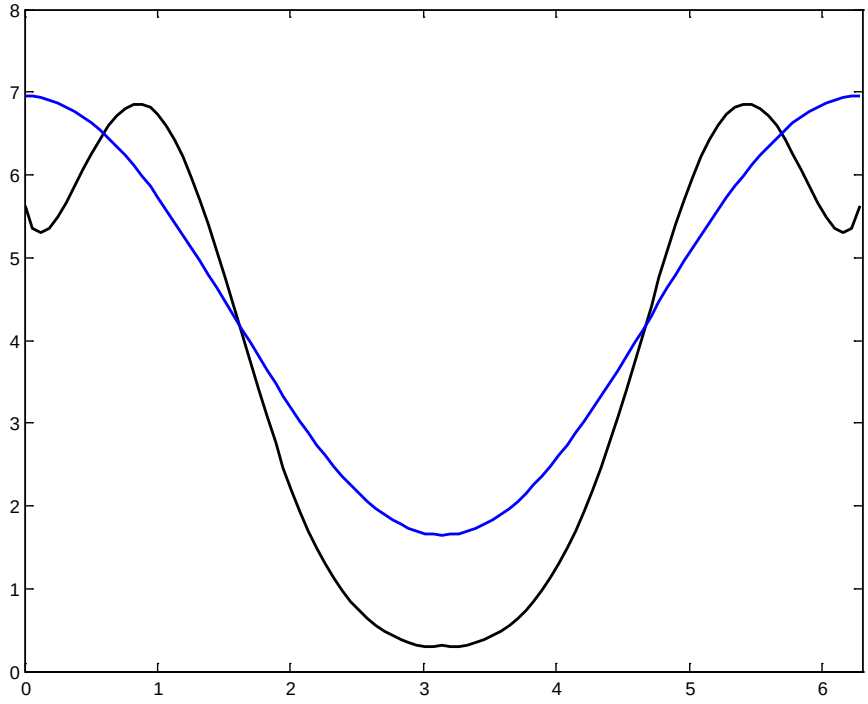


**Figure 8.** Kinetic energy (upper curve at $\varphi = \pi$) and the magnitude of potential energy in terms of $\varphi$. Vertical scale $\times 10^{41}$.

and the local negative potential energy is

$$E_P(\varphi) = \frac{-Gm^2}{2\rho(\varphi)}[\mathrm{J}]. \tag{42}$$

The corresponding local averages are $\bar{E}_k = 2.38257 \times 10^{41}[\mathrm{J}]$ and $\bar{E}_p = -4.369225 \times 10^{41}[\mathrm{J}]$. The ratio is $|\boldsymbol{E}_p| / E_k = 2.02435 \approx 2$, *i.e.*, almost the value defined by the circular system. It is reasonable to assume that the same ratio is valid for time averages.

**4) Concluding remarks about the PSR system**

Differently to the circular system the power emitted during a single revolution is a function of time and the radiation pattern $\sigma(\Omega)[\mathrm{W/steradian}]$ is a periodic function of time. Therefore, the reported by Taylor and Hulse power of the emitted gravitational waves P = 7.35 × $10^{24}$ [W] should be classified as a mean value.

## 5. Final Conclusions

- Both orbits, the circular and the elliptical, are defined by two forces of opposite directions: the centrifugal force and a term of the gravitational force (see Figure 3). It is logical to assume that both forces have the same physical explanation: the anisotropic energy exchange as described in reference [1]. Here, both anisotropies of radiation cancel. The other part of the gravitational force responsible for tangential acceleration or deceleration is the result of the tangential anisotropy of radiation.

- In the case of a circular orbit, the tangential acceleration is extremely small. We have shown that the notion of the instantaneous complex frequency is a convenient tool to study the process of inspiral of circular systems in the range of a linear gravitational force.

**Arguments in favor of the radiation recoil nature of gravity presented in [1 m]**

In 2015, the author presented a paper "Gravitational Forces Explained as the Result of Exchange between Baryonic Matter and the Quantum Vacuum" [1]. Let us present arguments in favor of this theory in terms of the description of orbiting double stars given in this paper:

- The orbit is defined by two forces: the gravitational force directed towards inside of the orbit and the centrifugal force directed towards the outside of the orbit. The forces are not collinear.
- The centripetal force is perpendicular to the tangent of the orbit.
- The gravitational force except some points is not perpendicular to the tangent and can be decomposed in two terms: the perpendicular compensates the centripetal force. The two forces cancel.
- The tangent force is responsible for acceleration or deceleration of the star.
- In the case of the common nearly circular orbit of the stars, we have an extremely small acceleration. In the case of a double-elliptical orbit, we have large accelerations and deceleration.
- The cancelation of the two forces shows that gravity and inertia have the same physical origin. They are recoil forces of radiation. The radiation pattern should be symmetric w.r.t. the tangent of the orbit. Differently, the pattern is asymmetric w.r.t. the line perpendicular to the orbit resulting in a recoil force of radiation.

In a word, it is logical to assume that all described here forces are recoil forces of radiation. The radiation pattern is symmetric w.r.t. the tangent of the orbit (cancellation of gravitation and inertia) and asymmetric w.r.t. the line perpendicular to the orbit, *i.e.*, the direction of the curvature radius.

## Conflicts of Interest

The authors declare no conflicts of interest regarding the publication of this paper.

## References

[1] Hahn, S.L. (2015) *Journal of Modern Physics*, **6**, 1135-1145. https://doi.org/10.4236/jmp.2015.68117

[2] Ferrari, V. (2010) The Quadrupole Formalism Applied to Binary Systems. https://www.-ego-gw.it/public/events/vesf

[3] Gasperini, M. (2017) Theory of Gravitational Interactions. 2nd Edition, Springer.

[4] Press Release (1993) About the Nobel Prize in Physics, Royal Swedish Academy of Sciences.

[5] The Binary Pulsar PSR1913+16. http://www.astrocornell.edu/academics/PSR1913+16

[6] Johnstone, R. http://www.johnstonsarchive.net./relativity/binarypulsar.html

[7] Hahn, S. (1939) The Instantaneous Complex Frequency Concept and Its Application in the Analysis of Building up Oscillations in Oscillator. *Proceedings of Vibrations Problems,* No. 1, 29-46.

[8] Hahn, S.L. and Snopek, K.M. (2016) Complex and Hypercomplex Analytic Signals. Theory and Applications, Artech House, Boston-Landon.

[9] Mironov, V.L. and Mironov, S.V. (2014) *Journal of Modern Physics*, **5**, 917-929. https://doi.org/10.4236/jmp.2014.510095

[10] The 2017 Nobel Prize in Physics-Press Release=Nobelprize.org.

[11] https://www.nobelprize.org/nobel_prizes/physics/laureates/2917/pr

## Appendix 1

This paper is illustrated by the properties of the binary pulsar PSR1913+16, a system of two binary neutron stars discovered and measured during many years by Taylor and Hulse [7] [8]. This great achievement of radioastronomy and also of time-frequency metrology was awarded by the Nobel Prize in physics in 1993. Let us repeat here the data compiled by Robert Johnston [8].

Mass of detected pulsar $m_1 = 1.441 \times \text{solar mass} = 2.8764 \times 10^{30}\left[\text{kg}\right]$ and of its companion $m_2 = 1.387 \times \text{s.m.} = 2.7205 \times 10^{30}\left[\text{kg}\right]$.

Orbital period $T_0 = 7.7511939106\left[\text{hr}\right] = 27807.19557\left[\text{s}\right]$.

Eccentricity of the elliptical orbits $\varepsilon = 0.617131$.

Semi-major axis $2a = 1950100\left[\text{km}\right]$ (remark of this author: the name semi-major axis should be replaced by major axis. Semi-major axis is equal not $2a$ but a. Periastron separation $= 746600\left[\text{km}\right]$,

Apastron separation $= 3153600\left[\text{km}\right]$

Orbital velocity of stars relative to the center of mass: at periastrone 450 [km/s], at apastrone: 110 [km/s].

## Appendix 2: The Derivation of the Curvature Radius of the in Spiral Orbit

Let us define the in spiral orbit by the equation

$$\psi(t) = \rho_0 \mathrm{e}^{\int_0^t s(t)\mathrm{d}t} \tag{A1}$$

$$s(t) = -(\alpha + \Delta\alpha * t) + j(\omega_0 + \Delta\omega * t) \tag{A2}$$

We assume that the binary stars have equal mass and rotate synchronously around common center of mass located at $x = y = 0$. The Cartesian coordinates of the first star are defined by the complex function $\psi(t) = x(t) + jy(t)$ with

$$x(t) = \rho_0 \mathrm{e}^{-\left(\alpha t + 0.5\Delta\alpha * t^2\right)} \cos\left(\omega_0 t + 0.5\Delta\omega * t^2\right) \tag{A3}$$

$$y(t) = \rho_0 \mathrm{e}^{-\left(\alpha t + 0.5\Delta\alpha * t^2\right)} \sin\left(\omega_0 t + 0.5\Delta\omega * t^2\right) \tag{A4}$$

and for the second star

$$x(t) = -\rho_0 \mathrm{e}^{-\left(\alpha t + 0.5\Delta\alpha * t^2\right)} \cos\left(\omega_0 t + 0.5\Delta\omega * t^2\right) \tag{A5}$$

$$y(t) = -\rho_0 \mathrm{e}^{-\left(\alpha t + 0.5\Delta\alpha * t^2\right)} \sin\left(\omega_0 t + 0.5\Delta\omega * t^2\right) \tag{A6}$$

The curvature radius at the point defined by $t = t_0$ is

$$\rho_c = \frac{\left[\left(\dot{x}(t_0)^2\right) + \left(\dot{y}(t_0)^2\right)\right]}{\left|\ddot{y}(t_0)\dot{x}(t_0) + \ddot{x}(t_0)\dot{y}(t_0)\right|} \tag{A7}$$

Let us calculate the derivatives beginning with zero values of $\Delta\alpha$ and $\Delta\omega$. We have

$$\dot{x}(t) = \rho_0\left[-\alpha_0 \mathrm{e}^{-\alpha_0 t}\cos(\omega_0 t) - \omega_0 \mathrm{e}^{-\alpha_0 t}\sin(\omega_0 t)\right] \tag{A8}$$

$$\dot{y}(t)=\rho_0\left[-\alpha_0 \mathrm{e}^{-\alpha_0 t}\sin(\omega_0 t)+\mathrm{e}^{-\alpha_0 t}\omega_0\cos(\omega_0 t)\right] \tag{A9}$$

$$\ddot{x}(t)=\rho_0\left[\alpha_0^2\mathrm{e}^{-\alpha_0 t}\cos(\omega_0 t)+\alpha_0\omega_0\mathrm{e}^{-\alpha t}\sin(\omega_0 t)+\alpha_0\omega_0\mathrm{e}^{-\alpha t}\sin(\omega_0 t)-\omega_0^2\mathrm{e}^{-\alpha_0 t}\cos(\omega_0 t)\right]$$

$$\ddot{y}(t)=R_0\left[\alpha_0^2\mathrm{e}^{-\alpha_0 t}\sin(\omega_0 t)-\alpha_0\omega_0\mathrm{e}^{-\alpha_0 t}\cos(\omega_0 t)-\alpha_0\omega_0\mathrm{e}^{-\alpha_0 t}\cos(\omega_0 t)-\omega_0^2\mathrm{e}^{-\alpha t}\sin(\omega_0 t)\right]$$

The insertion using $t=0$ yields

$$\rho_c(t)=\rho_0\mathrm{e}^{-\alpha_0 t}\frac{\left(\alpha_0^2+\omega_0^2\right)^{\frac{3}{2}}}{\left|\omega_0\left(\omega_0^2-\alpha_0^2\right)\right|}=\rho_0\mathrm{e}^{-\alpha_0 t}\frac{\left(1+\left(\alpha_0/\omega_0\right)^2\right)^{\frac{3}{2}}}{1-\left(\alpha_0/\omega_0\right)^2} \tag{A10}$$

Of course, for a circular orbit $\alpha_0 = 0$ and $\rho_c = \rho_0$. Otherwise, $\rho_c > \rho_0$. The center of the curvature radius is located at

$$\begin{aligned} x_c &= x(t_0)-\dot{y}(t_0)\frac{\left(\left(\dot{x}(t_0)\right)\right)^2+\left(\dot{y}(t_0)\right)^2}{\ddot{y}(t_0)\dot{x}(t_0)-\dot{y}(t_0)\ddot{x}(t_0)};\\ y_c &= y(t_0)+\dot{x}(t_0)\frac{\left(\left(\dot{x}(t_0)\right)\right)^2+\left(\dot{y}(t_0)\right)^2}{\ddot{y}(t_0)\dot{x}(t_0)-\dot{y}(t_0)\ddot{x}(t_0)}. \end{aligned} \tag{A11}$$

If $t=0$, $x(0)=\rho_0$, $y(0)=0$, $\dot{x}(0)=-\alpha_0\rho_0$, $\dot{y}(0)=\omega_0\rho_0$, $\ddot{x}(0)=\rho_0\left(\alpha_0^2-\omega_0^2\right)$, $\ddot{y}(0)=-2\alpha_0\omega_0 R_0$.

The insertion yields $x_c(0)=0, y_c(0)=-\frac{\alpha_0}{\omega_0}\rho_0$. The angle between $\rho_0$ and $\rho_c$ is

$$\tan\left(\varphi(t=0)\right)=-\frac{\alpha_0}{\omega_0},\ \sin\left(\varphi(t=0)\right)=\frac{\alpha_0/\omega_0}{\sqrt{1+\left(\alpha_0/\omega_0\right)^2}},$$

$$\cos\left(\varphi(t=0)\right)=\frac{1}{\sqrt{1+\left(\alpha_0/\omega_0\right)^2}}$$

The curvature radius of an ellipse in Cartesian coordinates (*x, y*) is $\rho_c=a^2b^2\left(\frac{x^2}{a^4}+\frac{y^2}{b^4}\right)^{\frac{3}{2}}$.

Journal of Modern Physics, 2018, 9, 1970-2007
http://www.scirp.org/journal/jmp
ISSN Online: 2153-120X
ISSN Print: 2153-1196

# Minkowski, Schwarzschild and Kerr Metrics Revisited

**J.-F. Pommaret**

CERMICS, Ecole des Ponts ParisTech, Paris, France
Email: jean-francois.pommaret@wanadoo.fr

**How to cite this paper:** Pommaret, J.-F. (2018) Minkowski, Schwarzschild and Kerr Metrics Revisited. *Journal of Modern Physics*, **9**, 1970-2007.
https://doi.org/10.4236/jmp.2018.910125

**Received:** June 19, 2018
**Accepted:** September 10, 2018
**Published:** September 13, 2018



## Abstract

In recent papers, a few physicists studying Black Hole perturbation theory in General Relativity (GR) have tried to construct the initial part of a differential sequence based on the Kerr metric, using methods similar to the ones they already used for studying the Schwarzschild geometry. Of course, such a differential sequence is well known for the Minkowski metric and successively contains the Killing (order 1), the Riemann (order 2) and the Bianchi (order 1 again) operators in the linearized framework, as a particular case of the *Vessiot structure equations*. In all these cases, they discovered that the *compatibility conditions* (CC) for the corresponding Killing operator were involving *a mixture of both second order and third order CC* and their idea has been to exhibit only a *minimal number of generating ones*. Unhappily, these physicists are neither familiar with the formal theory of systems of partial differential equations and differential modules, nor with the formal theory of Lie pseudogroups. Hence, even if they discovered a link between these differential sequences and the number of parameters of the Lie group preserving the background metric, they have been unable to provide an intrinsic explanation of this fact, being limited by the technical use of Weyl spinors, complex Teukolsky scalars or Killing-Yano tensors. The purpose of this difficult computational paper is to provide differential and homological methods in order to revisit and solve these questions, not only in the previous cases but also in the specific case of any Lie group or Lie pseudogroup of transformations. These new tools, which are now available as computer algebra packages, question the mathematical foundations of GR and the origin of gravitational waves.

## Keywords

General Relativity, Killing Operator, Riemann Tensor, Weyl Tensor, Bianchi Identities, Lie Algebroid, Differential Sequence, Differential Module, Homological Algebra, Extension Modules

## 1. Introduction

In many recent technical papers, a few physicists working on General Relativity (GR) are trying to construct high order differential sequences while starting with the Killing operator for a given metric (Minkowski, Schwarzschild, Kerr, ...) ([1] [2] [3] [4] [5]). The "*ad hoc*" (technical) methods involved are ranging from Killing/Killing-Yano tensors, Penrose spinors, Teukolski scalars or compexified frames.

Meanwhile, *on one side*, they have the feeling that the construction of these sequences has surely to do with the fact that the corresponding Killing systems of infinitesimal Lie equations have less linearly independent solutions than the $n(n+1)/2$ that were predicted by A. Eisenhart in 1949 for nondegenerate metrics with constant Riemannian curvature on a space of dimension $n$ ([6] along results first found by E. Vessiot in 1903 [7] [8]), that is 10 when $n=4$ (space-time) with the Minkowski metric, and discover that, *perhaps for this reason*, they have to exhibit an unexpected mixture of generating compatibility conditions (CC) of order 2 *and* 3.

However, *on another side*, they are clearly aware of the fact that *their results are far from being intrinsic* and cannot be adapted to other metrics or dimensions.

The purpose of this short but difficult paper, even though it is written in a rather self-contained computational way, is to solve this problem in its full intrinsic generality, using a few results ranging among the most delicate ones that can be found in the formal theory of systems of ordinary differential (OD) or partial differential (PD) equations and Lie pseudogroups introduced around 1970 by D. C. Spencer and coworkers ([9] [10] [11]). It must also be noticed that these new methods, though they can be found in many books ([12]-[18]) or papers ([19]-[25]) of the author of this paper to which we shall often refer, have rarely been acknowledged by the computer algebra community and/or by physicists. The essential new "trick" is to deal with sections of jet-bundles and *not* with solutions of systems of OD or PD equations.

In Section 2, we provide and illustrate the two crucial mathematical results needed for the applications presented in Section 3. The first result, roughly discovered by M. Janet in 1920 ([26]), describes the way to use a certain *prolongation*/*projection* (PP) procedure absolutely needed in order to transform any sufficiently regular system into a formally integrable system and, finally, even an involutive system, that is a situation where we know that the generating CC are described by a first order involutive system and the possibility to construct a *canonical* Janet or Spencer sequence. In this homological algebraic framework, the technique of diagram chasing is *absolutely needed* and we ask the reader to learn at least the so-called "snake" lemma in textbooks ([27]-[32]). As for the second result, it is allowing to study *effectively* Lie operators acting on vector fields and such that, if two vectors are solutions, their bracket is also a solution. It is thus also *absolutely needed* when dealing with the PP procedure

because it is not possible to work out solutions in general and the use of computer algebra is therefore a *pure nonsense* for the intrinsic study of most Lie operators as we shall see in Section 3.

The author thanks Prof. Lars Andersson from Albert Einstein Institute of Potsdam for many enlightening discussions during his last visit to AEI (October 23-27, 2017), in particular for bringing the problem of finding new generating CC to his attention when studying the specific Lie operators to be met in GR.

## 2. Mathematical Tools

### A) Formal Integrability

All operators and systems considered in this paper will have coefficients in a differential field $K$ with $n$ derivations $\partial_1,\cdots,\partial_n$, for example the standard derivations when $K=\mathbb{Q}\left(x^1,\cdots,x^n\right)$ is the differential field of rational functions. Starting with a given operator $\mathcal{D}$, a *direct problem* is to look for *generating compatibility conditions* (CC) described by an operator $\mathcal{D}_1$ in such a way that $\mathcal{D}_1\eta=0$ denotes the CC needed for solving (at least locally) the linear inhomogeneous system $\mathcal{D}\xi=\eta$. Going along this way, one may construct inductively a *differential sequence* $\mathcal{D},\mathcal{D}_1,\mathcal{D}_2,\cdots$ of operators such that not only $\mathcal{D}_{i+1}\circ\mathcal{D}_i=0$ of course but also each operator $\mathcal{D}_{i+1}$ generates the CC of $\mathcal{D}_i$. Such a result has been found for the first time as a footnote by M. Janet in 1920 ([26]) who even proved that, under slightly additional conditions, the sequence stops at $\mathcal{D}_n$ which is thus formally surjective, when $n$ is the number of independent variables.

The main problem is that, in general and though surprising it may look like, the word "*generating*" has no clear meaning at all, a result leading to refine the definition of a differential sequence in an intrinsic way. Apart from the Macaulay example that will be treated and revisited later on, our two favorite examples are the following ones that will also be revisited and are treated in a way adapted to the aim of this paper. We shall denote by $m$ the number of unknowns $\left(y^1,\cdots,y^m\right)$ also called *differential indeterminates*, by $n$ the number of independent variables $\left(x^1,\cdots,x^n\right)$ and by $q$ the order of the system/operator considered. We shall finally introduce the non-commutative ring $D=K\left[d\right]=K\left[d_1,\cdots,d_n\right]$ of differential operators $P,Q,\cdots$ with coefficients in $K$.

**EXAMPLE 2A.1**: With $m=1,n=2,K=\mathbb{Q}$, we shall use *formal derivatives* $\left(d_1,d_2\right)$ when using differential modules or computer algebra but will set $d_i\left(d_jy\right)=d_j\left(d_iy\right)=d_{ij}y=y_{ij}$ for simplicity while using jet coordinates and notations. Let us consider the second order system:

$$Py\equiv y_{22}=u,Qy\equiv y_{12}+y=v\Rightarrow y_2=v_2-u_1\Rightarrow y=v-v_{12}+u_{11}$$

There are many different ways to look at such a system. The first natural one is to say that *the only solution is* $y=0$ when $u=v=0$. The second one is to look for the CC that *must* be satisfied by $(u,v)$ and we may adopt two possible presentations:

- Substitute $y$ and obtain the 2 fourth order CC:

$$\begin{cases} A \equiv v_{1222} - v_{22} - u_{1122} + u = 0 \\ B \equiv v_{1122} - u_{1112} - u_{11} = 0 \end{cases}$$

which are not differentially independent because one can easily check:

$$B_{12} - B - A_{11} = 0$$

- However, we also have:

$$P \circ Q - Q \circ P = 0 \Rightarrow C \equiv Pv - Qu \equiv v_{22} - u_{12} - u = 0$$

that is a second order CC.

Finally, we obtain:

$$A \equiv C_{12} - C, B \equiv C_{11} \Leftrightarrow C \equiv B_{22} - A_{12} + A$$

and we discover that the CC of $\mathcal{D} = (P, Q)$ are generated by $(A, B)$ but also by $C$ alone, though any student will hesitate between the two possibilities!.

Referring to *differential homological algebra* as in ([25]) while indicating the order of an operator below its arrow, the same trivial differential module $M = 0$ (*care*) defined by $\mathcal{D}$ has therefore two split resolutions:

$$0 \to D \xrightarrow[2]{} D^2 \xrightarrow[4]{} D^2 \xrightarrow[2]{} D \to 0$$

$$0 \to D \xrightarrow[2]{} D^2 \xrightarrow[2]{} D \to 0$$

which are quite different even if the two Euler-Poincaré characteristics both vanish because we have:

$$1 - 2 + 2 - 1 = 0, \quad 1 - 2 + 1 = 0$$

**EXAMPLE 2A.2**: (Janet) Now with $m = 1, n = 3, q = 2$ and $K = \mathbb{Q}(x^2)$, let us consider the second order system (see [15] [16] for more details):

$$y_{33} - x^2 y_{11} = u, \quad y_{22} = v$$

We let the reader use computer algebra and Gröbner bases in order to find out the two generating CC of respective order 3 and 6 and work out the following possible resolution where $dim_K(M) = 12$:

$$0 \to D \to D^2 \xrightarrow[6]{} D^2 \xrightarrow[2]{} D \to M \to 0.$$

The main point in this subsection is to use the three following highly non-trivial theorems (Compare [10] [11] to [12] [16], in particular pp. 364-366 for details) and just follow their proofs on the two previous examples but the next example found by Macaulay will provide all details.

When $X$ is a manifold with $dim(X) = n$ and local coordinates $(x^1, \cdots, x^n)$, we denote by $T$ the tangent bundle and by $T^*$ the cotangent bundle. If $E$ is a vector bundle over $X$ with projection $\pi$, local coordinates $(x, y^k)$ for $k = 1, \cdots, m$, we use to denote by $dim(E) = m$ the fiber dimension of $E$. A local or global section $f$ can be locally described by $y^k = f^k(x)$. Using multi-indices $\mu = (\mu_1, \cdots, \mu_n)$ with *length* $|\mu| = \mu_1 + \cdots + \mu_n$, we shall denote by $J_q(E)$ the $q$-jet bundle of $E$ over $X$ with projection $\pi_q$ on $X$, local coordinates $x^i, y^k_\mu$

and sections $f_q=\left(f_\mu^k(x)\right)$ over $f$ for $j_q(f)=\left(\partial_\mu f^k(x)\right)$. The Spencer operator $D: J_{q+1}(E)\to T^*\otimes J_q(E): f_{q+1}\to j_1(f_q)-f_{q+1}$ $=\left(\partial_i f^k(x)-f_i^k(x),\partial_i f_j^k(x)-f_{ij}^k(x),\cdots\right)$ (care to the notation) will allow to distinguish among these two types of sections. We denote by $S_qT^*$ the vector bundle of (completely) symmetric tensors and by $\wedge^r T^*$ the vector bundle of (completely) skewsymmetric tensors over *X*. We set:

**DEFINITION 2A.3**: A *system* of order $q$ on $E$ is an open vector subbundle $R_q\subseteq J_q(E)$ with prolongations $\rho_r(R_q)=R_{q+r}=J_r(R_q)\cap J_{q+r}(E)\subseteq J_r(J_q(E))$ and symbols $\rho_r(g_q)=g_{q+r}=S_{q+r}T^*\otimes E\cap R_{q+r}\subseteq J_{q+r}(E)$ only depending on $g_q\subseteq S_qT^*\otimes E$. For $r,s\geq 0$, we denote by $R_{q+r}^{(s)}\subseteq R_{q+r}=\pi_{q+r}^{q+r+s}\left(R_{q+r+s}\right)$ the projection of $R_{q+r+s}$ on $R_{q+r}$, which is thus defined by more equations in general. The system $R_q$ is said to be *formally integrable* (FI) if we have $R_{q+r}^{(s)}=R_{q+r},\forall r,s\geq 0$, that is if all the equations of order $q+r$ can be obtained by means of only *r* prolongations. The system $R_q$ is said to be *involutive* if it is FI with an involutive symbol $g_q$. We shall simply denote by $\Theta=\left\{f\in E\,|\,j_q(f)\in R_q\right\}$ the "set" of (formal) solutions. It is finally easy to prove that the Spencer operator restricts to $D: R_{q+1}\to T^*\otimes R_q$.

Comparing the sequences obtained in the two previous examples, we may state:

**DEFINITION 2A.4**: A differential sequence is said to be *formally exact* if it is exact on the jet level composition of the prolongations involved. A formally exact sequence is said to be *strictly exact* if all the operators/systems involved are FI. A strictly exact sequence is called *canonical* if all the operators/systems are involutive. The only known canonical sequences are the Janet and Spencer sequences that can be defined independently from each other.

**EXAMPLE 2A.5**: In the first example with $dim(E)=1, dim(F_0)=2$, we let the reader prove that $dim(R_{2+r})=4,\forall r\geq 0$. Hence, if $(A,B)$ is a section of $F_1$ while *C* is a section of $F_1'$, the jet prolongation sequence:

$$0\to R_6\to J_6(E)\to J_4(F_0)\to F_1\to 0$$

$$0\to 4\to 28\to 30\to 2\to 0$$

is *not* formally exact because $4-28+30-2=4\neq 0$, while the corresponding long sequence:

$$0\to R_{r+4}\to J_{r+4}(E)\to J_{r+2}(F_0)\to J_r(F_1')\to 0$$

$$0\to 4\to (r+5)(r+6)/2\to (r+3)(r+4)\to (r+1)(r+2)/2\to 0$$

is indeed formally exact because

$$4-\frac{\left(r^2+11r+30\right)}{2}+\left(r^2+7r+12\right)-\frac{\left(r^2+3r+2\right)}{2}=0$$ but *not* strictly exact because $R_2$ is quite far from being FI.

With canonical projection $\Phi_0: J_q(E)\Rightarrow J_q(E)/R_q=F_0$, the case $r=0,s=1$ is described by the following commutative and exact diagram:

$$\begin{array}{ccccccccc}
 & & 0 & & 0 & & 0 & & \\
 & & \downarrow & & \downarrow & & \downarrow & & \\
0 & \to & g_{q+1} & \to & S_{q+1}T^*\otimes E & \to & T^*\otimes F_0 & \to & h_1 & \to 0 \\
 & & \downarrow & & \downarrow & & \downarrow & & \downarrow & \\
0 & \to & R_{q+1} & \to & J_{q+1}(E) & \to & J_1(F_0) & \to & Q_1 & \to 0 \\
 & & \downarrow & & \downarrow & & \downarrow & & \downarrow & \\
0 & \to & R_q & \to & J_q(E) & \to & F_0 & \to & 0 & \\
 & & & & \downarrow & & \downarrow & & & \\
 & & & & 0 & & 0 & & &
\end{array}$$

Chasing in this diagram while applying the "*snake*" lemma, we obtain the useful *long exact connecting sequence*:

$$0 \to g_{q+1} \to R_{q+1} \to R_q \to h_1 \to Q_1 \to 0$$

which is thus connecting in a tricky way FI (*lower left*) with CC (*upper right*).

Having in mind the fact that the *Riemann* ( $g_1$ is not 2-acyclics but $g_2 = 2$ is trivially involutive) and the *Weyl* ( $\hat{g}_1$ is not 2-acyclic but $\hat{g}_2$ is 2-acyclic $\forall n \geq 4$ while $\hat{g}_3 = 0, \forall n \geq 3$ ) operators (linearization of the respective tensors) are second order, a key stone is:

**THEOREM 2A.6**: If a system $R_q \subset J_q(E)$ is FI, then the corresponding operator $\mathcal{D}: E \xrightarrow{j_q} J_q(E) \xrightarrow{\Phi_0} J_q(E)/R_q = F_0$ admits (minimal) generating CC of order $s+1$ if $s$ is the smallest integer such that $g_{q+s}$ becomes 2-acyclic.

**THEOREM 2A.7**: (*prolongation/projection* (PP) *procedure*) If a system $R_q \subseteq J_q(E)$ has a 2-acyclic symbol $g_q \subseteq S_qT^*\otimes E$ and $g_{q+1}$ is a vector bundle, then $\rho_r\left(R_q^{(1)}\right) = R_{q+r}^{(1)}, \forall r \geq 0$. Hence, if an arbitrary system $R_q \subseteq J_q(E)$ is given, one can *effectively* find two integers $r, s \geq 0$ such that the system $R_{q+r}^{(s)}$ is formally integrable or even involutive, with the same solutions.

**THEOREM 2A.8**: Starting with *any* operator $\mathcal{D} = E \to F_0$ of order $q$ defined over a differential field $K$ by a system $R_q \subseteq J_q(E)$, one can construct a formally exact commutative diagram:

$$\begin{array}{ccccccccc}
0 & \to & \Theta & \to & E & \xrightarrow{\mathcal{D}} & F_0 & \xrightarrow{\mathcal{D}_1} & F_1 \\
 & & \| & & \| & & \downarrow\mathcal{P} & & \downarrow\mathcal{Q} \\
0 & \to & \Theta & \to & E & \xrightarrow{\mathcal{D}'} & F_0' & \xrightarrow{\mathcal{D}_1'} & F_1'
\end{array}$$

where $\mathcal{P}$ is an injective operator of order at least $r+s$ whenever $R_{q+r}^{(s)}$ is a formally integrable system with the same solutions as $R_q$ obtained by the PP procedure and the upper sequence is formally exact while the lower sequence is strictly exact with $ord\left(\mathcal{D}_1'\right) = 1$ when $\mathcal{D}'$ is involutive.

Starting with an arbitrary system $R_q \subset J_q(E)$, the main purpose of the next crucial example is to prove that the generating CC of the operator $\mathcal{D} = \Phi_0 \circ j_q : E \xrightarrow{j_q} J_q(E) \xrightarrow{\Phi_0} J_q(E)/R_q = F_0$, though they are of course fully determined by the first order CC of the final involutive system $R_{q+r}^{(s)}$ produced by the up/down PP procedure, are in general of order $r+s+1$ as we

shall see in the applications but may be of strictly lower order. All diagrams and chases will be described in actual practice. We invite the reader to study similarly the first example where $R_2^{(4)}=0, \mathcal{D}'=j_2$ and $\mathcal{D}_1'=D_1$ is the first Spencer operator.

**EXAMPLE 2A.9**: ([33], p 40 with the first feeling of Formal Integrability). With $m=1, n=3, q=2$, let us consider the second order linear system $R_2 \subset J_2(E)$ with $dim(E)=1, dim(R_2)=8$ and $par_2=\{y, y_1, y_2, y_3, y_{11}, y_{12}, y_{22}, y_{23}\}$ if we use jet coordinates, defined by the two inhomogeneous PD equations:

$$Py \equiv y_{33}=u, \quad Qy \equiv y_{13}+y_2=v$$

As we already said, the only existing intrinsic procedure has two steps:

- *Step* 1: First of all we have to look for the symbol $g_2$ defined by the two linear equations $v_{33}=0, v_{13}=0$. The coordinate system is not $\delta$-regular and exchanging $x^1$ with $x^2$, we get the Janet board:

$$\begin{cases} v_{33}=0 \\ v_{23}=0 \end{cases} \begin{array}{|ccc|} \hline 1 & 2 & 3 \\ 1 & 2 & \bullet \\ \hline \end{array}$$

It follows that $g_2$ is involutive, thus 2-acyclic and we obtain from the main theorem $\rho_r\left(R_2^{(1)}\right)=R_{2+r}^{(1)}$. However, $R_2^{(1)} \subset R_2$ with a strict inclusion because $R_2^{(1)}$ with $dim\left(R_2^{(1)}\right)=7$ is now defined by the 3 equations:

$$y_{33}=u, \quad y_{23}=v_3-u_1, \quad y_{13}+y_2=v$$

We may start again with $R_2^{(1)}$ and study its symbol $g_2^{(1)}$ defined by the 3 linear equations with Janet board:

$$\begin{cases} v_{33}=0 \\ v_{23}=0 \\ v_{13}=0 \end{cases} \begin{bmatrix} 1 & 2 & 3 \\ 1 & 2 & \bullet \\ 1 & \bullet & \bullet \end{bmatrix}$$

It follows that $g_2^{(1)}$ is again involutive but we have a strict inclusion $R_2^{(2)} \subset R_2^{(1)}$ because $dim\left(R_2^{(2)}\right)=6$ as $R_2^{(2)}$ is defined by the 4 equations with Janet board:

$$\begin{cases} y_{33}=u \\ y_{23}=v_3-u_1 \\ y_{22}=v_2-v_{13}+u_{11} \\ y_{13}-y_2=v \end{cases} \begin{bmatrix} 1 & 2 & 3 \\ 1 & 2 & \bullet \\ 1 & 2 & \bullet \\ 1 & \bullet & \bullet \end{bmatrix}$$

As $R_2^{(2)}$ is easily seen to be involutive, we achieve the PP procedure with the strict intrinsic inclusions and corresponding fiber dimensions:

$$R_2^{(2)} \subset R_2^{(1)} \subset R_2 \Leftrightarrow 6<7<8$$

Finally, we have $\rho_r\left(R_2^{(2)}\right)=\rho_r\left(\left(R_2^{(1)}\right)^{(1)}\right)=\left(\rho_r\left(R_2^{(1)}\right)\right)^{(1)}=\left(R_{2+r}^{(1)}\right)^{(1)}=R_{2+r}^{(2)}$.

- *Step* 2: It remains to find out the CC for $(u, v)$ in the initial inhomogeneous system. As we have used two prolongations in order to exhibit $R_2^{(2)}$, we have second order formal derivatives of $u$ and $v$ in the right members. Now, as we

have an involutive system, we have first order CC for the new right members and could hope therefore for third order generating CC. However, we have successively the 4 CC:

$$y_{233} = d_3(v_3 - u_1) = d_2 u \Rightarrow v_{33} - u_{13} - u_2 = 0$$

$$y_{223} = d_3(v_2 - v_{13} + u_{11}) = d_2(v_3 - u_1) \Rightarrow v_{133} - u_{113} - u_{12} = 0$$

$$y_{133} + y_{23} = d_3 v = d_1 u + (v_3 - u_1) \Rightarrow 0 = 0$$

$$y_{123} + y_{22} = d_2 v = d_1(v_3 - u_1) + (v_2 - v_{13} + u_{11}) \Rightarrow 0 = 0$$

It follows that we have *only* one second and one third order CC:

$$v_{33} - u_{13} - u_2 = 0, \quad v_{133} - u_{113} - u_{12} = 0$$

but, *surprisingly*, the *only* generating second order CC $v_{33} - u_{13} - u_2 = 0$ which is coming from the fact that the operator $P$ commutes with the operator $Q$.

We finally show how FI is related to CC by means of an homological procedure known as the "*long exact connecting sequence*" which is the main byproduct of the so-called *snake lemma* used when chasing in diagrams. Needless to say that absolutely no classical procedure can produce such a result which is thus totally absent from the GR papers already quoted. First of all, let us compute the dimensions of the bundles that will be used in the following diagrams while using *parametric* jets:

$$par_2 = \{y, y_1, y_2, y_3, y_{11}, y_{12}, y_{22}, y_{23}\}$$

$$par_3 = \{y, y_1, y_2, y_3, y_{11}, y_{12}, y_{22}, y_{111}, y_{112}, y_{122}, y_{222}, y_{223}\}$$

$$par_4 = \{y, y_1, y_2, y_3, y_{11}, y_{12}, y_{111}, y_{112}, y_{122}, y_{222}, y_{1111}, y_{1112}, y_{1122}, y_{1222}, y_{2222}, y_{2223}\}$$

and thus $dim(R_2) = 8, dim(R_3) = 12, dim(R_4) = 16$ in the following commutative and exact diagram where $E$ is the trivial vector bundle with $dim(E) = 1$ and $dim(g_{2+r}) = 4 + r$:

$$\begin{array}{ccccccccc}
 & & 0 & & 0 & & 0 & & \\
 & & \downarrow & & \downarrow & & \downarrow & & \\
0 & \to & g_4 & \to & S_4T^* \otimes E & \to & S_2T^* \otimes F_0 & \to & h_2 & \to 0 \\
 & & \downarrow & & \downarrow & & \downarrow & & \downarrow & \\
0 & \to & R_4 & \to & J_4(E) & \to & J_2(F_0) & \to & F_1 & \to 0 \\
 & & \downarrow & & \downarrow & & \downarrow & & \downarrow & \\
0 & \to & R_3 & \to & J_3(E) & \to & J_1(F_0) & \to & 0 & \\
 & & & & \downarrow & & \downarrow & & & \\
 & & & & 0 & & 0 & & &
\end{array}$$

$$\begin{array}{ccccccccc}
 & & 0 & & 0 & & 0 & & \\
 & & \downarrow & & \downarrow & & \downarrow & & \\
0 & \to & 6 & \to & 15 & \to & 12 & \to & 3 & \to 0 \\
 & & \downarrow & & \downarrow & & \downarrow & & \downarrow & \\
0 & \to & 16 & \to & 35 & \to & 20 & \to & 1 & \to 0 \\
 & & \downarrow & & \downarrow & & \downarrow & & \downarrow & \\
0 & \to & 12 & \to & 20 & \to & 8 & \to & 0 & \\
 & & & & \downarrow & & \downarrow & & & \\
 & & & & 0 & & 0 & & &
\end{array}$$

$$\begin{array}{ccccccccc}
 & & 0 & & 0 & & 0 & & 0 \\
 & & \downarrow & & \downarrow & & \downarrow & & \downarrow \\
0 \rightarrow & & g_4 & \rightarrow & S_4T^* \otimes E & \rightarrow & S_2T^* \otimes F_0 & \rightarrow & h_2 & \rightarrow 0 \\
 & & \downarrow \delta & & \downarrow \delta & & \downarrow \delta & & \downarrow \delta & \\
0 \rightarrow & & T^* \otimes g_3 & \rightarrow & T^* \otimes S_3T^* \otimes E & \rightarrow & T^* \otimes T^* \otimes F_0 & \rightarrow & T^* \otimes h_1 & \rightarrow 0 \\
 & & \downarrow \delta & & \downarrow \delta & & \downarrow \delta & & \downarrow & \\
0 \rightarrow & & \wedge^2 T^* \otimes g_2 & \rightarrow & \wedge^2 T^* \otimes S_2T^* \otimes E & \rightarrow & \wedge^2 T^* \otimes F_0 & \rightarrow & 0 & \\
 & & \downarrow \delta & & \downarrow \delta & & \downarrow & & & \\
0 \rightarrow & & \wedge^3 T^* \otimes T^* \otimes E & = & \wedge^3 T^* \otimes T^* \otimes E & \rightarrow & 0 & & & \\
 & & \downarrow & & \downarrow & & & & & \\
 & & 0 & & 0 & & & & &
\end{array}$$

$$\begin{array}{ccccccccc}
 & & 0 & & 0 & & 0 & & 0 \\
 & & \downarrow & & \downarrow & & \downarrow & & \downarrow \\
0 \rightarrow & & 6 & \rightarrow & 15 & \rightarrow & 12 & \rightarrow & 3 & \rightarrow 0 \\
 & & \downarrow \delta & & \downarrow \delta & & \downarrow \delta & & \downarrow \delta & \\
0 \rightarrow & & 15 & \rightarrow & 30 & \rightarrow & 18 & \rightarrow & 3 & \rightarrow 0 \\
 & & \downarrow \delta & & \downarrow \delta & & \downarrow \delta & & \downarrow & \\
0 \rightarrow & & 12 & \rightarrow & 18 & \rightarrow & 6 & \rightarrow & 0 & \\
 & & \downarrow \delta & & \downarrow \delta & & \downarrow & & & \\
0 \rightarrow & & 3 & = & 3 & \rightarrow & 0 & & & \\
 & & \downarrow & & \downarrow & & & & & \\
 & & 0 & & 0 & & & & &
\end{array}$$

where $S_4T^* \otimes E \simeq S_4T^*$ and $F_1 \simeq Q_2$. From the snake lemma and a chase, we obtain the *long exact connecting sequence*:

$$0 \rightarrow g_4 \rightarrow R_4 \rightarrow R_3 \rightarrow h_1 \rightarrow F_1 \rightarrow 0$$

$$0 \rightarrow 6 \rightarrow 16 \rightarrow 12 \rightarrow 3 \rightarrow 1 \rightarrow 0$$

relating FI (*lower left*) to CC (*upper right*). By composing the epimorphism $S_2T^* \otimes F_0 \rightarrow h_1$ with the epimorphism $h_1 \rightarrow F_1$, we obtain an epimorphism $S_2T^* \otimes F_0 \rightarrow F_1$ and the long exact sequence:

$$0 \rightarrow g_4 \rightarrow S_4T^* \otimes E \rightarrow S_2T^* \otimes F_0 \rightarrow F_1 \rightarrow 0$$

which is nevertheless not a long ker/coker exact sequence by counting the dimensions as we have $6-15+12-1=2 \neq 0$. In order to convince the reader about the usefulness of these new methods, even on such an elementary example, let us prove directly the exactness of the following long exact sequence $\forall r \geq 0$:

$$0 \rightarrow R_{r+4} \rightarrow J_{r+4}(E) \rightarrow J_{r+2}(F_0) \rightarrow J_r(F_1) \rightarrow 0$$

We let the reader check that $dim(R_{r+2}) = 4r+8, \forall r \geq 0$ and thus $dim(R_{r+4}) = 4r+16, \forall r \geq 0$ as a tricky exercise of combinatorics and then use the standard formulas:

$$dim(J_{r+4}(E)) = (r+5)(r+6)(r+7)/6$$

$$dim(J_{r+2}(F_0)) = (r+3)(r+4)(r+5)/3$$

$$dim\left(J_r\left(F_1\right)\right)=\left(r+1\right)\left(r+2\right)\left(r+3\right)/6$$

in order to check that the *Euler-Poincaré characteristics* (alternate sum of dimensions) is zero. We let the reader prove as a chasing exercise that the previous result is equivalent to prove that the following symbol sequence where $dim\left(g_{r+2}\right)=r+4\Rightarrow dim\left(g_{r+4}\right)=r+6,\forall r\geq 0$ :

$$0\to g_{r+4}\to S_{r+4}T^*\otimes E\to \boxed{S_{r+2}T^*\otimes F_0}\to S_rT^*\otimes F_1\to 0$$

is exact everywhere but at $S_{r+2}T^*\otimes F_0$ where the cohomology has dimension $r+2$, that is:

$$\begin{aligned}r+2&=\left(2\left(r+3\right)\left(r+4\right)/2-\left(r+1\right)\left(r+2\right)/2\right)-\left(\left(r+5\right)\left(r+6\right)/2-\left(r+6\right)\right)\\&=dim\left(R_{r+3}\right)-\left(dim\left(R_{r+4}\right)-dim\left(g_{r+4}\right)\right)\end{aligned}$$

but such a method cannot be used for the more complicate examples dealing with GR that we shall find in the next section. Referring to the general theorem, we may consider the commutative diagram where $\mathcal{P}$ is an injective operator:

$$\begin{array}{ccccccccc}0\to & \Theta & \to & 1 & \underset{2}{\overset{\mathcal{D}}{\to}} & 2 & \underset{2}{\overset{\mathcal{D}_1}{\to}} & 1\\ & \| & & \| & & \downarrow\mathcal{P} & \searrow & \downarrow\mathcal{Q}\\ 0\to & \Theta & \to & 1 & \underset{2}{\overset{\mathcal{D}'}{\to}} & 4 & \underset{1}{\overset{\mathcal{D}_1'}{\to}} & 4\end{array}$$

and the double prolongation diagram with $q=2,r=0,s=2,u\geq 0$ and $\mathcal{D}=\Phi\circ j_q,\mathcal{D}_1=\Psi_1\circ j_2$, where the two left upper downarrows are epimorphisms while the two left lower downarrows are monomorphisms:

$$\begin{array}{ccccccccc}0\to & R_{q+s+v+1} & \to & J_{q+s+v+1}\left(E\right) & \overset{\rho_{s+v+1}(\Phi)}{\to} & J_{s+v+1}\left(F_0\right) & \overset{\rho_{v+1}(\Psi_1)}{\to} & J_{v+1}\left(F_1\right)\\ & \downarrow & & \downarrow & & \downarrow & & \downarrow\\ 0\to & R^{(s)}_{q+v+1} & \to & J_{q+v+1}\left(E\right) & \overset{\rho_{v+1}(\Phi')}{\to} & J_{v+1}\left(F_0'\right) & \overset{\rho_v(\Psi_1')}{\to} & J_v\left(F_1'\right)\\ & \downarrow & & \downarrow & & \downarrow & & \\ 0\to & R_{q+v+1} & \to & J_{q+v+1}\left(E\right) & \overset{\rho_{v+1}(\Phi)}{\to} & J_{v+1}\left(F_0\right) & & \end{array}$$

because we have been able to choose $ord\left(\mathcal{D}_1\right)=r+s=s=2$ instead of $r+s+1$ as usual and where the columns are *not* sequences. Chasing now in an unusual way, we may start with any $b\in B_{s+u+1}=ker\left(\rho_u\left(\Psi_1\right)\right)$ whenever $u\geq 0$ that we can lift to $\overline{b}\in B_{s+v+1}$ because we have chosen an involutive CC system, whenever $v\geq u\geq 0$. Choosing $v=r+s+u=s+u$, we may use the fact that the central line defines a Janet sequence and is thus an exact sequence. Therefore, choosing $\overline{c}\in J_{q+v+1}\left(E\right)$ such that $\rho_{v+1}\left(\Phi'\right)\left(\overline{c}\right)$ is the image of $\overline{b}$ in $J_{v+1}\left(F_0'\right)$, we obtain by inclusion an element $c\in J_{q+v+1}\left(E\right)=J_{q+s+u+1}\left(E\right)$ such that $\rho_{v+1}\left(\Phi\right)\left(c\right)$ is $b$, ending the proof. In the differential module point of view, we have the commutative and exact diagram over $D=\mathbb{Q}\left[d_1,d_2,d_3\right]$ where the upper sequence comes from a Janet sequence:

$$\begin{array}{ccccccccccc}0\to & D & \underset{1}{\to} & D^4 & \underset{1}{\to} & D^4 & \underset{2}{\to} & D & \to & M & \to 0\\ & & & \downarrow & & \downarrow & & \| & & \| & \\ 0 & \to & D & \underset{2}{\to} & D^2 & \underset{2}{\to} & D & \to & M & \to 0 & \end{array}$$

The *Euler-Poincaré characteristic*, which is equal to the *differential rank* $rk_D(M)$ of $M$, vanishes in both resolutions which are called "*exact*" in algebraic analysis because *infinite jets are implicitly used*, even though the lower one is *not* "*strictly*" exact (*Care*, see [17] [18] [20] for more details).

**B) ALGEBROID BRACKET**

As we do not want to provide details about groupoids, we shall introduce a "copy" $Y$ (*target*) of $X$ (*source*) and define simply a Lie pseudogroup $\Gamma \subseteq aut(X)$ as a group of transformations solutions of a (in general nonlinear) system $R_q$, such that, whenever $y=f(x), z=g(y)\in\Gamma$ can be composed, then $z=g\circ f(x)\in\Gamma$, $x=f^{-1}(y)\in\Gamma$ and $y=id(x)=x\in\Gamma$. Setting $y=x+t\xi(x)+\cdots$ and passing to the limit when $t\to 0$, we may linearize the later system and obtain a (linear) system $R_q\subset J_q(T)$ such that $[\Theta,\Theta]\subset\Theta$. We may use the Frobenius theorem in order to find a generating fundamental set of *differential invariants* $\{\Phi^\tau(y_q)\}$ up to order $q$ which are such that $\Phi^\tau(\overline{y}_q)=\Phi^\tau(y_q)$ whenever $\overline{y}=g(y)\in\Gamma$. We obtain the *Lie form* $\Phi^\tau(y_q)=\Phi_\tau(id_q(x))=\Phi^\tau(j_q(id)(x))=\omega^\tau(x)$ of $R_q$.

Of course, in actual practice *one must use sections of* $R_q$ *instead of solutions* and we now prove why the use of the Spencer operator becomes crucial for such a purpose. Indeed, using the *algebraic bracket* $\{j_{q+1}(\xi), j_{q+1}(\eta)\}=j_q([\xi,\eta]), \forall\xi,\eta\in T$, we may obtain by bilinearity a *differential bracket* on $J_q(T)$ extending the bracket on $T$:

$$[\xi_q,\eta_q]=\{\xi_{q+1},\eta_{q+1}\}+i(\xi)D\eta_{q+1}-i(\eta)D\xi_{q+1}, \forall\xi_q,\eta_q\in J_q(T)$$

which does not depend on the respective lifts $\xi_{q+1}$ and $\eta_{q+1}$ of $\xi_q$ and $\eta_q$ in $J_{q+1}(T)$. This bracket on sections satisfies the *Jacobi identity* ([12] [13] [14] [15] [17]):

$$[[\xi_q,\eta_q],\zeta_q]+[[\eta_q,\zeta_q],\xi_q]+[[\zeta_q,\xi_q],\eta_q]=0$$

and we set ([12] [13] [14] [15]):

**DEFINITION 2B.1**: We say that a vector subbundle $R_q\subset J_q(T)$ is a *system of infinitesimal Lie equations* or a *Lie algebroid* if $[R_q,R_q]\subset R_q$, that is to say $[\xi_q,\eta_q]\in R_q, \forall\xi_q,\eta_q\in R_q$. Such a definition can be tested by means of computer algebra. We shall also say that $R_q$ is *transitive* if we have the short exact sequence $0\to R_q^0\to R_q\xrightarrow{\pi_0^q} T\to 0$.

**THEOREM 2B.2**: The bracket is compatible with prolongations:

$$[R_q,R_q]\subset R_q\Rightarrow[R_{q+r},R_{q+r}]\subset R_{q+r}, \forall r\geq 0$$

**Proof**: When $r=1$, we have $\rho_1(R_q)=R_{q+1}=\{\xi_{q+1}\in J_{q+1}(T)\,|\,\xi_q\in R_q, D\xi_{q+1}\in T^*\otimes R_q\}$ and we just need to use the following formulas showing how $D$ acts on the various brackets if we set $L(\xi_1)\zeta=[\xi,\zeta]+i(\zeta)D\xi_1$ (see [12] and [15] for more details):

$$i(\zeta)D\{\xi_{q+1},\eta_{q+1}\}=\{i(\zeta)D\xi_{q+1},\eta_q\}+\{\xi_q,i(\zeta)D\eta_{q+1}\},\quad\forall\zeta\in T$$

$$i(\zeta)D[\xi_{q+1},\eta_{q+1}]=[i(\zeta)D\xi_{q+1},\eta_q]+[\xi_q,i(\zeta)D\eta_{q+1}]+i(L(\eta_1)\zeta)D\xi_{q+1}-i(L(\xi_1)\zeta)D\eta_{q+1}$$

The right member of the second formula is a section of $R_q$ whenever $\xi_{q+1},\eta_{q+1}\in R_{q+1}$. The first formula may be used when $R_q$ is formally integrable.

Q.E.D.

**COROLLARY 2B.3**: The bracket is compatible with the PP procedure:

$$\left[R_q,R_q\right]\subset R_q\Rightarrow\left[R_{q+r}^{(s)},R_{q+r}^{(s)}\right]\subset R_{q+r}^{(s)},\forall r,s\geq 0$$

**EXAMPLE 2B.4**: With $n=1,q=3,X=\mathbb{R}$ and evident notations, the components of $\left[\xi_3,\eta_3\right]$ at order zero, one, two and three are defined by the totally unusual successive formulas:

$$\left[\xi,\eta\right]=\xi\partial_x\eta-\eta\partial_x\xi$$

$$\left(\left[\xi_1,\eta_1\right]\right)_x=\xi\partial_x\eta_x-\eta\partial_x\xi_x$$

$$\left(\left[\xi_2,\eta_2\right]\right)_{xx}=\xi_x\eta_{xx}-\eta_x\xi_{xx}+\xi\partial_x\eta_{xx}-\eta\partial_x\xi_{xx}$$

$$\left(\left[\xi_3,\eta_3\right]\right)_{xxx}=2\xi_x\eta_{xxx}-2\eta_x\xi_{xxx}+\xi\partial_x\eta_{xxx}-\eta\partial_x\xi_{xxx}$$

Affine transformations: $\xi_{xx}=0,\eta_{xx}=0\Rightarrow\left(\left[\xi_2,\eta_2\right]\right)_{xx}=0\Rightarrow\left[R_2,R_2\right]\subset R_2$.

Projective transformations:

$\xi_{xxx}=0,\eta_{xxx}=0\Rightarrow\left(\left[\xi_3,\eta_3\right]\right)_{xxx}=0\Rightarrow\left[R_3,R_3\right]\subset R_3$.

**EXAMPLE 2B.5**: With $n=m=2$ and $q=1$, let us consider the Lie pseudodogroup $\Gamma\subset aut(X)$ of finite transformations $y=f(x)$ such that $y^2dy^1=x^2dx^1=\alpha$. Setting $y=x+t\xi(x)+\cdots$ and linearizing, we get the Lie operator $\mathcal{D}\xi=\mathcal{L}(\xi)\alpha$ where $\mathcal{L}$ is the Lie derivative and the system $R_1\subset J_1(T)$ of linear infinitesimal Lie equations:

$$x^2\partial_1\xi^1+\xi^2=0,\quad \partial_2\xi^1=0$$

Replacing $j_1(\xi)$ by a section $\xi_1\in J_1(T)$, we have:

$$\xi_1^1=-\frac{1}{x^2}\xi^2,\quad \xi_2^1=0$$

Let us choose the two sections:

$$\xi_1=\left\{\xi^1=0,\xi^2=-x^2,\xi_1^1=1,\xi_2^1=0,\xi_1^2=0,\xi_2^2=0\right\}\in R_1$$

$$\eta_1=\left\{\eta^1=x^2,\eta^2=0,\eta_1^1=0,\eta_2^1=-x2,\eta_1^2=0,\eta_2^2=1\right\}\in R_1$$

We let the reader check that $\left[\xi_1,\eta_1\right]\in R_1$. However, we have the strict inclusion $R_1^{(1)}\subset R_1$ defined by the additional equation $\xi_1^1+\xi_2^2=0$ and thus $\xi_1,\eta_1\notin R_1^{(1)}$ though we have indeed $\left[R_1^{(1)},R_1^{(1)}\right]\subset R_1^{(1)}$, a result not evident at all because $\xi_1$ and $\eta_1$ have *nothing to do do* with solutions. We invite the reader to proceed in the same way with $\beta=x^2dx^1-x^1dx^2$ and compare.

### C) EXTENSION MODULES

Let $D=K\left[d_1,\cdots,d_n\right]=K\left[d\right]$ be the ring of differential operators with coefficients in a differential field $K$ of characteristic zero, that is such that $\mathbb{Q}\subset K$, with $n$ commuting derivations $\partial_1,\cdots,\partial_n$ and commutation relations

$d_i a = ad_i + \partial_i a, \forall a \in K$. If $y^1, \cdots, y^m$ are $m$ differential indeterminates, we may identify $Dy^1 + \cdots + Dy^m = Dy$ with $D^m$ and consider the finitely presented left differential module $M = {}_D M$ with presentation $D^p \to D^m \to M \to 0$ determined by a given linear multidimensional system with $n$ independent variables, $m$ unknowns and $p$ equations. Applying the functor $hom_D(\bullet, D)$, we get the exact sequence $0 \to hom_D(M, D) \to D^m \to D^p \to N_D \to 0$ of *right differential modules* that can be transformed by a side-changing functor to an exact sequence of finitely generated *left differential modules*. This new presentation corresponds to the *formal adjoint* $ad(\mathcal{D})$ of the linear differential operator $\mathcal{D}$ determined by the initial presentation but now with $p$ unknowns and $m$ equations, obtaining therefore a new finitely generated *left differential module* $N = {}_D N$ and we may consider $hom_D(M, D)$ as the *module of equations* of the *compatibility conditions* (CC) of $ad(\mathcal{D})$, a result not evident at first sight (see [16]). Using now a maximum free submodule $0 \to D^l \to hom_D(M, D)$ and repeating this standard procedure while using the well known fact that $ad(ad(\mathcal{D})) = \mathcal{D}$, we obtain therefore an embedding $0 \to hom_D(hom_D(M, D), D) \to D^l$ of left differential modules for a certain integer $1 \le l < m$ because $K$ is a field and thus $D$ is a noetherian bimodule over itself, a result leading to $l = rk_D(hom_D(M, D)) = rk_D(M) < m$ as in ([15] [16]). Now, setting $t(M) = \{m \in M \mid \exists 0 \neq P \in D, Pm = 0\}$, the kernel of the map $\epsilon : M \to hom_D(hom_D(M, D), D) : m \to \epsilon(m)(f) = f(m), \forall f \in hom_D(M, D)$ is the *torsion submodule* $t(M) \subseteq M$ and $\epsilon$ is injective if and only if $M$ is torsion-free, that is $t(M) = 0$. In that case, we obtain by composition an embedding $0 \to M \to D^l$ of $M$ into a free module. This result is quite important for applications as it provides a (minimal) parametrization of the linear differential operator $\mathcal{D}$ and amounts to the controllability of a classical control system when $n = 1$ ([16] [34]). This parametrization will be called an "*absolute parametrization*" as it only involves arbitrary "*potential-like*" functions (see [16] [18] [20] [21] [24] [31] [33] [35] [36] [37] for more details and examples, in particular [34] for the Einstein equations).

If $P = a^\mu d_\mu \in D = K[d]$, the highest value of $|\mu|$ with $a^\mu \neq 0$ is called the *order* of the *operator* $P$ and the ring $D$ with multiplication $(P, Q) \to P \circ Q = PQ$ is filtred by the order $q$ of the operators. We have the *filtration* $0 \subset K = D_0 \subset D_1 \subset \cdots \subset D_q \subset \cdots \subset D_\infty = D$. Moreover, it is clear that $D$, as an algebra, is generated by $K = D_0$ and $T = D_1 / D_0$ with $D_1 = K \oplus T$ if we identify an element $\xi = \xi^i d_i \in T$ with the vector field $\xi = \xi^i(x)\partial_i$ of differential geometry, but with $\xi^i \in K$ now. It follows that $D = {}_D D_D$ is a *bimodule* over itself, being at the same time a left $D$-module by the composition $P \to QP$ and a right $D$-module by the composition $P \to PQ$. We define the *adjoint* map $ad : D \to D^{op} : P = a^\mu d_\mu \to ad(P) = (-1)^{|\mu|} d_\mu a^\mu$ and we have $ad(ad(P)) = P$. It is easy to check that $ad(PQ) = ad(Q)ad(P), \forall P, Q \in D$. Such a definition can also be extended to any matrix of operators by using the transposed matrix of adjoint operators (see [21] [23] [25] [34] for more details

or applications to control theory and mathematical physics).

Accordingly, if $y=\left(y^1,\cdots,y^m\right)$ are differential indeterminates, then $D$ acts on $y^k$ by setting $d_\mu y^k=y^k_\mu$ with $d_i y^k_\mu=y^k_{\mu+1_i}$ and $y^k_0=y^k$. We may therefore use the jet coordinates in a formal way as in the previous section. Therefore, if a system of OD/PD equations is written in the form:

$$\Phi^\tau\equiv a^{\tau\mu}_k y^k_\mu=0$$

with coefficients $a^{\tau\mu}_k\in K$, we may introduce the free differential module $Dy=Dy^1+\cdots+Dy^m\simeq D^m$ and consider the differential submodule $I=D\Phi\subset Dy$ which is usually called the *module of equations*, both with the *differential module* $M=Dy/D\Phi$ or $D$-module and we may set $M={}_DM$ if we want to specify the ring of differential operators. Again, we may introduce the formal *prolongation* with respect to $d_i$ by setting:

$$d_i\Phi^\tau\equiv a^{\tau\mu}_k y^k_{\mu+1_i}+\left(\partial_i a^{\tau\mu}_k\right)y^k_\mu$$

with $\mu+1_i=\left(\mu_1,\cdots,\mu_{i-1},\mu_i+1,\mu_{i+1},\cdots,\mu_n\right)$ in order to induce maps $d_i:M\to M:\overline{y}^k_\mu\to\overline{y}^k_{\mu+1_i}$ by residue if we use to denote the residue $Dy\to M:y^k\to\overline{y}^k$ by a bar as in algebraic geometry. However, for simplicity, we shall not write down the bar when the background will indicate clearly if we are in $Dy$ or in $M$. We have a filtration

$0\subseteq M_0\subseteq M_1\subseteq\cdots\subseteq M_q\subseteq\cdots\subseteq M_\infty=M$ induced by that of $D$ and

$d_iM_q\subseteq M_{q+1}$ (compare to [35] and [37]).

As a byproduct, the differential modules we shall consider will always be *finitely generated* ($k=1,\cdots,m<\infty$) and *finitely presented* ($\tau=1,\cdots,p<\infty$). Equivalently, introducing the *matrix of operators* $\mathcal{D}=\left(a^{\tau\mu}_k d_\mu\right)$ with $m$ columns and $p$ rows, we may introduce the morphism

$D^p\xrightarrow{\mathcal{D}}D^m:\left(P_\tau\right)\to\left(P_\tau\Phi^\tau\right):P\to P\Phi=P\mathcal{D}$ over $D$ by acting with $\mathcal{D}$ *on the left of these row vectors* while acting with $D$ *on the right of these row vectors* and the *presentation* of $M$ is defined by the exact cokernel sequence $D^p\to D^m\to M\to 0$. It is essential to notice that the presentation only depends on $K,D$ and $\Phi$ or $\mathcal{D}$, that is to say never refers to the concept of (explicit or formal) solutions. It is at this moment that we have to take into account the results of the previous section in order to understant that certain presentations will be much better than others, in particular to establish a link with formal integrability and involution.

Having in mind that $K$ is a left $D$-module with the standard action $\left(D,K\right)\to K:\left(d_i,a\right)\to\partial_i a$ and that $D$ is a bimodule over itself, *we have only two possible constructions*:

**DEFINITION 2C.1**: We define the *system* $R=hom_K\left(M,K\right)=M^*$ and set $R_q=hom_K\left(M_q,K\right)=M^*_q$ as the *system of order q*. We have the *projective limit* $R=R_\infty\to\cdots\to R_q\to\cdots\to R_1\to R_0$. It follows that

$f_q\in R_q:y^k_\mu\to f^k_\mu\in K$ with $a^{\tau\mu}_k f^k_\mu=0$ defines a *section at order q* and we may set $f_\infty=f\in R$ for a *section* of $R$. For a ground field of constants $k$, this definition has of course to do with the concept of a formal power series solution.

However, for an arbitrary differential field $K$, *the main novelty of this new approach is that such a definition has nothing to do with the concept of a formal power series solution* (*care*) as illustrated in the next example.

**DEFINITION 2C.2**: We may define the right differential module $hom_D(M,D)$.

**PROPOSITION 2C.3**: When $M$ is a left $D$-module, then $R$ is also a left $D$-module.

*Proof*: As $D$ is generated by $K$ and $T$ as we already said, let us define:

$$(af)(m)=af(m), \quad \forall a\in K, \forall m\in M$$

$$(\xi f)(m)=\xi f(m)-f(\xi m), \quad \forall \xi=a^i d_i\in T, \forall m\in M$$

In the operator sense, it is easy to check that $d_i a=ad_i+\partial_i a$ and that $\xi\eta-\eta\xi=[\xi,\eta]$ is the standard bracket of vector fields. We finally get $(d_i f)^k_\mu=(d_i f)(y^k_\mu)=\partial_i f^k_\mu-f^k_{\mu+1_i}$ and thus recover *exactly* the Spencer operator of the previous section though *this is not evident at all*. We also get $(d_i d_j f)^k_\mu=\partial_{ij} f^k_\mu-\partial_i f^k_{\mu+1_j}-\partial_j f^k_{\mu+1_i}+f^k_{\mu+1_i+1_j}\Rightarrow d_i d_j=d_j d_i, \forall i,j=1,\cdots,n$ and thus $d_i R_{q+1}\subseteq R_q\Rightarrow d_i R\subset R$ induces a well defined operator $R\to T^*\otimes R: f\to dx^i\otimes d_i f$. This result has been discovered (up to sign) by Macaulay in 1916 ([33]). For more details on the Spencer operator and its applications, the reader may look at ([14] [15]).

Q.E.D.

We now recall the definition of the *extension modules* $ext^i_D(M,D)$ that we shall simply denote by $ext^i(M)$ when there cannot be any confusion. We divide the procedure into four steps that can be achieved by means of computer algebra ([17] [36] [38] [39]):

- Construct a *free resolution* of $M$, say:

$$\cdots\to F_i\to\cdots\to F_1\to F_0\to M\to 0$$

- Suppress $M$ in order to obtain the *deleted sequence*:

$$\cdots\to F_i\to\cdots\to F_1\to F_0\to 0$$

- Apply $hom_D(\bullet,D)$ in order to obtain the *dual sequence* heading backwards:

$$\cdots\leftarrow hom_D(F_i,D)\leftarrow\cdots\leftarrow hom_D(F_1,D)\leftarrow hom_D(F_0,D)\leftarrow 0$$

- Define $ext^i(M)$ to be the cohomology at $hom_D(F_i,D)$ in the dual sequence with $ext^0(M)=hom_D(M,D)$.

The following nested chain of difficult propositions and theorems can be obtained, *even in the non-commutative case*, by combining the use of extension modules and *double duality* in the framework of algebraic analysis ([16] [35] [39]).

**THEOREM 2C.4**: The extension modules do not depend on the resolution of $M$ used.

**PROPOSITION 2C.5**: Applying $hom_D(\bullet,D)$ provides right $D$-modules that can be transformed to left $D$-modules by means of the *side changing functor* and

vice-versa. Namely, if $N_D$ is a right $D$-module, then ${}_DN = \wedge^n T \otimes_K N_D$ is the *converted left* $D$-module while, if ${}_DN$ is a left $D$-module, then $N_D = \wedge^n T^* \otimes_K {}_DN$ is the *converted right* $D$-module.

**PROPOSITION 2C.6**: Instead of using $hom_D(\bullet, D)$ and the side changing functor in the module framework, we may use $ad$ in the operator framework. Namely, to any operator $\mathcal{D}: E \to F$ we may associate the formal adjoint $ad(\mathcal{D}): \wedge^n T^* \otimes F^* \to \wedge^n T^* \otimes E^*$ with the useful though striking relation $rk_D(ad(\mathcal{D})) = rk_D(\mathcal{D})$.

**PROPOSITION 2.C.7**: $ext^i(M)$ is a torsion module $\forall 1 \le i \le n$ but $ext^0(M) = hom_D(M, D)$ may not be a torsion module.

We shall say that an operator is *parametrizable* if it generates the CC of an operator and the next result will be essential for applications as it can be tested by means of computer algebra ([38]).

**THEOREM 2C.8**: An operator is *parametrizable* if and only if the corresponding differential module is torsion-free and double duality provides a constructive test for checking such a property.

## 3. Applications

**A) Minkowski Metric**:

If $n = 4$ and $\omega \in S_2T^*$ is the non-degenerate Minkowski metric, the corresponding Lie operator is $\xi \in T \to \Omega \equiv \mathcal{D}\xi = \mathcal{L}(\xi)\omega \in S_2T^*$ where $\mathcal{L}$ is the standard Lie derivative for tensors and we have to study the corresponding system $R_1 \subset J_1(T)$ of infinitesimal Lie equations. However, this system is finite type with $g_2 = 0$ but $g_1 \subset T^* \otimes T$ is *not* 2-acyclic and the CC are homogeneous of order 2, a result leading to the well-known finite length differential sequence where the order of an operator has been indicated under its arrow:

$$0 \to \Theta \to 4 \overset{\text{Killing}}{\underset{1}{\to}} 10 \overset{\text{Riemann}}{\underset{2}{\to}} 20 \overset{\text{Bianchi}}{\underset{1}{\to}} 20 \underset{1}{\to} 6 \to 0$$

In arbitrary dimension, we have successively:

$$n \to n(n+1)/2 \to n^2(n^2-1)/12 \to n^2(n^2-1)(n-2)/24 \to \cdots$$

or, introducing the Spencer $\delta$-cohomology:

$$T \to S_2T^* \to H^2(g_1) \to H^3(g_1) \to \cdots$$

However, this sequence is *not* canonical and we have to use the involutive system $R_2 \subset J_2(T)$ in the following *Fundamental Diagram I* relating the (upper) *canonical Spencer sequence* to the (lower) *canonical Janet sequence*, a result first found exactly 40 years ago in ([12]) that only depends on the left commutative square $\mathcal{D} = \Phi_0 \circ j_q$ when one has an involutive system $R_q \subseteq J_q(E)$ over $E$ and thus the involutive system $R_{q+1} \subset J_1(R_q)$ over $R_q$ when $dim(X) = n$.

SPENCER

$$
\begin{array}{ccccccccccccccc}
 & & & & 0 & & 0 & & 0 & & & & 0 & & \\
 & & & & \downarrow & & \downarrow & & \downarrow & & & & \downarrow & & \\
 & & & \overset{j_q}{\rightarrow} & C_0 & \overset{D_1}{\rightarrow} & C_1 & \overset{D_2}{\rightarrow} & C_2 & \overset{D_3}{\rightarrow} & \cdots & \overset{D_n}{\rightarrow} & C_n & \rightarrow 0 \\
 & & & & \downarrow & & \downarrow & & \downarrow & & & & \downarrow & & \\
0 & \rightarrow & \Theta & \overset{j_q}{\rightarrow} & C_0(E) & \overset{D_1}{\rightarrow} & C_1(E) & \overset{D_2}{\rightarrow} & C_2(E) & \overset{D_3}{\rightarrow} & \cdots & \overset{D_n}{\rightarrow} & C_n(E) & \rightarrow 0 \\
 & & \| & & \downarrow \Phi_0 & & \downarrow \Phi_1 & & \downarrow \Phi_2 & & & & \downarrow \Phi_n & & \\
0 \rightarrow & \Theta & \rightarrow & E & \overset{\mathcal{D}}{\rightarrow} & F_0 & \overset{\mathcal{D}_1}{\rightarrow} & F_1 & \overset{\mathcal{D}_2}{\rightarrow} & F_2 & \overset{\mathcal{D}_3}{\rightarrow} & \cdots & \overset{\mathcal{D}_n}{\rightarrow} & F_n & \rightarrow 0 \\
 & & & & & \downarrow & & \downarrow & & \downarrow & & & & \downarrow & \\
 & & & & & 0 & & 0 & & 0 & & & & 0 &
\end{array}
$$

JANET

Setting $n=4, q=2, E=T, C_r=\wedge^r T^*\otimes R_2$, the first order *first Spencer operator* $D_1$ is defined by the system $R_3\subset J_1(R_2)$ and the epimorphisms $\Phi_1,\cdots,\Phi_4$ are induced by the epimorphism $\Phi_0$. The corresponding fiber dimensions are indicated in the next diagram where $dim(R_2)=dim(T)+dim(g_1)=4+6=10$:

$$
\begin{array}{ccccccccccccccc}
 & & & & 0 & & 0 & & 0 & & 0 & & 0 & & \\
 & & & & \downarrow & & \downarrow & & \downarrow & & \downarrow & & \downarrow & & \\
 & & & \overset{j_2}{\rightarrow} & 10 & \overset{D_1}{\rightarrow} & 40 & \overset{D_2}{\rightarrow} & 60 & \overset{D_3}{\rightarrow} & 40 & \overset{D_4}{\rightarrow} & 10 & \rightarrow 0 \\
 & & & & \downarrow & & \downarrow & & \downarrow & & \downarrow & & \downarrow & & \\
0 & \rightarrow & \Theta & \overset{j_2}{\rightarrow} & 60 & \overset{D_1}{\rightarrow} & 160 & \overset{D_2}{\rightarrow} & 180 & \overset{D_3}{\rightarrow} & 96 & \overset{D_4}{\rightarrow} & 20 & \rightarrow 0 \\
 & & \| & & \downarrow & & \downarrow & & \downarrow & & \downarrow & & \downarrow & & \\
0 \rightarrow & \Theta & \rightarrow & 4 & \overset{\mathcal{D}}{\rightarrow} & 50 & \overset{\mathcal{D}_1}{\rightarrow} & 120 & \overset{\mathcal{D}_2}{\rightarrow} & 120 & \overset{\mathcal{D}_3}{\rightarrow} & 56 & \overset{\mathcal{D}_4}{\rightarrow} & 10 & \rightarrow 0 \\
 & & & & & \downarrow & & \downarrow & & \downarrow & & \downarrow & & \downarrow & \\
 & & & & & 0 & & 0 & & 0 & & 0 & & 0 &
\end{array}
$$

We recall that, apart from $j_2$ and $\mathcal{D}=\Phi_0\circ j_2$ which have order 2, then all the other operators have order 1. Of course, the reader may imagine easily that the author of this paper avoided computer algebra by using the following specific procedure:

1) First write down the Spencer sequence at once, keeping in mind that it is locally isomorphic to the tensor product of the Poincaré sequence:

$$\wedge^0 T^* \xrightarrow{d} \wedge^1 T^* \xrightarrow{d} \wedge^2 T^* \xrightarrow{d} \wedge^3 T^* \xrightarrow{d} \wedge^4 T^* \rightarrow 0$$

$$1 \xrightarrow{d} 4 \xrightarrow{d} 6 \xrightarrow{d} 4 \xrightarrow{d} 1 \rightarrow 0$$

by a Lie algebra of dimension $4+6=10$ and is thus locally exact.

2) Second, write down the central sequence just using some combinatorics on the Janet tabular for the trivially involutive second order operator $j_2$ (see [12], p. 157).

3) Then, obtain the Janet sequence by quotient.

4) Finally, use the vanishing of the three Euler-Poincaré characteristics for

checking the exactness of all these numbers, namely:

$$10-40+60-40+4=0,$$
$$4-60+160-180+96-20=0,$$
$$4-50+120-120+56-10=0$$

**B) SCHWARZSCHILD METRIC:**

In the Boyer-Lindquist coordinates $(t,r,\theta,\phi)=(x^0,x^1,x^2,x^3)$, we may consider the Schwarzschild metric $\omega=A(r)dt^2-(1/A(r))dr^2-r^2d\theta^2-r^2\sin^2(\theta)d\phi^2$ and $\xi=\xi^i d_i\in T$, let us introduce $\xi_i=\omega_{ri}\xi^r$ with the 4 *formal derivatives* $(d_0=d_t,d_1=d_r,d_2=d_\theta,d_3=d_\phi)$. With speed of light $c=1$ and $A=1-\frac{m}{r}$ where $m$ is a constant, the metric can be written in the diagonal form:

$$\begin{pmatrix} A & 0 & 0 & 0 \\ 0 & -1/A & 0 & 0 \\ 0 & 0 & -r^2 & 0 \\ 0 & 0 & 0 & -r^2\sin^2(\theta) \end{pmatrix}$$

Using the notations of differential modules theory, consider the Killing equations:

$$\Omega\equiv L(\xi)\omega=0\Leftrightarrow\Omega_{ij}\equiv d_i\xi_j+d_j\xi_i-2\gamma_{ij}^r\xi_r=0$$

where we have introduced the Christoffel symbols $\gamma$ through he standard Levi-Civita isomorphism $j_1(\omega)\simeq(\omega,\gamma)$ while setting $A'=\partial_r A$ in the differential field $K$ of coefficients ([40], p. 87). As in the later Macaulay and Janet examples and in order to avoid any further confusion between sections and derivatives, we shall use the sectional point of view and rewrite the previous equations in the symbolic form $\Omega\equiv L(\xi_1)\omega\in S_2T^*$ where $L$ is the *formal Lie derivative*:

$$\begin{cases} \frac{1}{2}\Omega_{33}\equiv\xi_{3,3}+\sin(\theta)\cos(\theta)\xi_2+rA\sin^2(\theta)\xi_1=0 \\ \Omega_{32}\equiv\xi_{2,3}+\xi_{3,2}-2\cot(\theta)\xi_3=0 \\ \Omega_{31}\equiv\xi_{1,3}+\xi_{3,1}-\frac{2}{r}\xi_3=0 \\ \Omega_{30}\equiv\xi_{0,3}+\xi_{3,0}=0 \\ \frac{1}{2}\Omega_{22}\equiv\xi_{2,2}+rA\xi_1=0 \\ \Omega_{21}\equiv\xi_{1,2}+\xi_{2,1}-\frac{2}{r}\xi_2=0 \\ \Omega_{20}\equiv\xi_{0,2}+\xi_{2,0}=0 \\ \frac{1}{2}\Omega_{11}\equiv\xi_{1,1}+\frac{A'}{2A}\xi_1=0 \\ \Omega_{10}\equiv\xi_{0,1}+\xi_{1,0}-\frac{A'}{A}\xi_0=0 \\ \frac{1}{2}\Omega_{00}\equiv\xi_{0,0}-\frac{AA'}{2}\xi_1=0 \end{cases}$$

Though this system $R_1 \subset J_1(T)$ has 4 equations of class 3, 3 equations of class 2, 2 equations of class 1 and 1 equation of class 0, it is far from being involutive because it is finite type with second symbol $g_2 = 0$ defined by the 40 equations $v_{ij}^k = 0$ in the initial coordinates. From the symmetry, it is clear that such a system has at least 4 solutions, namely the time translation $\partial_t \leftrightarrow \xi^0 = 1 \Leftrightarrow \xi_0 = A$ and, using cartesian coordinates $(t, x, y, z)$, the 3 space rotations $y\partial_z - z\partial_y, z\partial_x - x\partial_z, x\partial_y - y\partial_x$.

We may also write the Schwarzschild metric in cartesian coordinates as:

$$\omega = A(r)dt^2 + \left(1 - \frac{1}{A(r)}\right)dr^2 - \left(dx^2 + dy^2 + dz^2\right), \quad rdr = xdx + ydy + zdz$$

and notice that the $3 \times 3$ matrix of components of the three rotations has rank equal to 2, a result leading surely, before doing any computation to the existence of *one and only one* zero order Killing equation $x\xi^x + y\xi^y + z\xi^z = 0$. Such a result also amounts to say that the spatial projection of any Killing vector on the radial spatial unit vector $\left(x^1/r, x^2/r, x^3/r\right)$ vanishes because $r$ must stay invariant.

Caring only about the last three equations, we get formally:

$$\begin{aligned}
&\xi_{0,11} + \xi_{1,01} - d_1\left(\frac{A'}{A}\xi_0\right) \\
&= \xi_{0,11} - \frac{A'}{2A}\xi_{1,0} - \left(\frac{A''}{A} - \frac{(A')^2}{A^2}\right)\xi_0 - \frac{A'}{A}\xi_{0,1} \\
&= \xi_{0,11} + \frac{A'}{2A}\xi_{0,1} - \frac{(A')^2}{2A^2}\xi_0 - \left(\frac{A''}{A} - \frac{(A')^2}{A^2}\right)\xi_0 - \frac{A'}{A}\xi_{0,1} \\
&= \xi_{0,11} + \frac{A'}{2A}\xi_{1,0} - \frac{A''}{A}\xi_0
\end{aligned}$$

We obtain the linearized Christoffel symbols $\Gamma = L(\xi_2)\gamma \in S_2T^* \otimes T$ in the form:

$$\Gamma_{0,11} \equiv \xi_{0,11} + \frac{A'}{2A}\xi_{1,0} - \frac{A''}{A}\xi_0 = 0$$

and similarly in $R_2$ with lower indices as usual:

$$\Gamma_{0,01} \equiv \xi_{0,01} - \left(\frac{AA''}{2} + \frac{(A')^2}{4}\right)\xi_1 = 0$$

$$\Gamma_{0,00} \equiv \xi_{0,00} - \frac{AA'}{2}\xi_{1,0} = 0$$

$$\Gamma_{1,00} \equiv \xi_{1,00} + \left(\frac{AA''}{2} - \frac{A'^2}{4}\right)\xi_1 = 0$$

$$\Gamma_{1,01} \equiv \xi_{1,01} + \frac{A'}{2A}\xi_{1,0} = 0$$

$$\Gamma_{1,11} \equiv \xi_{1,11} + \left(\frac{A''}{2A} - \frac{3(A')^2}{4A^2}\right)\xi_1 = 0$$

It follows that we obtain in $R_3$ and thus finally in $R_1^{(2)}$ for constructing $\boxed{\rho_{01,01}}$:

$$+\xi_{1,001}+\frac{A'}{2A}\xi_{1,00}=0$$

$$-\xi_{1,001}-\left(\frac{AA''}{2}-\frac{(A')^2}{4}\right)'\xi_1-\left(\frac{AA''}{2}-\frac{(A')^2}{4}\right)\xi_{1,1}=0$$

$$-\frac{A'}{2A}\xi_{1,00}-\frac{A'}{2A}\left(\frac{AA''}{2}-\frac{(A')^2}{4}\right)\xi_1=0$$

$$\left(\frac{AA''}{2}-\frac{(A')^2}{4}\right)\xi_{1,1}+\frac{A'}{2A}\left(\frac{AA''}{2}-\frac{(A')^2}{4}\right)\xi_1=0$$

Summing these four prolongations, we get $\xi^1 d_1\left(\frac{AA''}{2}-\frac{(A')^2}{4}\right)=0\Rightarrow\boxed{\xi_1=0}$

because $A=1-\frac{m}{r}\Rightarrow A+rA'=1\Rightarrow 2A'+rA''=0$. Similarly, we could have obtained:

$$d_1\xi_{1,00}-d_0\xi_{1,01}=-\left(\frac{AA''}{2}-\frac{(A')^2}{4}\right)\xi_1=0$$

Using the relation $A+rA'=1$, we have also successively for constructing $\boxed{\rho_{02,01}}$:

$$d_1\Omega_{02}+d_0\Omega_{12}-d_2\Omega_{01}=2\xi_{2,01}-\left(\frac{2}{r}+\frac{A'}{A}\right)\xi_{2,0}\Rightarrow\xi_{2,01}=\left(\frac{1}{r}+\frac{A'}{2A}\right)\xi_{2,0}$$

$$\xi_{2,00}=-\xi_{0,20}=-\frac{AA'}{2}\xi_{1,2},\quad \xi_{0,12}=-\left(\frac{1}{r}+\frac{A'}{2A}\right)\xi_{2,0}$$

$$d_1(\xi_{2,00})-d_0(\xi_{2,01})-\frac{(AA')'}{2}\xi_{1,2}-\frac{AA'}{2}\xi_{1,12}-\left(\frac{1}{r}+\frac{A'}{2A}\right)\xi_{2,00}$$

$$=-\left(\frac{AA''}{2}+\frac{(A')^2}{4}\right)\xi_{1,2}+\frac{AA'}{2}\left(\frac{1}{r}+\frac{A'}{2A}\right)\xi_{1,2}$$

$$=\left(\frac{AA'}{2r}-\frac{AA''}{2}\right)\xi_{1,2}=\frac{3AA'}{2r}\xi_{1,2}$$

that is to say $\boxed{\xi_{1,2}=0}$. However, we have:

$$d_1(\xi_{1,01})-d_0(\xi_{1,11})=d_1\left(-\frac{A'}{2A}\xi_{1,0}\right)-\left(\frac{3(A')^2}{4A^2}-\frac{A''}{2A}\right)\xi_{1,0}$$

$$=-\frac{A'}{2A}\xi_{1,01}-\left(\frac{A''}{2A}-\frac{(A')^2}{2A^2}\right)\xi_{1,0}-\left(\frac{3(A')^2}{4A^2}-\frac{A''}{2A}\right)\xi_{1,0}$$

$$=\left(\frac{(A')^2}{4A^2}+\frac{(A')^2}{2A^2}-\frac{3(A')^2}{4A^2}\right)\xi_{1,0}=0$$

and such an approach does not bring $\xi_{1,0}=0$ for sections, even if it *must be surely true* for solutions. We may also notice that:

$$d_1\Omega_{02}+d_2\Omega_{01}-d_0\Omega_{12}=2\xi_{0,12}-\frac{A'}{A}\xi_{0,2}+\frac{2}{r}\xi_{2,0}$$

$$\Rightarrow \xi_{0,12}=\left(\frac{A'}{2A}+\frac{1}{r}\right)\xi_{0,2}$$

$$d_0\Omega_{12}+d_2\Omega_{01}-d_1\Omega_{02}=2\xi_{1,02}-\frac{2}{r}\xi_{2,0}-\frac{A'}{A}\xi_{0,2}$$

$$\Rightarrow \xi_{1,02}=\left(\frac{A'}{2A}-\frac{1}{r}\right)\xi_{0,2}$$

$$\xi_{0,11}=\frac{A''}{A}\xi_0-\frac{A'}{2A}\xi_{1,0}$$

Studying the component $\boxed{\rho_{01,12}}$, we obtain successively:

$$\begin{aligned}d_2\xi_{0,11}-d_1\xi_{0,12}&=\frac{A''}{A}\xi_{0,2}-\frac{A'}{2A}\xi_{1,02}-\left(\frac{A'}{2A}+\frac{1}{r}\right)'\xi_{0,2}-\left(\frac{A'}{2A}+\frac{1}{r}\right)\xi_{0,12}\\&=\left[\frac{A''}{A}-\frac{A'}{2A}\left(\frac{A'}{2A}-\frac{1}{r}\right)-\left(\frac{A'}{2A}+\frac{1}{r}\right)'-\left(\frac{A'}{2A}+\frac{1}{r}\right)^2\right]\xi_{0,2}\\&=-\frac{2A'}{rA}\xi_{0,2}\end{aligned}$$

and thus $\boxed{\xi_{0,2}=0}$. We also have:

$$d_3\Omega_{01}+d_1\Omega_{03}-d_0\Omega_{13}=2\xi_{0,13}-\frac{A'}{A}\xi_{0,3}+\frac{2}{r}\xi_{3,0}$$

$$\Rightarrow \xi_{0,13}=\left(\frac{A'}{2A}+\frac{1}{r}\right)\xi_{0,3}$$

$$d_0\Omega_{13}+d_3\Omega_{01}-d_1\Omega_{03}=2\xi_{1,03}-\frac{2}{r}\xi_{3,0}-\frac{A'}{A}\xi_{0,3}$$

$$\Rightarrow \xi_{1,03}=\left(\frac{A'}{2A}-\frac{1}{r}\right)\xi_{0,3}$$

Studying the component $\boxed{\rho_{01,13}}$, we obtain successively:

$$\xi_{0,11}=\frac{A''}{A}\xi_0-\frac{A'}{2A}\xi_{1,0}$$

$$d_3\Omega_{01}+d_1\Omega_{03}-d_0\Omega_{13}=2\xi_{0,13}-\frac{A'}{A}\xi_{0,3}$$

$$d_0\Omega_{13}+d_3\Omega_{01}-d_1\Omega_{0,3}=2\xi_{1,03}-\frac{2}{r}\xi_{3,0}-\frac{A'}{A}\xi_{0,3}$$

$$\Rightarrow \xi_{1,03}=\left(\frac{A'}{2A}-\frac{1}{r}\right)\xi_{0,3}$$

$$d_3\xi_{0,11}-d_1\xi_{0,13}=\frac{A''}{A}\xi_{0,3}-\frac{A'}{2A}\xi_{1,03}-\left(\frac{A'}{2A}+\frac{1}{r}\right)'\xi_{0,3}-\left(\frac{A'}{2A}+\frac{1}{r}\right)\xi_{0,13}$$

$$=\left[\frac{A''}{A}-\frac{A'}{2A}\left(\frac{A'}{2A}-\frac{1}{r}\right)-\left(\frac{A'}{2A}+\frac{1}{r}\right)'-\left(\frac{A'}{2A}+\frac{1}{r}\right)^2\right]\xi_{0,3}$$

$$=-\frac{3A'}{2rA}\xi_{0,3}$$

and thus $\boxed{\xi_{0,3}=0}$. We also have:

$$d_1\Omega_{03}+d_0\Omega_{13}-d_3\Omega_{01}=2\xi_{3,01}-\frac{2}{r}\xi_{3,0}-\frac{A'}{A}\xi_{0,3}$$

$$\Rightarrow \xi_{3,01}=\left(\frac{A'}{2A}-\frac{1}{r}\right)\xi_{0,3},\quad \xi_{3,00}=-\xi_{0,03}=-\frac{AA'}{2}\xi_{1,3}$$

Studying $\boxed{\rho_{03,01}}$, we obtain successively:

$$d_0\xi_{3,01}-d_1\xi_{3,00}=\left(\frac{A'}{2A}-\frac{1}{r}\right)\xi_{0,03}+\left(\frac{AA'}{2}\right)'\xi_{1,3}+\frac{AA'}{2}\xi_{1,13}$$

$$=\left[\frac{AA'}{2}\left(\frac{A'}{2A}-\frac{1}{r}\right)+\left(\frac{AA'}{2}\right)'-\frac{(A')^2}{4}\right]\xi_{1,3}$$

$$=\left(\frac{AA'}{2r}+\left(\frac{AA'}{2}\right)'\right)\xi_{1,3}$$

and thus $\boxed{\xi_{1,3}=0}$. We also have:

$$d_0\Omega_{12}+d_1\Omega_{02}-d_2\Omega_{01}=2\xi_{2,01}-\frac{2}{r}\xi_{2,0}-\left(\frac{A'}{A}\right)\xi_{2,0}=0$$

$$\Rightarrow \xi_{2,01}=\left(\frac{1}{r}+\frac{A'}{2A}\right)\xi_{2,0}$$

Finally, studying the component $\boxed{\rho_{21,02}}$ when $(rA)'=1$, we have successively:

$$d_0\left(\xi_{2,12}\right)-d_2\left(\xi_{2,01}\right)=d_0\left(-rA\xi_{1,1}\right)-\xi_1-\left(\frac{1}{r}+\frac{A'}{2A}\right)\xi_{2,02}$$

$$=\frac{rA'}{2}\xi_{1,0}+rA\left(\frac{1}{r}+\frac{A'}{2A}\right)\xi_{1,0}-\xi_{1,0}$$

$$=(A+rA')\xi_{1,0}-\xi_{1,0}=0$$

and thus $\xi_{1,0}=0$ *cannot be obtained*. As we already proved that we had $\xi_1=0$ and thus $\xi_{1,1}=0$ but also $\xi_{1,2}=0,\xi_{0,2}=0,\xi_{1,3}=0,\xi_{0,3}=0$, we have therefore obtained $10+5=15$ linearly independent first order equations after *only* 2 prolongations that can also be obtained by computer algebra in a rather "*brute*" way.

*It follows that one needs one more prolongation in order to obtain* $\xi_{1,0}=0$ *from* $\xi_1=0$ *by setting* $\xi_{1,0}=d_0\xi_1$ *formally.*

**REMARK 3B.1**: We present an alternative approach for finding the same results and illustrate it on two cases. First of all we obtain easily:

$$\xi_0^0+\frac{A'}{2A}\xi^1=0,\xi_1^1-\frac{A'}{2A}\xi^1=0,\xi_2^2+\frac{1}{r}\xi^1=0,\xi_3^3+\cot(\theta)\xi^2+\frac{1}{r}\xi^1=0$$

with $\xi_0=A\xi^0,\xi_1=-\frac{1}{A}\xi^1,\xi_2=-r^2\xi^2,\xi_3=-r^2\sin^2(\theta)\xi^3$. Then, using $r$ as a summation index, we have:

$$R_{kl,ij}\equiv\rho_{rl,ij}\xi_k^r+\rho_{kr,ij}\xi_l^r+\rho_{kl,rj}\xi_i^r+\rho_{kl,ir}\xi_j^r+\xi^r\partial_r\rho_{kl,ij}=0$$

and notice that $\rho_{ij}=0\Rightarrow R_{ij}\equiv\rho_{rj}\xi_i^r+\rho_{ir}\xi_j^r+\xi^r\partial_r\rho_{ij}=0$.

The 6 non-zero components of the Weyl tensor are:

$$\rho_{01,01}=+\frac{m}{r^3},\ \rho_{02,02}=-\frac{mA}{2r},\ \rho_{03,03}=-\frac{mA\sin^2(\theta)}{2r}$$

$$\rho_{12,12}=+\frac{m}{2rA},\ \rho_{13,13}=+\frac{m\sin^2(\theta)}{2rA},\ \rho_{23,23}=-mr\sin^2(\theta)$$

We obtain in particular:

$$R_{01,01}\equiv 2\rho_{01,01}\left(\xi_0^0+\xi_1^1\right)+\xi^r\partial_r\left(\rho_{01,01}\right)=\xi^1\partial_1\rho_{01,01}=0\Rightarrow\xi^1=0$$

and similarly:

$$R_{01,02}\equiv\rho_{01,01}\xi_2^1+\rho_{02,02}\xi_1^2+\xi^r\partial_r\rho_{01,02}=\frac{mA}{2r^3}\left(3\xi_{1,2}-\Omega_{12}\right)=0\Rightarrow\xi_2^1=0$$

and so on, as a way to avoid using computer algebra. However, the main consequence of this remark is to explain the existence of the 15 second order CC. Indeed, denoting by "~" a linear proportional dependence, we have:

$$R_{01,01}\sim R_{02,02}\sim R_{03,03}\sim R_{12,12}\sim R_{13,13}\sim R_{23,23}\to\xi_1=0$$

$$R_{01,02}\sim R_{13,23}\to\xi_{1,2}=0$$

$$R_{01,03}\sim R_{12,23}\to\xi_{1,3}=0$$

$$R_{01,12}\sim R_{03,23}\to\xi_{0,2}=0$$

$$R_{01,13}\sim R_{02,23}\to\xi_{0,3}=0$$

$$R_{01,23}\to 0,R_{02,03}\to 0,R_{02,12}\to 0,R_{02,13}\to 0,R_{03,13}\to 0,R_{12,13}\to 0$$

as a way to obtain the 5 equalities on the right and thus a total of $20-5=15$ second order CC obtained by elimination. We have to notice that $R_{01,23}=0,R_{02,31}=0\Rightarrow R_{03,12}=0$ from the identity $R\in ker(\delta)\Rightarrow R_{01,23}+R_{02,31}+R_{03,12}=0$ and there is no way to have two identical indices in the first jets appearing through the (formal) Lie derivative just described. As for the third order CC, using the equation $\xi_{1,1}=\frac{1}{2}\Omega_{11}-\frac{A'}{2A}\xi_1$, we have at least the first prolongations of the previous second order CC to which we have to add the new generating (where the first is the identity 0 = 0):

$$d_0\xi_1-\xi_{1,0}=0,d_1\xi_1-\xi_{1,1}=0,d_2\xi_1-\xi_{1,2}=0,d_3\xi_1-\xi_{1,3}=0,d_2\xi_{0,3}-d_3\xi_{0,2}=0$$

provided by the Spencer operator, leading to the crossed terms $d_i\xi_{1,j}-d_j\xi_{1,i}=0,\forall i,j=1,2,3$ because the Spencer operator is not FI. Finally, we have:

$$d_i\xi_{1,0}-d_0\xi_{1,i}\equiv d_0\left(d_i\xi_1-\xi_{1,i}\right)-d_i\left(d_0\xi_1-\xi_{1,0}\right)=0,\forall i=1,2,3$$

and do not find any new generating fourth order CC, even if the left member is fourth order. Of course, in each of the preceding situations, we have to replace the jets by their expressions in terms of $j_2(\Omega)$ or $j_3(\Omega)$ for obtaining the corresponding CC.

Such striking results are brought by the formal Lie derivative of the Weyl tensor because the Ricci tensor vanishes by assumption and we have the splitting $Riemann\simeq Ricci\oplus Weyl$ according to the *fundamental diagram II* that we discovered as early as in 1988 ([14]) but is still not acknowledged though it can be found in ([15] [21] [23] [24]). In particular, as the *Ricci* part is vanishing by assumption, we may identify the *Riemann* part with the *Weyl* part as tensors ([18] and [24], Th 4.8) and it is possible to prove (using a tedious direct computation or computer algebra) that the only 6 non-zero components are the ones just used in the remark. It is essential to notice that this result bringing a strong condition on the zero jets because of the Lie derivative of the Weyl tensor, thus on the first jets, involves indeed the first derivative of the Weyl tensor because we have a term in $\left(A''\right)'$. However, as we are dealing with sections, $\xi_1=0$ implies $\xi_{1,1}=0$ and we also have $\xi_{0,0}=0,\xi_{1,2}=0,\xi_{1,3}=0$ but *not* $\xi_{1,0}=0$, these later condition being only brought by another additional prolongation in $R_1^{(2)}\subset R_1^{(1)}=R_1$ and it remains to determine the dimensions of these subsystems, exactly again like in the Macaulay or Janet examples. Knowing that $10=dim(R_1)=dim(R_2)>dim(R_3)=5>dim(R_4)=4$, we have thus obtained the 16 equations defining $R_4$ with $dim(R_4)=20-16=4$, namely:

$$\begin{aligned}
&\xi_{3,3}+\sin(\theta)\cos(\theta)\xi_2=0\\
&\xi_{2,3}+\xi_{3,2}-2\cot(\theta)\xi_3=0\\
&\xi_{1,3}=0\\
&\xi_{0,3}=0\\
&\xi_{2,2}=0\\
&\xi_{1,2}=0\\
&\xi_{0,2}=0\\
&\xi_{3,1}-\frac{2}{r}\xi_3=0\\
&\xi_{2,1}-\frac{2}{r}\xi_2=0\\
&\xi_{1,1}=0\\
&\xi_{0,1}-\frac{A'}{A}\xi_0=0\\
&\xi_{3,0}=0\\
&\xi_{2,0}=0\\
&\xi_{1,0}=0\\
&\xi_{0,0}=0\\
&\xi_1=0
\end{aligned}$$

Setting now $\xi_0 = A\xi^0, \xi_1 = -\frac{1}{A}\xi^1, \xi_2 = -r^2\xi^2, \xi_3 = -r^2\xi^3$, we may even simplify these equations and get a system *not depending on A anymore*:

$$\left\{\begin{array}{l|cccc}
\xi_3^3 + \sin(\theta)\cos(\theta)\xi^2 = 0 & 2 & 0 & 1 & 3 \\
\xi_3^2 + \xi_2^3 - 2\cot(\theta)\xi^3 = 0 & 2 & 0 & 1 & 3 \\
\xi_3^1 = 0 & 2 & 0 & 1 & 3 \\
\xi_3^0 = 0 & 2 & 0 & 1 & 3 \\
\xi_1^3 = 0 & 2 & 0 & 1 & \bullet \\
\xi_1^2 = 0 & 2 & 0 & 1 & \bullet \\
\xi_1^1 = 0 & 2 & 0 & 1 & \bullet \\
\xi_1^0 = 0 & 2 & 0 & 1 & \bullet \\
\xi_0^3 = 0 & 2 & 0 & \bullet & \bullet \\
\xi_0^2 = 0 & 2 & 0 & \bullet & \bullet \\
\xi_0^1 = 0 & 2 & 0 & \bullet & \bullet \\
\xi_0^0 = 0 & 2 & 0 & \bullet & \bullet \\
\xi_2^2 = 0 & 2 & \bullet & \bullet & \bullet \\
\xi_2^1 = 0 & 2 & \bullet & \bullet & \bullet \\
\xi_2^0 = 0 & 2 & \bullet & \bullet & \bullet \\
\xi^1 = 0 & \bullet & \bullet & \bullet & \bullet
\end{array}\right.$$

It is easy to check that $R_1^{(3)}$, having minimum dimension equal to 4, is formally integrable, though not involutive as it is finite type, and to exhibit 4 solutions linearly independent over the constants. Indeed, we must have $\xi^0 = c$ where $c$ is a constant and we may drop the time variable not appearing elsewhere while using the equation $\xi^1 = 0$. It follows that $\xi^2 = f(\theta,\phi), \xi^3 = g(\theta,\phi)$ while $f, g$ are solutions of the first, second and fifth equations of Killing type with a general solution depending on 3 constants, a result leading to an elementary problem of 2-dimensional elasticity left to the reader as an exercise. The system $R_1^{(3)}$ is formally integrable while the system $R_2^{(2)}$ is involutive. Having in mind the PP procedure, it follows that the CC are of order 2, 3 *and* 4 along the following commutative and exact diagram and its various prolongations:

$$\begin{array}{ccccccccccc}
 & & & & 0 & & 0 & & & & \\
 & & & & \downarrow & & \downarrow & & & & \\
 & & 0 & \to & S_4T^*\otimes T & \to & S_3T^*\otimes F_0 & \to & h_3 & \to & 0 \\
 & & \downarrow & & \downarrow & & \downarrow & \searrow & \downarrow & & \\
0 & \to & R_4 & \to & J_4(T) & \to & J_3(F_0) & \to & Q_3 & \to & 0 \\
 & & \downarrow & & \downarrow \pi_3^4 & & \downarrow \pi_2^3 & & \downarrow & & \\
0 & \to & R_3 & \to & J_3(T) & \to & J_2(F_0) & \to & Q_2 & \to & 0 \\
 & & & & \downarrow & & \downarrow & & \downarrow & & \\
 & & & & 0 & & 0 & & 0 & &
\end{array}$$

$$\begin{array}{ccccccccccc}
 & & & & 0 & & 0 & & & & \\
 & & & & \downarrow & & \downarrow & & & & \\
 & & 0 & \to & 140 & \to & 200 & \to & 60 & \to & 0 \\
 & & \downarrow & & \downarrow & & \downarrow & \searrow & \downarrow & & \\
0 & \to & 4 & \to & 280 & \to & 350 & \to & 74 & \to & 0 \\
 & & \downarrow & & \downarrow \pi_3^4 & & \downarrow \pi_2^3 & & \downarrow & & \\
0 & \to & 5 & \to & 140 & \to & 150 & \to & 15 & \to & 0 \\
 & & & & \downarrow & & \downarrow & & \downarrow & & \\
 & & & & 0 & & 0 & & 0 & &
\end{array}$$

and its various prolongations like:

$$\begin{array}{ccccccccccc}
 & & & & 0 & & 0 & & 0 & & \\
 & & & & \downarrow & & \downarrow & & \downarrow & & \\
 & & 0 & \to & S_5T^*\otimes T & \to & S_4T^*\otimes F_0 & \to & h_4 & \to & 0 \\
 & & \downarrow & & \downarrow & & \downarrow & \searrow & \downarrow & & \\
0 & \to & R_5 & \to & J_5(T) & \to & J_4(F_0) & \to & Q_4 & \to & 0 \\
 & & \downarrow & & \downarrow \pi_3^4 & & \downarrow \pi_2^3 & & \downarrow & & \\
0 & \to & R_4 & \to & J_4(T) & \to & J_3(F_0) & \to & Q_3 & \to & 0 \\
 & & \downarrow & & \downarrow & & \downarrow & & \downarrow & & \\
 & & 0 & & 0 & & 0 & & 0 & &
\end{array}$$

$$\begin{array}{ccccccccccc}
 & & & & 0 & & 0 & & 0 & & \\
 & & & & \downarrow & & \downarrow & & \downarrow & & \\
 & & 0 & \to & 224 & \to & 350 & \to & 126 & \to & 0 \\
 & & \downarrow & & \downarrow & & \downarrow & \searrow & \downarrow & & \\
0 & \to & 4 & \to & 504 & \to & 700 & \to & 200 & \to & 0 \\
 & & \downarrow & & \downarrow \pi_3^4 & & \downarrow \pi_2^3 & & \downarrow & & \\
0 & \to & 4 & \to & 280 & \to & 350 & \to & 74 & \to & 0 \\
 & & \downarrow & & \downarrow & & \downarrow & & \downarrow & & \\
 & & 0 & & 0 & & 0 & & 0 & &
\end{array}$$

If we *define* $F_1 = Q_4$, we have the exact sequences with $dim(R_{3+r}) = dim(R_3) = 4, \forall r \geq 0$:

$$0 \to R_{5+r} \to J_{5+r}(T) \to J_{4+r}(F_0) \to J_r(F_1)$$

by applying the Spencer $\delta$-map inductively to the symbol sequences:

$$0 \to S_{5+r}T^* \otimes T \to S_{4+r}T^* \otimes F_0 \to S_rT^* \otimes F_1$$

and chasing as usual along the south-west to north-east diagonal. However, *exactly like in the Macaulay example* 2A.9 where we needed 2 prolongations while here we need 3 prolongations, we could also define $F_1 = Q_3$. Indeed, applying the Spencer operator $d$ of Proposition 2C.3 like in ([12], p. 190) or ([13], p. 688), the local exactnes of the sequence $T \to F_0 \to F_1$ is equivalent to the local exactness of the first Spencer sequence $R_4 \xrightarrow{d} T^* \otimes R_3 \xrightarrow{d} \wedge^2 T^* \otimes R_2$. As the second Spencer sequence is locally isomorphic to the tensor product of

the Poincaré sequence by a 4-dimensional Lie algebra, it is locally exact and the corresponding first Spencer sequence $R_5 \xrightarrow{d} T^* \otimes R_4 \xrightarrow{d} \wedge^2 T^* \otimes R_3$ is also locally exact. By projection, it is thus sufficient to prove the injectivity of $d$ in the sequence $0 \to T^* \otimes \left( R_3 / R_3^{(1)} \right) \xrightarrow{d} \wedge^2 T^* \otimes \left( R_2 / R_2^{(1)} \right)$. A tricky computation, justifying the use of the Spencer operator in Remark 3B.1, finally allows to construct inductively the *simplest, shortest, formally and locally exact* differential sequence:

$$0 \to \Theta \to 4 \xrightarrow[1]{} 10 \xrightarrow[3]{} 74 \xrightarrow[1]{} 170 \xrightarrow[1]{} 164 \xrightarrow[1]{} 76 \xrightarrow[1]{} 14 \to 0$$

However, this fact is of no importance compared to the following comments that we now provide and will be explained later on in a much simpler direct way.

First of all, denoting by $R_2' = R_2^{(1)} \subset R_2$ with $dim\left( R_2' \right) = 4$ the involutive system provided by the PP procedure, we are in position to construct the corresponding canonical/involutive (lower) Janet and (upper) Spencer sequences along the following *fundamental diagram I* already constructed in many books and papers (In particular, we advise the curious reader to look at the very striking Example 3.14 described in [17], p. 119 and showing the importance of involution) and presented in the last subsection *A*. In this diagram, *not depending any longer on m*, we have now $C_r = \wedge^r T^* \otimes R_2'$ and provide the fiber dimensions below:

$$\begin{array}{ccccccccccccccccc}
 & & & & & & 0 & & 0 & & 0 & & 0 & & 0 & & \\
 & & & & & & \downarrow & & \downarrow & & \downarrow & & \downarrow & & \downarrow & & \\
0 & \to & \Theta & \xrightarrow{j_2} & 4 & \xrightarrow{D_1} & 16 & \xrightarrow{D_2} & 24 & \xrightarrow{D_3} & 16 & \xrightarrow{D_4} & 4 & \to & 0 \\
 & & & & \downarrow & & \downarrow & & \downarrow & & \downarrow & & \downarrow & & & \\
0 & \to & 4 & \xrightarrow{j_2} & 60 & \xrightarrow{D_1} & 160 & \xrightarrow{D_2} & 180 & \xrightarrow{D_3} & 96 & \xrightarrow{D_4} & 20 & \to & 0 \\
 & & \| & & \downarrow & & \downarrow & & \downarrow & & \downarrow & & \downarrow & & & \\
0 & \to & \Theta & \to & 4 & \xrightarrow{\mathcal{D}} & 56 & \xrightarrow{\mathcal{D}_1} & 144 & \xrightarrow{\mathcal{D}_2} & 156 & \xrightarrow{\mathcal{D}_3} & 80 & \xrightarrow{\mathcal{D}_4} & 16 & \to & 0 \\
 & & & & & & \downarrow & & \downarrow & & \downarrow & & \downarrow & & \downarrow & & & \\
 & & & & & & 0 & & 0 & & 0 & & 0 & & 0 & &
\end{array}$$

We notice the vanishing of the Euler-Poincaré characteristics:

$$4 - 16 + 24 - 16 + 4 = 0,$$
$$4 - 60 + 160 - 180 + 96 - 20 = 0,$$
$$4 - 56 + 144 - 156 + 80 - 16 = 0$$

In actual practice, *all the preceding computations have been finally used to reduce the Poincaré group to its subgroup made with only one time translation and three space rotations*!. On the contrary, we have proved during the last forty years that one *must* increase the Poincaré group (10 parameters), first to the Weyl group (11 parameters by adding 1 dilatation) and finally to the conformal group of space-time (15 parameters by adding 4 elations) as in ([41]), while only dealing with the Spencer sequence in order to increase the dimensions of the Spencer bundles and thus the number of corresponding potentials and fields. In

view of the size of the matrices involved, we wish therefore good luck to the reader who should like to find back these results by using computer algebra!

Now, in order to convince the reader that *only new methods* can allow to study the strange phenomena happening in the constructions of CC (high order, sudden increase in the number of generators,...), we shall turn over totally the previous approach and use a totally different point of view in order to shortcut the use of computer algebra, having in mind that we already know the final formally integrable system $R_3 \subset J_3(T)$ with $dim(R_3)=4$ but the same method could be used for other cases. For this, we use the known Killing vector $\partial_t$ and the zero order equation $\xi^1=0$ in order to restrict $T$ to a sub-vector bundle $E \subset T$ of dimension 2 with section $(\xi^2,\xi^3)$ in order to have a first order system with 3 independent variables $(r,\theta,\phi)=(1,2,3)$ and 2 unknowns, obtained by eliminating $\xi^1$ and $\xi^0$ as follows in order to get an equivalent system for $\xi^2,\xi^3$ for the variables $(1,2,3)$ with only 5 equations:

$$\left\{\begin{array}{ll} \xi^3_3+\sin(\theta)\cos(\theta)\xi^2=0 & \boxed{\begin{array}{ccc} 2 & 1 & 3 \end{array}} \\ \xi^2_3+\xi^3_2-2\cot(\theta)\xi^3=0 & \begin{array}{ccc} 2 & 1 & 3 \end{array} \\ \xi^3_1=0 & \begin{array}{ccc} 2 & 1 & \bullet \end{array} \\ \xi^2_1=0 & \begin{array}{ccc} 2 & 1 & \bullet \end{array} \\ \xi^2_2=0 & \begin{array}{ccc} 2 & \bullet & \bullet \end{array} \end{array}\right.$$

As a byproduct, we have the following commutative diagrams:

$$\begin{array}{ccccccccccc} & & & & 0 & & 0 & & & & \\ & & & & \downarrow & & \downarrow & & & & \\ & & 0 & \rightarrow & S_3T^*\otimes E & \rightarrow & S_2T^*\otimes F_0 & \rightarrow & h_2 & \rightarrow 0 & \\ & & & & \downarrow\delta & & \downarrow\delta & & \downarrow & & \\ & & 0 & \rightarrow & T^*\otimes S_2T^*\otimes E & \rightarrow & T^*\otimes T^*\otimes F_0 & \rightarrow & T^*\otimes Q_1 & \rightarrow 0 & \\ & & & & \downarrow\delta & & \downarrow\delta & & \downarrow & & \\ 0 & \rightarrow & \wedge^2T^*\otimes g_1 & \rightarrow & \wedge^2T^*\otimes T^*\otimes E & \rightarrow & \wedge^2T^*\otimes F_0 & \rightarrow & 0 & & \\ & & \downarrow\delta & & \downarrow\delta & & \downarrow & & & & \\ 0 & \rightarrow & \wedge^3T^*\otimes E & = & \wedge^3T^*\otimes E & \rightarrow & 0 & & & & \\ & & \downarrow & & \downarrow & & & & & & \\ & & 0 & & 0 & & & & & & \end{array}$$

$$\begin{array}{ccccccccccc} & & & & & & 0 & & 0 & & \\ & & & & & & \downarrow & & \downarrow & & \\ & & & & 0 & \rightarrow & 20 & \rightarrow & 30 & \rightarrow 10 & \rightarrow 0 \\ & & & & & & \downarrow\delta & & \downarrow\delta & \downarrow & \\ & & & & 0 & \rightarrow & 36 & \rightarrow & 45 & \rightarrow 9 & \rightarrow 0 \\ & & & & & & \downarrow\delta & & \downarrow\delta & \downarrow & \\ & & 0 & \rightarrow & 3 & \rightarrow & 18 & \rightarrow & 15 & \rightarrow 0 & \\ & & & & \downarrow\delta & & \downarrow\delta & & \downarrow & & \\ & & 0 & \rightarrow & 2 & = & 2 & \rightarrow & 0 & & \\ & & & & \downarrow & & \downarrow & & & & \\ & & & & 0 & & 0 & & & & \end{array}$$

The next result points out the importance of the Spencer $\delta$-cohomology and will be justified later on in cartesian coordinates as it is intrinsic:

**LEMMA 3B.2**: The last symbol diagram is commutative and exact. In particular, the lower left map $\delta$ is surjective and thus the upper right induced map $h_2 \to T^* \otimes Q_1$ is also surjective while these two maps have isomorphic kernels.

*Proof*: The 3 components of $\wedge^2 T^* \otimes g_1$ are $\left\{v^3_{2,12}, v^3_{2,13}, v^3_{2,23}\right\}$ and the kernel of the map $\delta$ is described by the two linear equations:

$$v^2_{1,23} + v^2_{2,31} + v^2_{3,12} = 0, \quad v^3_{1,23} + v^3_{2,31} + v^3_{3,12} = 0$$

that is to say by the two linearly independent equations:

$$v^3_{2,12} = 0, \quad v^3_{2,13} = 0$$

Accordingly, in the left column we have:

$$dim\left(H^2\left(g_1\right)\right) = dim\left(Z^2\left(g_1\right)\right) = dim\left(ker\left(\delta\right)\right) = 1$$

An unusual snake-type diagonal chase left to the reader as an exercise proves that the induced map $h_2 \to T^* \otimes Q_1$ is surjective with a kernel isomorphic to $H^2\left(g_1\right)$. This is a *crucial result* because it also proves that the additional CC has only to do with the the single second order component of the Riemann tensor in dimension 2, a striking result that could not even be imagined by standard methods.

Q.E.D.

Now, we have explained why the new zero order PD equation $\xi_1 = 0 \Leftrightarrow \xi^1 = 0$ should be replaced by the condition $x^i \xi_i = 0$ by using the space euclidan metric for lowering the indices. Differentiating with respect to $x^j$, we obtain $\delta^i_j \xi_i + x^i \xi_{i,j} = 0$ with the Kronecker symbol $\delta$ and, contracting with $x^j$ we finally get $x^j \xi_j + x^i x^j \xi_{i,j} = 0$. hence *on space*, we get a new subsystem by adding to the standard Killing system of space $\left(n = 3\right)$ the above zero order constraint in order to get a system $R'_1$ with $dim\left(R'_1\right) = \left(3+9\right) - \left(6+2+1\right) = 3$. Coming back to the computation previously done with the Schwarzschild metric while using only $\xi^0$ and $\xi^1$, we discover that *the new system does not any longer depend on* "$A$" (See other examples in [16]).

Its study can be therefore replaced by that of the 3-dimensional system $R'_1$ which is defining a nontransitive system of infinitesimal lie equations, that is the map $\pi^1_0 : R'_1 \to T$ is no longer surjective, a result modifying the constructions of the Vessiot structure equations but this is out of our story. Suppressing from now on the "′" for simplicity, we are thus led to $n = 3$ and the *formally integrable* system of 9 linearly independent equations where $\omega$ is the Euclidean metric:

$$\xi_{i,j} + \xi_{j,i} = 0, \quad x^i \xi_{i,j} + \xi_j = 0, \quad x^i \xi_i = 0$$

because $x^j\left(x^i\xi_{i,j}+\xi_j\right)=x^ix^j\xi_{i,j}+x^i\xi_i=x^i\xi_i=0$.

Changing slighty the notations with now $n=3,m=dim(E)=2$ in order to keep an upper index for any unknown while setting $\xi^3=-\frac{x^1}{x^3}\xi^1-\frac{x^2}{x^3}\xi^2$, we get the following system $R_1\subset J_1(E)$ with $dim(R_1)=3$ because $par_1=\left\{\xi^1,\xi^2,\xi_1^2\right\}$ and corresponding Janet tabular:

$$\begin{cases}\Phi^5\equiv\xi_3^2+\frac{x^1}{x^3}\xi_1^2-\frac{1}{x^3}\xi^2=0\\ \Phi^4\equiv\xi_3^1-\frac{x^2}{x^3}\xi_1^2-\frac{1}{x^3}\xi^1=0\\ \Phi^3\equiv\xi_2^2=0\\ \Phi^2\equiv\xi_2^1+\xi_1^2=0=0\\ \Phi^1\equiv\xi_1^1=0\end{cases}\qquad\begin{array}{|ccc|}\hline 1&2&3\\ 1&2&3\\ 1&2&\bullet\\ 1&2&\bullet\\ 1&\bullet&\bullet\\ \hline\end{array}$$

It is easy to check that all the second order jets vanish and that the general solution $\left\{\xi^1=ax^2+bx^3,\xi^2=-ax^2+cx^3\right\}$ depends on 3 arbitrary constants $(a,b,c)$ in such a way that the three space rotations are separately and respectively obtained by each element of the basis $\left\{(1,0,0),(0,1,0),(0,0,1)\right\}$.

As before but with a different system, we have the following commutative diagrams:

$$\begin{array}{ccccccccccc}
 & & & & 0 & & 0 & & 0 & & \\
 & & & & \downarrow & & \downarrow & & \downarrow & & \\
 & & 0 & \to & S_3T^*\otimes E & \to & S_2T^*\otimes F_0 & \to & h_2 & \to & 0\\
 & & \downarrow & & \downarrow & & \downarrow & & \downarrow & & \\
0 & \to & R_3 & \to & J_3(E) & \to & J_2(F_0) & \to & F_1 & \to & 0\\
 & & \downarrow & & \downarrow\pi_4^3 & & \downarrow\pi_1^2 & & \downarrow & & \\
0 & \to & R_2 & \to & J_2(E) & \to & J_1(F_0) & \to & Q_1 & \to & 0\\
 & & \downarrow & & \downarrow & & \downarrow & & \downarrow & & \\
 & & 0 & & 0 & & 0 & & 0 & &
\end{array}$$

$$\begin{array}{ccccccccccc}
 & & & & 0 & & 0 & & 0 & & \\
 & & & & \downarrow & & \downarrow & & \downarrow & & \\
 & & 0 & \to & 20 & \to & 30 & \to & 10 & \to & 0\\
 & & \downarrow & & \downarrow & & \downarrow & & \downarrow & & \\
0 & \to & 3 & \to & 40 & \to & 50 & \to & 13 & \to & 0\\
 & & \downarrow & & \downarrow\pi_2^3 & & \downarrow\pi_1^2 & & \downarrow & & \\
0 & \to & 3 & \to & 20 & \to & 20 & \to & 3 & \to & 0\\
 & & \downarrow & & \downarrow & & \downarrow & & \downarrow & & \\
 & & 0 & & 0 & & 0 & & 0 & &
\end{array}$$

$$\begin{array}{ccccccccccc}
 & & & & 0 & & 0 & & & & \\
 & & & & \downarrow & & \downarrow & & & & \\
 & & 0 & \to & S_3T^*\otimes E & \to & S_2T^*\otimes F_0 & \to & h_2 & \to 0 & \\
 & & & & \downarrow\delta & & \downarrow\delta & & \downarrow & & \\
 & & 0 & \to & T^*\otimes S_2T^*\otimes E & \to & T^*\otimes T^*\otimes F_0 & \to & T^*\otimes Q_1 & \to 0 & \\
 & & & & \downarrow\delta & & \downarrow\delta & & \downarrow & & \\
0 & \to & \wedge^2T^*\otimes g_1 & \to & \wedge^2T^*\otimes T^*\otimes E & \to & \wedge^2T^*\otimes F_0 & \to & 0 & & \\
 & & \downarrow\delta & & \downarrow\delta & & \downarrow & & & & \\
0 & \to & \wedge^3T^*\otimes E & = & \wedge^3T^*\otimes E & \to & 0 & & & & \\
 & & \downarrow & & \downarrow & & & & & & \\
 & & 0 & & 0 & & & & & &
\end{array}$$

$$\begin{array}{ccccccccccc}
 & & & & & & 0 & & 0 & & \\
 & & & & & & \downarrow & & \downarrow & & \\
 & & & & 0 & \to & 20 & \to & 30 & \to 10 & \to 0 \\
 & & & & & & \downarrow\delta & & \downarrow\delta & \downarrow & \\
 & & & & 0 & \to & 36 & \to & 45 & \to 9 & \to 0 \\
 & & & & & & \downarrow\delta & & \downarrow\delta & \downarrow & \\
 & & 0 & \to & 3 & \to & 18 & \to & 15 & \to 0 & \\
 & & & & \downarrow\delta & & \downarrow\delta & & \downarrow & & \\
 & & 0 & \to & 2 & = & 2 & \to & 0 & & \\
 & & & & \downarrow & & \downarrow & & & & \\
 & & & & 0 & & 0 & & & &
\end{array}$$

The next result points out the importance of the Spencer $\delta$-cohomology:

**LEMMA 3B.3**: The last symbol diagram is commutative and exact. In particular, the lower left map $\delta$ is surjective and thus the upper right induced map $h_2 \to T^*\otimes Q_1$ is also surjective while these two maps have isomorphic kernels.

*Proof*: The 3 components of $\wedge^2T^*\otimes g_1$ are $\left\{v^2_{1,12}, v^2_{1,13}, v^2_{1,23}\right\}$ and the map $\delta$ is described by the two linear equations:

$$v^1_{1,23}+v^1_{2,31}+v^1_{3,12}=0, \quad v^2_{1,23}+v^2_{2,31}+v^2_{3,12}=0$$

that is to say by the two linearly independent equations:

$$v^2_{1,13}+\frac{x^2}{x^3}v^2_{1,12}=0, \quad v^2_{1,23}-\frac{x^1}{x^3}v^2_{1,12}=0$$

Accordingly, in the left column we have:

$$dim\left(H^2\left(g_1\right)\right)=dim\left(Z^2\left(g_1\right)\right)=dim\left(ker\left(\delta\right)\right)=1$$

An unusual snake-type diagonal chase left to the reader as an exercise proves that the induced map $h_2 \to T^*\otimes Q_1$ is surjective with a kernel isomorphic to $H^2\left(g_1\right)$. This is indeed a *crucial result* because it also proves that the additional CC has only to do with the the single second order component of the Riemann tensor in dimension 2, a striking result that could not even be imagined by standard methods.

Q.E.D.

Collecting the above results, we find the 3 *first order* differentially independent generating CC coming from the Janet tabular and *the additional single second order generating* CC describing the 2-dimensional *Riemann operator*, that is the linearized Riemann tensor in the space $\left(x^1, x^2\right)$:

$$\begin{cases} \Psi^4 \equiv d_{22}\Phi^1 + d_{11}\Phi^3 - d_{12}\Phi^2 = 0 \\ \Psi^3 \equiv d_3\Phi^3 - d_2\Phi^5 + \dfrac{x^1}{x^3}d_1\Phi^3 - \dfrac{1}{x^3}\Phi^3 = 0 \\ \Psi^2 \equiv d_3\Phi^2 - d_2\Phi^4 - d_1\Phi^5 - \dfrac{x^2}{x^3}d_1\Phi^3 + \dfrac{x^1}{x^3}\left(d_1\Phi^2 - d_2\Phi^1\right) - \dfrac{1}{x^3}\Phi^2 = 0 \\ \Psi^1 \equiv d_3\Phi^1 - d_1\Phi^4 - \dfrac{x^2}{x^3}\left(d_1\Phi^2 - d_2\Phi^1\right) - \dfrac{1}{x^3}\Phi^1 = 0 \end{cases}$$

An elementary but tedious computation provides the second order CC:

$$x^3\left(d_{22}\Psi^1 + d_{11}\Psi^3 - d_{12}\Psi^2\right) - \left(x^1d_1\Psi^4 + x^2d_2\Psi^4 + x^3d_3\Psi^4\right) - 2\Psi^4 = 0$$

The corresponding differential sequence written with differential modules over the ring $D = K\left[d_1, d_2, d_3\right]$ with $K = \mathbb{Q}\left(x^1, x^2, x^3\right)$ is:

$$0 \to D \xrightarrow[2]{} D^4 \xrightarrow[2]{} D^5 \xrightarrow[1]{} D^2 \xrightarrow{p} M \to 0$$

where $p$ is the canonical (residual) projection. We check indeed that $1-4+5-2=0$ but this sequence is quite far from being even strictly exact. Of course, as $R_2$ is involutive, we may set $C_r = \wedge^r T^* \otimes R_2$ and obtain the corresponding canonical second Spencer sequence which is induced by the Spencer operator:

$$0 \to \Theta \xrightarrow{j_2} C_0 \xrightarrow{D_1} C_1 \xrightarrow{D_2} C_2 \xrightarrow{D_3} C_3 \to 0$$

with dimensions:

$$0 \to \Theta \xrightarrow{j_2} 3 \xrightarrow[1]{D_1} 9 \xrightarrow[1]{D_2} 9 \xrightarrow[1]{D_3} 3 \to 0$$

We let the reader compute the corresponding Janet sequence as a first step towards the *Vessiot structure equations* which are not easily obtained because we have now:

$$x^i\xi_i = x^i\omega_{ij}\xi^j \Rightarrow \xi_{i,j} + \xi_{j,i} - 2\gamma_{ij}^r\xi_r = 0$$

where $\gamma$ denotes the Christoffel symbols.

This result justifies "*a fortiori*" the comments we have already provided. The reader may compare such an example with the Janet example (where we have one third order CC and one sixth order additional CC) with the major difference that we have now a formally integrable system. We do not know any other similar situation.

In order to achieve the study of the Schwarzschild metric in a purely intrinsic way, we prove that the situation of the previous example is just describing the way to exhibit the torsion part $t(M) \subseteq M$ of a differential module by computing a certain extension module. Coming back to the systems already obtained and keeping in mind that

$\xi_1=0\Rightarrow\xi_{0,0}=0,\xi_{0,1}-\frac{A'}{A}\xi_0=0,\xi_{0,2}=0,\xi_{0,3}=0\Rightarrow\xi^0=cst$ while replacing $r^2\xi_2,r^2\xi_3$ by $\xi^2,\xi^3$ respectively, we may therefore replace the integration of the previous system by that of the simpler system:

$$\left\{\begin{array}{ll}\Phi^5\equiv\xi_1^3=0 & 2\ 3\ 1\\ \Phi^4\equiv\xi_1^2=0 & 2\ 3\ 1\\ \Phi^3\equiv\xi_3^3+\sin(\theta)\cos(\theta)\xi^2=0 & 2\ 3\ \bullet\\ \Phi^2\equiv\xi_3^2+\xi_2^3-2\cot(\theta)\xi^3=0 & 2\ 3\ \bullet\\ \Phi^1\equiv\xi_2^2=0 & 2\ \bullet\ \bullet\end{array}\right.$$

allowing to define an isomorphic differential module because both systems are formally integrable though not involutive, with the same dimension $2+(2\times3)-5=3$ with $par_2=par_1=\{\xi^2,\xi^3,\xi_2^3\}$. We have now similarly the 3 *first order* CC and the single *second order* CC:

$$\left\{\begin{array}{l}\Psi^4\equiv d_{33}\Phi^1+d_{22}\Phi^3-d_{23}\Phi^2-\sin(\theta)\cos(\theta)d_2\Phi^1\\ \qquad -2\cot(\theta)d_2\Phi^3-2\sin^2(\theta)\Phi^1+\frac{2}{\sin^2(\theta)}\Phi^3=0\\ \Psi^3\equiv d_1\Phi^3-d_3\Phi^5-\sin(\theta)\cos(\theta)\Phi^4=0\\ \Psi^2\equiv d_1\Phi^2-d_3\Phi^4-d_2\Phi^5-2\cot(\theta)\Phi^5=0\\ \Psi^1\equiv d_1\Phi^1-d_2\Phi^4=0\end{array}\right.$$

describing again the single component of the linearized Riemann tensor for $(\theta,\phi)$ and the first Spencer cohomology group $H^2(g_1)$ of the first symbol $g_1\subset T^*\otimes E$ with $dim(E)=2$ and $dim(H^2(g_1))=dim(\wedge^2T^*\otimes g_1)-dim(\wedge^3T^*\otimes E)=3-2=1$. Of course, we could even simplified the later system by considering the new system:

$$\left\{\begin{array}{ll}\Phi^3\equiv\xi_3^3+\sin(\theta)\cos(\theta)\xi^2=0 & 2\ 3\\ \Phi^2\equiv\xi_3^2+\xi_2^3-2\cot(\theta)\xi^3=0 & 2\ 3\\ \Phi^1\equiv\xi_2^2=0 & 2\ \bullet\end{array}\right.$$

We let the reader fill in the details and discover again the only CC $\Psi^4=\Psi=0$.

Considering both situations already studied with $n=3,m=2$, we discover that the differential modules defined by the system $\Psi^1=0,\Psi^2=0,\Psi^3=0$ are isomoprphic, provided we extend conveniently the ground differential field. Hence, in both cases, we have $t(M)\neq0$ and the torsion submodule has a *single generator* namely the residue of $\Psi^4$ which is satisfying for example the so-called *autonomous* equation:

$$x^1d_1\Psi^4+x^2d_2\Psi^4+x^3d_3\Psi^4+2\Psi^4=0$$

Setting $M'=M/t(M)$, we have the short exact sequence:

$$0\to t(M)\to M\to M'\to0$$

where the torsion-free differential module $M'$ is now defined by

$\Psi^1=0,\cdots,\Psi^4=0$. The explanation can only be natural in the framework of *differential homological algebra* because, *by construction*, the CC operator $D_1$ is parametrized by $D$ and MUST therefore provide the torsion-free differential module $M'$. This result explains for the fiirst time the intrinsic character of the additional higher order generating CC that can be found in an apparently strange manner. In a more detailed way, let us proceed as follows in order to construct the following commutative diagram:

$$\begin{array}{ccccccc} & & & & & & 4 \\ & & & & & \overset{\mathcal{D}_1'}{\nearrow} & \\ 2 & \overset{\mathcal{D}}{\rightarrow} & 5 & \overset{\mathcal{D}_1}{\rightarrow} & 3 & & \\ 2 & \overset{ad(\mathcal{D})}{\leftarrow} & 5 & \overset{ad(\mathcal{D}_1)}{\leftarrow} & 3 & & \end{array}$$

1) Write down the operator $\mathcal{D}_1:\left(\Phi^1,\cdots,\Phi^5\right)\to\left(\Psi^1,\Psi^2,\Psi^3\right)$ as we did.

2) Multiply by test functions $\lambda=\left(\lambda^1,\lambda^2,\lambda^3\right)$, integrate by parts and construct the formal adjoint $ad\left(\mathcal{D}_1\right):\left(\lambda^1,\lambda^2,\lambda^3\right)\to\left(\mu^1,\cdots,\mu^5\right)$:

$$\begin{cases} -d_1\lambda^1=\mu^1 \\ -d_1\lambda^2=\mu^2 \\ -d_1\lambda^3=\mu^3 \\ d_3\lambda^2+d_2\lambda^1-\sin(\theta)\cos(\theta)\lambda^3=\mu^4 \\ d_3\lambda^3+d_2\lambda^2-2\cos(\theta)\lambda^2=\mu^5 \end{cases}$$

3) Construct generating CC as an operator $ad\left(\mathcal{D}\right):\left(\mu^1,\cdots,\mu^5\right)\to\left(\nu^1,\nu^2\right)$:

$$\begin{cases} d_1\mu^4+d_3\mu^2+d_2\mu^1-\sin(\theta)\cos(\theta)\mu^3=\nu^1 \\ d_1\mu^5+d_3\mu^3+d_2\mu^2-2\cos(\theta)\mu^2=\nu^2 \end{cases}$$

4) Exhibit $ad\left(ad\left(\mathcal{D}\right)\right)=\mathcal{D}:\left(\Upsilon^1,\Upsilon^2\right)\to\left(\Phi^1,\cdots,\Phi^5\right)$:

$$\begin{cases} -d_2\Upsilon^1=\Phi^1 \\ -d_3\Upsilon^1-d_2\Upsilon^2-2\cos(\theta)\Upsilon^2=\Phi^2 \\ -d_3\Upsilon^2-\sin(\theta)\cos(\theta)\Upsilon^1=\Phi^3 \\ -d_1\Upsilon^1=\Phi^4 \\ -d_1\Upsilon^2=\Phi^5 \end{cases}$$

5) Construct generating CC $\mathcal{D}':\left(\Phi^1,\cdots,\Phi^5\right)\to\left(\Psi^1,\Psi^2,\Psi^3,\Psi^4\right)$ and compare $\mathcal{D}\le\mathcal{D}'$. Then each new CC is a torsion element of the differential module determined by $\mathcal{D}$ which is thus parametrized by $\mathcal{D}_{-1}$ if and only if $\mathcal{D}'=\mathcal{D}$. In the present case, $\Psi^1,\Psi^2,\Psi^3$ being differentially independent, we find the only additional generating CC $\Psi^4=0$.

Accordingly, the situation in GR cannot evolve as long as people will not acknowledge the fact that the components of the Weyl tensor are *similarly* playing the part of torsion elements (the so-called *Lichnerowicz waves* in [42]

[43]) for the equations $Ricci=0$ for reasons only depending on the group structure of the conformal group of space-time and bring the splitting $Riemann=Weyl\oplus Ricci$.

**C) KERR METRIC:**

We now write the Kerr metric in Boyer-Lindquist coordinates:

$$ds^2=\frac{\rho^2-mr}{\rho^2}dt^2-\frac{\rho^2}{\Delta}dr^2-\rho^2d\theta^2+\frac{2amr\sin^2(\theta)}{\rho^2}dtd\phi$$
$$-\frac{\left(r^2+a^2\right)^2-a^2\Delta\sin^2(\theta)}{\rho^2}\sin^2(\theta)d\phi^2$$

where we have set $\Delta=r^2-mr+a^2,\rho^2=r^2+a^2\cos^2(\theta)$ and we check that:

$$a=0\Rightarrow ds^2=\left(1-\frac{m}{r}\right)dt^2-\frac{1}{1-\frac{m}{r}}dr^2-r^2d\theta^2-r^2\sin(\theta)^2d\phi^2$$

as a well-known way to recover the Schwarschild metric. Now, we notice that $t$ or $\phi$ do not appear in the coefficients of the metric and thus, as the maximum subgroup of invariance of the Kerr metric *must* be contained in the maximum subgroup of invariance of the Schwarzschild metric because of the above limit when $a\to 0$, we obtain the only possible 2 infinitesimal generators $\{\partial_t,\partial_\phi\}$ and we have the fundamental diagram I with fiber dimensions:

$$\begin{array}{ccccccccccccccccc}
 & & & & 0 & & 0 & & 0 & & 0 & & 0 & & \\
 & & & & \downarrow & & \downarrow & & \downarrow & & \downarrow & & \downarrow & & \\
0 & \to & \Theta & \overset{j_2}{\to} & 2 & \overset{D_1}{\to} & 8 & \overset{D_2}{\to} & 12 & \overset{D_3}{\to} & 8 & \overset{D_4}{\to} & 2 & \to & 0 \\
 & & & & \downarrow & & \downarrow & & \downarrow & & \downarrow & & \downarrow & & \\
0 & \to & 4 & \overset{j_2}{\to} & 60 & \overset{D_1}{\to} & 160 & \overset{D_2}{\to} & 180 & \overset{D_3}{\to} & 96 & \overset{D_4}{\to} & 20 & \to & 0 \\
 & & \| & & \downarrow & & \downarrow & & \downarrow & & \downarrow & & \downarrow & & \\
0 & \to & \Theta & \to & 4 & \overset{\mathcal{D}}{\to} & 58 & \overset{\mathcal{D}_1}{\to} & 152 & \overset{\mathcal{D}_2}{\to} & 168 & \overset{\mathcal{D}_3}{\to} & 88 & \overset{\mathcal{D}_4}{\to} & 18 & \to & 0 \\
 & & & & & & \downarrow & & \downarrow & & \downarrow & & \downarrow & & \downarrow & & \\
 & & & & & & 0 & & 0 & & 0 & & 0 & & 0 & &
\end{array}$$

with Euler-Poincaré characteristic $4-58+152-168+88-18=0$. Comparing the *surprisingly high* dimensions of the Janet bundles with the *surprisingly low* dimensions of the Spencer bundles needs no comment on the physical usefulness of the Janet sequence, despite its purely mathematical importance. In addition, using now the same notations as in the preceding section, we have the additional *zero order* equations $\xi^1=0,\xi^2=0$ produced by the non-zero components of the Weyl tensor and thus, *at best*,

$dim\left(R_0^{(3)}\right)=2\Leftrightarrow dim\left(R_1^{(2)}\right)=2$, if the zero order equations are obtained after *only* two prolongations. As these zero order equations depend on $j_2(\Omega)$, *at best*, we should obtain therefore eventually $dim(Q_2)=10+2=12$ CC of order 2 and $60-(4\times 12)=12$ CC of order 3 at least.

Using finally cartesian coordinates with $\xi^3=0, x^1\xi^1+x^2\xi^2=0$, we have only to study the following first order involutive system for $\xi^1=\xi$ with coefficients no longer depending on $(a,m)$, providing the only generator $x^1\partial_2-x^2\partial_1$

$$\begin{cases}\Phi^3\equiv\xi_3=0 & 1\ \ 2\ \ 3\\ \Phi^2\equiv\xi_2-\dfrac{1}{x^2}\xi=0 & 1\ \ 2\ \ \bullet\\ \Phi^1\equiv\xi_1=0 & 1\ \ \bullet\ \ \bullet\end{cases}$$

$$\begin{aligned}&\Psi^3\equiv d_3\Phi^2-d_2\Phi^3+\frac{1}{x^2}\Phi^3=0,\\ &\Psi^2\equiv d_3\Phi^1-d_1\Phi^3=0,\\ &\Psi^1\equiv d_2\Phi^1-d_1\Phi^2-\frac{1}{x^2}\Phi^1=0\end{aligned}$$

$$\Rightarrow d_3\Psi^1-d_2\Psi^2+d_1\Psi^3+\frac{1}{x^2}\Psi^2=0$$

$$\begin{array}{ccccccccccccccc}
 & & & & & & 0 & & 0 & & 0 & & 0 & & \\
 & & & & & & \downarrow & & \downarrow & & \downarrow & & \downarrow & & \\
0 & \to & \Theta & \overset{j_1}{\to} & 1 & \overset{D_1}{\to} & 3 & \overset{D_2}{\to} & 3 & \overset{D_3}{\to} & 1 & \to & 0 & & \\
 & & & & \downarrow & & \downarrow & & \downarrow & & \| & & & & \\
0 & \to & 1 & \overset{j_1}{\to} & 4 & \overset{D_1}{\to} & 6 & \overset{D_2}{\to} & 4 & \overset{D_3}{\to} & 1 & \to & 0 & & \\
 & & \| & & \downarrow & & \downarrow & & \downarrow & & \downarrow & & & & \\
0 & \to & \Theta & \to & 1 & \overset{\mathcal{D}}{\to} & 3 & \overset{\mathcal{D}_1}{\to} & 3 & \overset{\mathcal{D}_2}{\to} & 1 & \to & 0 & & \\
 & & & & & & \downarrow & & \downarrow & & \downarrow & & & & \\
 & & & & & & 0 & & 0 & & 0 & & & &
\end{array}$$

This result definitively proves that, *as far as differential sequences are concerned*, the only important object is the group, not the metric.

## 4. Conclusion

We may summarize the results obtained in the 3 previous subsections by saying:

*JANET AND SPENCER PLAY AT SEE - SAW*

because we have the formula $dim(C_r)+dim(F_r)=dim(C_r(E))$ and the sum thus only depends on $(n,m,q)$ but not on the underlying group when $E=T$. Hence, the smaller the background group is, the smaller the dimensions of the Spencer bundles are and the higher the dimensions of the Janet bundles are. As a byproduct, we claim that the only solution for escaping is to increase the dimension of the Lie group involved, adding successively 1 dilatation and 4 elations in order to deal with the conformal group of space-time while using the Spencer sequence instead of the Janet sequence ([23] [43]). The results of this paper thus question the mathematical foundations of GR and even strengthen the doubts we already had about the existence of gravitational waves in [23]. Two forthcoming publications will achieve this game.

## Conflicts of Interest

The authors declare no conflicts of interest regarding the publication of this paper.

## References


[1] Andersson, L. (2015) Spin Geometry and Conservation Laws in the Kerr Spacetime. arxiv:1504.02069.

[2] Shah, A.G., Whitting, B.F., Aksteiner, S., Andersson, L. and Bäckdahl, T. (2016) Gauge Invariant Perturbation of Schwarzschild Spacetime. arxiv:1611.08291.

[3] Aksteiner, S. and Bäckdahl, T. (2018) All Local Gauge Invariants for Perturbations of the Kerr Spacetime. arxiv:1803.05341.

[4] Khavkine, I. (2017) *Journal of Geometry and Physics*, **113**, 131-169. arxiv:1409.7212. https://doi.org/10.1016/j.geomphys.2016.06.009

[5] Khavkine, I. (2018) Compatibility Complexes of Overdetermined PDEs of Finite Type, with Applications to the Killing Equation. arxiv:1805.03751.

[6] Eisenhart, L.P. (1926) Riemannian Geometry. Princeton University Press, Princeton.

[7] Vessiot, E. (1903) *Annales Scientifiques de l'École Normale Supérieure*, **20**, 411-451. (Can Be Obtained from http://numdam.org)

[8] Vessiot, E. (1904) *Annales Scientifiques de l'École Normale Supérieure*, **21**, 9-85. (Can Be Obtained from http://numdam.org)

[9] Goldschmidt, H. (1968) *Annales Scientifiques de l'École Normale Supérieure*, **4**, 417-444. https://doi.org/10.24033/asens.1168

[10] Goldschmidt, H. (1968) *Annales Scientifiques de l'École Normale Supérieure*, **4**, 617-625. https://doi.org/10.24033/asens.1173

[11] Spencer, D.C. (1965) *Bulletin of the American Mathematical Society*, **75**, 1-114.

[12] Pommaret, J.-F. (1978) Systems of Partial Differential Equations and Lie Pseudogroups. Gordon and Breach, New York; Russian Translation: MIR, Moscow.

[13] Pommaret, J.-F. (1983) Differential Galois Theory. Gordon and Breach, New York.

[14] Pommaret, J.-F. (1988) Lie Pseudogroups and Mechanics. Gordon and Breach, New York.

[15] Pommaret, J.-F. (1994) Partial Differential Equations and Group Theory. Kluwer, Dordrecht. https://doi.org/10.1007/978-94-017-2539-2

[16] Pommaret, J.-F. (2001) Partial Differential Control Theory. Kluwer, Dordrecht, 1000 p.

[17] Pommaret, J.-F. (2016) Deformation Theory of Algebraic and Geometric Structures. Lambert Academic Publisher, Saarbrucken. http://arxiv.org/abs/1207.1964

[18] Pommaret, J.-F. (2018) New Mathematical Methods for Physics. NOVA Science Publisher, New York.

[19] Pommaret, J.-F.(1995) *Comptes rendus de l'Académie des Sciences*, **320**, 1225-1230.

[20] Pommaret, J.-F. (2013) *Multidimensional Systems and Signal Processing*, **26**, 405-437.

[21] Pommaret, J.-F. (2013) *Journal of Modern Physics*, **4**, 223-239. https://doi.org/10.4236/jmp.2013.48A022

[22] Pommaret, J.-F. (2014) *Journal of Modern Physics*, **5**, 157-170. https://doi.org/10.4236/jmp.2014.55026

[23] Pommaret, J.-F.(2017) *Journal of Modern Physics*, **8**, 2122-2158. https://doi.org/10.4236/jmp.2017.813130

[24] Pommaret, J.-F. (2017) Algebraic Analysis and Mathematical Physics. http://arxiv.org/abs/1706.04105

[25] Pommaret, J.-F. (2018) From Elasticity to Electromagnetism: Beyond the Mirror. http://arxiv.org/abs/1802.02430

[26] Janet, M. (1920) *Journal d'Analyse Mathematique*, **8**, 65-151.

[27] Assem, I. (1997) Algèbres et Modules. Masson, Paris.

[28] Bourbaki, N. (1980) Algébre. Ch. 10, Algébre Homologique, Masson, Paris.

[29] Hu, S.-T. (1968) Introduction to Homological Algebra, Holden-Day.

[30] Kunz, E. (1985) Introduction to Commutative Algebra and Algebraic Geometry. Birkhäuser, Boston.

[31] Northcott, D.G. (1966) An Introduction to Homological Algebra. Cambridge University Press, Cambridge.

[32] Rotman, J.J. (1979) An Introduction to Homological Algebra, Pure and Applied Mathematics. Academic Press, Cambridge.

[33] Macaulay, F.S. (1916) The Algebraic Theory of Modular Systems. Cambridge.

[34] Zerz, E. (2000) Topics in Multidimensional Linear Systems Theory. Lecture Notes in Control and Information Sciences (LNCIS) 256, Springer, Berlin.

[35] Bjork, J.E. (1993) Analytic D-Modules and Applications. Kluwer, Dordrecht. https://doi.org/10.1007/978-94-017-0717-6

[36] Quadrat, A. (2010) *Les cours du CIRM*, *Journees Nationales de Calcul Formel*, **1**, 281-471.

[37] Schneiders, J.-P. (1994) *Bulletin de la Societe Royale des Sciences de Liege*, **63**, 223-295.

[38] Quadrat, A. and Robertz, R. (2014) *Acta Applicandae Mathematicae*, **133**, 187-234. http://hal-supelec.archives-ouvertes.fr/hal-00925533 https://doi.org/10.1007/s10440-013-9864-x

[39] Kashiwara, M. (1995) Algebraic Study of Systems of Partial Differential Equations. Mémoires de la Société Mathématique de France 63 (Transl. from Japanese of His 1970 Master's Thesis).

[40] Foster, J. and Nightingale, J.D. (1979) A Short Course in General Relativity. Longman, London.

[41] Weyl, H. (1918) Space, Time, Matter. Springer, Dover.

[42] Choquet-Bruhat, Y. (2015) Introduction to General Relativity, Black Holes and Cosmology. Oxford University Press, Oxford.

[43] Hughston, L.P. and Tod, K.P. (1990) An Introduction to General Relativity. London Math. Soc. Students Texts 5, Cambridge University Press, Cambridge.

Journal of Modern Physics, 2018, 9, 2008-2020
http://www.scirp.org/journal/jmp
ISSN Online: 2153-120X
ISSN Print: 2153-1196

# Flat Space Cosmology as a Model of Light Speed Cosmic Expansion—Implications for the Vacuum Energy Density

**Eugene Terry Tatum[1], U. V. S. Seshavatharam[2]**

[1]760 Campbell Ln. Ste. 106 #161, Bowling Green, KY, USA
[2]Honorary Faculty, I-SERVE, S. No-42, Hitex Road, Hitech City, Hyderabad, India
Email: ett@twc.com, seshavatharam.uvs@gmail.com

**How to cite this paper:** Tatum, E.T. and Seshavatharam, U.V.S. (2018) Flat Space Cosmology as a Model of Light Speed Cosmic Expansion—Implications for the Vacuum Energy Density. *Journal of Modern Physics*, **9**, 2008-2020.
https://doi.org/10.4236/jmp.2018.910126

**Received:** August 22, 2018
**Accepted:** September 10, 2018
**Published:** September 13, 2018





## Abstract

Cosmologists have long ignored a stipulation by quantum field theorists that the vacuum pressure $p$ corresponding to the zero-state vacuum energy must always be equal in magnitude to the vacuum energy density $\rho$ (*i.e.*, $p=\rho$). Although general relativity stipulates the additional condition of proportionality between the vacuum gravitational field and ($\rho+3p$), the equation of state for the cosmic vacuum must fulfill both relativistic and quantum stipulations. This paper fully integrates Flat Space Cosmology (FSC) into the Friedmann equations containing a cosmological term, with interesting implications for the nature of dark energy, cosmic entropy and the entropic arrow of time. The FSC vacuum energy density is shown to be equal to the cosmic fluid bulk modulus at all times, thus meeting the quantum theory stipulation of ($p=\rho$). To date, FSC is the only viable dark energy cosmological model which has fully-integrated general relativity and quantum features.

## Keywords

Cosmology Theory, General Relativity, Dark Energy, Cosmic Flatness, Cosmic Entropy, Entropic Arrow of Time, Cosmic Inflation, Milne Universe, Black Holes, Cosmological Constant Problem

## 1. Introduction and Background

Flat Space Cosmology (FSC) is a mathematical model of universal expansion which has proven to be remarkably accurate in comparison to observations [1] [2] [3] [4]. FSC began as a heuristic model following the Penrose-Hawking idea of treating the expanding universe as a time-reversed giant black hole, which is

smoothly expanding as opposed to smoothly collapsing [5] [6]. However, we have also recently proven it to be a general relativity model by successfully integrating the FSC assumptions into the Friedmann equations which include a cosmological term and a global curvature term $k$ set to zero [7] [8]. The relevant equations will be repeated in this paper for clarity.

One of the results of integrating FSC into the Friedmann equations is that the following relation holds true in FSC:

$$\frac{3H^2c^2}{8\pi G} \cong \frac{\Lambda c^4}{8\pi G} \tag{1}$$

This is merely a reflection that global space-time in FSC is flat during the cosmic expansion. As stipulated by the space-time curvature rules of general relativity, a globally flat universe *must* have a net energy density of zero. Otherwise, if the positive energy density and negative energy density terms were not equal in magnitude, there would be an observable global space-time curvature representative of the greater energy density term.

Astronomical observations [9] [10] [11], in the context of general relativity, indicate that a mysterious energy presumably within the cosmic vacuum must be exerting a force in opposition to that of attractive gravity. Thus, this vacuum "dark energy" is defined as a negative energy with respect to the positive energy of cosmic matter. General relativity stipulates the associated vacuum gravitational field to be proportional to ( $\rho + 3p$ ). Quantum field theory makes the additional stipulation that the vacuum pressure $p$ corresponding to the zero-state vacuum energy must always be equal in magnitude to the vacuum energy density $\rho$ (*i.e.*, $p = \rho$ ). Cosmologists, who seem to be particularly focused on ( $\rho + 3p$ ), appear not to be strictly adhering to the quantum theory stipulation. If need be, they appear willing to consider an equation of state $w$ value other than exactly minus one. Nevertheless, the cosmic vacuum equation of state must follow *both* relativistic and quantum stipulations.

The purpose of this paper is to show how the FSC Friedmann equations evolve further from Equation (1) and what they imply, especially with respect to the vacuum energy conditions stipulated by general relativity and quantum field theory. Before doing so, however, it is useful to review the five current assumptions of FSC and its observational correlations.

### 1.1. The Five Assumptions of Flat Space Cosmology

1) The cosmic model is an ever-expanding sphere such that the cosmic horizon always translates at speed of light $c$ with respect to its geometric center at all times $t$. The observer is operationally defined to be at this geometric center at all times $t$.

2) The cosmic radius $R_t$ and total matter mass $M_t$ follow the Schwarzschild formula $R_t \cong 2GM_t/c^2$ at all times $t$.

3) The cosmic Hubble parameter is defined according to $H_t \cong c/R_t$ at all times $t$.

4) Incorporating our cosmological scaling adaptation of Hawking's black hole temperature formula, at any radius $R_t$, cosmic temperature $T_t$ is inversely proportional to the geometric mean of cosmic total matter mass $M_t$ and the Planck mass $M_{pl}$. $R_{pl}$ is defined as twice the Planck length (*i.e.,* as the Schwarzschild radius of the Planck mass black hole). With subscript $t$ for any time stage of cosmic evolution and subscript $pl$ for the Planck scale epoch, and incorporating the Schwarzschild relationship between $M_t$ and $R_t$,

$$\left.\begin{aligned} & k_B T_t \cong \frac{\hbar c^3}{8\pi G\sqrt{M_t M_{pl}}} \cong \frac{\hbar c}{4\pi\sqrt{R_t R_{pl}}} \\ & \begin{cases} M_t \cong \left(\dfrac{\hbar c^3}{8\pi G k_B T_t}\right)^2 \dfrac{1}{M_{pl}} & (2\mathrm{A}) \\ R_t \cong \dfrac{1}{R_{pl}}\left(\dfrac{\hbar c}{4\pi k_B}\right)^2\left(\dfrac{1}{T_t}\right)^2 & (2\mathrm{B}) \\ R_t T_t^2 \cong \dfrac{1}{R_{pl}}\left(\dfrac{\hbar c}{4\pi k_B}\right)^2 & (2\mathrm{C}) \\ H_t \cong \dfrac{c}{R_t} & (2\mathrm{D}) \end{cases} \end{aligned}\right\} \quad (2)$$

5) Total entropy of the cosmic model follows the Bekenstein-Hawking black hole entropy formula [12] [13]

$$S \cong \frac{\pi R^2}{L_p^2} \quad (3)$$

The first two assumptions are based upon a literal interpretation of the Hawking-Penrose conjecture as it would pertain to a smoothly-expanding Schwarzschild black hole. The third assumption (Hubble parameter) treats maximally redshifted radial photons at the cosmic model horizon as moving with speed of light *c relative* to the geometric center at a distance of horizon radius $R_t$. This is a stipulation of relativity. The fourth assumption is a cosmic temperature scaling assumption. While it shows similarity to the static Hawking black hole temperature formula, the FSC cosmic model is treated as scaling in Planck mass increments. This allows for dynamic cosmic expansion modeling from the Planck scale epoch. Finally, the fifth assumption utilizes the Bekenstein-Hawking entropy definition, which seems appropriate for a model of the Hawking-Penrose conjecture. The numerous observational correlations of FSC are given, most recently, in "Temperature Scaling in Flat Space Cosmology in Comparison to Standard Inflationary Cosmology" [7] and "Clues to the Fundamental Nature of Gravity, Dark Energy and Dark Matter" [8].

As previously reported [Tatum, *et al.* (2015)], a number of past, current and future cosmological parameters can be calculated using the FSC model. The accuracy of these correlations with observations is largely accomplished by incorporating the appropriate cosmological scaling formula for cosmic temperature [see the top equation in relation (2)]. This equation, by incorporating elementa-

ry and fundamental constants of nature, allows for FSC scaling from the Planck scale to the current scale. Thus, in this sense, *FSC can be considered a quantum cosmology model*.

### 1.2. Cosmological Parameter Derivations of FSC

Incorporation of the FSC assumptions into the cosmological scaling temperature formula allows for the following cosmological parameter definitions. Current observational parameters are calculated in the right-hand column. *The only free parameter in any of these equations is the cosmic temperature.* The currently observed cosmic temperature value: $T_0 = 2.72548\ ^0\text{K}$.

$$R \cong \frac{\hbar^{3/2}c^{7/2}}{32\pi^2 k_B^2 T^2 G^{1/2}} \qquad R_0 \cong \frac{\hbar^{3/2}c^{7/2}}{32\pi^2 k_B^2 T_0^2 G^{1/2}} \tag{4}$$

$$H \cong \frac{32\pi^2 k_B^2 T^2 G^{1/2}}{\hbar^{3/2}c^{5/2}} \qquad H_0 \cong \frac{32\pi^2 k_B^2 T_0^2 G^{1/2}}{\hbar^{3/2}c^{5/2}} \tag{5}$$

$$t \cong \frac{\hbar^{3/2}c^{5/2}}{32\pi^2 k_B^2 T^2 G^{1/2}} \qquad t_0 \cong \frac{\hbar^{3/2}c^{5/2}}{32\pi^2 k_B^2 T_0^2 G^{1/2}} \tag{6}$$

$$M \cong \frac{\hbar^{3/2}c^{11/2}}{64\pi^2 k_B^2 T^2 G^{3/2}} \qquad M_0 \cong \frac{\hbar^{3/2}c^{11/2}}{64\pi^2 k_B^2 T_0^2 G^{3/2}} \tag{7}$$

$$Mc^2 \cong \frac{\hbar^{3/2}c^{15/2}}{64\pi^2 k_B^2 T^2 G^{3/2}} \qquad M_0c^2 \cong \frac{\hbar^{3/2}c^{15/2}}{64\pi^2 k_B^2 T_0^2 G^{3/2}} \tag{8}$$

$$H_0 = 2.167862848658891\times 10^{-18}\ \text{s}^{-1}\left(66.89325791854758\ \text{km}\cdot\text{s}^{-1}\cdot\text{Mpc}^{-1}\right)$$

This derived current Hubble parameter value fits very closely with the low end range of the 2015 Planck Collaboration consensus observational value of 67.8 +/− 0.9 $\text{km}\cdot\text{s}^{-1}\cdot\text{Mpc}^{-1}$.

$$t_0 \cong \frac{1}{H_0} = 4.612837941379141\times 10^{17}\ \text{s}\left(14.61694683819266\times 10^9\ \text{sidereal yrs}\right)$$

(multiplying by 1 sidereal yr/3.155814954 × $10^7$ s)

This value is the reciprocal of the derived Hubble parameter, as one would expect for a flat space-time cosmic model in comparison to the standard inflationary model. 13.7 billion years is now consensus for the standard model.

$$R_0 \cong \frac{c}{H_0} = 1.382894024801713\times 10^{26}\ \text{m}\left(14.61720137583068\times 10^9\ \text{light-yrs}\right)$$

(multiplying by 1 Julian light-yr/9.4607304725808 × $10^{15}$ m)

This current cosmic radius value correlates with current cosmic time by $R_o = ct_o$. For reasons given in the seminal FSC papers, a perpetually flat and finite space-time cosmology model has no need to incorporate a superluminal inflationary mechanism to solve the flatness and horizon problems.

$$Vol_0 = \frac{4\pi}{3}\left(\frac{c}{H_0}\right)^3 = 1.107784564915062\times 10^{79}\ \text{m}^3$$

$$M_0 = \frac{c^3}{2GH_0} = 9.311265291518025\times 10^{52} \text{ kg}$$

This total matter mass number can be compared very favorably to a rough estimate made from astronomical observations. The visible matter consists of roughly 100 billion galaxies averaging roughly 100 billion stars each, of average star mass equal to roughly $1.4 \times 10^{30}$ kg (70 percent of solar mass), totaling to roughly $1.4 \times 10^{52}$ kg. The 2015 Planck Collaboration report indicates a universal matter ratio of approximately 5.47 parts dark matter to 1 part visible (baryonic) matter. This brings the total estimated matter in the observable universe to approximately $9.1 \times 10^{52}$ kg. A recent study [14] of average mass density of intergalactic dust gives a value of approximately $10^{-30}$ kg·m$^{-3}$. Since this is approximately 1 part intergalactic dust to 1000 parts galactic and perigalactic matter, intergalactic dust does not appreciably modify the total observational estimated mass of matter given above. Accordingly, this observational estimate is remarkably close to the above FSC theoretical calculation of total cosmic matter mass. By the FSC Friedmann equations (below), the positive matter mass-energy must always be equal in absolute magnitude to the negative dark energy. This predicts a 50/50 cosmic energy density percentage ratio as opposed to the approximately 30/70 ratio currently claimed by standard cosmology proponents. However, without unequivocally *proving* cosmic acceleration, standard cosmology cannot yet rightfully claim this 30/70 ratio (see Discussion section).

$$M_0c^2 = \frac{c^5}{2GH_0} = 8.368547901344209\times 10^{69} \text{ J}$$

$$\rho_0 = \frac{3H_0^2}{8\pi G} = 8.405303329200976\times 10^{-27} \text{ kg}\cdot\text{m}^{-3} \quad \text{(critical mass density)}$$

This closely approximates the observational critical density.

$$\rho_0c^2 = \frac{3H_0^2c^2}{8\pi G} = 7.554309895973191\times 10^{-10} \text{ J}\cdot\text{m}^{-3}$$

This closely approximates the observational critical energy density and the observational vacuum energy density. They are equal in absolute magnitude in FSC.

## 2. Flat Space Cosmology Friedmann Equations

With respect to the Friedmann equations, those incorporating a non-zero cosmological term (*i.e.,* a dark energy term) are now the most relevant since the 1998 Type Ia supernovae discoveries. Therefore, accepting Friedmann's starting assumptions of homogeneity, isotropism and an expanding cosmic system with a stress-energy tensor of a perfect fluid, we have his cosmological equation

$$\frac{\dot{a}^2 + kc^2}{a^2} \cong \frac{8\pi G\rho + \Lambda c^2}{3} \tag{9}$$

This equation is derived from the 00 (*i.e.*, energy density) component of the Einstein field equations. Since the global curvature term $k$ is always zero in FSC,

Equation (9) reduces to

$$\left(\frac{\dot{a}}{a}\right)^2 \cong H^2 \cong \frac{8\pi G\rho}{3} + \frac{\Lambda c^2}{3} \tag{10}$$

With rearrangement, we have

$$\frac{3H^2}{8\pi G} - \frac{\Lambda c^2}{8\pi G} \cong \rho \tag{11}$$

This is the relevant Friedmann equation for cosmic mass density. Multiplying all terms by $c^2$ gives us the relevant Friedmann equation for cosmic energy density

$$\frac{3H^2c^2}{8\pi G} - \frac{\Lambda c^4}{8\pi G} \cong \rho c^2 \tag{12}$$

At this point it is crucial to remember that Friedmann's energy density derivation of Einstein's field equations for the cosmic system as a whole (*i.e.,* globally) can be interpreted in the form of additive space-time curvatures represented by the individual terms. The first term can be read as the positive energy density (*i.e.,* the positive space-time curvature) term; the second term can be read as the negative energy density (*i.e.,* the negative space-time curvature) term; and the third term can be read as the summation (*i.e., net*) energy density term for global cosmic space-time curvature. Since global space-time is treated as constantly and perfectly flat in FSC, the third term must always have a net value of zero energy density. This is entirely in keeping with the general theory of relativity, as applied to cosmology, as well as current cosmological observations of flatness (*i.e.,* critical density). Hence, in FSC

$$\frac{3H^2}{8\pi G} \cong \frac{\Lambda c^2}{8\pi G} \tag{13}$$

And

$$\frac{3H^2c^2}{8\pi G} \cong \frac{\Lambda c^4}{8\pi G} \tag{14}$$

From these respective critical mass density and energy density equations, it is obvious that the FSC model defines the Lambda term $\Lambda$ by

$$\Lambda \cong \frac{3H^2}{c^2} \tag{15}$$

In FSC and other realistic linear Milne-type models, Hubble parameter $H$ is a quantity which scales with cosmic time and is defined as

$$H \cong \frac{c}{R} \tag{16}$$

where $c$ is the speed of light and $R$ is the cosmic radius as defined by the Schwarzschild formula

$$R \cong \frac{2GM}{c^2} \tag{17}$$

where $M$ represents the total matter mass of the cosmic system and $G$ is the uni-

versal gravitational constant. Therefore, FSC Equation (15) substituted by Equation (16) gives

$$\Lambda \cong \frac{3}{R^2} \tag{18}$$

So the Lambda term $\Lambda$ is also a scalar quantity (*i.e.,* like the Hubble parameter, not actually a constant) over the great span of cosmic time. This indicates that *FSC is a dynamic dark energy quintessence model.*

Crucially, Equation (18) allows one to compare the Lambda term $\Lambda$ with total entropy for the FSC cosmic system over the span of cosmic time. Recalling the Bekenstein-Hawking derivation of black hole entropy [Bekenstein (1974); Hawking (1976)] as directly proportional to the event horizon surface area $\left(4\pi R^2\right)$, we can apply their formula for cosmic entropy

$$S \cong \frac{\pi R^2}{L_p^2} \tag{19}$$

Then substituting Equation (18) into Equation (19) and rearranging terms

$$\Lambda \cong \frac{3\pi}{SL_p^2} \tag{20}$$

Thus, the Lambda term $\Lambda$ in FSC is inversely proportional to total cosmic entropy $S$ at all times. Substituting Equation (20) into Equation (15) gives

$$S \cong \frac{\pi c^2}{H^2 L_p^2} \tag{21}$$

and

$$H \cong \frac{c}{L_p}\sqrt{\frac{\pi}{S}} \tag{22}$$

And, since the reciprocal of the Hubble parameter is the measure of cosmic time $t$ in FSC

$$t \cong \frac{L_p}{c}\sqrt{\frac{S}{\pi}} \tag{23}$$

So cosmic time is always directly proportional to $\sqrt{S}$, with entropy $S$ as defined by Bekenstein and Hawking. Thus, the "entropic arrow of time" is clearly defined in the FSC model.

The dark energy density cosmological term is not only expressed as $\left(\Lambda c^4/8\pi G\right)$ in FSC Friedmann equation (14) but, by incorporating equation (20) into this term, we now have a dark energy density equation

$$\frac{\Lambda c^4}{8\pi G} \cong \frac{3c^4}{8GSL_p^2} \cong \frac{3H^2c^2}{8\pi G} \tag{24}$$

wherein any of these terms can be used interchangeably to quantify the absolute magnitude of the cosmic dark energy density at all times.

Since the FSC cosmic expansion model follows the Friedmann starting assumptions of homogeneity, isotropism, and an expanding cosmic system with a

stress-energy tensor of an ideal fluid, one can consider the bulk modulus $B$ of classical mechanics to apply to such a fluid. Thus, the wave velocity $v_w$ of the cosmic fluid should have the following relationship

$$v_w = \sqrt{\frac{B}{d}} \tag{25}$$

In a realistic cosmic model, where $v_w = c$, and $d = p$, and $B$ is the cosmic vacuum bulk modulus, this can be expressed as

$$c = \sqrt{\frac{B}{p}} \tag{26}$$

Thus,

$$B = pc^2 \tag{27}$$

Therefore, the pressure of this particular ideal fluid (the cosmic vacuum) must always equal its energy density by virtue of the fact that the cosmic vacuum always has a wave velocity of *c.* This satisfies the quantum theory ( $p = \rho$ ) stipulation for the zero-state vacuum energy.

## 3. Discussion

Cosmologists have long ignored a stipulation by quantum field theorists that the vacuum pressure $p$ corresponding to the zero-state vacuum energy must always be equal in *absolute magnitude* to the vacuum energy density $\rho$ (*i.e.,* $p = \rho$). While general relativity further stipulates proportionality between the repulsive gravity field of dark energy and ( $\rho + 3p$ ), there appears to be little interest within the standard inflationary cosmology community concerning strict adherence to the above quantum theory stipulation. Unfortunately, the effect of ignoring the quantum field stipulation is that it becomes difficult for cosmologists to otherwise explain an *observed* equation of state term $w = -1.006 +/- 0.045$ (Planck 2015). Whereas, a value of exactly −1.0 is a *prediction* of the FSC model, as is obvious from equation (27), when adopting the *convention* of opposite pressure and density signages.

The discovery of dark energy within the cosmic vacuum applies to cosmic models an accelerator pedal in opposition to the brake pedal of attractive gravity. An important question yet to be resolved is whether the cosmic acceleration value is precisely zero or *very slightly* positive. Deep statistical analysis of the Supernova Cosmology Project compilation data shows only two remaining viable categories of dark energy cosmological models: realistic Milne-type $R_h = ct$ models (with a zero acceleration value, by definition); and the standard model (with an exceedingly small positive acceleration value). A number of very recent papers [15] [16] [17] [18] show strong statistical support for the continued viability of realistic Milne-type $R_h = ct$ models.

The FSC model is the most realistic Milne-type $R_h = ct$ model to date, by virtue of the fact that it is now fully integrated into the Friedmann equations, as shown in this paper, and shows tight correlations with the 2015 Planck Collabo-

ration report findings, including their consensus *observational* Hubble parameter value of 67.8 +/− 0.9 km·s$^{-1}$·Mpc$^{-1}$. A realistic Milne-type model, in sharp contrast to Milne's original "empty universe" model [19], is one which contains gravitational matter. As further evidence of the continued viability of realistic $R_h = ct$ models, the following open source graph from the Supernova Cosmology Project [20] is shown in **Figure 1**.

The FSC realistic Milne-type $R_h = ct$ model is mathematically a perpetual critical density (*i.e.,* "flat") model, as shown in the seminal FSC papers [Tatum, *et al.* (2015)]. Therefore, it falls on the "Flat" universe model line in **Figure 1**.

Those with knowledge of the observational studies of the ratio of dark matter to visible matter realize the difficulty of determining a *precise co-moving* value for this ratio at the present time. Too little is yet known about dark matter for such precision. Galactic and perigalactic distributions of dark matter can be surprisingly variable, as evidenced by the 29 March 2018 report in *Nature* [21] of a galaxy apparently completely lacking in dark matter! Although the 2015 Planck Collaboration consensus is a *large-scale* approximate ratio of 5.47 parts dark matter to 1 part visible matter, this can only be a rough estimate of the actual *co-moving* ratio, particularly if this ratio varies significantly over cosmic time. A 10-to-1 actual ratio in co-moving galaxies remains a possibility, and would change the actual ratio of total matter mass-energy to dark energy to essentially unity (*i.e.,* 50% matter and 50% dark energy). The intersection zone of tightest constraints shown in **Figure 1** would then correlate with 0.5 Omega_ matter and 0.5 Omega_Lambda. This is one of several important *testable predictions* discriminating the FSC model from the standard model.

So long as these models are in a statistical dead heat, it is reasonable to ask if one of the two models is more compatible with the quantum theory stipulation of equality between the vacuum pressure and the vacuum energy density. The answer to this question is clearly in favor of FSC, because the predicted 50/50 percentage ratio for FSC meets the quantum theory stipulation, whereas the standard model 30/70 percentage ratio does not.

The reason why the 50/50 percentage ratio of FSC implies equality between the vacuum pressure and the vacuum energy density (and why the standard model 30/70 percentage ratio does *not* imply such equality) is contained in the final four equations of this paper [Equations (24) thru (27)]. The crucial equations are (24) and (27). Only in the FSC model can the vacuum energy density $\left(\Lambda c^4/8\pi G\right)$ be shown to be equal in absolute magnitude to both the total matter mass-energy density $\left(3H^2c^2/8\pi G\right)$ and the vacuum pressure represented by the bulk modulus $B$ term in Equation (27).

One of the unexpected findings of integrating the FSC model into the Friedmann equations is the intriguing *discovery of a possible close relationship between dark energy and total cosmic entropy* [see relations (18) through (24)]. A review of prior publications concerning this possible relationship indicates that theoretical physicist Roger Penrose explores this subject in great detail in his recent book entitled "Fashion Faith and Fantasy in the New Physics of the

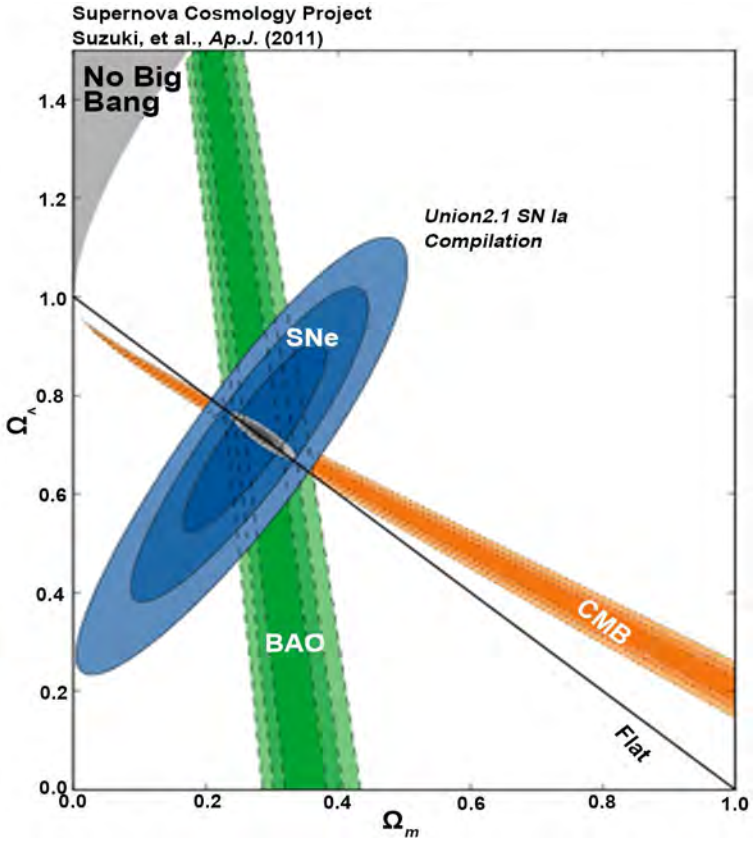


**Figure 1.** Accumulated Supernova (SNe), BAO and CMB data with highlighted constraints.

Universe" [22] (pages 275-285). Perhaps most notably, Penrose uses the Bekenstein-Hawking black hole entropy formula to derive the same equation (in rearranged form, on his page 277) as FSC relation (18) in this paper. This gives us great confidence that resulting FSC Equations (19) through (24), showing mathematical relationships between total cosmic entropy and the Hubble parameter, cosmic time ("entropic arrow of time") and vacuum energy density, are indeed realistic and correct. *Thus, FSC also may prove to be a useful cosmological model correlate to Erik Verlinde's "entropic gravity"* [23] *and "emergent gravity"* [24] *theories.*

It is important to reiterate that the equation of state for the cosmic vacuum is stipulated by *both* relativistic and quantum considerations. By apparently ignoring the stipulation from quantum field theory that ( $p = \rho$ ) must always hold true for the cosmic vacuum, standard cosmology practitioners appear to have reached an impasse between general relativity and quantum theory. The FSC model, on the other hand, has fully integrated these relativistic and quantum stipulations, while maintaining remarkable accuracy with respect to current observations.

## 4. Summary and Conclusions

The FSC model of cosmology was developed as a heuristic mathematical model

of the Hawking-Penrose idea that an expanding universe arising from a singularity state can be modeled as a time-reversed giant black hole. This idea was an extension of Penrose's paper [Penrose (1965)] on the singularities of black holes and cosmology. Hawking's doctoral thesis took the idea further by proving the validity of time-reversal in the treatment of general relativity as it concerns cosmology [Hawking and Penrose (1970)]. Finally, the FSC model completes this idea by incorporating scaling black hole equations suitable for cosmology. Thus, the proven accuracy of FSC with respect to current astronomical observations does not appear to be an accident.

To overcome any potential objections that FSC does not fit within general relativity, this paper fully integrates FSC into the Friedmann equations. The implications of the FSC Friedmann equations offer unique insights into the possible nature of dark energy with respect to total cosmic entropy and the entropic arrow of time (see especially FSC reference [8]).

The primary purpose of this paper concerns the vacuum energy density implications of the FSC Friedmann equations. Particular attention is paid to Equation (1) as it relates to Equations (24) thru (27). Since a perpetually flat universe model implies (by the global curvature rules of general relativity) perpetual equality of the absolute magnitudes of global positive energy density and global negative energy density, the magnitude of the vacuum pressure can be equated with the magnitude of critical energy density (now approximately $10^{-9}$ J·m$^{-3}$). Remembering that Friedmann's assumptions included treatment of the cosmic fluid (*i.e.,* the cosmic vacuum) as a perfect fluid, classical wave velocity equation (25) would seem to be appropriate for the FSC model. Thus, the cosmic wave velocity (speed of light $c$) should be directly proportional to the square root of the cosmic fluid bulk modulus, and inversely proportional to the square root of the cosmic fluid density. This relationship leads to Equation (27), indicating perpetual equality between the *absolute magnitudes* of the vacuum pressure and the vacuum energy density. So FSC *predicts* an equation of state $w$ term value of −1.0 exactly (assuming the convention of opposite pressure and density signages). This follows directly from the small number of FSC assumptions incorporated into the Friedmann equations. It is not an *ad hoc* adjustment to cosmology theory, as has clearly been the case for the various theories of cosmic inflation ([25], page 238, [26]).

In conclusion, so long as standard cosmology proponents accept, as fact that cosmic expansion is undergoing positive acceleration, *however small,* as implied by their claim of a 30/70 percentage ratio of total cosmic matter mass-energy to dark energy, standard cosmology is not adhering strictly to the ( $\rho = p$ ) stipulation of quantum field theory. To date, FSC is the only viable dark energy cosmological model which has fully-integrated general relativity and quantum features.

## Dedications and Acknowledgements

Both authors dedicate this paper to the late Dr. Stephen Hawking and to Dr.

Roger Penrose for their groundbreaking work on black holes and their possible application to cosmology. Dr. Tatum thanks Dr. Rudolph Schild of the Harvard Center for Astrophysics for his past support and encouragement. Author Seshavatharam UVS is indebted to professors Brahmashri M. Nagaphani Sarma, Chairman, Shri K.V. Krishna Murthy, founding Chairman, Institute of Scientific Research in Vedas (I-SERVE), Hyderabad, India, and to Shri K.V.R.S. Murthy, former scientist IICT (CSIR), Govt. of India, Director, Research and Development, I-SERVE, for their valuable guidance and great support in developing this subject.

## Conflicts of Interest

The authors declare no conflicts of interest regarding the publication of this paper.

## References

[1] Tatum, E.T., Seshavatharam, U.V.S. and Lakshminarayana, S. (2015) *International Journal of Astronomy and Astrophysics,* **5**, 116-124. https://doi.org/10.4236/ijaa.2015.52015

[2] Tatum, E.T., Seshavatharam, U.V.S. and Lakshminarayana, S. (2015) *Journal of Applied Physical Science International,* **4**, 18-26.

[3] Tatum, E.T., Seshavatharam, U.V.S. and Lakshminarayana, S. (2015) *Frontiers of Astronomy, Astrophysics and Cosmology,* **1**, 98-104.

[4] Planck Collaboration XIII. (2015) Cosmological Parameters. http://arxiv.org/abs/1502.01589

[5] Hawking, S. and Penrose, R. (1970) *Proceedings of the Royal Society of London A*, **314**, 529-548. https://doi.org/10.1098/rspa.1970.0021

[6] Penrose, R. (1965) *Physical Review Letters*, **14**, 57. https://doi.org/10.1103/PhysRevLett.14.57

[7] Tatum, E.T. and Seshavatharam, U.V.S. (2018) *Journal of Modern Physics*, **9**, 1404-1414. https://doi.org/10.4236/jmp.2018.97085

[8] Tatum, E.T. and Seshavatharam, U.V.S. (2018) *Journal of Modern Physics*, **9**, 1469-1483. https://doi.org/10.4236/jmp.2018.98091

[9] Perlmutter, S., *et al.* (1999) *Astrophysical Journal*, **517**, 565-586.

[10] Schmidt, B., *et al.* (1998) *Astrophysical Journal*, **507**, 46-63. https://doi.org/10.1086/306308

[11] Riess, A.G., *et al.* (1998) *Astronomical Journal*, **116**, 1009-1038. https://doi.org/10.1086/300499

[12] Hawking, S. (1976) *Physical Review D*, **13**, 191-197. https://doi.org/10.1103/PhysRevD.13.191

[13] Bekenstein, J.D. (1974) *Physical Review D*, **9**, 3292-3300. https://doi.org/10.1103/PhysRevD.9.3292

[14] Inoue, A.K. (2004) *Monthly Notices of the Royal Astronomical Society,* **350**, 729-744. https://doi.org/10.1111/j.1365-2966.2004.07686.x

[15] Tutusaus, I., *et al.* (2017). *Astronomy & Astrophysics,* **602**, A73. arXiv:1706.05036v1 [astro-ph.CO].

[16] Nielsen, J.T., *et al.* (2015) Marginal Evidence for Cosmic Acceleration from Type Ia Supernovae. arXiv:1506.01354v1.

[17] Wei, J.-J., *et al.* (2015) *Astronomical Journal*, **149**, 102-112. https://doi.org/10.1088/0004-6256/149/3/102

[18] Melia, F. (2012) *Astronomical Journal*, **144**, 110. arXiv:1206.6289 [astro-ph.CO]. https://doi.org/10.1088/0004-6256/144/4/110

[19] Milne, E.A. (1935) Relativity Gravitation and World Structure. The Clarendon Press, Oxford.

[20] Suzuki, *et al.* (2011) The Hubble Space Telescope Cluster Supernovae Survey: V. Improving the Dark Energy Constraints above Z>1 and Building an Early-Type-Hosted Supernova Sample. arXiv.org/abs/1105.3470.

[21] Van Dokkum, P., *et al.* (2018) *Nature*, **555**, 629-632. https://doi.org/10.1038/nature25767

[22] Penrose, R. (2016) Fashion Faith and Fantasy in the New Physics of the Universe. Princeton University Press, Princeton. https://doi.org/10.1515/9781400880287

[23] Verlinde, E. (2011) *Journal of High Energy Physics*, **4**, 29-55. arXiv:1001.0785v1 [hep-th]. https://doi.org/10.1007/JHEP04(2011)029

[24] Verlinde, E. (2016) Emergent Gravity and the Dark Universe. arXiv:1611.02269v2 [hep-th].

[25] Guth, A.H. (1997) The Inflationary Universe. Basic Books, New York.

[26] Steinhardt, P.J. (2011) *Scientific American*, **304**, 18-25. https://doi.org/10.1038/scientificamerican0411-36


# Call for Papers

# Journal of Modern Physics

**ISSN: 2153-1196 (Print)  ISSN: 2153-120X (Online)**
**http://www.scirp.org/journal/jmp**

***Journal of Modern Physics*** **(JMP)** is an international journal dedicated to the latest advancement of modern physics. The goal of this journal is to provide a platform for scientists and academicians all over the world to promote, share, and discuss various new issues and developments in different areas of modern physics.

## Editor-in-Chief

**Prof. Yang-Hui He** City University, UK

## Executive Editor-in-Chief

**Prof. Marko Markov** Research International, Buffalo Office, USA

## Subject Coverage

Journal of Modern Physics publishes original papers including but not limited to the following fields:

Biophysics and Medical Physics
Complex Systems Physics
Computational Physics
Condensed Matter Physics
Cosmology and Early Universe
Earth and Planetary Sciences
General Relativity
High Energy Astrophysics
High Energy/Accelerator Physics
Instrumentation and Measurement
Interdisciplinary Physics
Materials Sciences and Technology
Mathematical Physics
Mechanical Response of Solids and Structures
New Materials: Micro and Nano-Mechanics and Homogeneization
Non-Equilibrium Thermodynamics and Statistical Mechanics
Nuclear Science and Engineering
Optics
Physics of Nanostructures
Plasma Physics
Quantum Mechanical Developments
Quantum Theory
Relativistic Astrophysics
String Theory
Superconducting Physics
Theoretical High Energy Physics
Thermology

We are also interested in: 1) Short Reports—2-5 page papers where an author can either present an idea with theoretical background but has not yet completed the research needed for a complete paper or preliminary data; 2) Book Reviews—Comments and critiques.

## Notes for Intending Authors

Submitted papers should not have been previously published nor be currently under consideration for publication elsewhere. Paper submission will be handled electronically through the website. All papers are refereed through a peer review process. For more details about the submissions, please access the website.

## Website and E-Mail

**http://www.scirp.org/journal/jmp  E-mail: jmp@scirp.org**

## What is SCIRP?

Scientific Research Publishing (SCIRP) is one of the largest Open Access journal publishers. It is currently publishing more than 200 open access, online, peer-reviewed journals covering a wide range of academic disciplines. SCIRP serves the worldwide academic communities and contributes to the progress and application of science with its publication.

## What is Open Access?

All original research papers published by SCIRP are made freely and permanently accessible online immediately upon publication. To be able to provide open access journals, SCIRP defrays operation costs from authors and subscription charges only for its printed version. Open access publishing allows an immediate, worldwide, barrier-free, open access to the full text of research papers, which is in the best interests of the scientific community.

- High visibility for maximum global exposure with open access publishing model
- Rigorous peer review of research papers
- Prompt faster publication with less cost
- Guaranteed targeted, multidisciplinary audience


Scientific Research Publishing

**Website: http://www.scirp.org**

**Subscription: sub@scirp.org**

**Advertisement: service@scirp.org**